Heinrich Heine Universität Düsseldorf

SecYEG/YidC-Mediated Membrane Protein Biogenesis

Inaugural dissertation

for the attainment of the title of doctor
in the Faculty of Mathematics and Natural Sciences
at the Heinrich Heine University Düsseldorf

presented by

Michael Kamel
from Cairo, Egypt

Düsseldorf/Germany, August 2023

From Synthetic Membrane Systems, Institute of Biochemistry
at the Heinrich Heine University Düsseldorf

Wir dürfen die Hoffnung niemals verlieren.
Claudia Tiedermann, Dark.

Abstract

Proteins destined to leave the cytosol of the cell are transported to and across the cytoplasmic membrane in prokaryotes or the endoplasmic reticulum in eukaryotes using the universal Sec machinery. In a simple view, proteins destined to cross the cytoplasmic membrane in prokaryotes are delivered post-translationally to the SecYEG: SecA translocon where they get transported through the SecYEG channel using ATP hydrolysis of the motor protein SecA. On the other hand, proteins destined to be transported to the cytoplasmic membrane are delivered co-translationally to SecYEG or the membrane protein insertase, YidC, where they get inserted and properly folded into the membrane. Advances in membrane mimetic systems allowed for better studying and characterization of key processes associated with the membrane. Here, the advances in membrane mimetic systems were employed to study key steps in protein transport to and across the cytoplasmic membrane of bacteria.

Combining the use of membrane vesicles and nanodisc technology with biochemical and biophysical methods (fluorescence spectroscopy, SPR, and QCM), it was shown that mono-unsaturated fatty acids (UFAs) stimulate protein transport via the SecYEG: SecA translocon. Mono-UFAs induce lipid packing defects into the membrane that might promote SecA binding to the membrane via its N-terminal amphipathic helix. The N-terminal helix of SecA is split into helices, a small and a long helix as confirmed by the AlphaFold2 model of the *E.coli* SecA and the crystal structure of *B. subtilis* SecA. The results suggest that the long helix promotes electrostatic interactions with the anionic lipids of the membrane via its positively charged face to recruit SecA to the membrane. On the other hand, the small helix promotes hydrophobic interactions with the membrane, where it gets inserted. This step primes SecA for the functional assembly with SecYEG and activates its translocating ATPase activity. Additionally, the N-terminal helix regulates the binding of SecA homologs to the diverse membranes across different bacterial species.

Using supported lipid bilayers with single-molecule fluorescence microscopy, the oligomeric state of the Sec translocon, and the assembly of the SecYEG: SecA and SecYEG: ribosomes nascent chain complexes (RNCs) were addressed. The results showed that SecYEG exists mainly as a monomer in the membrane, and the dimer fraction increases once bound to SecA. Moreover, the lateral mobility of translocon was measured and has been shown to be slower once bound to RNCs.

Finally, combining the use of cell-free protein synthesis (CFPS) and nanodisc technology, the co-translational assembly of the bacterial membrane protein insertion pathway was established. SecYEG and/or YidC reconstituted in MSP-based nanodiscs or directly isolated using maleic acid copolymers were supplied to CFPS reactions, where they formed complexes with SecM-stalled RNCs. The assembled complexes were purified and can be further used for structural studies using cryo-EM. Nascent chains with different lengths were designed that can be used with the established platform to provide different snapshots of the insertion pathway and provide more details about the path of the nascent chain from the ribosome exit tunnel to the membrane.

Contents

Chapter 1

Introduction

1.1 The Sec system

About one-third of the protein in bacteria are destined to leave the cytosol and be transported to or across the cytoplasmic membrane to execute their functions [1]. Most of the proteins destined to be exported or integrated into the membrane interact with the universal Sec system. The Sec system is a conserved system that resides in the cytoplasmic membrane of bacteria, archaea, and also the endoplasmic reticulum of eukaryotes. It is commonly composed of the heterotrimeric complex SecY/SecE/SecG in bacteria and Sec61α/Sec61γ/Sec61β in eukaryotes, that form a channel in the membrane. The Sec system executes two major functions, the transport of secretory, periplasmic, and outer membrane protein across the cytoplasmic membrane, and the insertion of membrane proteins in the cytoplasmic membrane. Therefore, it engages with different types of substrates, and delivery/targeting machinery in order to execute these functions [2].

In principle, two different pathways exist for targeting substrates to the Sec system. SecA-dependent pathway targets secretory, periplasmic, and outer membrane proteins, that are destined to be exported across the cytoplasmic membrane. Substrates belonging to this pathway possess a cleavable N-terminal signal peptide and are normally targeted to the Sec system in a post-translational mode. On the other hand, membrane proteins destined to be inserted into the cytoplasmic membrane are targeted to the Sec system using the signal recognition particle (SRP)-dependant pathway in a co-translational mode [2].

In the post-translational mode, SecYEG interacts with SecA, which is a peripheral membrane protein that uses ATP hydrolysis as a source of energy to drive protein translocation across the membrane. Substrates harboring cleavable N-terminal signal peptides bind chaperones and holdases like Trigger Factor and SecB, which keep the substrate in an unfolded, secretion-competent state. These chaperones then deliver the substrate to the ATPase SecA, which interacts with the cytoplasmic membrane, and the membrane-embedded channel SecYEG. The substrate is translocated through the SecYEG-based channel upon ATP hydrolysis on SecA [3].

On the other hand, during membrane protein insertion, which typically occurs in a co-translational mode, SecYEG interacts with the translating ribosomes and inserts membrane protein into the membrane during their ongoing translation. In this mode, ribosome nascent chain complexes (RNCs) bind the SRP, a GTPase which targets the RNCs to the Sec system via interaction with SecYEG-bound SR receptor FtsY. Afterward, the RNCs are transferred to the Sec translocon, and GTP hydrolysis by the SRP: FtsY causes the dissociation of the targeting complex. SecYEG then inserts the nascent chain into the membrane co-translationally [4]. SecYEG has been shown to interact with other different types of machinery like YidC and SecD-FYajC. YidC is an insertase that belongs to the YidC/OxaI/Alb3 family. It has been shown to insert small membrane proteins into the membrane. It can do its function dependently or independently from the Sec translocon. Substrates can be targeted to YidC post-translationally or co-translationally in an SRP-dependent manner (Figure 1.1) [2, 5].
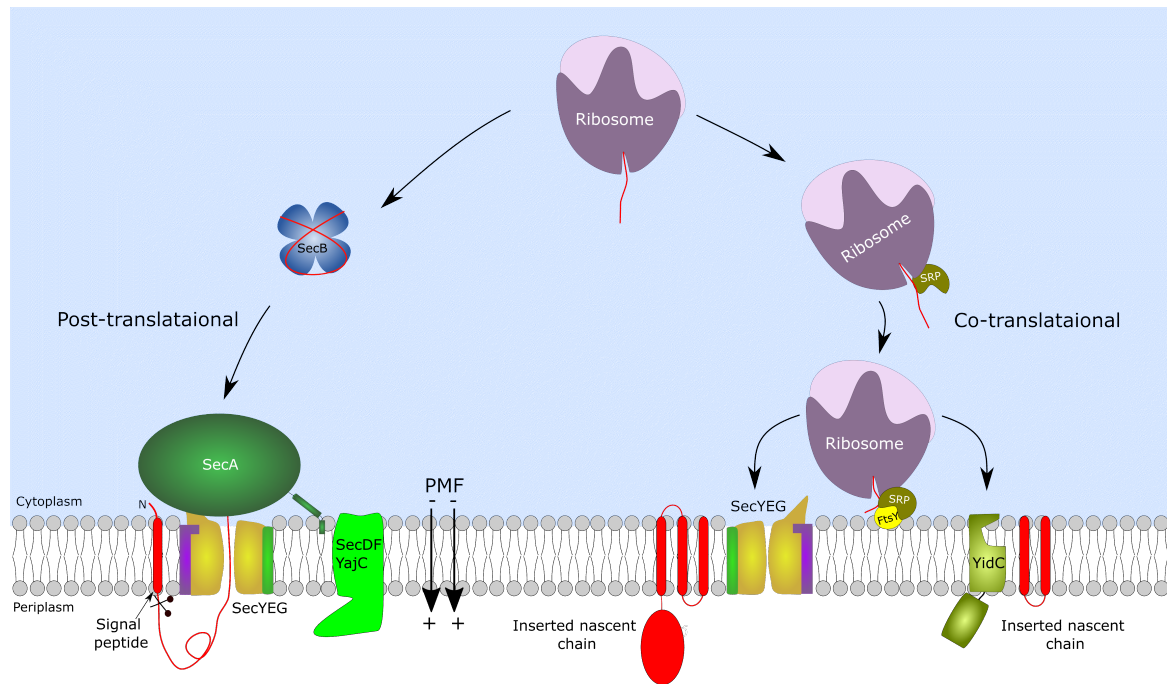
Figure 1.1: Post-translational and co-translational modes of the Sec system. Post-translational mode is usually used for the transport of protein across the cytoplasmic membrane and involves the holdase SecB, which keeps the nascent chain unfolded for secretion, and the motor protein SecA, which uses ATP hydrolysis to transport the nascent chain through the SecYEG channel. The co-translational mode is used for membrane protein insertion through SecYEG and/or YidC. It involves the SRP that targets the ribosome nascent chain complex to the membrane where it binds its receptor FtsY and then the RNCs are transferred to SecYEG for co-translational insertion.

It has been shown that there are exceptions to this simple picture. For instance, the inner membrane protein, RodZ, which has a large cytosolic domain, followed by a single transmembrane domain, is targeted co-translationally to the Sec system using SecA [6, 7]. The periplasmic maltose binding protein, MBP is another example of SecA-dependent co-translational targeting [8]. On the other hand, the SRP can also target nascent chains in a post-translational mode. It has been shown that small membrane proteins, like YohP and YkgR, and tail-anchored proteins, such as DjlC, Flk, and SciP can be post-translationally targeted to the Sec system using SRP [9–11].

1.1.1   The protein conducting membrane channel, SecYEG

The first crystal structure of SecYEβ was obtained from the Archeon, *Methanococcus janaschii*, and it represented the resting state of the membrane-embedded channel (Figure 1.2 A and B) [12]. SecY is composed of ten transmembrane helices (TMHs) that are organized into two halves composed of TMHs 1 to 5 and 6 to 10 respectively, forming a pseudosymmetric clamshell-like structure. The two halves are connected by a periplasmic loop between TMHs 5 and 6 (hinge region). A side section of SecY shows that it resembles an hourglass with two funnels separated by a central constriction called the pore ring. The pore ring is comprised of hydrophobic and bulky amino acids, six isoleucines in *E.coli*, and it is sealed from the periplasmic side with the TMH 2a, which is called the plug domain, that seals the channel against ion diffusion. A lateral

gate is located between TMH 2, 3, and TMH 7/8 in the front of SecY, it facilitates the entrance of the signal peptide and TMHs of the substrates into the lipid bilayer. Long cytosolic loops between TMH 6/7 and TMH 8/9 provide the binding site for SecA, ribosomes, and FtsY, the SRP receptor. SecY channel has different states, quiescent (Figure 1.2 A and B), pre-open (Figure 1.2 C), and open state (Figure 1.2 D), depending on the stage of protein translocation.

SecE is another essential subunit. In *E.coli*, SecE has 3 TMHs and an amphipathic helix that lies parallel to the membrane, but only the third TMH and the amphipathic helix have been shown to be essential for protein transport. SecE is located at the back of SecY opposite to the lateral gate (Figure 1.2 A and B), and it has been shown to stabilize the two halves of SecY [12, 13]. In the absence of SecE, SecY is rapidly degraded by the membrane protease, FtsH [14].

In *E.coli*, SecG is composed of two TMHs and it has been shown to be not essential for protein transport *in vitro* [15] and for cell viability. The cytosolic loops of SecG has been suggested to seal the cytoplasmic funnel of SecY [16]. SecG deletion strains show transport and cold-sensitive growth defects *in vivo* [17–19]. However, these defects could be suppressed by various gene products that are involved in phospholipids biosynthesis [20, 21]. SecG has also been shown to promote SecYEG: SecA binding [22] and is important for translocation in the absence of proton motive force (PMF) (Figure 1.2) [23, 24].

1.2   Post-translational protein transport across the cytoplasmic membrane

In a simple view, substrates with an N-terminal signal peptide are destined for post-translational protein transport. They are targeted to the Sec translocon by chaperones like SecB [25]. The N-terminal signal peptide is characterized by having a positively charged N-terminus, a hydrophobic core, and a polar C-terminus [26]. At the ribosomes, signal peptides of the pre-proteins are less hydrophobic than TMHs and therefore become bound by Trigger Factor (TF) that aims to decrease their affinity for SRP, and this act as a selection mechanism for the post-translational pathway prior to handing the pre-protein over to SecB [27, 28]. The holdase chaperone SecB is a tetramer formed of a dimer of dimers. It contains a solvent-exposed hydrophobic groove that can bind hydrophobic stretches of the pre-protein. SecB serves to keep the pre-protein unfolded and targets the pre-protein to the ATPase motor protein SecA [29–31], which then translocates the pre-protein through the SecY channel using ATP hydrolysis as an energy source.

The proton motive force has been shown to further stimulate the translocation of the polypeptide chain [32]. After translocation is completed, the signal peptide is cleaved to release the mature protein on the periplasmic side of the membrane [33].
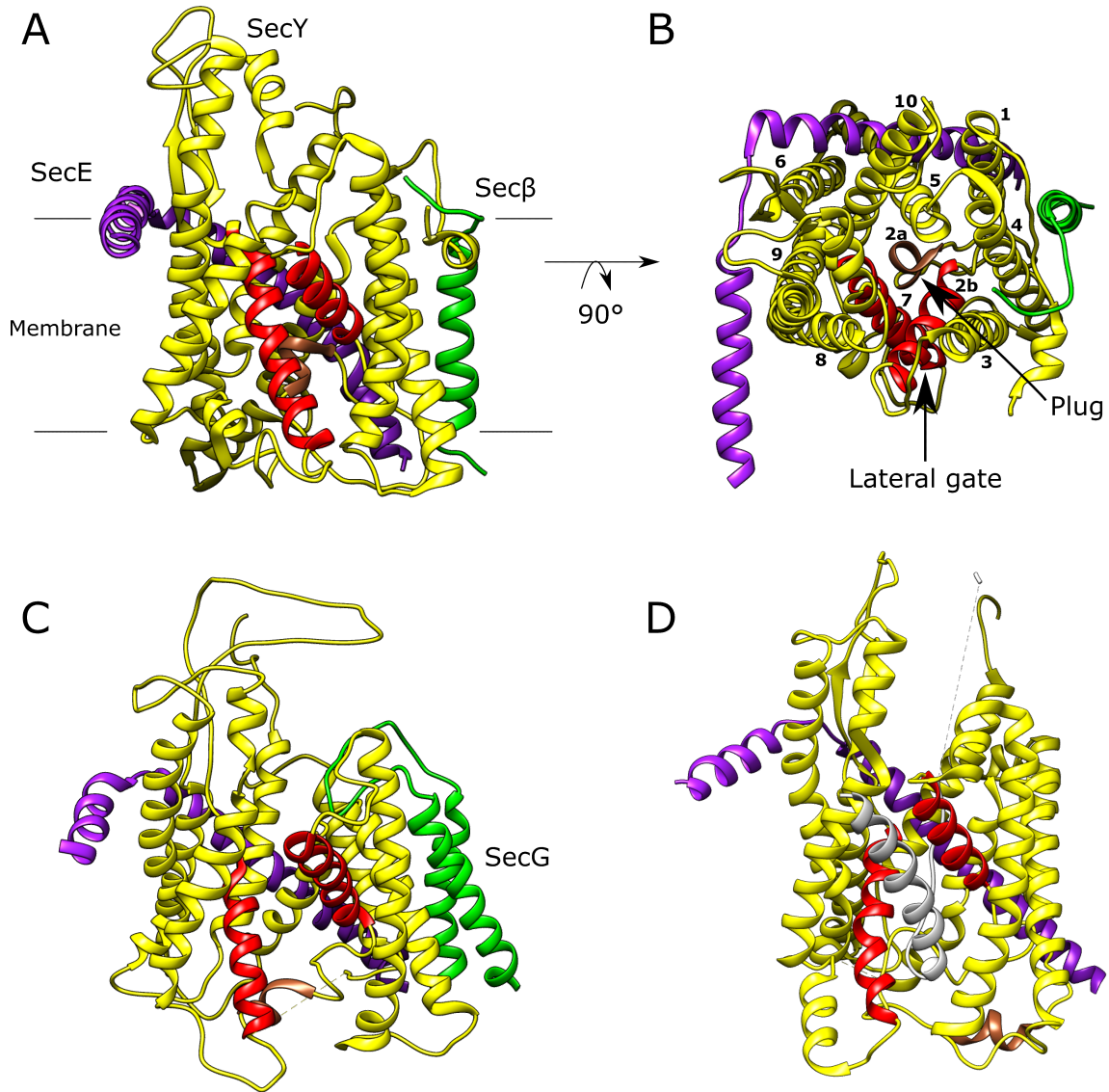
Figure 1.2: The structure of the membrane-embedded channel, SecYEG. SecY has ten TMHs, and a lateral gate (red) between TMH 2b and TMH 7. SecE is made of 3 TMHs and an amphipathic helix (purple, TMH 1, and 2 are missing from this structure) and SecG has 2 TMHs (green). The SecYEG channel exists in different states depending on the opening or closing of the lateral gate. A and B) The Quinescent or resting state from the structure of SecYEβ from *Methanococcus janaschii* (PDB: 1RHZ) with a closed lateral gate. C) The pre-open state from SecYEG from *Thermotoga maritima* (PDB: 3DIN). D) The open translocating state from SecYE of *Geobacillus thermodenitrificans* (PDB: 6ITC) with an open lateral gate. The lateral gate is depicted in red color, the plug domain in brown and signal peptide is white.

1.2.1 SecA

SecA is a peripheral membrane motor protein that provides the energy for protein transport by ATP hydrolysis (Figure 1.3 A). It is a multidomain protein, which is composed of two nucleotide-binding domains, NBD1 and NBD2 (also called the intramolecular regulator of ATPase 2 (IRA-2)). ATP binds at the interface between the two NBDs, they move relative to each other during ATP hydrolysis. The two NBDs form the so-called DEAD motor, which is also present in the

DNA/RNA helicases [34, 35]. SecA contains a polypeptide crosslinking domain (PPXD), where the pre-protein can bind and that has an important role in the activation of the ATPase activity of SecA [36, 37]. The C-domain is composed of four subdomains, the helical scaffold domain (HSD), the two helix finger (THF), the helical wing domain (HWD), and the C-terminal linker domain (CTD). The THF is a part of the intramolecular regulator of ATPase 1 (IRA-1) [38] that inhibits the ATPase activity of SecA [39]. The CTD contains a zinc finger and has an important role in SecA interaction with the holdase SecB [40, 41] and the membrane [42]. SecA has an N-terminal amphipathic helix that has an important role in membrane binding. Moreover, SecA has a clamp domain, which forms by the rotation of the PPXD domain towards NBD2, which is suggested to hold the substrate during protein translocation [43].
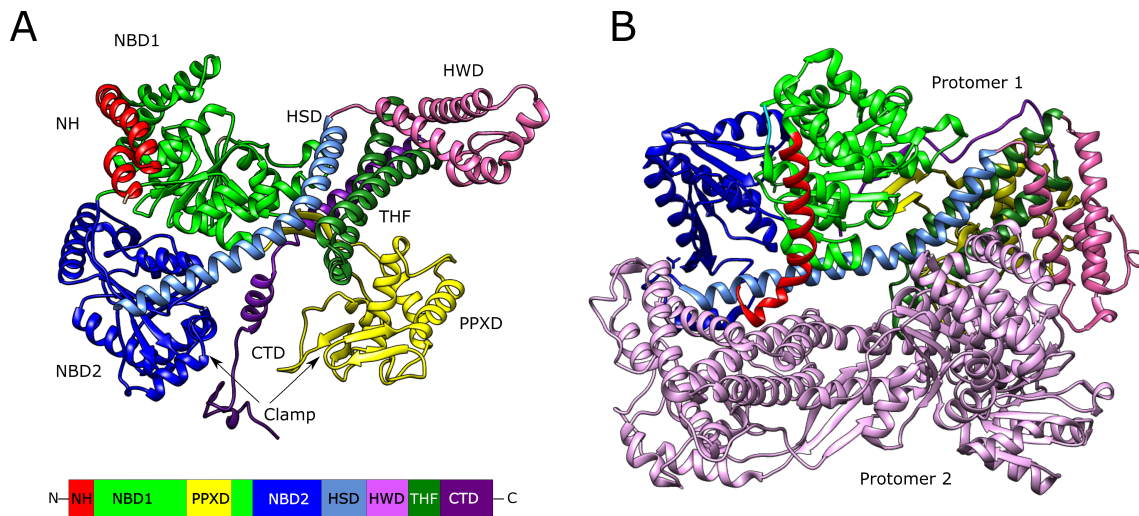
Figure 1.3: The structure of ATPase motor protein, SecA. A) AlphaFold2 model of *E. coli* SecA. SecA is a multidomain protein composed of two nucleotide binding domains, preprotein crosslinking domain (PPXD) and the C-domain which is composed of the helical wing domain (HWD), the two helix finger (THF), the helical scaffold domain (HSD), the C-terminal linker domain (CTD) and N-terminal amphipathic helix (NH). A clamp is formed by the rotation of the PPXD domain towards the NBD2. B) The probable physiological dimer of SecA from *Bacillus subtilis* (PDB: 1M6N). The second copy is shown in salmon.

1.2.2   Different models describe the mechanism of action of SecA

The translocation process starts with the pre-protein binding to SecA, which in turn binds to the SecYEG channel. This cause the signal peptide of the pre-protein to interact with the lateral gate of SecYEG at the interface of the lipid bilayer. This causes the channel to partially open (unlocked state) and the plug that keeps the channel closed to be displaced from the channel. This interaction causes a change in the conformation of SecA priming it for elevated ATP hydrolysis and priming the channel to translocate the pre-protein [44, 45]. However, several models have been proposed for how SecA translocates the pre-protein through the SecYEG channel.

Firstly inspired by the first SecYEG: SecA structure, Erlandson et al 2008 proposed a sole power stroke mechanism in which the THF of SecA would bind the polypeptide chain and push the substrate into the SecY channel in the ATP-bound state. After ATP hydrolysis, SecA disengages from the substrate leading to the backsliding of the substrate. Possibly, SecY provides

enough friction through its pore ring that slows down the backsliding rate, while SecA grabs the next segment of the substrate providing unidirectionality [38, 46]. Zimmer et al 2008 showed that SecA contains a clamp that forms by the rotation of the PPXD domain towards the NBD2. They propose that the clamp will hold the substrate during the ADP-bound state of SecA preventing it from backsliding. The translocating polypeptide chain would form a β sheet with two β strands connecting NBD1 with PPXD stabilizing the clamp. However, this model contradicts the fact that during the ADP-bound state of SecA, passive diffusion of the polypeptide chain is observed [43].

Then, Bauer et al. 2014 proposed a refined "push-and-slide" mechanism, where both power stroke and passive sliding are parts of the translocation process. Here, SecA interacts with the polypeptide chain through the THF domain and pushes the substrate into the channel during the ATP-bound state. After ATP hydrolysis, the two helix fingers will disengage from the polypeptide chain, allowing passive sliding in both directions. This active pushing provides directionality of the transport. They explain that the THF does not interact strongly with all amino acids, and when it encounters weakly interacting amino acids, the polypeptide chain will passively move in both directions resulting in no active pushing, which explains the promiscuity of SecA. In vivo, the translocation efficiency can be improved by SecDF pulling and the folding of the polypeptide chain on the extracellular side of the membrane [47]. However, both of these models did not take into account, how the THF retracts without the simultaneous retraction of the polypeptide chain erasing the work done from the power stroke. Using single-molecule FRET between SecA and SecY, Captovic et al 2019 proposed a model supporting the push and slide model while addressing this problem. They proposed that the THF insert deeply into the channel in the ATP-bound state pushing the substrate to the periplasmic side of the membrane (Figure 1.4 A-II). Afterward, the SecA clamp tightens around the polypeptide chain holding it in position (Figure 1.4 A-III). In the transition state of ATP hydrolysis, the THF starts to retract (Figure 1.4 A-IV). Once ATP is hydrolyzed, the THF retracts completely, while the clamp still remains closed (Figure 1.4 A-V). The clamp reopens only after the release of P_i allowing for passive sliding in both directions (Figure 1.4 A-I). They argue that passive sliding can be reduced *in vivo* by the proton motive force, or the substrating folding and binding to periplasmic chaperones on the periplasmic side of the membrane [48].

Alternatively, Allen et al 2016 proposed a "Brownian ratchet" model. Here, the polypeptide chain normally diffuses freely within the closed channel backward and forwards (Figure 1.4 B-I). However, when a bulky region of the polypeptide chain (bulky residues or secondary structure elements) reaches the channel that can not pass causing a blockage, this will trigger nucleotide exchange in SecA from ADP to ATP (Figure 1.4 B-II). The conformational changes within SecA will cause the opening of the channel, where the bulky region can then diffuse freely (Figure 1.4 B-III). After ATP hydrolysis, the channel will close trapping the bulky region at the periplasmic side of the membrane, thus preventing backsliding (Figure 1.4 B-IV). Here, the THF act as a sensor for the bulky regions in the substrate rather than actively pushing the polypeptide chain inside the channel. The forward directionality is ensured because SecA is only present in the cytoplasmic side of the membrane, therefore the resolution of the channel blockage induced by the nucleotide exchange can only happen in the cytoplasmic side of the channel. Consequently, a bulky region trapped on the periplasmic side of the channel will not induce the nucleotide

exchange on SecA and the opening of the channel [49]. Corey et al 2019 expanded the Brownian ratchet model using MD simulation, electron paramagnetic resonance, and hydrogen-deuterium exchange mass spectrometry (HDX-MS). They showed that the pre-protein can form secondary structures within the cytoplasmic and periplasmic cavities of the SecYEG channel in the ADP-bound state of SecA. When the THF encounters a secondary structure, it promotes nucleotide exchange and the opening of the channel. However, in the ATP-bound state, there is a bias for the pre-protein to form secondary structures in the periplasmic cavity of the channel. After ATP hydrolysis and the closure of the channel, the pre-protein secondary structures present in the periplasmic cavity prevent the backsliding, which then favors the forward translocation of the pre-protein [50].

Using single-molecule intramolecular FRET to monitor the plug dynamics within SecY, Fessl et al 2018 were able to provide more details on the steps of pre-protein translocation. They described that the signal peptide unlocks the translocon in an ATP-independent manner, followed by the displacement of the plug which requires ATP and leads to the opening of the channel. Afterward, a slow phase that is independent of pre-protein length occurs. In this phase, structural rearrangements of the translocon may occur, like placing the signal peptide within the lateral gate or the complete threading of the pre-protein loop following the signal peptide through the channel. This phase is then proceeded by a fast phase which is dependent on the pre-protein length. Finally, the relocation of the plug and the closure of the channel occur, independent of ATP [51].

Based on hydrogen-deuterium exchange mass spectrometry (HDX-MS), Krishnamurthy et al 2022 proposed an alternative "catch-and-release" model. They showed that conformationally locally frustrated prongs around the SecA clamp catch and release trapped pre-protein frustrated segments. Frustration is a phenomenon that occurs within certain regions in a protein that is forced into energetically unfavorable arrangements by well-folded parts of the protein [52, 53]. In this model, the binding of the signal peptide to SecA promotes the closure of the SecA clamp and opening of the SecY channel (Figure 1.4 C-II). Here frustrated regions within the signal peptide will interact with frustrated regions within the SecA clamp (Catch). Afterward, the binding of mature domain regions of the polypeptide chain to SecA promotes the release of ADP and the binding of ATP (Figure 1.4 C-III). ATP binding stimulates the release of the mature domain regions of the polypeptide chain inside the channel (Release) (Figure 1.4 C-IV). During the transition state of ATP hydrolysis, the SecA clamp will interact with the preceding mature domain targeting signals (MTS) within the polypeptide chain through frustrated regions on both partners (Catch) (Figure 1.4 C-V). After ATP hydrolysis, a succeeding region of the mature domain will bind to SecA and induce ADP release and the restart of the ATP cycle. These cycles of catch and release repeat until no more mature domain segments are present to bind SecA. This model shows that pre-protein can interact with high affinity but transiently with SecA through the frustrated segments, allowing for SecA processivity, and explains how SecA can promiscuously recognize its substrates. This model is also compatible with the "Brownian ratchet" model, where the pre-protein enters the channel by diffusion as well as the "push and slide" model. In the latter case, the THF can push the substrate into the channel during the catch phase [54].

Finally, in a recently published cryo-EM structure of the SecYEG: SecA complex by Dong et al 2023 in the presence of both ADP and ATP, the authors proposed a new model called the "Hand-Switching model". They showed that the substrate formed a β-strand that is sandwiched between two structural elements within the clamp, the TCβ, which is two β strands that link NBD1 to the PPXD, and a loop from the PPXD domain called the PP loop. They demonstrated that in the ADP bound state, the TCβ has stronger interactions with the polypeptide chain than the PP loop (Figure 1.4 D-I), while in the ATP bound state, the PP loop forms stronger interactions with the polypeptide chain bending it and weakening the interaction with the TCβ (Figure 1.4 D-II). After ATP hydrolysis, the PP loop holds the substrate tightly, and TCβ returns to its original conformation in the ADP state forming strong interaction with the polypeptide chain and weakening the interaction with the PP loop (Figure 1.4 D-III). These repeated cycles of loose and tight interaction result in the forward movement of the polypeptide chain inside the channel [55].

1.2.3 The effect of the membrane composition on the SecYEG: SecA translocon

The effect of the inner membrane composition on protein transport through SecYEG: SecA translocon has been extensively documented. de Vrije et al 1988 showed that anionic lipids are involved in protein translocation across the inner membrane *in vivo* [56]. Lill et al 1990 showed that acidic phospholipids stimulate the ATPase activity of SecA, which they named SecA/lipid ATPase. They also showed that acidic phospholipids are necessary for the translocation ATPase activity of SecA and the translocation of pre-protein across the inner membrane [57] and that SecA interacts with liposomes containing acidic phospholipids. Breukink et al 1992 showed that SecA interacts with monolayers containing acidic phospholipids and that these interactions are not inhibited by high salt concentrations indicating that both electrostatic and hydrophobic interactions between SecA and the membrane exist [58]. It has also been shown that SecA penetrates deep into the membrane [59–61]. Hendrick et al. 1991 showed that inner membrane vesicles depleted of acidic phospholipids are unable to bind SecA and do neither support protein translocation nor the translocation ATPase activity of SecA [62]. Moreover, van der Does et al 2000 showed that the non-bilayer forming lipid phosphatidylethanolamine stimulates protein translocation [63]. Prabudiansyah et al 2015 showed using styrene-maleic acid-lipid particles the enrichment of anionic lipids, phosphatidylglycerol, and cardiolipin around the SecYEG channel [64].
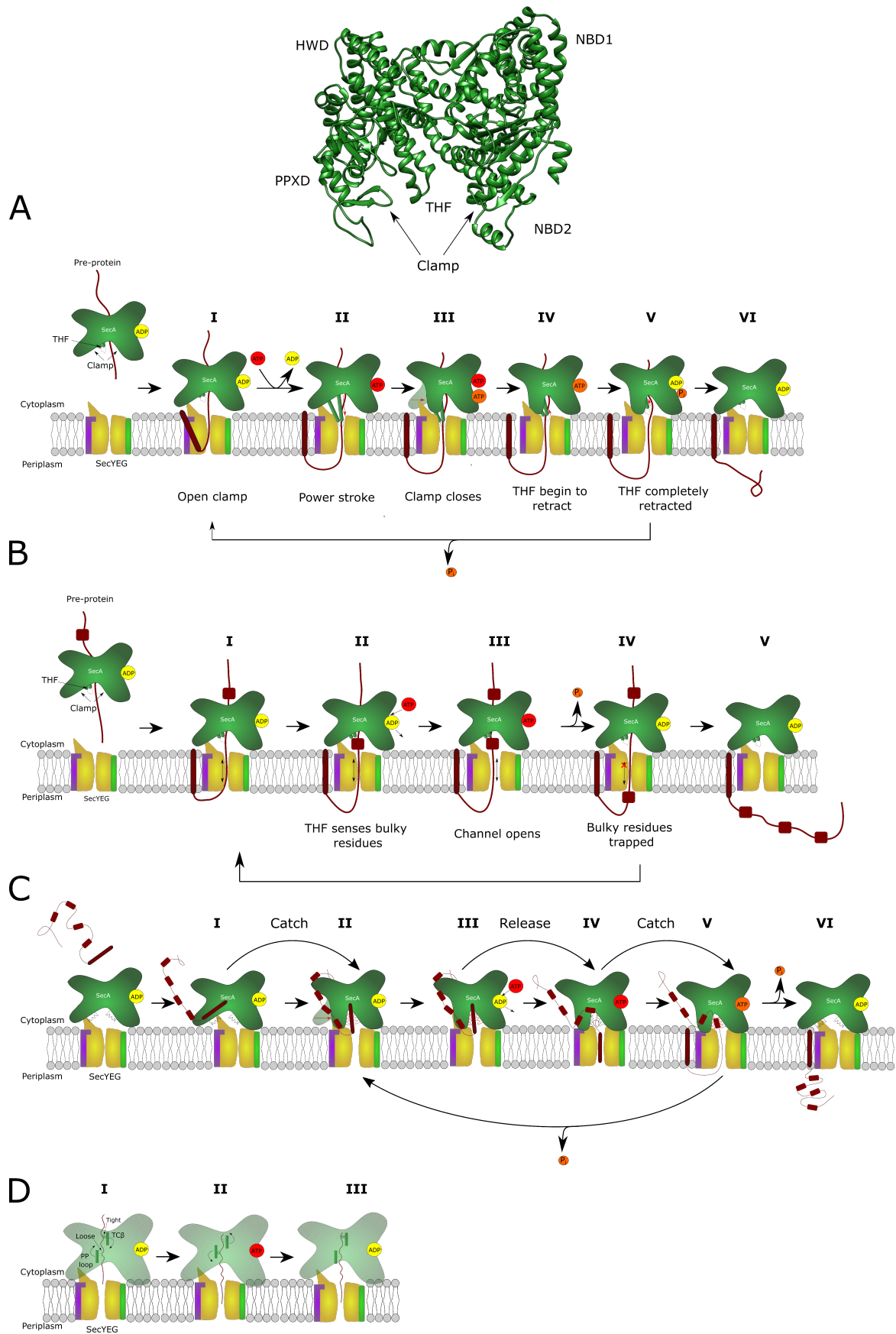
Figure 1.4: Differend models of SecA mediated protein translocation. Top: AlphaFold2 model of *E. coli* SecA showing the clamp and the THF domains. A) The push and slide model. The two helix finger of SecA binds the pre-protein and actively pushes it inside the channel. B) The Brownian ratchet model. The two helix finger of SecA acts as a sensor for bulky residue inducing the opening of the channel, while the pre-protein randomly diffuses backward and forward, when the bulky residues cross the channel and the channel closes, this lead to trapping the bulky residues on the other side preventing backsliding. C) The catch and release model, here frustrated domain within the SecA clamp transiently interacts (catch) with frustrated domains within the signal peptide and MTS within the pre-protein and then releases it (release). This catch-and-release mechanism promotes the forward motion of the pre-protein. D) The Hand-switching model. Here, the subsequent loose and tight interaction of the TCβ and PP loop within the SecA clamp with the pre-protein biases the forward motion of the pre-protein through the channel. ADP is depicted in yellow, ATP is red, while orange colored ATP indicate the transition state of ATP hydrolysis.

Floyd et al 2014 showed that the N-terminal helix of SecA is important for its ability to complement the growth of SecA temperature-sensitive mutant strain and they show that this loss of activity is correlated with the ability of SecA to bind the membrane. They identified that the first 23 residues of the N-terminal helix are dispensable, but deleting them reduces transport activity. Deleting the additional residues 23 to 25 leads to the reduction of membrane binding and activity, while deleting more than 25 amino acids abolishes membrane binding and transport activity. They argued that the N-terminal helix of SecA has positive residues that can interact with acidic lipids in the membrane [65]. Bauer et al 2014 showed that deleting the first 20 amino acids of the N-terminal helix of SecA leads to the loss of the *in vitro* translocation activity which correlates well with its inability to bind liposomes. When a Histidine tag was introduced instead of the N-terminal helix, both membrane binding and activity were restored in Ni-NTA-containing SecYEG proteoliposomes. They also showed that the rebinding of SecA to a translocating SecY channel requires that SecA interacts firstly with the membrane with its N-terminal helix. This probably helps to concentrate SecA at the translocation site and restricts its diffusion to the membrane plane [47]. Koch et al 2016 demonstrated that the N-terminal helix of SecA is necessary for membrane binding and that SecA binding to the membrane allosterically changes its conformation, priming it for high-affinity binding to SecYEG. They argue that the SecA membrane-bound state is an intermediate in the translocation cycle where it undergoes 2D diffusion in the membrane until it encounters SecYEG [66]. Winkler et 2020 analyzed SecA: membrane interaction using surface plasmon resonance and showed that SecA binds to the membrane in two states, the first state is electrostatically driven and mediated by the positive residues on the N-terminal helix of SecA, while the second state involves the insertion of the N-terminal helix of SecA, probably mediated by hydrophobic interactions of the amphipathic helix with the membrane confirming what has been previously proposed that SecA inserts into the membrane [67].

The exact binding interface of SecA to the membrane has not been completely clarified. As mentioned above, the N-terminal helix of SecA is a crucial component of SecA membrane interaction. Earlier studies show that the C-terminus is also involved in membrane binding [42]. In a new study, the author created 25 surface-exposed cysteine mutations of SecA conjugated to the

polarity-sensitive fluorophore NBD. By measuring the change in fluorescence intensity and shift in wavelength upon incubation with liposomes made from *E.coli* polar lipids, they determined three domains of SecA involved in binding to the membrane. The first domain comprises the positively charged N-terminal amphipathic helix of SecA as expected. Interestingly, they discovered a second domain that is composed of an alpha helix that is located between NBD II and the first half of the helical scaffold domain (HSD). They described that the third domain is the CTD region of SecA forming a weak lipid binding domain [68].
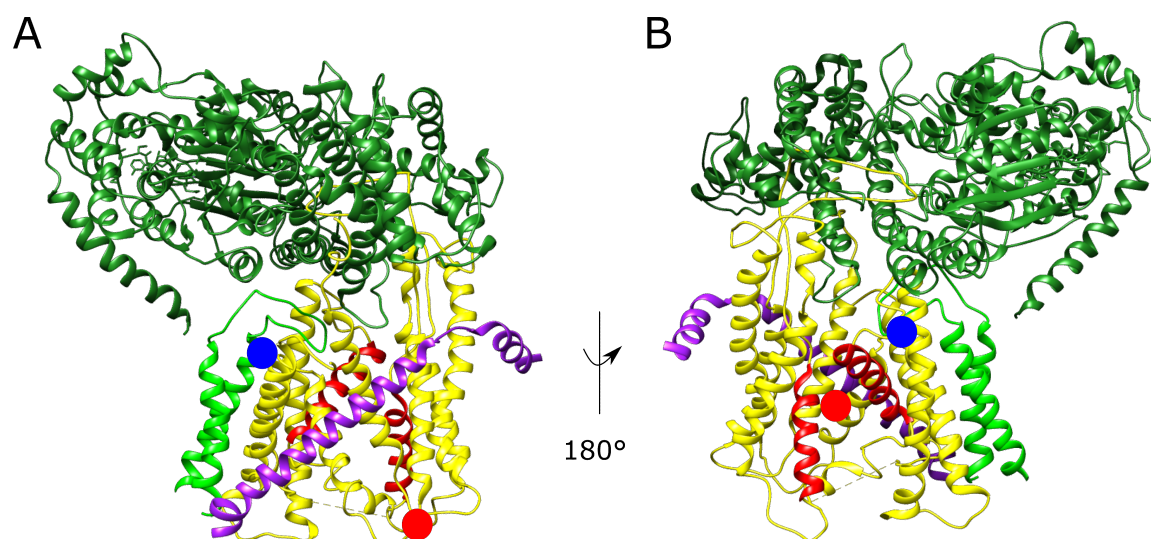
Figure 1.5: Specific lipid binding sites on SecYEG: SecA translocon as determined by MD simulations. SecA is depicted in green, SecY in yellow, SecE in violet, and SecG in light green. Blue circles indicate the positions in the back (A) and front (B) of the translocon, where anionic lipids, either phosphatidyl glycerol (PG) or cardiolipin have been found using molecular dynamics simulations to specifically bind SecYEG. Red circles indicate the additional SecY contact positions that were found for PG by Koch et al 2019.

Phosphatidylglycerol (PG) and cardiolipin (CL) are bacteria's most common acidic lipids. The exact role of cardiolipin has been extensively disputed. Gold et al 2009 demonstrated that the acidic lipid cardiolipin associates tightly with the SecYEG channel stabilizing its dimeric form. It also provides a high-affinity binding interface for SecA and stimulates its ATPase activity [69]. However, Prabudiansyah et al 2015 showed that cardiolipin has no further stimulatory role on the SecYEG:SecA protein translocation as compared to phosphatidylglycerol. This was further supported by a study that showed that inactivation of the three paralogues of the cardiolipin synthetase genes resulted in the inhibition of cardiolipin biosynthesis, while cell viability was marginally affected. This shows that cardiolipin is not essential for protein translocation [70].

Corey et al 2019 identified using coarse-grained molecular dynamics (MD) simulation two specific cardiolipin sites on the SecYEG: SecA translocon (Figure 1.5). The first site is located in the proximity of the lateral gate of the SecY, helical scaffold domain of SecA and SecG. They argue accordingly that CL has a role in the stabilization of the open or closed state of the channel and may have a role in mediating the signal peptide membrane interaction. The second site is

at the back of the translocon and comprises positive residues of TMH 1 and 4 at the interface of SecY and SecG. The second site is in direct contact with the N-terminal helix of SecA which has been shown to be crucial for SecA: lipid binding as discussed above. They show that these cardiolipin-specific sites are required for the activation of the ATPase activity of SecA, rather than the stabilization of the dimeric state of SecY. They also demonstrate that these cardiolipin-specific sites are required for the PMF stimulation of protein translocation [71]. Koch et al 2019 identified using coarse-grained MD simulation specific anionic lipids sites around SecY. On the cytoplasmic side of SecY, two spots were identified, the first site is located at the SecG: SecA N-terminal helix interface. The second site is on the other side of SecY at the SecY-SecG interface. These sites are in good agreement with the cardiolipin-specific sites observed by Corey et al 2019. From the periplasmic side, two more sites were identified. The third site involves the interaction of the anionic lipids with a loop between TMH5 and 6 of SecY. Interestingly, the fourth site is located near the lateral gate with a preference for PG over CL. Moreover, they indicate that the headgroup of the PG inserts in the open lateral gate, while that was not observed with CL. They explain that the insertion of the PG headgroup in the lateral gate could promote the binding of the signal peptide which contains a positively charged N-terminus (Figure 1.5) [72].

All of these studies indeed confirm the role of lipids within the membrane on the activity of SecYEG: SecA translocon and confirm the essential role of anionic lipids and the N-terminal helix of SecA. However, the exact role of cardiolipin is not yet clarified and moreover, the effect of the acyl chain composition of the membrane on protein transport has never been investigated.

1.2.4   Oligomeric state of SecA

SecA forms dimers in solution [73–75] with a dissociation constant that ranges from 1 nM to 3 μM depending on the ionic strength and temperature [75, 76]. However, the quaternary structure of the translocating SecA has been a matter of great debate. The cellular concentration of SecA is around 5 to 8 μM, so cytoplasmic SecA is expected to mainly exist as a dimer [73, 77]. However, a new single molecule study showed that cellular SecA concentration is in the range of 20 to 200 nM, nevertheless, they show that it mainly exists as a dimer in the cytoplasm [78].

Different structures of SecA have been determined with a variety of methods: X-ray crystallography [35, 43, 79–84], nuclear magnetic resonance (NMR) [85] and cryogenic electron microscopy [55, 86, 87]. Many of the resolved structures reveals a dimer, however, the position of the protomers and the dimeric interface differs between structures. The reasons for that firstly could be that many of the crystalized dimers might not reflect the actual physiological dimer, due to the conditions used for crystallization, and as mentioned above, dimerization is sensitive to ionic strength. Secondly, SecA might indeed exist in various dimeric forms in the cytoplasm, but one or two of the reported dimers might form the active translocating dimer when bound to SecY [88]. Many of the reported dimers have an antiparallel organization with their C-domain facing opposite directions, and only one structure has a parallel orientation [81]. However, several studies have shown that *Bacillus subtilis* anti-parallel dimer is the most abundant dimer in solution (Figure 1.3 B) [35, 89–91].

Several studies proposed that SecA remains dimeric during the translocation cycle [74, 76]. Crosslinked SecA protomers either at their native cysteine or genetically engineered cysteines at

the *B. subtilis* anti-parallel dimer and a tandem fusion of SecA were able to interact with SecY and promote protein translocation *in vitro*. This indicates that the dissociation of the dimer is not necessary for protein translocation [92–94]. Nevertheless, other studies show that the dimeric SecA dissociates once bound to the membrane and SecY [67, 77, 95–98] and that a crosslinked dimeric SecA at the interface of the *B.subtilis* dimer is not active [99]. Other studies showed that SecA dimers can weakly bind the membrane [97, 98]. Moreover, there have been various reports that showed that signal peptides can either induce the monomerization or dimerization of SecA [100, 101]. Several studies showed the deletion of the N-terminal 11 residues of SecA shifted the equilibrium of the dimeric SecA to monomers in solution, however, they disagree on whether or not this mutant is active both *in vivo* and *in vitro* [96, 102, 103]. Other studies showed that this mutant is both dimeric and functional [91, 93, 104].
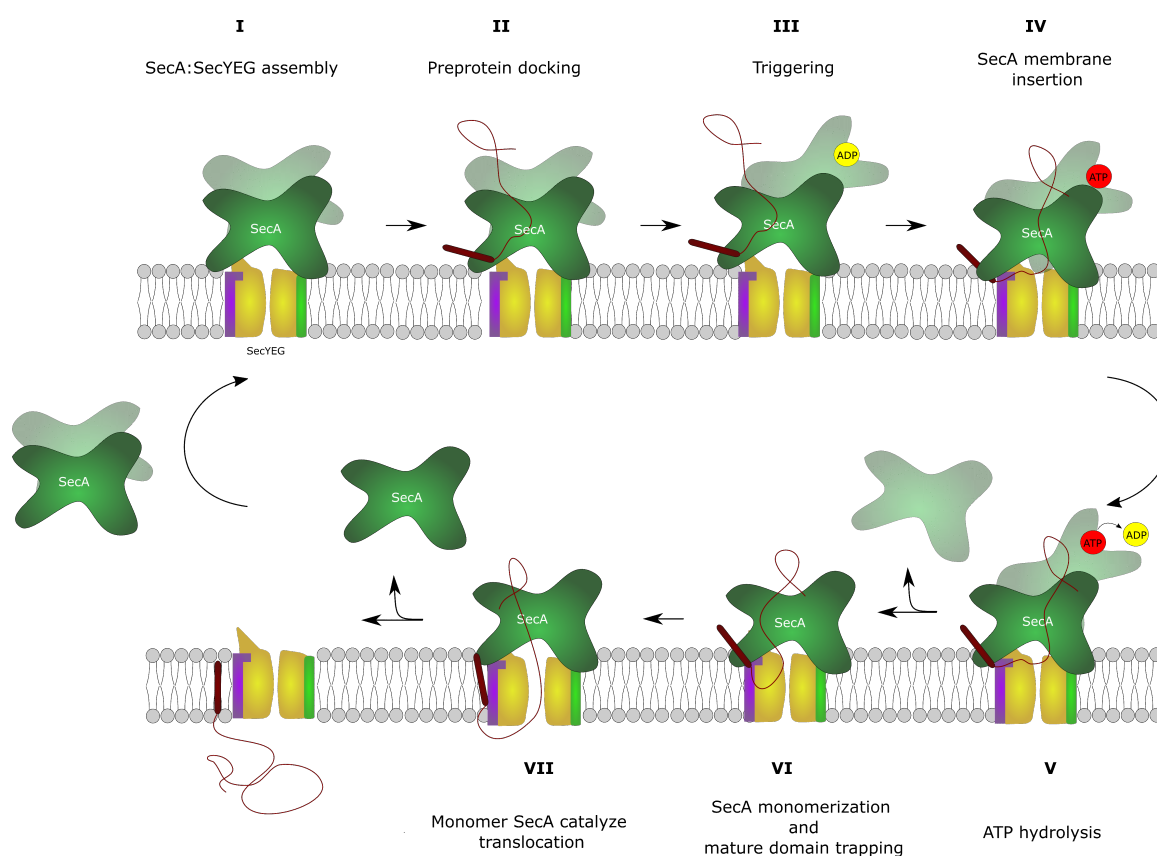
Figure 1.6: Monomer-dimer model of membrane-bound and translocating SecA [91]. This model shows that SecA binds the membrane and SecYEG as a dimer, but it monomerizes to catalyze protein translocation. Here, the SecA dimer binds with one of its protomers to SecYEG (I), the SecY-protomer then binds the pre-protein (II). The binding of the signal peptide triggers SecYEG: SecA where the SecA dimers slide over each other forming the triggered dimer (III). ADP is released from the SecY unbound protomer, and ATP binds which triggers the membrane insertion of SecA (IV). ATP hydrolysis (V) induces the monomerization of SecA and trapping of the mature domain of the pre-protein (VI). Monomeric SecA catalyzes multiple rounds of stepwise translocation of the pre-protein through the SecY channel (VII).

Based on extensive biochemical analysis, Gouridis et al 2013 investigated the oligomeric state of SecA in great detail. They showed that SecA dimerization is mediated by both electrostatic and hydrophobic interactions. They described that three interconvertible dimers of SecA exist,

an electrostatic dimer (ED), a salt-resistant dimer (SRD), and a triggered dimer (TD) that exist in equilibrium with the SecA monomer. They elaborated that the N-terminal helix of SecA plays an important role in mediating SecA dimerization. The N-terminal helix of SecA is predicted to be divided into a small helix (α0) followed by a longer helix (α1). The positive residues within the (α1) helix are needed for the formation of the ED dimer, while the (α0) helix is responsible for the formation of the SRD dimer. Ionic strength, SecY, signal peptides, nucleotides, and mutations can modulate the equilibrium between the SecA conformations.

They demonstrated that all the SecA conformations contribute to the translocation cycle in different stages and proposed a model describing that (Figure 1.6). Firstly, the cytoplasmic SecA is in the ADP-bound state and exists as the electrostatic dimer (1M6N), SecA docks to SecYEG with only one of its protomers, while the other protomer acts as a regulatory protomer (Figure 1.6 I). This SecY: SecA interaction makes SecA dimer asymmetric and the SecY bound protomer binds with high affinity to the pre-protein (Figure 1.6 II), while the regulatory protomer is unable to bind pre-proteins. The signal peptide triggers the SecY: SecA translocon, where SecA dimers slide over each other forming the TD dimer (Figure 1.6 III). The SRD dimer is necessary for the transition of ED to the TD dimer. ADP is then released from the regulatory protomer and ATP binds, this step drives the insertion of the SecY-bound SecA protomer into the membrane (Figure 1.6 IV). ATP hydrolysis is then stimulated by allosteric regulation of the regulatory protomer and binding of the mature pre-protein domain (Figure 1.6 V). ATP hydrolysis then triggers the monomerization of SecA and the pre-protein mature domain becomes trapped, and the signal peptide intercalates with the lateral gate of SecY (Figure 1.6 VI). The monomeric SecA then catalyzes the translocation of the pre-protein through the channel until it is completely translocated (Figure 1.6 VII). Subsequently, the monomeric SecA loses its affinity for the SecY channel, dimerizes, and starts another cycle of translocation [91]. This model shows for the first time the possibility that the translocating SecA can exist in both dimer and monomeric states explaining the contradicting results observed in the literature. Nevertheless, this model still contradicts the *in vitro* studies that showed the monomerization of SecA once bound to the membrane and the weak affinity of the crosslinked SecA dimer to the membrane [97, 98].

Despite the recent advances in studying the post-translational protein transport through the Sec translocon. Certain issues still remain unresolved. What is the exact role of cardiolipin? Does the membrane acyl chain composition have an effect on SecA-membrane binding and protein transport? Are both SecA and SecYEG sensitive to the lipid environment? What is the exact oligomeric state of the membrane-bound and SecYEG-bound SecA? What is the exact role of the N-terminal helix of SecA in protein transport? The membrane composition varies substantially between gram-negative, gram-positive, and extremophilic bacteria. Is the N-terminal helix of SecA homologs evolutionarily tuned to interact with membranes with different headgroups and acyl chain compositions? Does SecA needs to first bind the membrane in order to find SecY or can it already dock to the SecY channel directly from the cytoplasm? These challenging questions rationalize the need for different membrane mimetic systems and biophysical approaches to characterize the SecYEG: SecA translocon: membrane interaction.

1.3   Co-translational membrane protein insertion and folding

Membrane proteins make up 20-30 % of the cellular proteome. Proteins in the cytoplasmic membrane contain hydrophobic TMHs that can be misfolded or aggregate if not directly inserted into the membrane. Integral membrane proteins (IMPs) are normally inserted in the membrane co-translationally with the help of the Sec translocon and the insertase, YidC. Ribosomes translating nascent chains of membrane proteins with exposed highly hydrophobic signal peptides, which is called signal anchor or TMHs in this case, are recognized by the signal recognition particle (SRP) which targets the ribosome nascent chain complexes (RNCs) to the membrane insertion machinery [105]. Signal peptides of the SRP pathway do not all contain positively charged residues on the N-terminus and are more hydrophobic than the signal peptides that target the pre-proteins to the post-translational pathway [106, 107]. They are not conserved in sequence, but rather highly hydrophobic with a high propensity to form alpha helices [108, 109].

1.3.1   SRP dependent targeting

The bacterial SRP is a ribonucleoprotein that comprises the minimal functional core required for RNC binding and targeting. It mainly consists of 4.5S RNA and the protein Ffh, which is a homolog of the eukaryotic SRP54 protein [110]. Ffh is a GTPase protein that contains a methionine-rich domain called the M-domain that has the ability to recognize hydrophobic stretches typical for membrane protein nascent chains. Moreover, it contains an N-terminal NG-domain including the GTPase domain and the binding site for the SRP receptor [111, 112]. The 4.5S RNA is required for the stable complex formation between the SRP and the SRP receptor (SR) by modulating the GTP hydrolysis [113–116]. The Ffh M-domain binds to the ribosome at the exit tunnel, where it contacts uL23 and uL29 ribosomal protein and 23S rRNA as well. The C-terminus of the Ffh protrudes inside the exit tunnel where it contacts uL23 [117, 118]. The number of SRP in the cell is in the range of a few hundred copies, however, they are capable of efficiently interacting with a nanomolar to a subnanomolar affinity to RNCs translating membrane proteins even before the signal anchor or TMHs emerge from the ribosomal exit tunnel [119]. Therefore, SRP rapidly scans the ribosomes by binding and dissociating until it recognizes a signal anchor or a TMH. Subsequently, the SRP: RNCs complex is stabilized and SRP switches from scanning mode to targeting mode [119, 120].

SRP targets the RNCs to the membrane, where it binds to the SRP receptor, called FtsY in bacteria [105]. FtsY is a peripheral membrane protein that interacts with the membrane and SecY via its A-domain and also has an NG-domain homologous to that of the SRP which can bind and hydrolyze GTP, and it provides the binding domain for SRP. It has been shown that anionic lipids are needed for the binding of FtsY to the membrane, where it forms an amphipathic helix at the membrane interface. Deleting the A-domain causes loss of FtsY membrane binding, however, that does not have an effect on the membrane protein targeting process [121–123]. The assembly of the SRP: FtsY complex stimulates the GTPase activity of the Ffh, which causes a conformational change within the complex that is necessary for the transfer of the RNC to the translocon and the disassembly of the SRP: FtsY complex.

Thus, the SRP cycle starts with the SRP scanning the ribosomes at the exit tunnel for a

signal anchor or a TMH. Once found, the SRP binds with high affinity to RNCs and targets them to the membrane where it binds the SR receptor, FtsY via the NG domains (closed state) (Figure 1.7 B). The NG domain heterodimer then relocates to the distal end of the 4.5S RNA (open state) to promote the handover of the RNC to the SecYEG translocon (Figure 1.7 A) [124]. GTP binding stabilizes the complex formation between SRP: RNCs with FtsY and initiates the transfer of the RNCs to the Sec translocon. The Sec translocon in turn causes conformational changes within the SRP: FtsY complex and activates GTP hydrolysis, which then stimulates the dissociation of the SRP: FtsY complex [2, 120, 125, 126].
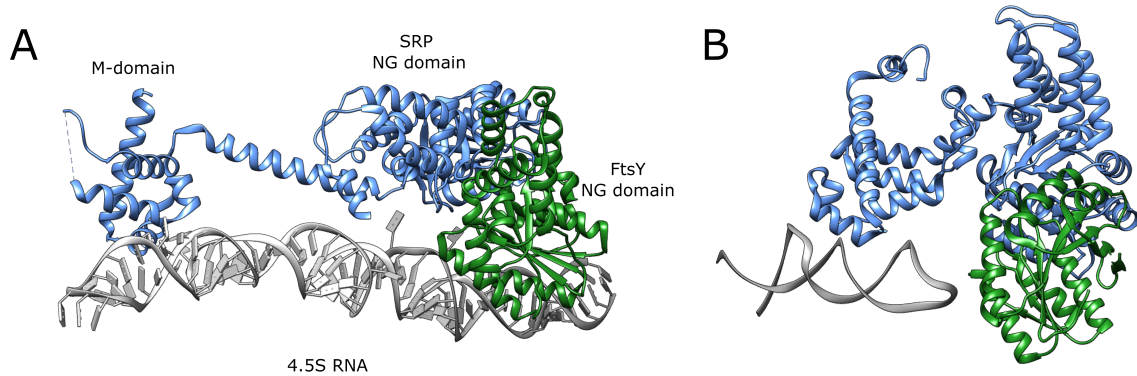
Figure 1.7: Structure of the SRP: FtsY. A) Structure of the SRP receptor, FtsY, bound to SRP (PDB: 2XXA) in the open state. B) Structure of the SRP: FtsY in the closed state (PDB: 5GAD).

1.3.2 SecYEG and SecYEG/SecA-dependent insertion

The Sec translocon can work independently or associate with accessory proteins to insert different membrane protein types. The classical and the most conserved pathway starts once the RNCs are targeted via SRP to the translocon. SecYEG binds to RNCs at the ribosomal tunnel exit with its cytoplasmic loops between TMH 6 and 7 and TMH 8 and 9 as well as the amphipathic helix of SecE [127, 128]. The exit tunnel of the ribosomes forms a continuous conduit with the translocon pore allowing for a direct passage of the nascent chain to the translocon [129]. During the insertion of membrane protein, the transmembrane segment binds to the lateral gate of SecY, while the downstream hydrophilic region translocates through the central pore of the channel, and cytoplasmic regions are released from SecYEG. Different structures of SecYEG: RNCs carrying membrane protein have been visualized using cryo-EM and they showed that the lateral gate could be opened by the presence of TMH but to different degrees. However, other studies showed that the lateral gate opening occurs also in the absence of substrates and TMH insertion do not require the lateral gate opening. They demonstrated that stochastic lateral gate opening is enough for the TMHs to be integrated into the lipid bilayer and the rate of TMH insertion is only determined by the translation rate of the ribosome [130]. Due to the low resolution of the available structures, it was difficult to determine the exact position of the TMH within the SecYEG channel, some structures showed that a TMH was located at the lateral gate, or partially at the lateral gate and partially in the lipids bilayer, while other structures show that the TMH was completely located in the bilayer [129, 131–133].

Typical substrates for SecYEG only-dependent insertion are membrane proteins with short periplasmic domains like MtlA or TatC [106, 134]. Membrane proteins with large periplasmic domains are inserted with the help of SecYEG/SecA, where SecA is responsible for the translocation of periplasmic domains or loops across the cytoplasmic membrane. In this pathway, first, the RNC is targeted in an SRP-dependent manner to the SecYEG translocon. After the integration of the hydrophobic TMH, RNC will detach to allow for SecA binding to promote the translocation of the periplasmic domain. One of the best-studied substrates for SecYEG/SecA pathway is FtsQ which has one TMH and a long periplasmic tail [135] and the leader peptidase LPase, which has two transmembrane helices and a large C-terminal periplasmic domain [136].

1.3.3   YidC only dependent insertion

The membrane insertion of several membrane proteins was shown to be completely performed by YidC, independently of SecYEG. YidC is an essential protein in bacteria, that has homologs in mitochondria (Oxa1), chloroplasts (Alb3), and in the endoplasmic reticulum (Get1 and EMC3). In *E.coli*, YidC is composed of six TMHs, a large periplasmic domain called the P1 domain between TMH1 and 2, and a coiled-coil region in the cytoplasmic side between TMH2 and 3 (Figure 1.8). P1 domain has been shown to be non-essential as many YidC homologs do not contain it and it can also be deleted in *E.coli* without any defects [137]. Between the P1 domain and TMH2, a conserved amphipathic helix called EH1 is located. EH1 deletion leads to the loss of YidC function both *in vivo* and *in vitro* [137, 138] The coiled-coil domain between TMH2 and 3, called the C1 region, is made of two α helices that protrude to the cytoplasm. Many studies showed that this domain is essential for YidC activity, however, its exact function is not clear [139–141]. TMH2 to 6 forms a globular bundle with a hydrophilic groove in the inner leaflet of the membrane which is open towards the cytoplasmic side and closed on the periplasmic side of the membrane. This groove has been proposed to host the substrate hydrophilic domains destined to be translocated to the periplasm [138]. TMH3 and 5 form a transmembrane gap that can clamp an incoming substrate forming a hydrophobic slide mechanism. The outer face of the TMH3 and 5 have hydrophobic residues that contact an inserting substrate [142]. Another important domain of YidC is the C-terminal region, which is called the C2 loop, it is rich in positively charged amino acids that have been shown to form a binding site for translating ribosomes. Interestingly the deletion of this site does neither affect the insertion activity of YidC nor the viability of the cells [141, 143].

A common feature of YidC-only substrates is that they are small proteins with a small periplasmic domain. YidC-only substrates include the small phage-encoded proteins M13 procoat and Pf3 coat [144, 145], the c-subunit of the F_1F_o ATP synthase (F_oc) [146], the large conductance mechanosensitive channel, MscL [147, 148], the tail anchored protein TssL [149]. Targeting of substrates to YidC can occur either post or co-translationally and in an SRP-dependent or independent manner. The small phage protein Pf3 and M13 procoat are targeted independently of the SRP. It is believed that the electrostatic interactions between the phospholipid bilayer and the phage protein ensure the targeting of these proteins to YidC [144, 150]. Some substrates clearly require the SRP targeting pathway like MscL, while the requirement for SRP for other substrates including F_oc is controversial [146–148, 151].

Interestingly, the TMHs of YidC are short and are not sufficient to span the whole membrane. The resulting hydrophobic mismatch induces membrane thinning. The membrane thinning has been proposed to reduce the energy barrier for the insertion of the nascent chain [140].
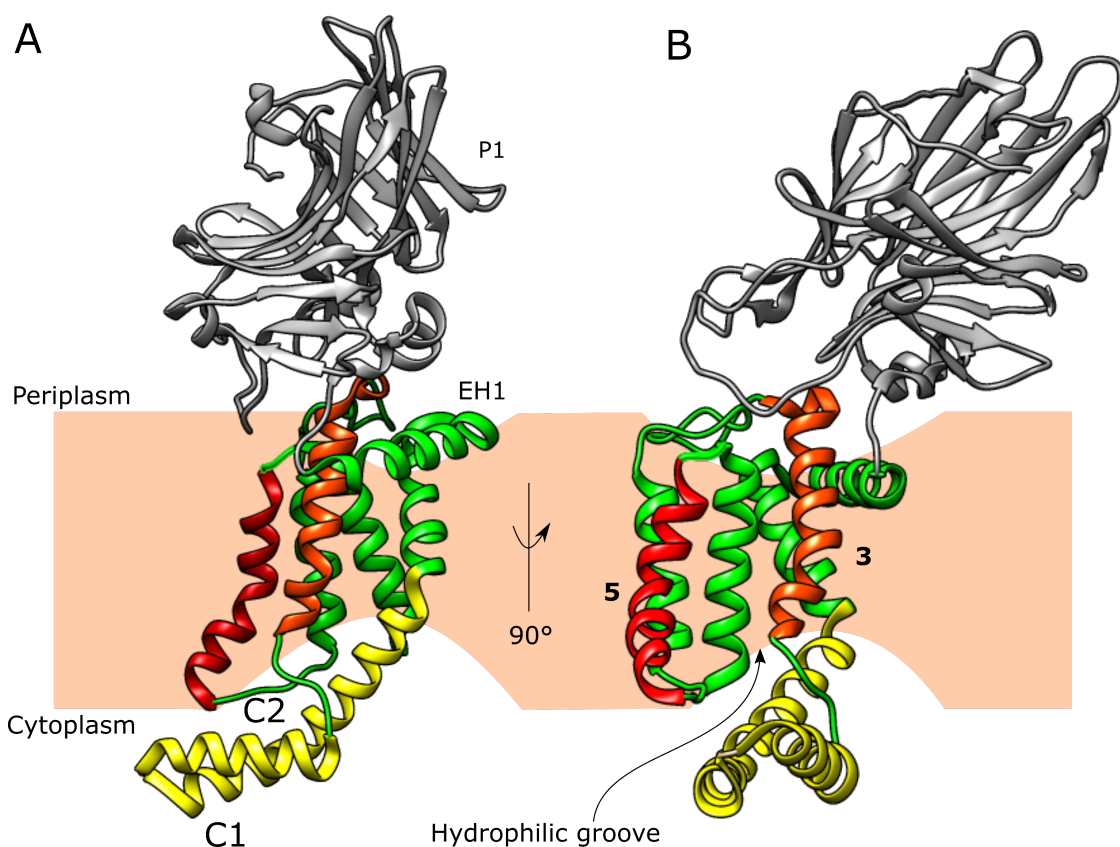
Figure 1.8: Structure of the membrane insertase, YidC (PDB: 6AL2). *E.coli* YidC is composed of 6 TMHs, a periplasmic domain (P1), and a cytoplasmic domain (C1). A hydrophilic groove is formed by TMH2 to 6 in the inner leaflet of the membrane. YidC promotes membrane thinning that was proposed to decrease the energy barrier of insertion of nascent chains.

1.3.4   SecYEG/YidC and the Holo-translocon dependent insertion

Many membrane proteins require both SecYEG and YidC for insertion and proper folding. For some substrates, both SecYEG and YidC are required for insertion, while for others YidC is only needed for the folding of the membrane protein. Therefore, it has been proposed that SecYEG and YidC form a complex in the membrane. Crosslinking and co-purification studies have shown that FtsQ, leader peptidase, and MtlA interact with both SecYEG and YidC [135, 152, 153]. YidC has been shown to contact the lateral gate of SecY and help the release of the nascent chain from the lateral gate. Indeed, crosslinks of YidC with TMH2b, 7, 3, and 8 of SecY have been shown [154]. FtsQ requires SecYEG/SecA for insertion, but crosslinking studies have shown that YidC contacts the TMHs of FtsQ during membrane insertion [135]. CyoA, an essential protein of the electron transfer chain, has been shown to require both SecYEG and YidC for insertion. The signal peptide, short periplasmic loop, and the first TMH are inserted by YidC, while the second TMH and a large periplasmic domain require SecYEG/SecA for insertion [155, 156]. NuoK, a membrane protein with 3 TMHs, also requires both SecYEG and YidC, with TMH 2 and 3

being YidC dependent [157]. LacY and MalF have been shown to require only SecY/SecA for insertion, however, YidC has been shown to be important for the correct folding of the protein after insertion [153, 158, 159].

In addition to SecYEG interactions with YidC, it can also interact with SecDFYajC forming all together the so-called holo-translocon. SecDF has been proposed to be required for the proton motive force-driven translocation of substrates. SecDF has been shown to crosslink with SecG and to bind with the P1 domain of YidC [160, 161]. The holo-translocon has been shown to be more effective in protein translocation, ribosome binding, and insertion of membrane proteins such as CyoA [160, 162, 163]. Subunit a of the F_1F_o ATP synthase also requires both SecYEG and YidC and SecDF for insertion [151, 164]. It has been suggested that a central lipid pool exists between the seven subunits of the holo-translocon that can provide a flexible environment for the proper folding of membrane proteins and the assembly of membrane protein complexes [165, 166]. Recently, biochemical studies and a low-resolution cryo-EM structure showed an interaction between the holo-translocon and β-barrel assembly machinery (BAM complex) forming an intermembrane super complex, where the periplasmic domain of SecDF and YidC contacts the periplasmic domains of the BAM complex. They argue that the formation of this complex is important for outer membrane proteins folding and insertion [167].

Recent advances in studying membrane protein insertion supported by diverse cryo-EM structures provided insights into the mechanism of membrane protein insertion and folding. Nevertheless, the available structures have been obtained using either detergent-solubilized SecYEG or YidC, indicating a non-native structure. Other structures were obtained using a nanodisc-reconstituted SecYEG or YidC in a complex with RNCs, in which the components of the complex were individually isolated and artificially assembled which might not reflect the continuous process of co-translational insertion and the native environment. Moreover, the available structures often provide a low or mid-resolution. Consequently, different questions still remain to be addressed, such as what is the exact path of the nascent chain from the ribosomal exit tunnel to the membrane? what are the prerequisites for the substrate selection for the different insertion pathways? What is the exact functional architecture of the SecYEG/YidC complex and the holo-translocon? and what are the principles of SecYEG/YidC cooperation during the multiple stages of membrane protein insertion?

1.4   Approaches to studying integral and peripheral membrane proteins

Studying membrane protein remains quite challenging for many reasons. They are insoluble in aqueous solutions and they normally operate within and at the interface of the membrane. Therefore, different membrane mimetic systems have been developed in order to facilitate the study of the structure and function of membrane proteins and ensure compatibility with various biochemical and biophysical tools.

1.4.1 Membrane mimetics

A membrane mimetic is a system that aims to substitute the native bilayer membrane by mimicking the hydrophobic environment produced by the lipid bilayer. The aim of a membrane mimetic is to improve the stability of membrane protein *in vitro* and provide a convenient platform to study them in an environment that mimics the chemical and physical composition of their native environment.

Detergent micelles

Detergents are the most common and extensively used membrane mimetic for the solubilization, purification, and characterization of membrane proteins. Detergents are amphiphilic molecules that can self-assemble to form detergent micelles above a certain concentration called the critical micelle concentration (CMC) (Figure 1.10 A). Detergents can be classified into three categories: ionic detergents that can be both positively or negatively charged. They are harsh detergents and strong denaturants such as sodium dodecyl sulfate (SDS). Zwitterionic detergents that have no net charge, they are less denaturants compared to ionic detergents and have strong solubilization potential compared to nonionic detergents such as 3-((3-cholamidopropyl) dimethylammonio)-1-propanesulfonate (CHAPS) and lauryl dimethylamine oxide (LDAO). Lastly, non-ionic detergents, which are mild detergents preserving the structural integrity of membrane proteins such as dodecyl-L-D-maltoside (DDM) and lauryl-maltose neopentyl-glycol (LMNG). Phospholipid-like detergents also exist that can be either charged or zwitterionic and have been extensively used to study membrane proteins like Lyso PG and Fos-Choline 12. Detergents have been extensively used to study membrane proteins using different biophysical approaches like X-ray crystallography, cryogenic electron microscopy, nuclear magnetic resonance, electron paramagnetic resonance, and others [168].

Nevertheless, using detergents has certain drawbacks. A major drawback is the shorter chain lengths that detergents normally have compared to the length of the acyl chains in the native membrane. This causes a hydrophobic mismatch between the detergent micelles and the isolated membrane proteins leading to the formation of nonphysiological conformations of membrane proteins inside the micelle. Furthermore, the hydrophobic packing within the detergent micelles is weaker than in the native membrane allowing for water penetration into the micelles and causing structural instabilities for the membrane proteins [169, 170].

Amphipols

Amphipols are amphipathic polymers that have the ability to replace detergent micelles and keep membrane protein soluble in solution. Amphipols are soluble in an aqueous solution and assemble into micelle-like particles. The most commonly used amphipol is the A8-35 (Figure 1.9 A). The solubility of A8-35 is pH-dependent, where its solubility drops when pH drops below 7 due to protonation of the carboxylate group or in the presence of multivalent cations. Other amphipols that do not have these limitations have also been developed, for instance, phosphatidylcholine-based amphipols (PC-APols) and sulfonated-based amphipols (SA-APols) [171].

Amphipols can adsorb and permeabilize lipid vesicles, and under optimized experimental conditions like temperature, pH, and ionic strength, they can break lipid vesicles into small fragments or nanodisc or bicelle-like structures and/or mixed micelles. However, they can not solubilize biological membranes or extract membrane protein with few exceptions. Therefore, membrane proteins are normally extracted and purified in detergents and then replaced by amphipols. In the case of a detergent-sensitive membrane protein, solubilization can be done in detergent while purification can be done in the amphipol-trapped state. Typically, membrane proteins purified in detergents are supplemented with a concentrated stock of amphipols in water, during this stage amphipols mix with the detergent both in solution and at the transmembrane region of the protein forming a ternary amphipol/detergent/ membrane protein complex. After a short incubation time, the detergent concentration is then dropped below the CMC either by dilution or adsorption on polystyrene beads (Bio-beads SM2) causing the detergent molecule to be replaced forming an amphipol/membrane protein complex. Lipids can also be incorporated in amphipols/membrane protein complexes either from lipids purified with the protein or added afterward in order to stabilize the protein. Amphipols have a very low critical aggregation concentration, making it easy to handle amphipol/ membrane protein complexes, for instance, extensive dilution in an amphipol-free buffer is feasible. Using amphipols has many advantages, they improve the stability of membrane protein compared to detergent micelles. They do not affect the function and ligand binding capability of membrane proteins. They have been used in the refolding of membrane proteins and can be used in cell-free expression systems for membrane protein production. Many biophysical methods have also been applied to membrane proteins in amphipols to characterize their structure and function [171, 172].
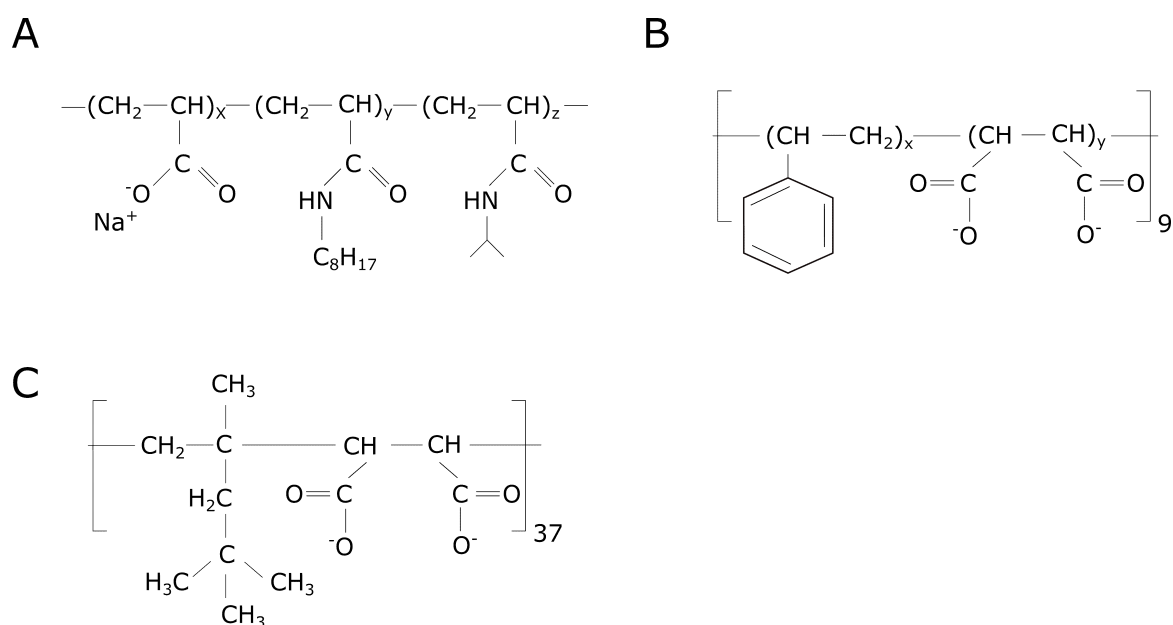
Figure 1.9: Chemical structure of polymers commonly used as membrane mimetics. A) A8-35 amphipol. B) Styrene-maleic acid copolymer (SMA). C) Diisobutylene-maleic acid copolymer (DIBMA).

Bicelles

Bicelles are the first membrane mimetic to be able to incorporate a large amount of lipids and create a bilayer-like environment. Bicelles are disc-shaped nano-aggregates that contain bilayer-forming long-chain phospholipids mixed with either a detergent or a short-chain phospholipid in an aqueous solution (Figure 1.10 B). They can be formed by mixing the long-chain lipid DMPC with the detergent CHAPS or by mixing the long-chain lipids DMPG and DMPC with the short-chain lipid DHPC. Bicelles have the advantage of providing membrane proteins with a native-like environment [173, 174]. Different lipid composition has also been incorporated within bicelles which can be useful for specific interactions of membrane proteins with lipids. Moreover, paramagnetic ions can be added to the lipid mixtures to allow alignment in an external magnetic field for NMR and EPR studies on membrane proteins [175, 176]. Nevertheless, they fail to sufficiently mimic the lateral pressure of the membrane which could disturb the structure and dynamics of the integrated membrane protein. One other disadvantage is that their size and geometry are sensitive to the concentration of lipids in solution and any dilution could change the system properties [168, 177, 178]. Small isotropic bicelles have been extensively used to probe the structure and dynamics of membrane proteins in solution NMR spectroscopy as they provide a native-like environment and fast tumbling required for good NMR spectra. The structure of many membrane proteins such as sensory rhodopsin II [179], EmrE [180], and the transmembrane domain of ephA1 [181] was determined in bicelles using solution NMR. Large bicelles have been used in solid-state NMR as they provide a larger bilayer area for the incorporation of membrane proteins while allowing the control of their orientation in the external magnetic field [182]. X-ray crystallography has also been used to determine the high-resolution structure of membrane proteins embedded in bicelles such as the rhomboid protease [183], VDAC-1 [184], and the β_2-adrenergic G-protein coupled receptor [185].

Nanodiscs

Nanodisc is a discoidal particle formed by the noncovalent assembly of a membrane scaffold protein (MSP) and phospholipids. The MSP is derived from the human serum protein apolipoprotein A1, which is the main component of high-density lipoprotein particles (HDL) involved in the transport of cholesterol. A single nanodisc is formed from phospholipids that are organized as bilayers and interact with two molecules of MSP. MSP forms a belt that wraps around the self-assembled lipid bilayer, where the hydrophobic part of each MSP molecule interacts with the hydrophobic acyl chain of each leaflet of the bilayer (Figure 1.10 C). The hydrophilic part of the MSP is therefore oriented outwards ensuring the aqueous solubility of the assembled nanodisc. The prototypical MSP comprises an N-terminal truncation of the apolipoprotein A1 and is called MSP1. It is made of 10 α helices capped with prolines and interconnected by short linkers to ensure flexibility. It can form discs of around 10 nm in diameter. Introducing helical repeats or deletions in the central portion of the MSP produces discs with diverse sizes that range from 4 to 17 nm. Therefore, the lateral dimension of the bilayer within the nanodisc is determined by the length of MSP used and therefore can be adapted to different membrane proteins. To reconstitute membrane protein in nanodiscs, they need first to be purified in a detergent micelle, then mixed with lipid and the membrane scaffold protein. Afterward, the detergent can be removed

by polystyrene beads (Bio-beads SM2) [186, 187].

Nanodiscs have been used to study the structure and dynamics of membrane proteins by means of different biophysical approaches [188, 189]. The structure of multiple membrane proteins in nanodiscs has been determined using cryo-EM to high resolution [190, 191]. However, due to the limitation imposed on the size of the membrane protein by the available cryo-EM and single particle analysis approaches, only membrane proteins with sufficiently large molecular weight could be visualized. The structure of small membrane proteins could still be determined when prepared as fusion proteins to increase their size or using antibody-antigen fragments to increase their stability and limit their flexibility [87, 192, 193]. Nanodiscs have been also useful for studying membrane proteins using both NMR [194] and EPR spectroscopy [195]. Furthermore, fluorescence-based approaches have been employed on membrane protein reconstituted in nanodiscs like total internal reflection microscopy (TIRFM), fluorescence correlation microscopy (FCS) and Förster resonance energy transfer (FRET) [196–198].

Saposins

Saposins have also been utilized to form nanodiscs for the characterization of membrane proteins Here, the lipid binding protein Saposin A (SapA) is mixed with lipids and the membrane protein of interest to form lipid nanoparticles called Salipro. Multiple SapA forms a scaffold that surrounds a disc-like nanoparticle made of a lipid bilayer core and the membrane protein of interest (Figure 1.10 D). One major advantage of using SapA is its flexibility to adjust itself to the size of the membrane protein used making it suitable for both small and large membrane proteins. SapA forms highly homogenous nanoparticles with increased stability [199, 200]. Recently, it has been shown that membrane protein can also be directly reconstituted in saposin nanoparticles from the crude membrane with a technique named DirectMX. This technique allows the reconstitution of membrane protein surrounded by native membrane lipids [201]. Many membrane proteins have already been studied in saposin nanoparticles and have shown to be functional and structurally intact using different biochemical and biophysical methods. For instance, the functional reconstitution of the ABC transporter, HlyB has been established in Salipro [202]. Differential scanning fluorimetry and microscale thermophoresis have been used to characterize the peptide transporter, PepT [200]. Moreover, the cryo-EM structure of various membrane proteins, for example, the fungal mitochondrial calcium uniporter [203] and the ion channel, TPC1 [204] have been resolved in Salipro.

Peptidisc

Peptidisc is a peptide scaffold that is used to keep membrane proteins soluble in solution. The peptide used is based on the apolipoprotein AI peptide but has a reversed sequence. It can form two amphipathic helical stretches separated by prolines. When the peptide is mixed with detergent-solubilized membrane proteins, many copies of the peptide interact with the transmembrane regions of the protein embedding it in a disc-like structure termed peptidisc once the detergent is removed (Figure 1.10 E). This approach has been used with both α-helical and β-barrel membrane proteins and the reconstitution protocol is quite straightforward [205]. It has also been shown that membrane proteins reconstituted in peptidisc can be used for structural

studies using cryo-EM. For instance, the high-resolution cryo-EM structures of the ABC transporter, MsbA, and the mechanosensitive channel, MscS have been resolved in peptidisc [206].

Maleic acid copolymers

Most of the described above membrane mimetic systems have the disadvantage that membrane protein must be first solubilized and purified in detergents. Knowles et al 2009 proposed a new kind of copolymer, called styrene-maleic acid (SMA), that has the ability to extract membrane proteins directly from the membrane without the use of any detergents (Figure 1.9 B). Once mixed with biological membranes, discoidal particles of around 10 nm in diameter are formed that contain among others the membrane protein of interest surrounded by its native lipids. These particles have been named SMA lipid particles or SMALPs. SMALP contains a central lipid bilayer surrounded by the SMA copolymer where the hydrophobic styrene group interacts with the acyl chains of the lipids and the maleic acid group is oriented toward the aqueous solvent. SMA has already been used to extract many proteins, for example, AcrB, the ABC transporter P-gp, the potassium channel KcsA, bacteriorhodopsin, the respiratory chain complex IV, and so on. Membrane proteins encapsulated in SMALPs have also been amenable to different biophysical studies like circular dichroism, analytical ultracentrifugation, differential scanning calorimetry, cryo-EM, and small angle neutron scattering. However, SMALPs have some limitations, since the diameter of the disc can reach a maximum of 15 nm, large membrane protein complexes might not be successfully extracted, as they will not fit within the size of the disc. The SMA polymer losses its solubility below pH of 6.5, due to the protonation of the maleic acid group. Moreover, SMA can chelate divalent cations like Ca^{2+} and Mg^{2+} and become insoluble. Therefore, it is incompatible with experiments that require a high concentration of divalent cations (above 5 mM), Thus, it is not suitable to be used with proteins like ABC transporters and ATPases. It also interferes with the far UV optical spectroscopy making it difficult to determine protein concentrations [207, 208].

Therefore, a new maleic acid-based copolymer has been developed that lacks the styrene group, called diisobutylene-maleic acid (DIBMA) (Figure 1.9 C) which lacks the disadvantages of SMA. It does not interfere with the UV absorption of protein, can tolerate higher concentrations of divalent cations, and can form bigger discs compared to SMA up to $\approx$ 40 nm. However, it has lower solubilization efficiency compared to SMA. Moreover, DIBMA lipid particles (DIBMALPs) have a broader size distribution compared to SMALPs [209–211]. A modified version of DIBMA has also been developed that is partially amidated with the amino sugar N-methy-D-glucamine called Glyco-DIBMA. This polymer is less charged and hydrophobic, providing higher solubilization efficiency than DIBMA and producing lipid particles with smaller and narrower size distribution [212].

Vesicles

Liposomes are spherical vesicles with an aqueous compartment surrounded by a lipid bilayer and can provide a robust artificial mimic of the cell (Figure 1.10 G). They can be unilamellar, containing a single bilayer, or multilamellar, containing multiple bilayers. Liposomes can be further classified to small unilamellar vesicles (SUVs), with a size range below 100 nm, large unilamellar

vesicles (LUVs) with a size range between 100 nm and 1 μm, and giant unilamellar vesicles (GUVs) with size more than 1 μm [213, 214]. They can be prepared either from synthetic lipids, where the composition can be substantially varied to match the need of the protein to be studied, or native membrane extracts which provide a near-native environment to study membrane proteins [215]. Reconstituting membrane proteins in liposomes has many advantages, first, the membrane potential can be sustained across the bilayer of the liposome due to the different aqueous compartments across the bilayer. It also provides a continuous membrane where the diffusion behavior of phospholipids and proteins can be studied [216, 217].

To reconstitute membrane proteins in liposomes, they need first to be purified in detergent micelles, followed by mixing with detergent-solubilized or swelled liposomes. Subsequently, the detergent is removed by rapid dilution, dialysis, or incubation with polystyrene beads (Bio-beads, SM2) forming proteoliposomes [218]. Proteoliposomes offer a cell-like nature to a certain extent, due to the different compartments introduced, different ions, compounds or pH can be maintained on the inside and outside of the liposome. Therefore, proteoliposomes are a great system to establish functional assays to study membrane proteins, for instance, the uptake or transport of labeled substrates from the outside to the inside of the liposomes or vice versa [219–221]. The *in vitro* transport of fluorescently labeled proOmpA (precursor of outer membrane protein A) into the lumen of SecYEG reconstituted liposomes or inner membrane vesicles [222, 223], the fluorescent-based measurement of the ADP/ATP exchange rate of the adenine translocase in liposomes are examples of functional assays established to study membrane proteins [221]. Furthermore, liposomes can be used to study specific protein-lipid interactions by monitoring the activity of a protein when reconstituted in liposomes of different compositions [63, 224] or by checking protein binding to lipid vesicles by the co-flotation of the protein with the liposomes in sucrose density gradients [225].

Liposomes have also been used to crystallize membrane proteins in a lipid bilayer forming the so-called 2D crystals in which their structure can be analyzed using electron microscopy [226, 227].

GUVs have also been used to study membrane proteins. GUVs can be formed by controlled hydration of lipid films usually using electroformation. They have been extensively used to study diffusion processes within the membrane and at the membrane interface, and to monitor the assembly of macromolecular complexes using fluorescence microscopy techniques [228–231].

Supported lipid bilayers

Supported lipid bilayers (SLBs) offer a robust system to study protein dynamics (Figure 1.10 H). The most common method to form SLBs is by fusion of lipid vesicles on solid surfaces, for instance, glass, mica, or gold [232, 233]. Other methods have been employed to form SLBs like Langumir-Blodgett, and Langumir-Schaefer, these methods require the formation of one monolayer at a time, which is advantageous when asymmetric SLBs with different lipid compositions on each leaflet are required [234–236]. They are attractive to be used because they are relatively easy to prepare, different lipid compositions can be incorporated and the fluidity of the membrane can be maintained at least at the upper leaflets which makes them a good option to investigate protein dynamics [237]. They can be readily used to investigate the properties of the

different membranes using, for example, fluorescence recovery after photobleaching to investigate the fluidity of the investigated membranes [238]. They have been employed to investigate protein:membrane interactions using techniques like surface plasmon resonance (SPR) or quartz crystal microbalance (QCM) [239]. Moreover, they can be easily employed in surface imaging techniques down to the single molecule level like atomic force microscopy (AFM) or total internal reflection fluorescence microscopy (TIRFm) [240, 241]. Nevertheless, one limitation of using supported lipid bilayers is that there is only a thin aqueous layer between the solid support and bilayer, which can substantially affect the diffusion behavior of incorporated membrane proteins with large loops or soluble domains [242].
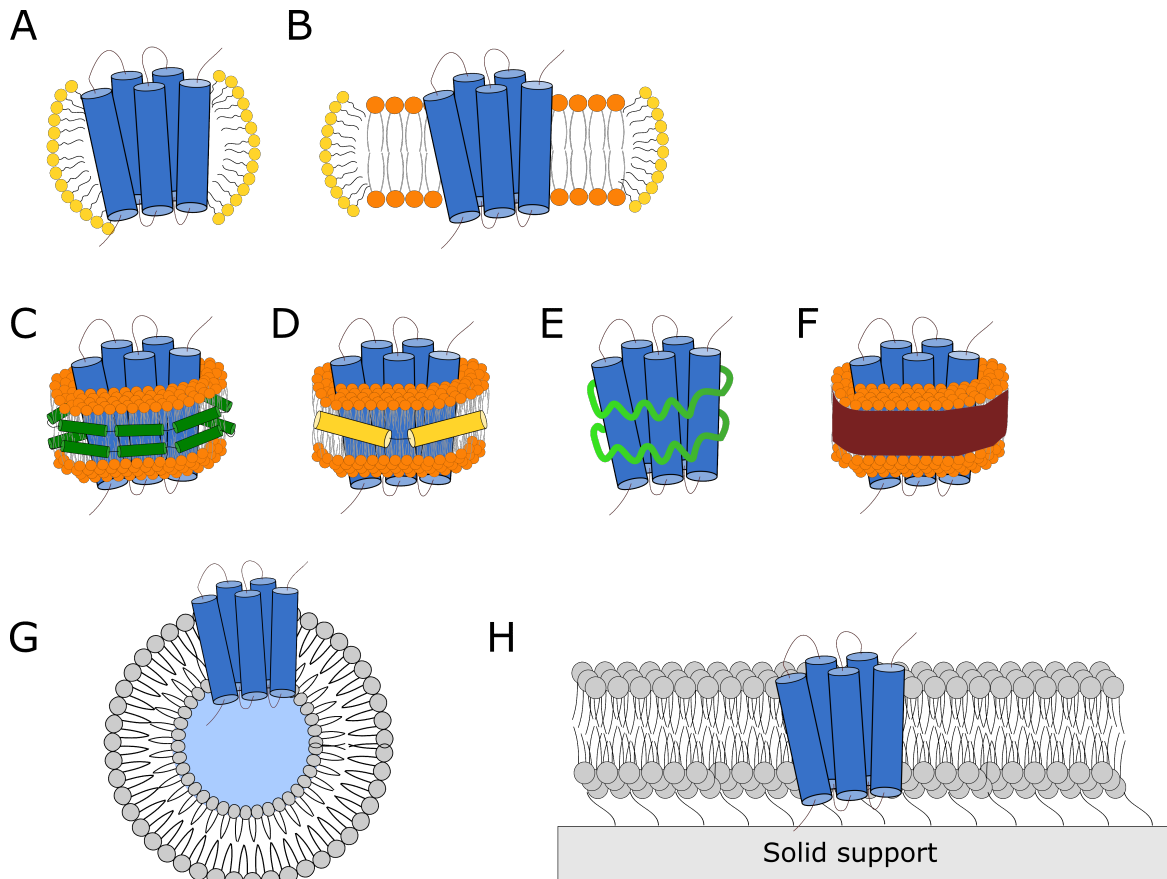
Figure 1.10: Different types of membrane mimetics. A) Detergent micelles. B) Bicelles. C) Membrane scaffold protein nanodiscs. D) Saposin nanodiscs (Salipro). E) Peptidiscs. F) Styrene maleic acids lipid particles (SMALPs). G) Vesicles. H) Supported lipids bilayer.

1.4.2 Examples of biophysical tools to characterize protein-membrane interactions

Surface plasmon resonance

Surface plasmon resonance (SPR) is a real-time, label-free method that has been extensively implemented to study biomolecular interactions. It relies on the SPR phenomenon that mainly occurs in thin conducting films at an interface between media of different refractive indices (Figure 1.11 A). In SPR, polarized light is directed through a prism to a glass surface that provides a media of high refractive index, coated with a conducting gold layer on the border of a flow cell that contains the sample solution, providing a media of low refractive index. Under a certain angle called the critical angle, total internal reflection is achieved in which the incident light is reflected from the glass surface and detected by the detector. This creates an evanescent wave that leaks into the media of low refractive index and excites surface plasmons (electron charge density wave) within the gold layer. The plasmons then absorb some of the energy of the incident light causing a decrease in the intensity of the reflected light reaching the detector. When the refractive index in the flow cell changes, for instance, due to changes in solute or protein concentration, this will cause a change in the critical angle needed to achieve the surface plasmon phenomena which can then be measured as a response. The signal in an SPR sensorgram is then a plot of change in the critical angle over time. However, response units are the preferred term to describe the change in signal and there is a linear relationship between the amount of analyte on the surface and the rise of the signal. In SPR, one interacting partner is immobilized on the surface and is called the ligand, while the other partner is injected in solution and flows over the surface inside the flow cell and is called the analyte. Different chemistry approaches have been utilized to immobilize or capture the ligand on the surface of the sensor chip. The advantages of using SPR are that it allows for label-free detection, real-time monitoring of the interaction, and consumption of a low amount of samples. However, the main advantage of using SPR is its ability to determine kinetic rate constants as well as affinity constants [243, 244].

SPR has been used to study protein: membrane interactions. Different sensor chip designs have been employed to form a membrane mimetic on the surface of the SPR chip. The most commonly used sensor chips are HPA and L1 sensor chips from Biacore. HPA chip has a dextran matrix functionalized with alkanethiol layer which adsorbs lipids from micelles or liposomes injected over the surface forming a lipid monolayer with the hydrophobic acyl chains of the lipid molecules oriented toward the surface, while the head groups are oriented toward the solution. This approach is suitable to study peripheral membrane proteins, while integral membrane proteins can not be used in such a system as only one monolayer is formed. The second approach is the L1 sensor chip which contains a dextran matrix functionalized with hydrophobic residues that can capture lipid vesicles on the surface of the sensor chip. Here, integral membrane proteins can be easily studied since they can be reconstituted beforehand in the vesicles to be captured on the surface. Another commonly used approach is capturing liposomes containing biotinylated lipids on the surface of streptavidin functionalized chips [244–246].

SPR has been used to characterize many membrane-associated processes. For instance, it can provide information about the requirement of specific lipids for the membrane binding of certain

proteins [247] and monitor the kinetics of protein binding to the membrane (Figure 1.11 B) [67]. Moreover, some proteins are only able to bind to their interacting partners once they are bound to the membrane, which can be nicely monitored by SPR [248, 249]. It can also track the ability of certain proteins to extract lipids from the membrane like saposin and CERT protein [250, 251]. It was also used to monitor the pore-forming ability of the pore-forming protein, perforin [252]. SPR has been used to immobilize native inner membrane vesicles for *E.coli* where overexpressed membrane proteins have been studied [253, 254].
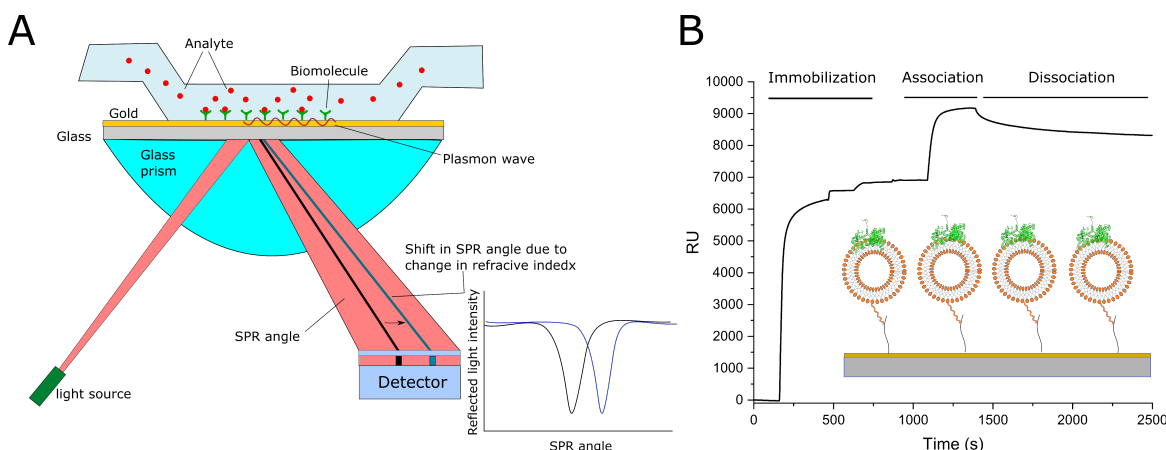
Figure 1.11: Surface plasmon resonance. A) Principle of surface plasmon resonance. B) Protein-membrane interaction can be measured on liposomes captured on sensor chips made of lipophilic anchors. Immobilization indicates capturing of liposomes on the chip surface. Association indicates the binding phase of the protein of interest to the liposomes, while dissociation indicates the dissociation of the protein from liposomes after the binding phase is over.

Quartz crystal microbalance

Quartz crystal microbalance with dissipation (QCM-D) is a method that has been utilized to study membranes as well as biomolecular interactions that occur on the surface of a supported lipid bilayer. It allows the quantification of the absorbed mass on the surface as well as the viscoelastic properties of the surface. Like SPR, QCM-D has a sensor chip, that is made of a quartz crystal that is sandwiched between two gold electrodes. The quartz crystal manifests a piezoelectric effect that is exploited in QCM-D. When an external voltage is applied to the crystal, it deforms, and by alternating the voltage, a shear wave is generated in the crystal between the two electrodes which has a specific resonance frequency. The shear wave decays evanescently in the liquid above the surface with a characteristic decay length which is around 250 nm in water, which is the permitted detection range in QCM-D. Fitting a decaying oscillating curve to the data allows the extraction of the resonating frequency of the crystal, (f), and the energy dissipation, (D). A solvent above the surface of the quartz is detected as a coupled mass that has a thickness corresponding to its density. The decay length of the shear wave depends on the density and the viscosity of the solvent used. Therefore, a shift in the resonance frequency of the crystal (Δf) and energy dissipation (ΔD) can be measured when the mass above the surface is changed, for instance, due to added biomolecules or changing the thickness of the deposited layer, or when the solvent used is changed. Therefore, Δf and ΔD are the measured responses

in QCM-D [255].

For thin rigid films formed above the surface of the sensor chip, the principle of the measurement depends on a simple relationship between the change in the frequency of the crystal and the change in mass using the Sauerbay equation

$$\Delta m = -C \times \Delta f / n$$

where n is the harmonic number, C is the material-specific Sauerbay constant, Δm is the change in mass and Δf is the change in frequency. This is often the case when working in a vacuum or gas phase, for example during monitoring metal plating in vacuum deposition systems or in case of gas adsorption or desorption processes. However, working with biological system requires the presence of an aqueous solution above the surface, which incorporate viscous and elastic contribution to the change of frequency of the crystal. In that case, the Saurerbay equation underestimates the changes in mass and thickness of the film. Here comes the dissipation monitoring in play. QCM-D measures the dissipation of energy (D) as the dampening of the oscillations of the crystal when the driving voltage is cut off. It allows measuring Δf and ΔD values at several overtones and by fitting the data to viscoelastic models, it increases the sensitivity of the measurement and gives useful information about the viscoelastic properties of the film. Moreover, using different overtones allows for different penetration depths within the liquid above the surface, for instance, a high overtone number will dissipate within the adsorbed layer, while low overtones can sense the solution above the layer. This allows for estimation of the homogeneity of the adsorbed layer as a function of distance from the surface [255].

QCM-D has been widely used to produce supported lipid bilayers using the vesicle fusion method. Briefly, vesicles are injected and adsorbed on the surface of the sensor chip causing a decrease in Δf due to the increase in mass over the surface and an increase in the ΔD due to the softness and viscoelastic properties of the vesicles. Once the vesicles reach a critical concentration on the surface, they fuse forming a supported planar bilayer on the surface, releasing the water from the vesicle lumen, increasing the Δf due to the decrease in the total mass on the surface, and a decrease ΔD due to the formation of thinner and more rigid bilayer film on the surface (Figure 1.12 A and B) [239, 256–258]. Due to the ability of QCM-D to form and characterize supported lipid bilayers, it has been widely employed to study membrane-associated processes when using SLBs as a membrane mimetic like membrane- protein, membrane- peptide, and membrane-drug interactions (Figure 1.12 C) [259–265].

Other biophysical methods also exist to characterize protein-membrane interactions like neutron reflectometry. This method can provide information about the complex lipid composition of the membrane, and the relative location of lipids and proteins within the membrane. It has the advantage of its ability to determine the penetration of protein across the membrane not only at the interface as in SPR and QCM [266, 267]. Surface imaging techniques have also been used to study protein-membrane interaction like atomic force microscopy (AFM). Here, different information could be obtained, for instance, membrane proteins reconstituted in a lipid bilayer could be visualized in the free and ligand-bound state. It also allows monitoring of conformational changes within the membrane protein, for example, those induced by a bound ligand [268–270]. Single-molecule force spectroscopy has also been employed to study membrane protein- ligands

interactions within the membrane and to mechanically unfold membrane proteins in the membrane to probe the molecular interactions necessary to maintain protein structure and function. Moreover, It has been used to monitor membrane protein insertion and folding into the membrane [271, 272]. Total internal reflection microscopy (TIRFM) has also been used to study membrane protein in supported lipid bilayers. Here, one can obtain information about membrane protein dynamics, for instance, diffusion coefficients of membrane proteins in the presence and absence of a binding partner, oligomerization, and formation of protein complexes within the membrane [241, 273]. Hydrogen deuterium exchange mass spectrometry (HDX MS) has also been used to identify the binding interfaces of proteins to the membrane and to identify conformational changes of the protein once bound to the membrane [274].
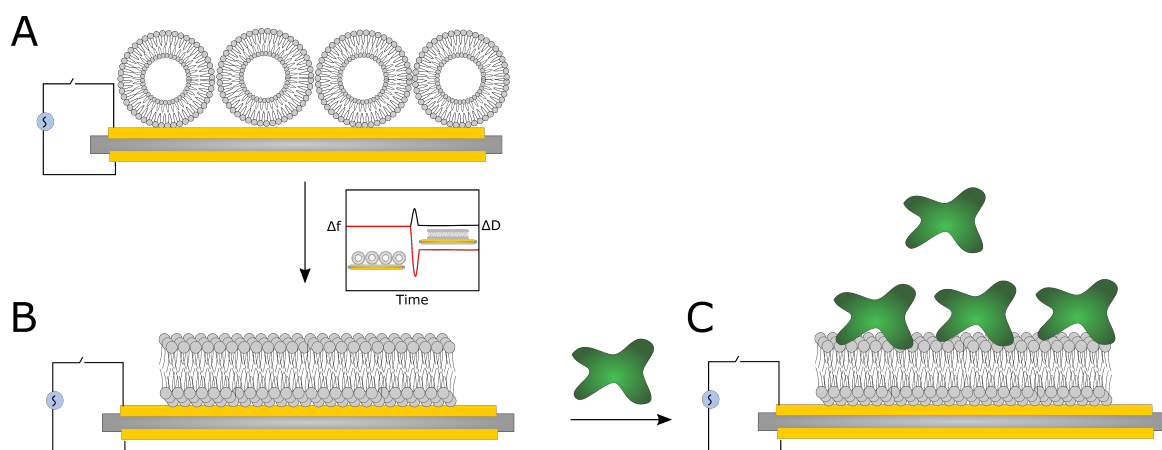
Figure 1.12: Quartz crystal microbalance. A) Principle of quartz crystal microbalance. B) Supported lipid bilayer immobilized on quartz microbalance. C) Protein binding on supported lipid bilayer on QCM chip.

References

[1] G.-W. Li, D. Burkhardt, C. Gross, and J. S. Weissman, "Quantifying absolute protein synthesis rates reveals principles underlying allocation of cellular resources," *Cell*, vol. 157, no. 3, pp. 624–635, 2014.

[2] K. Denks, A. Vogt, I. Sachelaru, N.-A. Petriman, R. Kudva, and H.-G. Koch, "The Sec translocon mediated protein transport in prokaryotes and eukaryotes," *Molecular membrane biology*, vol. 31, no. 2-3, pp. 58–84, 2014.

[3] A. G. Komarudin and A. J. Driessen, "SecA-mediated protein translocation through the SecYEG Channel," *Microbiology Spectrum*, vol. 7, no. 4, pp. 7–4, 2019.

[4] J. Oswald, R. Njenga, A. Natriashvili, P. Sarmah, and H.-G. Koch, "The dynamic SecYEG translocon," *Frontiers in Molecular Biosciences*, vol. 8, p. 664241, 2021.

[5] D. Smets, M. S. Loos, S. Karamanou, and A. Economou, "Protein transport across the bacterial plasma membrane by the Sec pathway," *The Protein Journal*, vol. 38, pp. 262–273, 2019.

[6] S. Rawat, L. Zhu, E. Lindner, R. E. Dalbey, and S. H. White, "SecA drives transmembrane insertion of RodZ, an unusual single-span membrane protein," *Journal of molecular biology*, vol. 427, no. 5, pp. 1023–1037, 2015.

[7] S. Wang, C.-I. Yang, and S.-o. Shan, "SecA mediates cotranslational targeting and translocation of an inner membrane protein," *Journal of Cell Biology*, vol. 216, no. 11, pp. 3639–3653, 2017.

[8] D. Huber, M. Jamshad, R. Hanmer, D. Schibich, K. Döring, I. Marcomini, G. Kramer, and B. Bukau, "SecA cotranslationally interacts with nascent substrate proteins in vivo," *Journal of bacteriology*, vol. 199, no. 2, pp. e00622–16, 2017.

[9] R. Steinberg, A. Origi, A. Natriashvili, P. Sarmah, M. Licheva, P. M. Walker, C. Kraft, S. High, J. Luirink, W. Q. Shi, *et al.*, "Posttranslational insertion of small membrane proteins by the bacterial signal recognition particle," *PLoS biology*, vol. 18, no. 9, p. e3000874, 2020.

[10] E. Pross, L. Soussoula, I. Seitl, D. Lupo, and A. Kuhn, "Membrane targeting and insertion of the c-tail protein SciP," *Journal of molecular biology*, vol. 428, no. 20, pp. 4218–4227, 2016.

[11] M. Peschke, M. Le Goff, G. M. Koningstein, A. Karyolaimos, J.-W. de Gier, P. van Ulsen, and J. Luirink, "SRP, FtsY, DnaK and YidC are required for the biogenesis of the E. coli tail-anchored membrane proteins DjlC and Flk," *Journal of molecular biology*, vol. 430, no. 3, pp. 389–403, 2018.

[12] B. V. D. Berg, W. M. Clemons, I. Collinson, Y. Modis, E. Hartmann, S. C. Harrison, and T. A. Rapoport, "X-ray structure of a protein-conducting channel," *nature*, vol. 427, no. 6969, pp. 36–44, 2004.

[13] J. A. L. a Nijeholt, J. de Keyzer, I. Prabudiansyah, and A. J. Driessen, "Characterization of the supporting role of SecE in protein translocation," *FEBS letters*, vol. 587, no. 18, pp. 3083–3088, 2013.

[14] A. Kihara, Y. Akiyama, and K. Ito, "FtsH is required for proteolytic elimination of un-complexed forms of SecY, an essential protein translocase subunit.," *Proceedings of the National Academy of Sciences*, vol. 92, no. 10, pp. 4532–4536, 1995.

[15] L. Brundage, J. P. Hendrick, E. Schiebel, A. J. Driessen, and W. Wickner, "The purified E. coli integral membrane protein SecYE is sufficient for reconstitution of SecA-dependent precursor protein translocation," *Cell*, vol. 62, no. 4, pp. 649–657, 1990.

[16] Y. Tanaka, Y. Sugano, M. Takemoto, T. Mori, A. Furukawa, T. Kusakizako, K. Kumazaki, A. Kashima, R. Ishitani, Y. Sugita, *et al.*, "Crystal structures of SecYEG in lipidic cubic phase elucidate a precise resting and a peptide-bound state," *Cell reports*, vol. 13, no. 8, pp. 1561–1568, 2015.

[17] K.-i. Nishiyama, M. Hanada, and H. Tokuda, "Disruption of the gene encoding p12 (SecG) reveals the direct involvement and important function of SecG in the protein translocation of Escherichia coli at low temperature.," *The EMBO journal*, vol. 13, no. 14, pp. 3272–3277, 1994.

[18] A. M. Flower, "SecG function and phospholipid metabolism in Escherichia coli," *Journal of bacteriology*, vol. 183, no. 6, pp. 2006–2012, 2001.

[19] A. Flower, L. Hines, and P. Pfennig, "SecG is an auxiliary component of the protein export apparatus of Escherichia coli," *Molecular and General Genetics MGG*, vol. 263, no. 1, pp. 131–136, 2000.

[20] V. P. Kontinen, I. M. Helander, and H. Tokuda, "The secG deletion mutation of Escherichia coli is suppressed by expression of a novel regulatory gene of Bacillus subtilis," *FEBS letters*, vol. 389, no. 3, pp. 281–284, 1996.

[21] H. Suzuki, K.-i. Nishiyama, and H. Tokuda, "Increases in Acidic Phospholipid Contents Specifically Restore Protein Translocation in a Cold-sensitive secA orsecG Null Mutant," *Journal of Biological Chemistry*, vol. 274, no. 43, pp. 31020–31024, 1999.

[22] S. Das and D. B. Oliver, "Mapping of the SecA· SecY and SecA· SecG interfaces by site-directed in vivo photocross-linking," *Journal of Biological Chemistry*, vol. 286, no. 14, pp. 12371–12380, 2011.

[23] K.-i. Nishiyama, S. Mizushima, and H. Tokuda, "A novel membrane protein involved in protein translocation across the cytoplasmic membrane of Escherichia coli.," *The EMBO Journal*, vol. 12, no. 9, pp. 3409–3415, 1993.

[24] M. Hanada, K.-i. Nishiyama, and H. Tokuda, "SecG plays a critical role in protein translocation in the absence of the proton motive force as well as at low temperature," *FEBS letters*, vol. 381, no. 1-2, pp. 25–28, 1996.

[25] F.-U. Hartl, S. Lecker, E. Schiebel, J. P. Hendrick, and W. Wickner, "The binding cascade of SecB to SecA to SecYE mediates preprotein targeting to the e. coli plasma membrane," *Cell*, vol. 63, no. 2, pp. 269–279, 1990.

[26] G. Von Heijne, "Signal sequences: the limits of variation," *Journal of molecular biology*, vol. 184, no. 1, pp. 99–105, 1985.

[27] T. Bornemann, W. Holtkamp, and W. Wintermeyer, "Interplay between trigger factor and other protein biogenesis factors on the ribosome," *Nature communications*, vol. 5, no. 1, pp. 1–8, 2014.

[28] A. Ariosa, J. H. Lee, S. Wang, I. Saraogi, and S.-o. Shan, "Regulation by a chaperone improves substrate selectivity during cotranslational protein targeting," *Proceedings of the National Academy of Sciences*, vol. 112, no. 25, pp. E3169–E3178, 2015.

[29] C. Huang, P. Rossi, T. Saio, and C. G. Kalodimos, "Structural basis for the antifolding activity of a molecular chaperone," *Nature*, vol. 537, no. 7619, pp. 202–206, 2016.

[30] P. Bechtluft, A. Kedrov, D.-J. Slotboom, N. Nouwen, S. J. Tans, and A. J. Driessen, "Tight hydrophobic contacts with the SecB chaperone prevent folding of substrate proteins," *Biochemistry*, vol. 49, no. 11, pp. 2380–2388, 2010.

[31] J. Zhou and Z. Xu, "Structural determinants of SecB recognition by SecA in bacterial protein translocation," *Nature Structural & Molecular Biology*, vol. 10, no. 11, pp. 942–947, 2003.

[32] A. Driessen and W. Wickner, "Proton transfer is rate-limiting for translocation of precursor proteins by the Escherichia coli translocase.," *Proceedings of the National Academy of Sciences*, vol. 88, no. 6, pp. 2471–2475, 1991.

[33] L.-G. Josefsson and L. L. Randall, "Different exported proteins in E. coli show differences in the temporal mode of processing in vivo," *Cell*, vol. 25, no. 1, pp. 151–157, 1981.

[34] K. Sato, H. Mori, M. Yoshida, and S. Mizushima, "Characterization of a potential catalytic residue, Asp-133, in the high affinity ATP-binding site of Escherichia coli SecA, translocation ATPase," *Journal of Biological Chemistry*, vol. 271, no. 29, pp. 17439–17444, 1996.

[35] J. F. Hunt, S. Weinkauf, L. Henry, J. J. Fak, P. McNicholas, D. B. Oliver, and J. Deisenhofer, "Nucleotide control of interdomain interactions in the conformational reaction cycle of SecA," *Science*, vol. 297, no. 5589, pp. 2018–2026, 2002.

[36] H. Ding, I. Mukerji, and D. Oliver, "Nucleotide and phospholipid-dependent control of PPXD and C-domain association for SecA ATPase," *Biochemistry*, vol. 42, no. 46, pp. 13468–13475, 2003.

[37] N. Chada, K. Chattrakun, B. P. Marsh, C. Mao, P. Bariya, and G. M. King, "Single-molecule observation of nucleotide induced conformational changes in basal SecA-ATP hydrolysis," *Science advances*, vol. 4, no. 10, p. eaat8797, 2018.

[38] K. J. Erlandson, S. Miller, Y. Nam, A. R. Osborne, J. Zimmer, and T. A. Rapoport, "A role for the two-helix finger of the SecA ATPase in protein translocation," *Nature*, vol. 455, no. 7215, pp. 984–987, 2008.

[39] S. Karamanou, E. Vrontou, G. Sianidis, C. Baud, T. Roos, A. Kuhn, A. S. Politou, and A. Economou, "A molecular switch in SecA protein couples ATP hydrolysis to protein translocation," *Molecular microbiology*, vol. 34, no. 5, pp. 1133–1145, 1999.

[40] P. Fekkes, C. van der Does, and A. J. Driessen, "The molecular chaperone SecB is released from the carboxy-terminus of SecA during initiation of precursor protein translocation," *The EMBO journal*, vol. 16, no. 20, pp. 6105–6113, 1997.

[41] P. Fekkes and A. J. Driessen, "Protein targeting to the bacterial cytoplasmic membrane," *Microbiology and Molecular Biology Reviews*, vol. 63, no. 1, pp. 161–173, 1999.

[42] E. Breukink, N. Nouwen, A. van Raalte, S. Mizushima, J. Tommassen, and B. de Kruijff, "The C terminus of SecA is involved in both lipid binding and SecB binding," *Journal of Biological Chemistry*, vol. 270, no. 14, pp. 7902–7907, 1995.

[43] J. Zimmer, Y. Nam, and T. A. Rapoport, "Structure of a complex of the ATPase SecA and the protein-translocation channel," *Nature*, vol. 455, no. 7215, pp. 936–943, 2008.

[44] D. Hizlan, A. Robson, S. Whitehouse, V. A. Gold, J. Vonck, D. Mills, W. Kühlbrandt, and I. Collinson, "Structure of the SecY complex unlocked by a preprotein mimic," *Cell reports*, vol. 1, no. 1, pp. 21–28, 2012.

[45] L. Li, E. Park, J. Ling, J. Ingram, H. Ploegh, and T. A. Rapoport, "Crystal structure of a substrate-engaged SecY protein-translocation channel," *Nature*, vol. 531, no. 7594, pp. 395–399, 2016.

[46] K. J. Erlandson, E. Or, A. R. Osborne, and T. A. Rapoport, "Analysis of polypeptide movement in the SecY channel during SecA-mediated protein translocation," *Journal of Biological Chemistry*, vol. 283, no. 23, pp. 15709–15715, 2008.

[47] B. W. Bauer, T. Shemesh, Y. Chen, and T. A. Rapoport, "A "push and slide" mechanism allows sequence-insensitive translocation of secretory proteins by the SecA ATPase," *Cell*, vol. 157, no. 6, pp. 1416–1429, 2014.

[48] M. A. Catipovic, B. W. Bauer, J. J. Loparo, and T. A. Rapoport, "Protein translocation by the SecA ATPase occurs by a power-stroke mechanism," *The EMBO journal*, vol. 38, no. 9, p. e101140, 2019.

[49] W. J. Allen, R. A. Corey, P. Oatley, R. B. Sessions, S. A. Baldwin, S. E. Radford, R. Tuma, and I. Collinson, "Two-way communication between SecY and SecA suggests a brownian ratchet mechanism for protein translocation," *Elife*, vol. 5, 2016.

[50] R. A. Corey, Z. Ahdash, A. Shah, E. Pyle, W. J. Allen, T. Fessl, J. E. Lovett, A. Politis, and I. Collinson, "ATP-induced asymmetric pre-protein folding as a driver of protein translocation through the Sec machinery," *Elife*, vol. 8, p. e41803, 2019.

[51] T. Fessl, D. Watkins, P. Oatley, W. J. Allen, R. A. Corey, J. Horne, S. A. Baldwin, S. E. Radford, I. Collinson, and R. Tuma, "Dynamic action of the Sec machinery during initiation, protein translocation and termination," *Elife*, vol. 7, p. e35112, 2018.

[52] J. D. Bryngelson and P. G. Wolynes, "Spin glasses and the statistical mechanics of protein folding.," *Proceedings of the National Academy of sciences*, vol. 84, no. 21, pp. 7524–7528, 1987.

[53] D. U. Ferreiro, E. A. Komives, and P. G. Wolynes, "Frustration in biomolecules," *Quarterly reviews of biophysics*, vol. 47, no. 4, pp. 285–363, 2014.

[54] S. Krishnamurthy, M.-F. Sardis, N. Eleftheriadis, K. E. Chatzi, J. H. Smit, K. Karathanou, G. Gouridis, A. G. Portaliou, A.-N. Bondar, S. Karamanou, *et al.*, "Preproteins couple the intrinsic dynamics of SecA to its ATPase cycle to translocate via a catch and release mechanism," *Cell Reports*, vol. 38, no. 6, p. 110346, 2022.

[55] L. Dong, S. Yang, J. Chen, X. Wu, D. Sun, C. Song, and L. Li, "Structural basis of SecA-mediated protein translocation," *Proceedings of the National Academy of Sciences*, vol. 120, no. 2, p. e2208070120, 2023.

[56] T. De Vrije, R. De Swart, W. Dowhan, J. Tommassen, and B. De Kruijff, "Phosphatidyl-glycerol is involved in protein translocation across Escherichia coli inner membranes," *Nature*, vol. 334, no. 6178, pp. 173–175, 1988.

[57] R. Lill, W. Dowhan, and W. Wickner, "The ATPase activity of SecA is regulated by acidic phospholipids, SecY, and the leader and mature domains of precursor proteins," *Cell*, vol. 60, no. 2, pp. 271–280, 1990.

[58] E. Breukink, R. A. Demel, G. De Korte-Kool, and B. De Kruijff, "SecA insertion into phospholipids is stimulated by negatively charged lipids and inhibited by ATP: a monolayer study," *Biochemistry*, vol. 31, no. 4, pp. 1119–1124, 1992.

[59] N. D. Ulbrandt, E. London, and D. Oliver, "Deep penetration of a portion of Escherichia coli SecA protein into model membranes is promoted by anionic phospholipids and by partial unfolding.," *Journal of Biological Chemistry*, vol. 267, no. 21, pp. 15184–15192, 1992.

[60] R. C. Keller, M. M. Snel, B. de Kruijff, and D. Marsh, "SecA restricts, in a nucleotide-dependent manner, acyl chain mobility up to the center of a phospholipid bilayer," *FEBS letters*, vol. 358, no. 3, pp. 251–254, 1995.

[61] R. Cabelli, K. M. Dolan, L. Qian, and D. B. Oliver, "Characterization of membrane-associated and soluble states of SecA protein from wild-type and SecA51 (ts) mutant strains of Escherichia coli.," *Journal of Biological Chemistry*, vol. 266, no. 36, pp. 24420–24427, 1991.

[62] J. Hendrick and W. Wickner, "SecA protein needs both acidic phospholipids and SecY/E protein for functional high-affinity binding to the Escherichia coli plasma membrane.," *Journal of Biological Chemistry*, vol. 266, no. 36, pp. 24596–24600, 1991.

[63] C. van der Does, J. Swaving, W. van Klompenburg, and A. J. Driessen, "Non-bilayer lipids stimulate the activity of the reconstituted bacterial protein translocase," *Journal of Biological Chemistry*, vol. 275, no. 4, pp. 2472–2478, 2000.

[64] I. Prabudiansyah, I. Kusters, A. Caforio, and A. J. Driessen, "Characterization of the annular lipid shell of the Sec translocon," *Biochimica et Biophysica Acta (BBA)-Biomembranes*, vol. 1848, no. 10, pp. 2050–2056, 2015.

[65] J. H. Floyd, Z. You, Y.-H. Hsieh, Y. Ma, H. Yang, and P. C. Tai, "The dispensability and requirement of SecA N-terminal aminoacyl residues for complementation, membrane binding, lipid-specific domains and channel activities," *Biochemical and biophysical research communications*, vol. 453, no. 1, pp. 138–142, 2014.

[66] S. Koch, J. G. de Wit, I. Vos, J. P. Birkner, P. Gordiichuk, A. Herrmann, A. M. van Oijen, and A. J. Driessen, "Lipids activate SecA for high affinity binding to the SecYEG complex," *Journal of Biological Chemistry*, vol. 291, no. 43, pp. 22534–22543, 2016.

[67] K. Winkler, A. Karner, A. Horner, C. Hannesschlaeger, D. Knyazev, C. Siligan, M. Zimmermann, R. Kuttner, P. Pohl, and J. Preiner, "Interaction of the motor protein SecA and the bacterial protein translocation channel SecYEG in the absence of ATP," *Nanoscale Advances*, vol. 2, no. 8, pp. 3431–3443, 2020.

[68] G. Roussel, E. Lindner, and S. H. White, "Topology of the SecA ATPase Bound to Large Unilamellar Vesicles," *Journal of Molecular Biology*, vol. 434, no. 12, p. 167607, 2022.

[69] V. A. Gold, A. Robson, H. Bao, T. Romantsov, F. Duong, and I. Collinson, "The action of cardiolipin on the bacterial translocon," *Proceedings of the National Academy of Sciences*, vol. 107, no. 22, pp. 10044–10049, 2010.

[70] B. K. Tan, M. Bogdanov, J. Zhao, W. Dowhan, C. R. Raetz, and Z. Guan, "Discovery of a cardiolipin synthase utilizing phosphatidylethanolamine and phosphatidylglycerol as substrates," *Proceedings of the National Academy of Sciences*, vol. 109, no. 41, pp. 16504–16509, 2012.

[71] R. A. Corey, E. Pyle, W. J. Allen, D. W. Watkins, M. Casiraghi, B. Miroux, I. Arechaga, A. Politis, and I. Collinson, "Specific cardiolipin–SecY interactions are required for proton-motive force stimulation of protein secretion," *Proceedings of the National Academy of Sciences*, vol. 115, no. 31, pp. 7967–7972, 2018.

[72] S. Koch, M. Exterkate, C. A. López, M. Patro, S. J. Marrink, and A. J. Driessen, "Two distinct anionic phospholipid-dependent events involved in SecA-mediated protein translocation," *Biochimica et Biophysica Acta (BBA)-Biomembranes*, vol. 1861, no. 11, p. 183035, 2019.

[73] M. Akita, A. Shinkai, S.-i. Matsuyama, and S. Mizushima, "SecA, an essential component of the secretory machinery of Escherichia coli, exists as homodimer," *Biochemical and biophysical research communications*, vol. 174, no. 1, pp. 211–216, 1991.

[74] A. J. Driessen, "SecA, the peripheral subunit of the Escherichia coli precursor protein translocase, is functional as a dimer," *Biochemistry*, vol. 32, no. 48, pp. 13190–13197, 1993.

[75] R. L. Woodbury, S. J. Hardy, and L. L. Randall, "Complex behavior in solution of homodimeric SecA," *Protein Science*, vol. 11, no. 4, pp. 875–882, 2002.

[76] I. Kusters, G. van den Bogaart, A. Kedrov, V. Krasnikov, F. Fulyani, B. Poolman, and A. J. Driessen, "Quaternary structure of SecA in solution and bound to SecYEG probed at the single molecule level," *Structure*, vol. 19, no. 3, pp. 430–439, 2011.

[77] E. Or, A. Navon, and T. Rapoport, "Dissociation of the dimeric SecA ATPase during protein translocation across the bacterial membrane," *The EMBO journal*, vol. 21, no. 17, pp. 4470–4479, 2002.

[78] A.-B. Seinen, D. Spakman, A. M. van Oijen, and A. J. Driessen, "Cellular dynamics of the SecA ATPase at the single molecule level," *Scientific reports*, vol. 11, no. 1, pp. 1–16, 2021.

[79] V. Sharma, A. Arockiasamy, D. R. Ronning, C. G. Savva, A. Holzenburg, M. Braunstein, W. R. Jacobs Jr, and J. C. Sacchettini, "Crystal structure of Mycobacterium tuberculosis SecA, a preprotein translocating ATPase," *Proceedings of the National Academy of Sciences*, vol. 100, no. 5, pp. 2243–2248, 2003.

[80] A. R. Osborne, W. M. Clemons Jr, and T. A. Rapoport, "A large conformational change of the translocation ATPase SecA," *Proceedings of the National Academy of Sciences*, vol. 101, no. 30, pp. 10937–10942, 2004.

[81] D. G. Vassylyev, H. Mori, M. N. Vassylyeva, T. Tsukazaki, Y. Kimura, T. H. Tahirov, and K. Ito, "Crystal structure of the translocation ATPase SecA from Thermus thermophilus reveals a parallel, head-to-head dimer," *Journal of molecular biology*, vol. 364, no. 3, pp. 248–258, 2006.

[82] Y. Papanikolau, M. Papadovasilaki, R. B. Ravelli, A. A. McCarthy, S. Cusack, A. Economou, and K. Petratos, "Structure of dimeric SecA, the Escherichia coli preprotein translocase motor," *Journal of molecular biology*, vol. 366, no. 5, pp. 1545–1557, 2007.

[83] J. Zimmer, W. Li, and T. A. Rapoport, "A novel dimer interface and conformational changes revealed by an X-ray structure of B. subtilis SecA," *Journal of molecular biology*, vol. 364, no. 3, pp. 259–265, 2006.

[84] J. Zimmer and T. A. Rapoport, "Conformational flexibility and peptide interaction of the translocation ATPase SecA," *Journal of molecular biology*, vol. 394, no. 4, pp. 606–612, 2009.

[85] I. Gelis, A. M. Bonvin, D. Keramisanou, M. Koukaki, G. Gouridis, S. Karamanou, A. Economou, and C. G. Kalodimos, "Structural basis for signal-sequence recognition by the translocase motor SecA as determined by NMR," *Cell*, vol. 131, no. 4, pp. 756–769, 2007.

[86] Y. Chen, X. Pan, Y. Tang, S. Quan, P. C. Tai, and S.-F. Sui, "Full-length Escherichia coli SecA dimerizes in a closed conformation in solution as determined by cryo-electron microscopy," *Journal of Biological Chemistry*, vol. 283, no. 43, pp. 28783–28787, 2008.

[87] C. Ma, X. Wu, D. Sun, E. Park, M. A. Catipovic, T. A. Rapoport, N. Gao, and L. Li, "Structure of the substrate-engaged SecA-SecY protein translocation machine," *Nature communications*, vol. 10, no. 1, pp. 1–9, 2019.

[88] M. F. Sardis and A. Economou, "SecA: a tale of two protomers," *Molecular microbiology*, vol. 76, no. 5, pp. 1070–1081, 2010.

[89] H. Ding, J. F. Hunt, I. Mukerji, and D. Oliver, "Bacillus subtilis SecA ATPase exists as an antiparallel dimer in solution," *Biochemistry*, vol. 42, no. 29, pp. 8729–8738, 2003.

[90] S. M. Auclair, D. B. Oliver, and I. Mukerji, "Defining the solution state dimer structure of Escherichia coli SecA using Forster resonance energy transfer," *Biochemistry*, vol. 52, no. 14, pp. 2388–2401, 2013.

[91] G. Gouridis, S. Karamanou, M. F. Sardis, M. A. Schärer, G. Capitani, and A. Economou, "Quaternary dynamics of the SecA motor drive translocase catalysis," *Molecular cell*, vol. 52, no. 5, pp. 655–666, 2013.

[92] J. de Keyzer, E. O. van der Sluis, R. E. Spelbrink, N. Nijstad, B. de Kruijff, N. Nouwen, C. van der Does, and A. J. Driessen, "Covalently dimerized SecA is functional in protein translocation," *Journal of Biological Chemistry*, vol. 280, no. 42, pp. 35255–35260, 2005.

[93] H. Wang, B. Na, H. Yang, and P. C. Tai, "Additional in vitro and in vivo evidence for SecA functioning as dimers in the membrane: dissociation into monomers is not essential for protein translocation in Escherichia coli," *Journal of bacteriology*, vol. 190, no. 4, pp. 1413–1418, 2008.

[94] L. B. Jilaveanu and D. Oliver, "SecA dimer cross-linked at its subunit interface is functional for protein translocation," *Journal of bacteriology*, vol. 188, no. 1, pp. 335–338, 2006.

[95] M. Alami, K. Dalal, B. Lelj-Garolla, S. G. Sligar, and F. Duong, "Nanodiscs unravel the interaction between the SecYEG channel and its cytosolic partner SecA," *The EMBO journal*, vol. 26, no. 8, pp. 1995–2004, 2007.

[96] E. Or, D. Boyd, S. Gon, J. Beckwith, and T. Rapoport, "The bacterial ATPase SecA functions as a monomer in protein translocation," *Journal of Biological Chemistry*, vol. 280, no. 10, pp. 9097–9105, 2005.

[97] G. Roussel and S. H. White, "Binding of SecA ATPase monomers and dimers to lipid vesicles," *Biochimica et Biophysica Acta (BBA)-Biomembranes*, vol. 1862, no. 2, p. 183112, 2020.

[98] G. Roussel and S. H. White, "The SecA ATPase motor protein binds to Escherichia coli liposomes only as monomers," *Biochimica et Biophysica Acta (BBA)-Biomembranes*, vol. 1862, no. 9, p. 183358, 2020.

[99] E. Or and T. Rapoport, "Cross-linked SecA dimers are not functional in protein translocation," *FEBS letters*, vol. 581, no. 14, pp. 2616–2620, 2007.

[100] M. Musial-Siwek, S. L. Rusch, and D. A. Kendall, "Probing the affinity of SecA for signal peptide in different environments," *Biochemistry*, vol. 44, no. 42, pp. 13987–13996, 2005.

[101] J. Benach, Y.-T. Chou, J. J. Fak, A. Itkin, D. D. Nicolae, P. C. Smith, G. Wittrock, D. L. Floyd, C. M. Golsaz, L. M. Gierasch, *et al.*, "Phospholipid-induced monomerization and signal-peptide-induced oligomerization of SecA," *Journal of Biological Chemistry*, vol. 278, no. 6, pp. 3628–3638, 2003.

[102] L. B. Jilaveanu, C. R. Zito, and D. Oliver, "Dimeric SecA is essential for protein translocation," *Proceedings of the National Academy of Sciences*, vol. 102, no. 21, pp. 7511–7516, 2005.

[103] S. Das, E. Stivison, E. Folta-Stogniew, and D. Oliver, "Reexamination of the role of the amino terminus of SecA in promoting its dimerization and functional state," *Journal of bacteriology*, vol. 190, no. 21, pp. 7302–7307, 2008.

[104] S. Karamanou, G. Sianidis, G. Gouridis, C. Pozidis, Y. Papanikolau, E. Papanikou, and A. Economou, "Escherichia coli SecA truncated at its termini is functional and dimeric," *FEBS letters*, vol. 579, no. 5, pp. 1267–1271, 2005.

[105] D. Akopian, K. Shen, X. Zhang, and S.-o. Shan, "Signal recognition particle: an essential protein-targeting machine," *Annual review of biochemistry*, vol. 82, pp. 693–721, 2013.

[106] A. Kuhn, H.-G. Koch, and R. E. Dalbey, "Targeting and insertion of membrane proteins," *EcoSal Plus*, vol. 7, no. 2, 2017.

[107] R. Steinberg, L. Knüpffer, A. Origi, R. Asti, and H.-G. Koch, "Co-translational protein targeting in bacteria," *FEMS microbiology letters*, vol. 365, no. 11, p. fny095, 2018.

[108] J. H. Peterson, C. A. Woolhead, and H. D. Bernstein, "The conformation of a nascent polypeptide inside the ribosome tunnel affects protein targeting and protein folding," *Molecular microbiology*, vol. 78, no. 1, pp. 203–217, 2010.

[109] H. Adams, P. A. Scotti, H. De Cock, J. Luirink, and J. Tommassen, "The presence of a helix breaker in the hydrophobic core of signal sequences of secretory proteins prevents recognition by the signal-recognition particle in Escherichia coli," *European journal of biochemistry*, vol. 269, no. 22, pp. 5564–5571, 2002.

[110] M. Halic, M. Blau, T. Becker, T. Mielke, M. R. Pool, K. Wild, I. Sinning, and R. Beckmann, "Following the signal sequence from ribosomal tunnel exit to signal recognition particle," *Nature*, vol. 444, no. 7118, pp. 507–511, 2006.

[111] P. F. Egea, S.-o. Shan, J. Napetschnig, D. F. Savage, P. Walter, and R. M. Stroud, "Substrate twinning activates the signal recognition particle and its receptor," *Nature*, vol. 427, no. 6971, pp. 215–221, 2004.

[112] P. J. Focia, I. V. Shepotinovskaya, J. A. Seidler, and D. M. Freymann, "Heterodimeric GTPase core of the SRP targeting complex," *Science*, vol. 303, no. 5656, pp. 373–377, 2004.

[113] S. F. Ataide, N. Schmitz, K. Shen, A. Ke, S.-o. Shan, J. A. Doudna, and N. Ban, "The crystal structure of the signal recognition particle in complex with its receptor," *Science*, vol. 331, no. 6019, pp. 881–886, 2011.

[114] J. R. Jagath, N. B. Matassova, E. De Leeuw, J. M. Warnecke, G. Lentzen, M. V. Rodnina, J. Luirink, and W. Wintermeyer, "Important role of the tetraloop region of 4.5 S RNA in SRP binding to its receptor FtsY," *Rna*, vol. 7, no. 2, pp. 293–301, 2001.

[115] J. D. Miller, H. D. Bernstein, and P. Walter, "Interaction of E. coli Ffh/4.5 S ribonucleo-protein and FtsY mimics that of mammalian signal recognition particle and its receptor," *Nature*, vol. 367, no. 6464, pp. 657–659, 1994.

[116] N. Zheng and L. M. Gierasch, "Domain interactions in E. coli SRP: stabilization of M domain by RNA is required for effective signal sequence modulation of NG domain," *Molecular cell*, vol. 1, no. 1, pp. 79–87, 1997.

[117] A. Jomaa, D. Boehringer, M. Leibundgut, and N. Ban, "Structures of the E. coli translating ribosome with SRP and its receptor and with the translocon," *Nature communications*, vol. 7, no. 1, p. 10471, 2016.

[118] K. Denks, N. Sliwinski, V. Erichsen, B. Borodkina, A. Origi, and H.-G. Koch, "The signal recognition particle contacts uL23 and scans substrate translation inside the ribosomal tunnel," *Nature microbiology*, vol. 2, no. 4, pp. 1–10, 2017.

[119] E. Mercier, W. Holtkamp, M. V. Rodnina, and W. Wintermeyer, "Signal recognition particle binds to translating ribosomes before emergence of a signal anchor sequence," *Nucleic acids research*, vol. 45, no. 20, pp. 11858–11866, 2017.

[120] W. Holtkamp, S. Lee, T. Bornemann, T. Senyushkina, M. V. Rodnina, and W. Winter-meyer, "Dynamic switch of the signal recognition particle from scanning to targeting," *Nature structural & molecular biology*, vol. 19, no. 12, pp. 1332–1337, 2012.

[121] R. Parlitz, A. Eitan, G. Stjepanovic, L. Bahari, G. Bange, E. Bibi, and I. Sinning, "Escherichia coli signal recognition particle receptor FtsY contains an essential and autonomous membrane-binding amphipathic helix," *Journal of Biological Chemistry*, vol. 282, no. 44, pp. 32176–32184, 2007.

[122] G. Stjepanovic, K. Kapp, G. Bange, C. Graf, R. Parlitz, K. Wild, M. P. Mayer, and I. Sinning, "Lipids trigger a conformational switch that regulates signal recognition particle (SRP)-mediated protein targeting," *Journal of Biological Chemistry*, vol. 286, no. 26, pp. 23489–23497, 2011.

[123] A. Eitan and E. Bibi, "The core Escherichia coli signal recognition particle receptor contains only the N and G domains of FtsY," *Journal of bacteriology*, vol. 186, no. 8, pp. 2492–2494, 2004.

[124] A. Jomaa, Y.-H. H. Fu, D. Boehringer, M. Leibundgut, S.-o. Shan, and N. Ban, "Structure of the quaternary complex between SRP, SR, and translocon bound to the translating ribosome," *Nature communications*, vol. 8, no. 1, p. 15470, 2017.

[125] G. Bacher, H. Lütcke, B. Jungnickel, T. A. Rapoport, and B. Dobberstein, "Regulation by the ribosome of the GTPase of the signal-recognition particle during protein targeting," *Nature*, vol. 381, no. 6579, pp. 248–251, 1996.

[126] D. Akopian, K. Dalal, K. Shen, F. Duong, and S.-o. Shan, "SecYEG activates GTPases to drive the completion of cotranslational protein targeting," *Journal of Cell Biology*, vol. 200, no. 4, pp. 397–405, 2013.

[127] T. Becker, S. Bhushan, A. Jarasch, J.-P. Armache, S. Funes, F. Jossinet, J. Gumbart, T. Mielke, O. Berninghausen, K. Schulten, *et al.*, "Structure of monomeric yeast and mammalian Sec61 complexes interacting with the translating ribosome," *science*, vol. 326, no. 5958, pp. 1369–1373, 2009.

[128] Z. Cheng, Y. Jiang, E. C. Mandon, and R. Gilmore, "Identification of cytoplasmic residues of Sec61p involved in ribosome binding and cotranslational translocation," *The Journal of cell biology*, vol. 168, no. 1, pp. 67–77, 2005.

[129] J. Frauenfeld, J. Gumbart, E. O. v. d. Sluis, S. Funes, M. Gartmann, B. Beatrix, T. Mielke, O. Berninghausen, T. Becker, K. Schulten, *et al.*, "Cryo-EM structure of the ribosome–SecYE complex in the membrane environment," *Nature structural & molecular biology*, vol. 18, no. 5, pp. 614–621, 2011.

[130] E. Mercier, X. Wang, M. Maiti, W. Wintermeyer, and M. V. Rodnina, "Lateral gate dynamics of the bacterial translocon during cotranslational membrane protein insertion," *Proceedings of the National Academy of Sciences*, vol. 118, no. 26, p. e2100474118, 2021.

[131] E. Park, J.-F. Ménétret, J. C. Gumbart, S. J. Ludtke, W. Li, A. Whynot, T. A. Rapoport, and C. W. Akey, "Structure of the SecY channel during initiation of protein translocation," *Nature*, vol. 506, no. 7486, pp. 102–106, 2014.

[132] L. Bischoff, S. Wickles, O. Berninghausen, E. O. Van Der Sluis, and R. Beckmann, "Visualization of a polytopic membrane protein during SecY-mediated membrane insertion," *Nature communications*, vol. 5, no. 1, p. 4103, 2014.

[133] L. Kater, B. Frieg, O. Berninghausen, H. Gohlke, R. Beckmann, and A. Kedrov, "Partially inserted nascent chain unzips the lateral gate of the Sec translocon," *EMBO reports*, vol. 20, no. 10, p. e48191, 2019.

[134] T. Welte, R. Kudva, P. Kuhn, L. Sturm, D. Braig, M. Müller, B. Warscheid, F. Drepper, and H.-G. Koch, "Promiscuous targeting of polytopic membrane proteins to SecYEG or YidC by the Escherichia coli signal recognition particle," *Molecular biology of the cell*, vol. 23, no. 3, pp. 464–479, 2012.

[135] M. L. Urbanus, P. A. Scotti, L. Fröderberg, A. Sääf, J.-W. L. de Gier, J. Brunner, J. C. Samuelson, R. E. Dalbey, B. Oudega, and J. Luirink, "Sec-dependent membrane protein insertion: sequential interaction of nascent FtsQ with SecY and YidC," *EMBO reports*, vol. 2, no. 6, pp. 524–529, 2001.

[136] P. B. Wolfe, M. Rice, and W. Wickner, "Effects of two sec genes on protein assembly into the plasma membrane of Escherichia coli.," *Journal of Biological Chemistry*, vol. 260, no. 3, pp. 1836–1841, 1985.

[137] F. Jiang, M. Chen, L. Yi, J.-W. de Gier, A. Kuhn, and R. E. Dalbey, "Defining the regions of Escherichia coli YidC that contribute to activity," *Journal of Biological Chemistry*, vol. 278, no. 49, pp. 48965–48972, 2003.

[138] K. Kumazaki, S. Chiba, M. Takemoto, A. Furukawa, K.-i. Nishiyama, Y. Sugano, T. Mori, N. Dohmae, K. Hirata, Y. Nakada-Nakura, *et al.*, "Structural basis of Sec-independent membrane protein insertion by YidC," *Nature*, vol. 509, no. 7501, pp. 516–520, 2014.

[139] Y. Chen, R. Soman, S. K. Shanmugam, A. Kuhn, and R. E. Dalbey, "The role of the strictly conserved positively charged residue differs among the Gram-positive, Gram-negative, and chloroplast YidC homologs," *Journal of Biological Chemistry*, vol. 289, no. 51, pp. 35656–35667, 2014.

[140] S. Wickles, A. Singharoy, J. Andreani, S. Seemayer, L. Bischoff, O. Berninghausen, J. Soeding, K. Schulten, E. O. van der Sluis, and R. Beckmann, "A structural model of the active ribosome-bound membrane protein insertase YidC," *Elife*, vol. 3, p. e03035, 2014.

[141] Y. Geng, A. Kedrov, J. J. Caumanns, A. H. Crevenna, D. C. Lamb, R. Beckmann, and A. J. Driessen, "Role of the cytosolic loop C2 and the C terminus of YidC in ribosome binding and insertion activity," *Journal of Biological Chemistry*, vol. 290, no. 28, pp. 17250–17261, 2015.

[142] C. Klenner and A. Kuhn, "Dynamic disulfide scanning of the membrane-inserting Pf3 coat protein reveals multiple YidC substrate contacts," *Journal of Biological Chemistry*, vol. 287, no. 6, pp. 3769–3776, 2012.

[143] I. Seitl, S. Wickles, R. Beckmann, A. Kuhn, and D. Kiefer, "The C-terminal regions of YidC from Rhodopirellula baltica and Oceanicaulis alexandrii bind to ribosomes and partially substitute for SRP receptor function in Escherichia coli," *Molecular microbiology*, vol. 91, no. 2, pp. 408–421, 2014.

[144] M. Chen, J. C. Samuelson, F. Jiang, M. Muller, A. Kuhn, and R. E. Dalbey, "Direct interaction of YidC with the Sec-independent Pf3 coat protein during its membrane protein insertion," *Journal of Biological Chemistry*, vol. 277, no. 10, pp. 7670–7675, 2002.

[145] J. C. Samuelson, F. Jiang, L. Yi, M. Chen, J.-W. de Gier, A. Kuhn, and R. E. Dalbey, "Function of YidC for the insertion of M13 procoat protein in Escherichia coli: Translocation of mutants that show differences in their membrane potential dependence and sec requirement," *Journal of Biological Chemistry*, vol. 276, no. 37, pp. 34847–34852, 2001.

[146] M. van der Laan, P. Bechtluft, S. Kol, N. Nouwen, and A. J. Driessen, "F_1F_0 ATP synthase subunit c is a substrate of the novel YidC pathway for membrane protein biogenesis," *The Journal of cell biology*, vol. 165, no. 2, pp. 213–222, 2004.

[147] S. J. Facey, S. A. Neugebauer, S. Krauss, and A. Kuhn, "The mechanosensitive channel protein MscL is targeted by the SRP to the novel YidC membrane insertion pathway of Escherichia coli," *Journal of molecular biology*, vol. 365, no. 4, pp. 995–1004, 2007.

[148] S. A. Neugebauer, A. Baulig, A. Kuhn, and S. J. Facey, "Membrane protein insertion of variant MscL proteins occurs at YidC and SecYEG of Escherichia coli," *Journal of molecular biology*, vol. 417, no. 4, pp. 375–386, 2012.

[149] M.-S. Aschtgen, A. Zoued, R. Lloubes, L. Journet, and E. Cascales, "The C-tail anchored TssL subunit, an essential protein of the enteroaggregative Escherichia coli Sci-1 Type VI secretion system, is inserted by YidC," *Microbiologyopen*, vol. 1, no. 1, pp. 71–82, 2012.

[150] A. Gallusser and A. Kuhn, "Initial steps in protein membrane insertion. Bacteriophage M13 procoat protein binds to the membrane surface by electrostatic interaction.," *The EMBO journal*, vol. 9, no. 9, pp. 2723–2729, 1990.

[151] L. Yi, N. Celebi, M. Chen, and R. E. Dalbey, "Sec/SRP requirements and energetics of membrane insertion of subunits a, b, and c of the Escherichia coli F_1F_0 ATP synthase," *Journal of Biological Chemistry*, vol. 279, no. 38, pp. 39260–39267, 2004.

[152] E. N. Houben, P. A. Scotti, Q. A. Valent, J. Brunner, J.-W. L. de Gier, B. Oudega, and J. Luirink, "Nascent Lep inserts into the Escherichia coli inner membrane in the vicinity of YidC, SecY and SecA," *FEBS letters*, vol. 476, no. 3, pp. 229–233, 2000.

[153] S. Wagner, O. Pop, G.-J. Haan, L. Baars, G. Koningstein, M. M. Klepsch, P. Genevaux, J. Luirink, and J.-W. de Gier, "Biogenesis of MalF and the MalFGK2 maltose transport

complex in Escherichia coli requires YidC," *Journal of Biological Chemistry*, vol. 283, no. 26, pp. 17881–17890, 2008.

[154] I. Sachelaru, N. A. Petriman, R. Kudva, P. Kuhn, T. Welte, B. Knapp, F. Drepper, B. Warscheid, and H.-G. Koch, "YidC occupies the lateral gate of the SecYEG translocon and is sequentially displaced by a nascent membrane protein," *Journal of Biological Chemistry*, vol. 288, no. 23, pp. 16295–16307, 2013.

[155] N. Celebi, L. Yi, S. J. Facey, A. Kuhn, and R. E. Dalbey, "Membrane biogenesis of subunit II of cytochrome bo oxidase: contrasting requirements for insertion of N-terminal and C-terminal domains," *Journal of molecular biology*, vol. 357, no. 5, pp. 1428–1436, 2006.

[156] E. van Bloois, G.-J. Haan, J.-W. de Gier, B. Oudega, and J. Luirink, "Distinct requirements for translocation of the N-tail and C-tail of the Escherichia coli inner membrane protein CyoA," *Journal of Biological Chemistry*, vol. 281, no. 15, pp. 10002–10009, 2006.

[157] C. E. Price and A. J. Driessen, "Conserved negative charges in the transmembrane segments of subunit K of the NADH: Ubiquinone Oxidoreductase determine its dependence on YidC for membrane insertion 2," *Journal of Biological Chemistry*, vol. 285, no. 6, pp. 3575–3581, 2010.

[158] S. Nagamori, I. N. Smirnova, and H. R. Kaback, "Role of YidC in folding of polytopic membrane proteins," *The Journal of cell biology*, vol. 165, no. 1, pp. 53–62, 2004.

[159] L. Zhu, H. R. Kaback, and R. E. Dalbey, "YidC protein, a molecular chaperone for LacY protein folding via the SecYEG protein machinery," *Journal of Biological Chemistry*, vol. 288, no. 39, pp. 28180–28194, 2013.

[160] R. J. Schulze, J. Komar, M. Botte, W. J. Allen, S. Whitehouse, V. A. Gold, J. A. Lycklama a Nijeholt, K. Huard, I. Berger, C. Schaffitzel, *et al.*, "Membrane protein insertion and proton-motive-force-dependent secretion through the bacterial holo-translocon SecYEG–SecDF–YajC–YidC," *Proceedings of the National Academy of Sciences*, vol. 111, no. 13, pp. 4844–4849, 2014.

[161] K. Xie, D. Kiefer, G. Nagler, R. E. Dalbey, and A. Kuhn, "Different regions of the nonconserved large periplasmic domain of Escherichia coli YidC are involved in the SecF interaction and membrane insertase activity," *Biochemistry*, vol. 45, no. 44, pp. 13401–13408, 2006.

[162] J. Komar, S. Alvira, R. J. Schulze, R. Martin, J. A. Lycklama a Nijeholt, S. C. Lee, T. R. Dafforn, G. Deckers-Hebestreit, I. Berger, C. Schaffitzel, *et al.*, "Membrane protein insertion and assembly by the bacterial holo-translocon SecYEG–SecDF–YajC–YidC," *Biochemical journal*, vol. 473, no. 19, pp. 3341–3354, 2016.

[163] M. Botte, N. R. Zaccai, J. L. À. Nijeholt, R. Martin, K. Knoops, G. Papai, J. Zou, A. Deniaud, M. Karuppasamy, Q. Jiang, *et al.*, "A central cavity within the holo-translocon suggests a mechanism for membrane protein insertion," *Scientific reports*, vol. 6, no. 1, p. 38399, 2016.

[164] L. Yi, F. Jiang, M. Chen, B. Cain, A. Bolhuis, and R. E. Dalbey, "YidC is strictly required for membrane insertion of subunits a and c of the F_1F_0 ATP synthase and SecE of the SecYEG translocase," *Biochemistry*, vol. 42, no. 35, pp. 10537–10544, 2003.

[165] R. Martin, A. H. Larsen, R. A. Corey, S. R. Midtgaard, H. Frielinghaus, C. Schaffitzel, L. Arleth, and I. Collinson, "Structure and dynamics of the central lipid pool and proteins of the bacterial holo-translocon," *Biophysical journal*, vol. 116, no. 10, pp. 1931–1940, 2019.

[166] W. Dowhan, H. Vitrac, and M. Bogdanov, "Lipid-assisted membrane protein folding and topogenesis," *The protein journal*, vol. 38, pp. 274–288, 2019.

[167] S. Alvira, D. W. Watkins, L. Troman, W. J. Allen, J. S. Lorriman, G. Degliesposti, E. J. Cohen, M. Beeby, B. Daum, V. A. Gold, *et al.*, "Inter-membrane association of the Sec and BAM translocons for bacterial outer-membrane biogenesis," *Elife*, vol. 9, p. e60669, 2020.

[168] S. Majeed, A. B. Ahmad, U. Sehar, and E. R. Georgieva, "Lipid membrane mimetics in functional and structural studies of integral membrane proteins," *Membranes*, vol. 11, no. 9, p. 685, 2021.

[169] H.-X. Zhou and T. A. Cross, "Influences of membrane mimetic environments on membrane protein structures," *Annual review of biophysics*, vol. 42, pp. 361–392, 2013.

[170] S. Lee, A. Mao, S. Bhattacharya, N. Robertson, R. Grisshammer, C. G. Tate, and N. Vaidehi, "How do short chain nonionic detergents destabilize G-protein-coupled receptors?," *Journal of the American Chemical Society*, vol. 138, no. 47, pp. 15425–15433, 2016.

[171] M. Zoonens and J.-L. Popot, "Amphipols for each season," *The Journal of membrane biology*, vol. 247, pp. 759–796, 2014.

[172] J.-L. Popot, T. Althoff, D. Bagnard, J.-L. Banères, P. Bazzacco, E. Billon-Denis, L. J. Catoire, P. Champeil, D. Charvolin, M. J. Cocco, *et al.*, "Amphipols from A to Z," *Annual review of biophysics*, vol. 40, pp. 379–408, 2011.

[173] P. Ram and J. Prestegard, "Magnetic field induced ordering of bile salt/phospholipid micelles: new media for NMR structural investigations," *Biochimica et Biophysica Acta (BBA)-Biomembranes*, vol. 940, no. 2, pp. 289–294, 1988.

[174] C. R. Sanders and G. C. Landis, "Reconstitution of membrane proteins into lipid-rich bilayered mixed micelles for NMR studies," *Biochemistry*, vol. 34, no. 12, pp. 4030–4040, 1995.

[175] E. K. Tiburu, D. M. Moton, and G. A. Lorigan, "Development of magnetically aligned phospholipid bilayers in mixtures of palmitoylstearoylphosphatidylcholine and dihexanoylphosphatidylcholine by solid-state NMR spectroscopy," *Biochimica Et Biophysica Acta (BBA)-Biomembranes*, vol. 1512, no. 2, pp. 206–214, 2001.

[176] T. B. Cardon, E. K. Tiburu, A. Padmanabhan, K. P. Howard, and G. A. Lorigan, "Magnetically aligned phospholipid bilayers at the parallel and perpendicular orientations for X-band spin-label EPR studies," *Journal of the American Chemical Society*, vol. 123, no. 12, pp. 2913–2914, 2001.

[177] B.-B. Lucyanna, R. Gelen, C. Merce, R. Laia, L.-I. Carmen, d. l. M. Alfons, and L. Olga, "Structural versatility of bicellar systems and their possibilities as colloidal carriers," *Pharmaceutics*, vol. 3, no. 3, pp. 636–664, 2011.

[178] G. E. Fanucci, J. Y. Lee, and D. S. Cafiso, "Membrane mimetic environments alter the conformation of the outer membrane protein BtuB," *Journal of the American Chemical Society*, vol. 125, no. 46, pp. 13932–13933, 2003.

[179] A. Gautier, H. R. Mott, M. J. Bostock, J. P. Kirkpatrick, and D. Nietlispach, "Structure determination of the seven-helix transmembrane receptor sensory rhodopsin II by solution NMR spectroscopy," *Nature structural & molecular biology*, vol. 17, no. 6, pp. 768–774, 2010.

[180] E. A. Morrison, G. T. DeKoster, S. Dutta, R. Vafabakhsh, M. W. Clarkson, A. Bahl, D. Kern, T. Ha, and K. A. Henzler-Wildman, "Antiparallel EmrE exports drugs by exchanging between asymmetric structures," *Nature*, vol. 481, no. 7379, pp. 45–50, 2012.

[181] E. V. Bocharov, M. L. Mayzel, P. E. Volynsky, M. V. Goncharuk, Y. S. Ermolyuk, A. A. Schulga, E. O. Artemenko, R. G. Efremov, and A. S. Arseniev, "Spatial structure and pH-dependent conformational diversity of dimeric transmembrane domain of the receptor tyrosine kinase EphA1," *Journal of Biological Chemistry*, vol. 283, no. 43, pp. 29385–29395, 2008.

[182] V. Yeh, A. Goode, and B. B. Bonev, "Membrane protein structure determination and characterisation by solution and solid-state NMR," *Biology*, vol. 9, no. 11, p. 396, 2020.

[183] K. R. Vinothkumar, "Structure of rhomboid protease in a lipid environment," *Journal of molecular biology*, vol. 407, no. 2, pp. 232–247, 2011.

[184] R. Ujwal, D. Cascio, J.-P. Colletier, S. Faham, J. Zhang, L. Toro, P. Ping, and J. Abramson, "The crystal structure of mouse VDAC1 at 2.3 Å resolution reveals mechanistic insights into metabolite gating," *Proceedings of the National Academy of Sciences*, vol. 105, no. 46, pp. 17742–17747, 2008.

[185] S. G. Rasmussen, H.-J. Choi, D. M. Rosenbaum, T. S. Kobilka, F. S. Thian, P. C. Edwards, M. Burghammer, V. R. Ratnala, R. Sanishvili, R. F. Fischetti, *et al.*, "Crystal structure of the human $\beta2$ adrenergic G-protein-coupled receptor," *Nature*, vol. 450, no. 7168, pp. 383–387, 2007.

[186] T. H. Bayburt, Y. V. Grinkova, and S. G. Sligar, "Self-assembly of discoidal phospholipid bilayer nanoparticles with membrane scaffold proteins," *Nano letters*, vol. 2, no. 8, pp. 853–856, 2002.

[187] T. Ritchie, Y. Grinkova, T. Bayburt, I. Denisov, J. Zolnerciks, W. Atkins, and S. Sligar, "Reconstitution of membrane proteins in phospholipid bilayer nanodiscs," *Methods in enzymology*, vol. 464, pp. 211–231, 2009.

[188] S. Ly, F. Bourguet, N. O. Fischer, E. Y. Lau, M. A. Coleman, and T. A. Laurence, "Quantifying interactions of a membrane protein embedded in a lipid nanodisc using fluorescence correlation spectroscopy," *Biophysical journal*, vol. 106, no. 2, pp. L05–L08, 2014.

[189] K. Malhotra and N. N. Alder, "Advances in the use of nanoscale bilayers to study membrane protein structure and function," *Biotechnology and Genetic Engineering Reviews*, vol. 30, no. 1, pp. 79–93, 2014.

[190] R. G. Efremov, C. Gatsogiannis, and S. Raunser, "Lipid nanodiscs as a tool for high-resolution structure determination of membrane proteins by single-particle cryo-EM," in *Methods in enzymology*, vol. 594, pp. 1–30, Elsevier, 2017.

[191] V. Kalienkova, C. Alvadia, V. Clerico Mosina, and C. Paulino, "Single-particle cryo-EM of membrane proteins in lipid nanodiscs," *Expression, Purification, and Structural Biology of Membrane Proteins*, pp. 245–273, 2020.

[192] Y. Gao, E. Cao, D. Julius, and Y. Cheng, "TRPV1 structures in nanodiscs reveal mechanisms of ligand and lipid action," *Nature*, vol. 534, no. 7607, pp. 347–351, 2016.

[193] I. G. Denisov and S. G. Sligar, "Nanodiscs in membrane biochemistry and biophysics," *Chemical reviews*, vol. 117, no. 6, pp. 4669–4713, 2017.

[194] J. M. Gluck, M. Wittlich, S. Feuerstein, S. Hoffmann, D. Willbold, and B. W. Koenig, "Integral membrane proteins in nanodiscs can be studied by solution nmr spectroscopy," *Journal of the American Chemical Society*, vol. 131, no. 34, pp. 12060–12061, 2009.

[195] E. R. Georgieva, "Nanoscale lipid membrane mimetics in spin-labeling and electron paramagnetic resonance spectroscopy studies of protein structure and function," *Nanotechnology Reviews*, vol. 6, no. 1, pp. 75–92, 2017.

[196] A. Kedrov, S. Wickles, A. H. Crevenna, E. O. van der Sluis, R. Buschauer, O. Berninghausen, D. C. Lamb, and R. Beckmann, "Structural dynamics of the YidC: ribosome complex during membrane protein biogenesis," *Cell reports*, vol. 17, no. 11, pp. 2943–2954, 2016.

[197] A. Nath, A. J. Trexler, P. Koo, A. D. Miranker, W. M. Atkins, and E. Rhoades, "Single-molecule fluorescence spectroscopy using phospholipid bilayer nanodiscs," in *Methods in enzymology*, vol. 472, pp. 89–117, Elsevier, 2010.

[198] A. Nath, P. K. Koo, E. Rhoades, and W. M. Atkins, "Allosteric effects on substrate dissociation from cytochrome P450 3A4 in nanodiscs observed by ensemble and single-molecule fluorescence spectroscopy," *Journal of the American Chemical Society*, vol. 130, no. 47, pp. 15746–15747, 2008.

[199] J. Frauenfeld, R. Löving, J.-P. Armache, A. F. Sonnen, F. Guettou, P. Moberg, L. Zhu, C. Jegerschöld, A. Flayhan, J. A. Briggs, *et al.*, "A saposin-lipoprotein nanoparticle system for membrane proteins," *Nature methods*, vol. 13, no. 4, pp. 345–351, 2016.

[200] A. Flayhan, H. D. Mertens, Y. Ural-Blimke, M. M. Molledo, D. I. Svergun, and C. Löw, "Saposin lipid nanoparticles: A highly versatile and modular tool for membrane protein research," *Structure*, vol. 26, no. 2, pp. 345–355, 2018.

[201] P. Lloris-Garcerá, S. Klinter, L. Chen, M. J. Skynner, R. Löving, and J. Frauenfeld, "DirectMX–One-Step reconstitution of membrane proteins from crude cell membranes into Salipro nanoparticles," *Frontiers in Bioengineering and Biotechnology*, vol. 8, p. 215, 2020.

[202] K. Kanonenberg, S. H. Smits, and L. Schmitt, "Functional reconstitution of HlyB, a type I secretion ABC transporter, in saposin-A nanoparticles," *Scientific Reports*, vol. 9, no. 1, pp. 1–12, 2019.

[203] N. X. Nguyen, J.-P. Armache, C. Lee, Y. Yang, W. Zeng, V. K. Mootha, Y. Cheng, X.-c. Bai, and Y. Jiang, "Cryo-EM structure of a fungal mitochondrial calcium uniporter," *Nature*, vol. 559, no. 7715, pp. 570–574, 2018.

[204] A. F. Kintzer, E. M. Green, P. K. Dominik, M. Bridges, J.-P. Armache, D. Deneka, S. S. Kim, W. Hubbell, A. A. Kossiakoff, Y. Cheng, *et al.*, "Structural basis for activation of voltage sensor domains in an ion channel TPC1," *Proceedings of the National Academy of Sciences*, vol. 115, no. 39, pp. E9095–E9104, 2018.

[205] M. L. Carlson, J. W. Young, Z. Zhao, L. Fabre, D. Jun, J. Li, J. Li, H. S. Dhupar, I. Wason, A. T. Mills, *et al.*, "The Peptidisc, a simple method for stabilizing membrane proteins in detergent-free solution," *Elife*, vol. 7, p. e34085, 2018.

[206] G. Angiulli, H. S. Dhupar, H. Suzuki, I. S. Wason, F. Duong Van Hoa, and T. Walz, "New approach for membrane protein reconstitution into peptidiscs and basis for their adaptability to different proteins," *Elife*, vol. 9, p. e53530, 2020.

[207] T. J. Knowles, R. Finka, C. Smith, Y.-P. Lin, T. Dafforn, and M. Overduin, "Membrane proteins solubilized intact in lipid containing nanoparticles bounded by styrene maleic acid copolymer," *Journal of the American Chemical Society*, vol. 131, no. 22, pp. 7484–7485, 2009.

[208] S. C. Lee, T. J. Knowles, V. L. Postis, M. Jamshad, R. A. Parslow, Y.-P. Lin, A. Goldman, P. Sridhar, M. Overduin, S. P. Muench, *et al.*, "A method for detergent-free isolation of membrane proteins in their local lipid environment," *Nature protocols*, vol. 11, no. 7, pp. 1149–1162, 2016.

[209] A. O. Oluwole, B. Danielczak, A. Meister, J. O. Babalola, C. Vargas, and S. Keller, "Solubilization of membrane proteins into functional lipid-bilayer nanodiscs using a diisobutylene/maleic acid copolymer," *Angewandte Chemie International Edition*, vol. 56, no. 7, pp. 1919–1924, 2017.

[210] A. O. Oluwole, J. Klingler, B. Danielczak, J. O. Babalola, C. Vargas, G. Pabst, and S. Keller, "Formation of lipid-bilayer nanodiscs by diisobutylene/maleic acid (DIBMA) copolymer," *Langmuir*, vol. 33, no. 50, pp. 14378–14388, 2017.

[211] B. Danielczak, A. Meister, and S. Keller, "Influence of Mg2+ and Ca2+ on nanodisc formation by diisobutylene/maleic acid (DIBMA) copolymer," *Chemistry and physics of lipids*, vol. 221, pp. 30–38, 2019.

[212] B. Danielczak, M. Rasche, J. Lenz, E. P. Patallo, S. Weyrauch, F. Mahler, M. T. Agbadaola, A. Meister, J. O. Babalola, C. Vargas, *et al.*, "A bioinspired glycopolymer for capturing membrane proteins in native-like lipid-bilayer nanodiscs," *Nanoscale*, vol. 14, no. 5, pp. 1855–1867, 2022.

[213] A. D. Bangham and R. Horne, "Negative staining of phospholipids and their structural modification by surface-active agents as observed in the electron microscope," *Journal of molecular biology*, vol. 8, no. 5, pp. 660–IN10, 1964.

[214] A. Akbarzadeh, R. Rezaei-Sadabady, S. Davaran, S. W. Joo, N. Zarghami, Y. Hanifehpour, M. Samiei, M. Kouhi, and K. Nejati-Koshki, "Liposome: classification, preparation, and applications," *Nanoscale research letters*, vol. 8, no. 1, pp. 1–9, 2013.

[215] K. D. Hickey, M. M. Buhr, *et al.*, "Lipid bilayer composition affects transmembrane protein orientation and function," *Journal of lipids*, vol. 2011, 2011.

[216] O. G. Mouritsen, "Model answers to lipid membrane questions," *Cold Spring Harbor perspectives in biology*, vol. 3, no. 9, p. a004622, 2011.

[217] A. J. Jones, J. N. Blaza, H. R. Bridges, B. May, A. L. Moore, and J. Hirst, "A Self-Assembled respiratory chain that catalyzes NADH oxidation by Ubiquinone-10 cycling between Complex I and the Alternative Oxidase," *Angewandte Chemie International Edition*, vol. 55, no. 2, pp. 728–731, 2016.

[218] R. Skrzypek, S. Iqbal, and R. Callaghan, "Methods of reconstitution to investigate membrane protein function," *Methods*, vol. 147, pp. 126–141, 2018.

[219] M. Scalise, L. Pochini, N. Giangregorio, A. Tonazzi, and C. Indiveri, "Proteoliposomes as tool for assaying membrane transporter functions and interactions with xenobiotics," *Pharmaceutics*, vol. 5, no. 3, pp. 472–497, 2013.

[220] Z. L. Johnson and S.-Y. Lee, "Liposome reconstitution and transport assay for recombinant transporters," in *Methods in Enzymology*, vol. 556, pp. 373–383, Elsevier, 2015.

[221] J. Kreiter, E. Beitz, and E. E. Pohl, "A Fluorescence-based method to measure ADP/ATP exchange of recombinant adenine nucleotide translocase in liposomes," *Biomolecules*, vol. 10, no. 5, p. 685, 2020.

[222] J. De Keyzer, C. Van Der Does, and A. J. Driessen, "Kinetic analysis of the translocation of fluorescent precursor proteins into Escherichia coli membrane vesicles," *Journal of Biological Chemistry*, vol. 277, no. 48, pp. 46059–46065, 2002.

[223] A. Kedrov, I. Kusters, V. V. Krasnikov, and A. J. Driessen, "A single copy of SecYEG is sufficient for preprotein translocation," *The EMBO journal*, vol. 30, no. 21, pp. 4387–4397, 2011.

[224] R. C. Hresko, T. E. Kraft, A. Quigley, E. P. Carpenter, and P. W. Hruz, "Mammalian glucose transporter activity is dependent upon anionic and conical phospholipids," *Journal of Biological Chemistry*, vol. 291, no. 33, pp. 17271–17282, 2016.

[225] H. F. Hofbauer, M. Gecht, S. C. Fischer, A. Seybert, A. S. Frangakis, E. H. Stelzer, R. Covino, G. Hummer, and R. Ernst, "The molecular recognition of phosphatidic acid by an amphipathic helix in Opi1," *Journal of Cell Biology*, vol. 217, no. 9, pp. 3109–3126, 2018.

[226] D. L. Stokes, W. J. Rice, M. Hu, C. Kim, and I. Ubarretxena-Belandia, "Two-dimensional crystallization of integral membrane proteins for electron crystallography," *Membrane Protein Structure Determination: Methods and Protocols*, pp. 187–205, 2010.

[227] C. Jiko, K. M. Davies, K. Shinzawa-Itoh, K. Tani, S. Maeda, D. J. Mills, T. Tsukihara, Y. Fujiyoshi, W. Kühlbrandt, and C. Gerle, "Bovine F_1F_o ATP synthase monomers bend the lipid bilayer in 2D membrane crystals," *Elife*, vol. 4, p. e06119, 2015.

[228] M. K. Doeven, J. H. Folgering, V. Krasnikov, E. R. Geertsma, G. van den Bogaart, and B. Poolman, "Distribution, lateral mobility and function of membrane proteins incorporated into giant unilamellar vesicles," *Biophysical journal*, vol. 88, no. 2, pp. 1134–1142, 2005.

[229] T. Eierhoff, B. Bastian, R. Thuenauer, J. Madl, A. Audfray, S. Aigal, S. Juillot, G. E. Rydell, S. Müller, S. de Bentzmann, *et al.*, "A lipid zipper triggers bacterial invasion," *Proceedings of the National Academy of Sciences*, vol. 111, no. 35, pp. 12895–12900, 2014.

[230] D. Merkle, N. Kahya, and P. Schwille, "Reconstitution and anchoring of cytoskeleton inside giant unilamellar vesicles," *ChemBioChem*, vol. 9, no. 16, pp. 2673–2681, 2008.

[231] S. Kohyama, A. Merino-Salomón, and P. Schwille, "In vitro assembly, positioning and contraction of a division ring in minimal cells," *Nature Communications*, vol. 13, no. 1, p. 6098, 2022.

[232] H. M. McConnell, T. H. Watts, R. Weis, and A. A. Brian, "Supported planar membranes in studies of cell-cell recognition in the immune system," *Biochimica et Biophysica Acta (BBA)-Reviews on Biomembranes*, vol. 864, no. 1, pp. 95–106, 1986.

[233] T. H. Watts, A. A. Brian, J. W. Kappler, P. Marrack, and H. M. McConnell, "Antigen presentation by supported planar membranes containing affinity-purified I-Ad.," *Proceedings of the National Academy of Sciences*, vol. 81, no. 23, pp. 7564–7568, 1984.

[234] A. Hughes, S. Roser, M. Gerstenberg, A. Goldar, B. Stidder, R. Feidenhans'l, and J. Bradshaw, "Phase behavior of DMPC free supported bilayers studied by neutron reflectivity," *Langmuir*, vol. 18, no. 21, pp. 8161–8171, 2002.

[235] L. A. Clifton, M. W. Skoda, E. L. Daulton, A. V. Hughes, A. P. Le Brun, J. H. Lakey, and S. A. Holt, "Asymmetric phospholipid: lipopolysaccharide bilayers; a Gram-negative bacterial outer membrane mimic," *Journal of the royal society interface*, vol. 10, no. 89, p. 20130810, 2013.

[236] V. Rondelli, G. Fragneto, S. Motta, E. Del Favero, and L. Cantù, "Reflectivity from floating bilayers: can we keep the structural asymmetry?," in *Journal of Physics: conference series*, vol. 340, p. 012083, IOP Publishing, 2012.

[237] A. A. Brian and H. M. McConnell, "Allogeneic stimulation of cytotoxic T cells by supported planar membranes.," *Proceedings of the National Academy of Sciences*, vol. 81, no. 19, pp. 6159–6163, 1984.

[238] D. Axelrod, D. Koppel, J. Schlessinger, E. Elson, and W. W. Webb, "Mobility measurement by analysis of fluorescence photobleaching recovery kinetics," *Biophysical journal*, vol. 16, no. 9, pp. 1055–1069, 1976.

[239] N.-J. Cho, C. W. Frank, B. Kasemo, and F. Höök, "Quartz crystal microbalance with dissipation monitoring of supported lipid bilayers on various substrates," *Nature protocols*, vol. 5, no. 6, pp. 1096–1106, 2010.

[240] A. Matysik and R. S. Kraut, "Preparation of mica supported lipid bilayers for high resolution optical microscopy imaging," *JoVE (Journal of Visualized Experiments)*, no. 88, p. e52054, 2014.

[241] P. A. Nguyen, C. M. Field, A. C. Groen, T. J. Mitchison, and M. Loose, "Using supported bilayers to study the spatiotemporal organization of membrane-bound proteins," in *Methods in cell biology*, vol. 128, pp. 223–241, Elsevier, 2015.

[242] L. K. Tamm and H. M. McConnell, "Supported phospholipid bilayers," *Biophysical journal*, vol. 47, no. 1, pp. 105–113, 1985.

[243] H. H. Nguyen, J. Park, S. Kang, and M. Kim, "Surface plasmon resonance: a versatile technique for biosensor applications," *Sensors*, vol. 15, no. 5, pp. 10481–10510, 2015.

[244] V. Hodnik and G. Anderluh, "Capture of intact liposomes on biacore sensor chips for protein–membrane interaction studies," *Surface plasmon resonance: methods and protocols*, pp. 201–211, 2010.

[245] M. Beseničar, P. Maček, J. H. Lakey, and G. Anderluh, "Surface plasmon resonance in protein–membrane interactions," *Chemistry and physics of lipids*, vol. 141, no. 1-2, pp. 169–178, 2006.

[246] V. Hodnik and G. Anderluh, "Surface plasmon resonance for measuring interactions of proteins with lipid membranes," *Lipid-Protein Interactions: Methods and Protocols*, pp. 23–36, 2013.

[247] A. Bavdek, N. O. Gekara, D. Priselac, I. Gutiérrez Aguirre, A. Darji, T. Chakraborty, P. Macek, J. H. Lakey, S. Weiss, and G. Anderluh, "Sterol and pH interdependence in the binding, oligomerization, and pore formation of Listeriolysin O," *Biochemistry*, vol. 46, no. 14, pp. 4425–4437, 2007.

[248] A. Bahloul, V. Michel, J.-P. Hardelin, S. Nouaille, S. Hoos, A. Houdusse, P. England, and C. Petit, "Cadherin-23, myosin VIIa and harmonin, encoded by Usher syndrome type I genes, form a ternary complex and interact with membrane phospholipids," *Human molecular genetics*, vol. 19, no. 18, pp. 3557–3565, 2010.

[249] M. Hekman, S. Albert, A. Galmiche, U. E. Rennefahrt, J. Fueller, A. Fischer, D. Puehringer, S. Wiese, and U. R. Rapp, "Reversible membrane interaction of BAD requires two C-terminal lipid binding domains in conjunction with 14-3-3 protein binding," *Journal of Biological Chemistry*, vol. 281, no. 25, pp. 17321–17336, 2006.

[250] S. Locatelli-Hoops, N. Remmel, R. Klingenstein, B. Breiden, M. Rossocha, M. Schoeniger, C. Koenigs, W. Saenger, and K. Sandhoff, "Saposin A mobilizes lipids from low cholesterol and high bis (monoacylglycerol) phosphate-containing membranes: patient variant Saposin A lacks lipid extraction capacity," *Journal of Biological Chemistry*, vol. 281, no. 43, pp. 32451–32460, 2006.

[251] T. Sugiki, H. Takahashi, M. Nagasu, K. Hanada, and I. Shimada, "Real-time assay method of lipid extraction activity," *Analytical biochemistry*, vol. 399, no. 2, pp. 162–167, 2010.

[252] T. Praper, M. P. Besenicar, H. Istinic, Z. Podlesek, S. S. Metkar, C. J. Froelich, and G. Anderluh, "Human perforin permeabilizing activity, but not binding to lipid membranes, is affected by pH," *Molecular immunology*, vol. 47, no. 15, pp. 2492–2504, 2010.

[253] J. de Keyzer, C. van der Does, T. G. Kloosterman, and A. J. Driessen, "Direct demonstration of ATP-dependent release of SecA from a translocating preprotein by surface plasmon resonance," *Journal of Biological Chemistry*, vol. 278, no. 32, pp. 29581–29586, 2003.

[254] Z. C. Wu, J. de Keyzer, A. Kedrov, and A. J. Driessen, "Competitive binding of the SecA ATPase and ribosomes to the SecYEG translocon," *Journal of Biological Chemistry*, vol. 287, no. 11, pp. 7885–7895, 2012.

[255] T. K. Lind and M. Cárdenas, "Understanding the formation of supported lipid bilayers via vesicle fusion-A case that exemplifies the need for the complementary method approach," *Biointerphases*, vol. 11, no. 2, p. 020801, 2016.

[256] C. Keller and B. Kasemo, "Surface specific kinetics of lipid vesicle adsorption measured with a quartz crystal microbalance," *Biophysical journal*, vol. 75, no. 3, pp. 1397–1402, 1998.

[257] M. Rodahl, F. Höök, A. Krozer, P. Brzezinski, and B. Kasemo, "Quartz crystal microbalance setup for frequency and Q-factor measurements in gaseous and liquid environments," *Review of Scientific Instruments*, vol. 66, no. 7, pp. 3924–3930, 1995.

[258] B. Seantier, C. Breffa, O. Felix, and G. Decher, "Dissipation-enhanced quartz crystal microbalance studies on the experimental parameters controlling the formation of supported lipid bilayers," *The Journal of Physical Chemistry B*, vol. 109, no. 46, pp. 21755–21765, 2005.

[259] A. Mechler, S. Praporski, K. Atmuri, M. Boland, F. Separovic, and L. L. Martin, "Specific and selective peptide-membrane interactions revealed using quartz crystal microbalance," *Biophysical Journal*, vol. 93, no. 11, pp. 3907–3916, 2007.

[260] K. Glasmästar, C. Larsson, F. Höök, and B. Kasemo, "Protein adsorption on supported phospholipid bilayers," *Journal of colloid and interface science*, vol. 246, no. 1, pp. 40–47, 2002.

[261] G. E. Rydell, A. B. Dahlin, F. Höök, and G. Larson, "QCM-D studies of human norovirus VLPs binding to glycosphingolipids in supported lipid bilayers reveal strain-specific characteristics," *Glycobiology*, vol. 19, no. 11, pp. 1176–1184, 2009.

[262] J. Kotarek and M. Moss, "Impact of phospholipid bilayer saturation on amyloid-β protein aggregation intermediate growth: A quartz crystal microbalance analysis," *Analytical biochemistry*, vol. 399, no. 1, pp. 30–38, 2010.

[263] K. F. Wang, R. Nagarajan, C. M. Mello, and T. A. Camesano, "Characterization of supported lipid bilayer disruption by chrysophsin-3 using QCM-D," *The Journal of Physical Chemistry B*, vol. 115, no. 51, pp. 15228–15235, 2011.

[264] K. F. Wang, R. Nagarajan, and T. A. Camesano, "Antimicrobial peptide alamethicin insertion into lipid bilayer: A QCM-D exploration," *Colloids and Surfaces B: Biointerfaces*, vol. 116, pp. 472–481, 2014.

[265] K.-C. Liu, H. Pace, E. Larsson, S. Hossain, A. Kabedev, A. Shukla, V. Jerschabek, J. Mohan, C. A. Bergström, M. Bally, *et al.*, "Membrane insertion mechanism of the caveola coat protein Cavin1," *Proceedings of the National Academy of Sciences*, vol. 119, no. 25, p. e2202295119, 2022.

[266] L. A. Clifton, "Unravelling the structural complexity of protein–lipid interactions with neutron reflectometry," *Biochemical Society Transactions*, vol. 49, no. 4, pp. 1537–1546, 2021.

[267] H. P. Wacklin, "Neutron reflection from supported lipid membranes," *Current Opinion in Colloid & Interface Science*, vol. 15, no. 6, pp. 445–454, 2010.

[268] A. M. Whited and P. S.-H. Park, "Atomic force microscopy: a multifaceted tool to study membrane proteins and their interactions with ligands," *Biochimica et Biophysica Acta (BBA)-Biomembranes*, vol. 1838, no. 1, pp. 56–68, 2014.

[269] D. Pogoryelov, C. Reichen, A. L. Klyszejko, R. Brunisholz, D. J. Muller, P. Dimroth, and T. Meier, "The oligomeric state of c rings from cyanobacterial F-ATP synthases varies from 13 to 15," *Journal of bacteriology*, vol. 189, no. 16, pp. 5895–5902, 2007.

[270] R. R. Sanganna Gari, K. Chattrakun, B. P. Marsh, C. Mao, N. Chada, L. L. Randall, and G. M. King, "Direct visualization of the E. coli Sec translocase engaging precursor proteins in lipid bilayers," *Science Advances*, vol. 5, no. 6, p. eaav9404, 2019.

[271] T. Serdiuk, S. A. Mari, and D. J. Müller, "Pull-and-paste of single transmembrane proteins," *Nano letters*, vol. 17, no. 7, pp. 4478–4488, 2017.

[272] T. Serdiuk, A. Steudle, S. A. Mari, S. Manioglu, H. R. Kaback, A. Kuhn, and D. J. Müller, "Insertion and folding pathways of single membrane proteins guided by translocases and insertases," *Science advances*, vol. 5, no. 1, p. eaau6824, 2019.

[273] S. Wilmes, M. Hafer, J. Vuorio, J. A. Tucker, H. Winkelmann, S. Löchte, T. A. Stanly, K. D. Pulgar Prieto, C. Poojari, V. Sharma, *et al.*, "Mechanism of homodimeric cytokine receptor activation and dysregulation by oncogenic mutations," *Science*, vol. 367, no. 6478, pp. 643–652, 2020.

[274] O. Vadas, M. Jenkins, G. Dornan, and J. Burke, "Using hydrogen–deuterium exchange mass spectrometry to examine protein–membrane interactions," *Methods in enzymology*, vol. 583, pp. 143–172, 2017.

Chapter 2

Aim

The bacterial Sec translocon is responsible for the post-translational transport of secretory, periplasmic, and outer membrane proteins as well as the co-translational insertion of membrane proteins into the cytoplasmic membrane of bacteria. This work mainly aimed to combine different membrane mimetic systems with the biochemical and biophysical characterization of the post-translational and co-translational pathways of the Sec translocon.

The first part of the work focussed on the effect of the membrane composition on the protein transport activity of SecYEG: SecA translocon. It was previously reported that anionic lipids are essential for the activity of the Sec translocon. This has been linked to the N-terminal helix of SecA, which has positively charged residues that interact with the membrane's anionic lipids. Depleting anionic lipids from the membrane or deleting the N terminal helix of SecA abolishes the membrane binding ability of SecA as well as protein transport. In bacteria, phosphatidylglycerol and cardiolipin are the major anionic lipids, however, there have been strong discrepancies about the stimulatory role of cardiolipin. The effect of acyl chain composition on protein transport has never been investigated, even though the acyl chain composition in bacterial membranes changes substantially between different growth, temperature, and environmental conditions. Therefore, in this work, the effect of cardiolipin was investigated and compared to phosphatidyl glycerol. Moreover, the effect of the acyl chain composition by varying the degree of mono-unsaturated fatty acids was investigated. To that aim, different membrane mimetics (liposomes and nanodiscs) with different lipid compositions were generated and compared for both SecA membrane binding and protein transport using a variety of biochemical and biophysical tools.

The second part of the work aimed to study the role of the membrane binding of SecA on protein transport. SecA is a peripheral membrane protein that exists mostly in the membrane based on a recent study. It was also previously reported that SecA initially binds the membrane and undergoes 2D dimensional diffusion to find the channel, SecYEG. Therefore, the aim was to elucidate how SecA binds to the membrane and its effect on protein transport. It is controversial which domains of SecA other than the N-terminal helix interact with the membrane. Therefore, identifying the exact domain of SecA that contact the membrane was the first goal in this part. Afterward, mutations were introduced within the N-terminal helix of SecA to change the helix's hydrophobic and hydrophilic properties and examine how that affects both SecA: membrane binding and protein transport.

The membrane composition of the cytoplasmic membrane of bacteria varies substantially

across different bacterial species from gram-negative to gram-positive to extremophilic bacteria. Consequently, it was argued that the N-terminal helix of SecA homologs might have been evolutionarily tuned to interact with different membranes. Therefore, the membrane binding of different SecA homologs was characterized and correlated to the membrane composition of the respective species.

In the third part of the work, the membrane channel dynamics, SecYEG was studied in supported lipid bilayers using single-molecule fluorescence microscopy. The oligomeric state of SecYEG was extensively disputed, consequently, the oligomeric state of the translocon was addressed in this study. Moreover, the lateral mobility of the translocon was measured and monitored how it change when in a complex with SecA or ribosomes nascent chain complex (RNC).

Membrane proteins destined to be inserted into the membrane are targeted co-translationally to the membrane, where they get inserted via SecYEG or the membrane insertase, YidC, or both of them. The exact selection mechanism for the insertion machinery is not yet clear. Moreover, the exact path of the nascent chain from the ribosome exit tunnel to the membrane is not fully resolved. Therefore, the final aim of this work was to establish a platform, where the co-translational assembly of the membrane protein insertion pathway could be reconstituted in membrane mimetic systems. Cell-free protein synthesis was used to allow for the co-translation assembly of the RNCs with the insertion machinery for structural studies. This nicely imitates the continuous process and the native conditions that happen *in vivo*. Different nanodisc types were used as membrane mimetics like membrane scaffold protein-based nanodiscs and maleic acid copolymers-based nanodiscs. They provide the lipid bilayer for the nascent chain to be inserted which further simulates the *in vivo* condition of membrane protein insertion into the membrane. The established platform can be employed for nascent chains with different lengths to get snapshots of different stages of the membrane protein insertion pathway.

Chapter 3

Unsaturated fatty acids augment protein transport via the SecA:SecYEG translocon

Authors: Michael Kamel, Maryna Löwe, Stephan Schott-Verdugo, Holger
                    Gohlke and Alexej Kedrov.

Own work: 70%.
Contribution: Michael Kamel performed all biochemical and fluorescence-based
                    measurements.

                    Michael Kamel and Maryna Löwe performed SPR experiments.

                    Maryna Löwe performed QCM experiments.

                    Stephan Schot-Verdugo and Holger Gohlke performed MD simu-
                    lations.

                    Michael Kamel and Alexej Kedrov analyzed and interpreted the
                    data in contribution with Stephan Schot-Verdugo and Holger
                    Gohlke .

                    All authors contributed to writing and editing the manuscript.

Unsaturated fatty acids augment protein transport via the SecA:SecYEG translocon

Michael Kamel[1], Maryna Löwe[1], Stephan Schott-Verdugo[2,3] (iD), Holger Gohlke[2,3] and Alexej Kedrov[1] (iD)

1 Synthetic Membrane Systems, Institute for Biochemistry, Heinrich Heine University Düsseldorf, Germany
2 Institute for Pharmaceutical and Medicinal Chemistry, Heinrich Heine University Düsseldorf, Germany
3 John von Neumann Institute for Computing (NIC), Jülich Supercomputing Centre (JSC), Institute of Biological Information Processing (IBI-7: Structural Bioinformatics), and Institute of Bio- and Geosciences (IBG-4: Bioinformatics), Forschungszentrum Jülich GmbH, Germany

The translocon SecYEG and the associated ATPase SecA form the primary protein secretion system in the cytoplasmic membrane of bacteria. The secretion is essentially dependent on the surrounding lipids, but the mechanistic understanding of their role in SecA : SecYEG activity is sparse. Here, we reveal that the unsaturated fatty acids (UFAs) of the membrane phospholipids, including tetraoleoyl-cardiolipin, stimulate SecA : SecYEG-mediated protein translocation up to ten-fold. Biophysical analysis and molecular dynamics simulations show that UFAs increase the area per lipid and cause loose packing of lipid head groups, where the N-terminal amphipathic helix of SecA docks. While UFAs do not affect the translocon folding, they promote SecA binding to the membrane, and the effect is enhanced up to fivefold at elevated ionic strength. Tight SecA : lipid interactions convert into the augmented translocation. Our results identify the fatty acid structure as a notable factor in SecA : SecYEG activity, which may be crucial for protein secretion in bacteria, which actively change their membrane composition in response to their habitat.

Introduction

Protein transport across the cytoplasmic bacterial membrane is an essential step in biogenesis of cell envelope and secretory proteins [1]. Most of these proteins cross the membrane post-translationally as unfolded precursors (preproteins). The preproteins with cleavable N-terminal hydrophobic signal sequences are picked up by holdase chaperones, such as SecB, and delivered to the Sec machinery (Fig. 1A). The core of the Sec machinery consists of the heterotrimeric membrane-embedded channel, or *translocon*, SecYEG, and the membrane-associated ATPase SecA. The translocon builds a narrow transmembrane conduit for the unfolded preproteins, and it is primed by insertion of the signal sequence at the translocon : lipid interface. The activity of the SecYEG-bound ATPase SecA provides the energy for directional transport of the preprotein through the translocon [2].

The crucial role of the lipid environment for Sec-mediated protein transport has been generally acknowledged, with a primary focus on electrostatic interactions at the membrane interface [3–6]. The anionic lipids, mainly phosphatidylglycerol (PG) and cardiolipin (CL), mediate anchoring of SecA at the membrane interface even in the absence of SecYEG [3,7], as they interact with the basic residues within the N-terminal helix of the ATPase. In contrast to the lipid head groups, only limited insights on the effect of the constituting fatty acids are available. Initial *in vitro* experiments revealed that dioleoyl-phosphatidylethanolamine (DOPE) stimulates preprotein translocation [5]. The effect was attributed to the conical shape of DOPE molecules built of two mono-unsaturated fatty acids (UFAs) and the small head group, but the mechanistic explanation of the stimulation remained obscure. This limited knowledge contrasts the essential complexity of cellular membranes, where the diversity of fatty acids that constitute lipids arises from variations in their length and the unsaturation level. Furthermore, cells regulate the UFA content in response to changing environmental factors, the habitat style and the growth phase, so the ratio of UFAs to saturated fatty acids in the inner membrane of *E. coli* changes from 1 : 1 to 2 : 1 when the growth temperature is reduced to 17 °C [8,9]. Several membrane-associated protein complexes in bacteria and eukaryotes appear to be sensitive to the UFA content, having an effect on signalling reactions, protein folding and degradation [10–12].

Here, we demonstrate for the first time that changes in the UFA content in phospholipids have a notable effect on SecA : SecYEG-mediated protein translocation. Increasing the *cis*-UFA content from 50 to 100 mol % within the fluid phase membrane leads to a fivefold increase in the translocon activity. Biophysical analysis and all-atom molecular dynamics simulations show that the structure of the fatty acids does not affect SecYEG stability, but UFAs determine a loosely packed membrane interface and facilitate apolar SecA : lipid interactions. The stimulated association of the ATPase with the lipid membrane leads to the augmented activity of the SecA : SecYEG complex. We further demonstrate that the UFA-enriched tetraoleoyl-CL stimulates the translocation up to ten-fold, and the stimulation does not involve oligomerization of SecYEG. Our results reveal that the organization of the lipid membrane plays a prominent role in the regulation of protein translocation and suggest that the regulation may be employed upon the bacterial adaptation to various habitat conditions.

Results

Unsaturated fatty acids stimulate protein translocation

The effect of the fatty acid structure on SecA : SecYEG-mediated translocation was examined using liposomes of defined and tailored lipid compositions. The inner membranes of *E. coli* are composed mainly of the zwitterionic lipid phosphatidylethanolamine (PE; up to 70 mol %) and anionic lipids, PG (20–25 mol%) and CL (3–5 mol %) [13]. Due to the small radius of their head groups, some PE species, such as DOPE, do not form planar lipid bilayers *in vitro*, and their gel-to-fluid transition temperatures are substantially higher than those of PG or another zwitterionic lipid phosphatidylcholine (PC) with the same fatty acid composition. Thus, to avoid potential nonlamellar structures and phase separation in the composite liposomes, PC lipids were employed here as the zwitterionic component. SecYEG was reconstituted into liposomes containing 30 mol % PG and 70 mol % PC; that way, the fraction of anionic lipids (PG) mirrored the abundance in the inner membrane of *E. coli* and should be sufficient to enable the electrostatically driven SecA : lipid interactions [3,5]. Indeed, the translocon remained active when reconstituted into POPC : POPG lipids, thus validating PC : PG liposomes as a functional membrane mimetic (Fig. 1B).

To examine the effect of the lipid-constituting UFAs on translocation, the fatty acid composition in the proteoliposomes was varied, while keeping the PC : PG molar ratio of 7 : 3 constant. Phospholipids composed
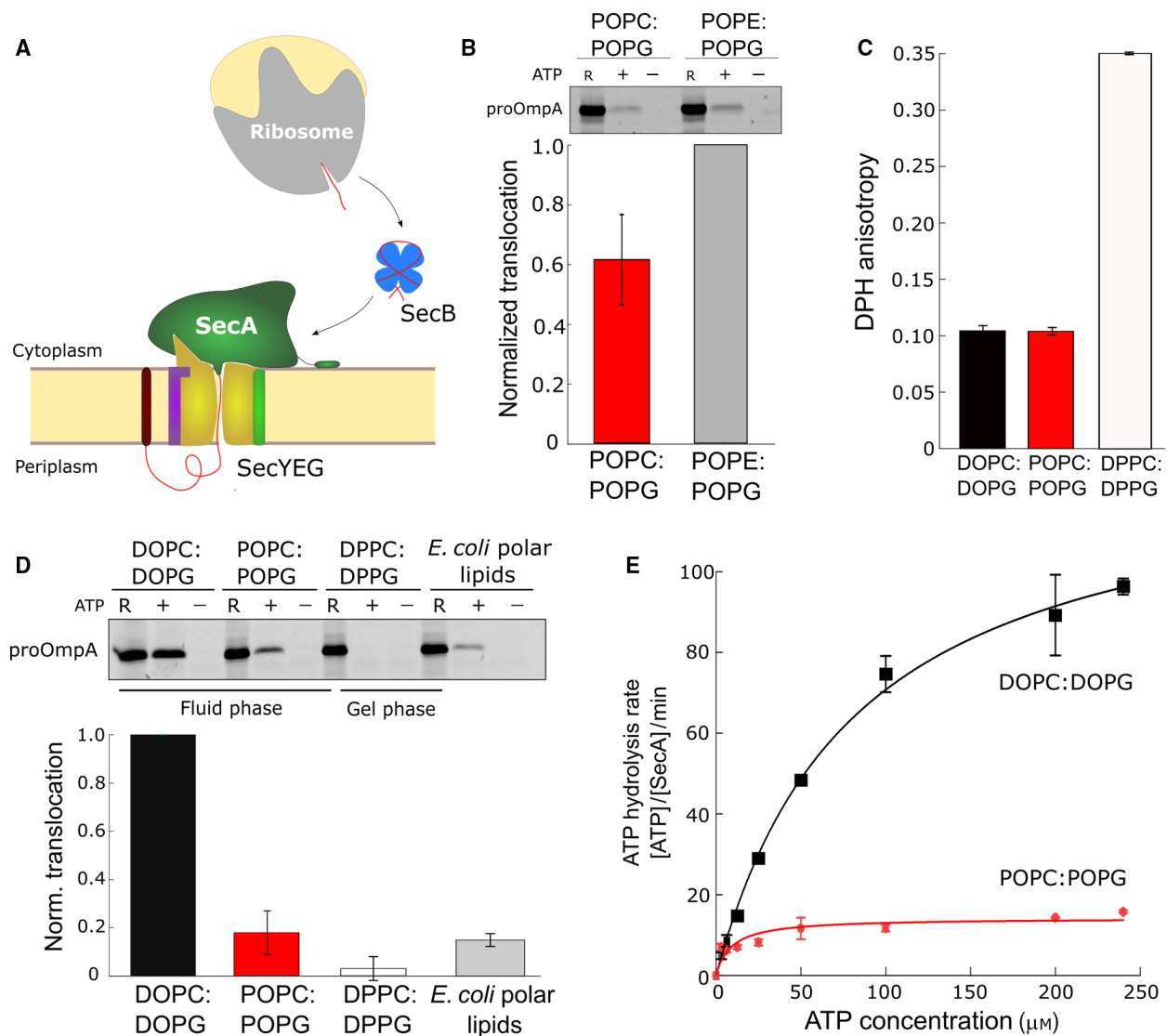
Fig. 1. Unsaturated fatty acids stimulate Sec-mediated translocation. (A) The primary bacterial pathway for protein translocation is composed of the cytoplasmic holdase chaperone SecB, the membrane-associated ATPase SecA and the transmembrane translocon SecYEG. (B) POPC : POPG lipid composition supports SecYEG activity. Translocation of the model substrate proOmpA was measured in SecYEG-containing proteoliposomes composed of 30 mol % POPG and 70 mol % zwitterionic lipids, either POPC or POPE. (C) Low fluorescence anisotropy of the DPH dye in either DOPC : DOPG or POPC : POPG confirms that both lipid bilayers are present in the fluid phase at 37 °C. In contrast, a high fluorescence anisotropy value measured in DPPC : DPPG membranes indicates the low-mobile gel phase. (D) Translocation of the preprotein proOmpA is sensitive to the content of the unsaturated fatty acids (UFAs), being maximal for DOPC : DOPG membranes. The translocation efficiency in DOPC : DOPG bilayers was used for normalization. Error bars show standard deviation (SD) values, as measured in triplicates. (E) The ATPase activity of SecA associated with proOmpA translocation is strongly stimulated in DOPC:DOPG proteoliposomes (K_M of 83 ± 6 μM). The uniform molar ratio of PC:PG lipids of 7 : 3 was used for all samples.

of dipalmitoyl (16 : 0/16 : 0, DP; no mono-UFA), 1-palmitoyl-2-oleoyl (16 : 0/18 : 1 Δ9-*cis*, PO; 50% mono-UFA) and dioleoyl (18 : 1/18 : 1 Δ9-*cis*, DO; 100% mono-UFA) fatty acids, as well as the natural extract of *E. coli* polar lipids (average mono-UFA content ~ 50 mol %), were tested. Fully saturated fatty

acids of DPPC : DPPG lipids resulted in a gel-phase membrane (transition temperatures 42 °C), but both POPC : POPG and DOPC : DOPG membranes (phase transition temperatures −2 °C and −18 °C, respectively) were present in the disordered fluid phase, as confirmed by the fluorescence anisotropy analysis of

the conventional bilayer-incorporated reporter DPH (Fig. 1C) [14]. The membrane fluidity was essential for SecA : SecYEG-mediated translocation at 37 °C : Transport of the preprotein proOmpA was nearly zero in the gel-phase DPPC : DPPG liposomes; hence, the essential SecA : SecYEG dynamics must be severely suppressed (Fig. 1D). The fluid-phase membranes ensured the preprotein translocation, but the translocation efficiency manifested striking variations : DOPC : DOPG lipids strongly stimulated the activity of SecA : SecYEG, as up to 5-fold more proOmpA was accumulated in liposomes, in comparison to POPC : POPG membranes (Fig. 1D). The translocation efficiency correlated with the ATPase activity of SecA (Fig. 1E), suggesting that the length of the polypeptide chain translocated per cycle of ATP hydrolysis was not altered. The translocation in native *E. coli* extracts enriched with partially unsaturated PE lipids was substantially lower than in DOPC : DOPG liposomes, so that the stimulatory effect must originate from the fatty acid structure and presence of UFAs, but not the head group composition.

To investigate whether UFAs of phospholipids modulate the translocation rate, we analysed the kinetics of a single translocation cycle using the Förster's resonance energy transfer (FRET)-based transport assay [15]. The N-terminal proOmpA domain of the fusion preprotein proOmpA-DHFR is translocated into the liposome lumen (Fig. 2A). The preprotein stays trapped within the Sec complex, once the folded C-terminal DHFR domain blocks the SecA : SecYEG machinery, so the translocation cycle results in a stable stalled intermediate. Once the translocation intermediate is assembled, the fluorophores placed in the C-terminal part of proOmpA (Cyanine3, donor) and at the periplasmic side of SecYEG (Atto 643, acceptor) come into proximity allowing for FRET. The increase in the acceptor fluorescence is assigned to the assembly of the intermediate and, once recorded over time, it provides an insight into the translocation kinetics [15]. SecYEG reconstituted in the UFA-enriched DOPC : DOPG liposomes displayed approx. twofold higher rates of the intermediate formation compared to SecYEG in POPC : POPG liposomes (Fig. 2B and C). Next to that, the threefold lower amplitude of the FRET signal observed in POPC : POPG further suggested that a fraction of SecA : SecYEG complexes did not completely translocate the proOmpA domain, likely due to the slower translocation kinetics accompanied by inactivation of the temperature-labile SecA ATPase [16]. Together, the results of the functional assays reveal that UFAs within the physiologically fluid lipid membrane stimulate the efficiency of the

SecA : SecYEG translocon and increase the rate of the polypeptide chain transport.

SecYEG stability and topology are not affected by fatty acid composition

The prominent effect of the lipid fatty acid composition on Sec-mediated translocation suggests that the hydrophobic core of the membrane could either affect stability and dynamics of the SecYEG translocon or be a novel factor that regulates SecA binding and SecA : SecYEG assembly. SecYEG is known to interact with specific lipids, such as PG and CL, and the interactions may cause heterogeneity in the structural dynamics [17–19]. To probe the effect of various environments on the translocon folding and stability, we established differential scanning fluorimetry (DSF) measurements, which report on the protein denaturation based on changes in the fluorescence emission of tryptophan residues [20]. Loss of the native protein structure leads to exposure of tryptophan residues to the aqueous solvent, so that their fluorescence is red-shifted. The SecYEG translocon contains eight tryptophan residues positioned at the ends of transmembrane helices (Fig. 3A), and their fluorescence was recorded over the temperature range from 20 to 90 °C. An abrupt change observed both in detergent micelles and in liposomes indicated the cooperative denaturation of the translocon (Fig. 3B). Notably, the lipid environment greatly stabilized SecYEG : The denaturation temperature T_m in DDM micelles was measured at 47 °C, but it increased to 66 °C in DOPC : DOPG liposomes (Fig. 3B). Variations in the lipid UFA content had a minor effect on the T_m value indicating that SecYEG was equally stable and correctly folded in the examined lipid bilayers (Fig. 3C). As the lipid composition had a minor effect on the reconstitution efficiency of the translocon, and POPC : POPG lipids rather favoured its functional topology in lipid membranes (Fig. 4A and B), UFA-specific SecYEG inactivation upon the reconstitution was excluded. Importantly, a recent mass spectrometry analysis of SecYEG-associated fatty acids in native membranes did not reveal deviations from the overall UFA distribution in *E. coli* inner membranes, so that the translocon does not form preferential interactions with specific fatty acids [17]. Finally, the SecYEG[prlA4] mutant, which demonstrates elevated preprotein translocation due to the altered structure of the central pore [21], was similarly sensitive to the UFA content as the wild-type translocon (SecYEG[WT], Fig. 4C). Thus, the dominant effect of UFAs on SecA : SecYEG-mediated translocation could not be related
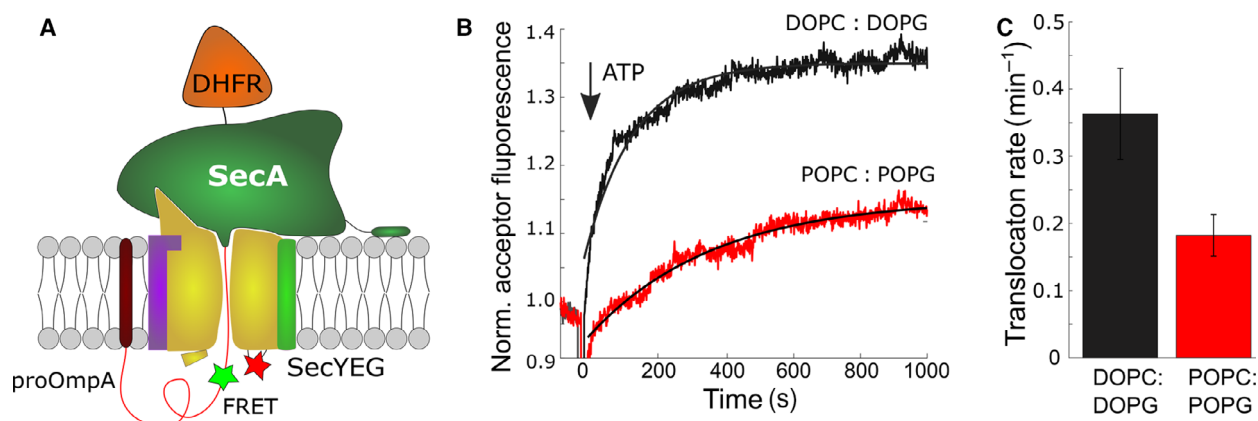
Fig. 2. Unsaturated fatty acids stimulate the kinetics of SecA : SecYEG translocation. (A) Scheme of the assembled translocation intermediate. The unfolded proOmpA domain is translocated via SecA : SecYEG, but the folded domain DHFR stalls the transport and jams the translocon. Two fluorophores positioned within proOmpA and at the periplasmic side of SecY allow for FRET once the stalled complex is formed. (B) Assembly of the translocation intermediate is followed as the fluorescence of the FRET acceptor is increasing with time after addition of ATP (arrow). The UFA-enriched DOPC : DOPG membranes (black) stimulate the proOmpA translocation and ensure formation of the stalled translocation intermediate. (C) Apparent translocation rates determined from the FRET-based assay validate the faster translocation reaction in the UFA-enriched DOPC : DOPG membrane. The molar ratio of PC : PG lipids of 7 : 3 was used for both samples. The error bars correspond to SD values based on measurements in duplicates.

to SecYEG : lipid contacts, but possibly originated from altered SecA : lipid interactions at the membrane interface.

Unsaturated fatty acids cause loose packing of lipid head groups

To study whether the lipid-constituting UFAs alter the lipid membrane organization, we employed the environment-sensitive dye laurdan to examine the lipid packing at the membrane : water interface. The dye spontaneously intercalates between the lipid head groups, and its general fluorescence polarization value decreases with higher water permeation, which is characteristic for loose lipid packing [22]. The fluorescence polarization measured in DOPC : DOPG liposomes was significantly lower than that in POPC : POPG membranes (-0.52 ± 0.02 vs. -0.40 ± 0.01; Fig. 5A), thus suggesting more disordered interface structure for the UFA-enriched lipid bilayer.

To scrutinize the lipid organization within the membrane at the molecular level, all-atom molecular dynamics (MD) simulations of DOPC : DOPG and POPC : POPG lipid bilayers were carried out. Both systems showed very similar electron density profiles and membrane thicknesses (Fig. 5B and Table 1). However, a comparison of the lateral pressure profiles and the lipid packing revealed prominent differences between these lipid bilayers (Fig. 5C–E). Pressure differences were observed in 1) the head group region

($15–17$ Å, the repulsive component is stronger in DOPC : DOPG); 2) close to the ester bonding ($11–14$ Å, attractive pressure in DOPC : DOPG); 3) in the region of the unsaturation ($\sim 5–10$ Å, the repulsive component is stronger in DOPC : DOPG); and 4) in the membrane centre (0 Å, only the POPC : POPG system has a repulsive component). Thus, the presence of an additional double bond in DOPC : DOPG membrane shifts repulsive pressure from the acyl chain region towards the water interface, as suggested by analytical studies and found for similar lipid compositions of varying unsaturation degrees [23,24] and to some extent to the head group region. For DOPC : DOPG, the more attractive pressure at the ester bond region and at the membrane centre comes at the expense of the stronger repulsive components in the regions of the head groups and the unsaturation, reflecting more pronounced steric interactions between the polar groups and the acyl chains, respectively. Indeed, the packing density in the DOPC : DOPG system is higher in the ester bond region and the membrane centre, but lower in the regions of the head groups and the unsaturation (Fig. 5E), similar to what has been previously found for pure DOPC versus POPC systems [11]. The lower particle density on the surface of the membrane bilayer is associated with a larger area per lipid of the DOPC : DOPG system (70.25 ± 0.05 Å^2, mean $\pm$ SEM) compared to the POPC : POPG system (66.74 ± 0.02 Å^2; Fig. 5D and Table 1), in agreement with the results from laurdan
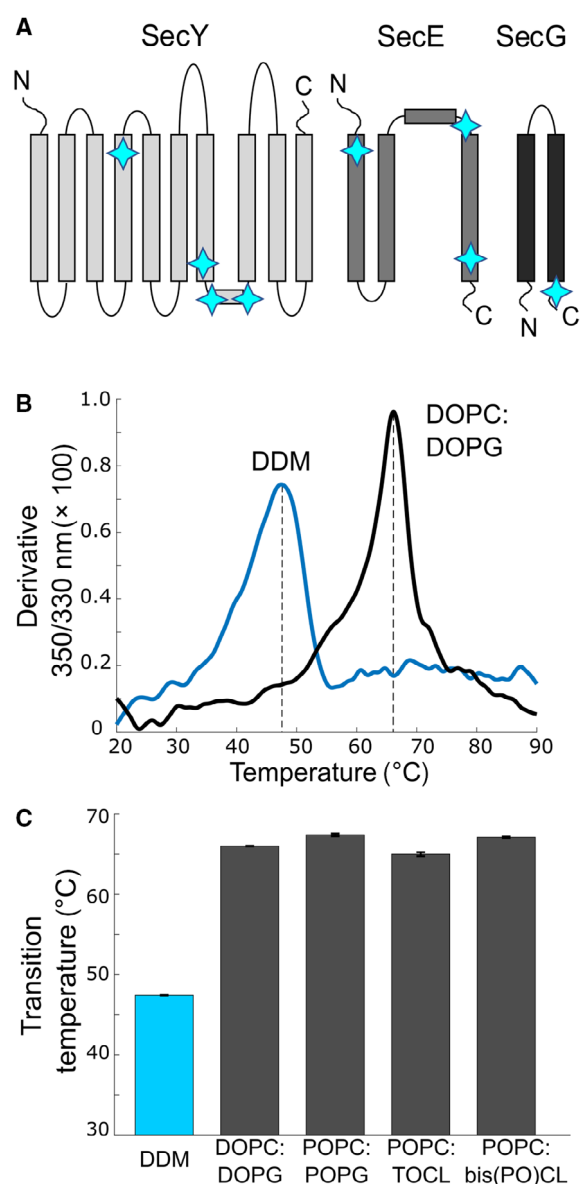
Fig. 3. The fatty acids content does not affect the stability and dynamics of the SecYEG translocon. (A) The scheme of the SecYEG secondary structure. Positions of the tryptophan residues are indicated with star symbols. Changes in tryptophan fluorescence were used to describe the thermal unfolding of SecYEG in DSF experiments. (B) Profiles of the thermal denaturation of SecYEG, as measured by differential scanning fluorometry based on the changes in the intrinsic tryptophan fluorescence. The lipid membrane substantially stabilizes the reconstituted translocon. (C) Thermal stability of SecYEG in liposomes is not influenced by the fatty acid composition of the membrane. Error bars show SD values, as measured in duplicates. The liposomes were composed of either 70 mol % PC and 30 mol % PG or 85 mol % PC and 15 mol % CL.

fluorescence (Fig. 5A). Thus, both experimental test and MD simulations indicate that the elevated UFA content leads to redistribution of the pressure within the membrane and induces looser packing of the lipid head groups.

Unsaturated fatty acids facilitate SecA binding to the lipid bilayer

SecA : lipid interactions at the membrane interface are recognized as an essential factor in Sec-mediated translocation [3,5,25]. Peripheral SecA : lipid binding may be a prerequisite to activate the ATPase and ensure the downstream SecA : SecYEG assembly [7,26]. Although the effect of UFAs on SecA binding has not yet been examined, it has been shown for several eukaryotic proteins that defects in the lipid packing and transiently exposed hydrophobic areas enhance the affinity of amphipathic helices to membranes [10,12]. The N-terminal tail of SecA (residues 1–25) forms an amphipathic helix that binds to and likely sinks into the lipid membrane in the presence of anionic head groups due to electrostatic interactions (Fig. 6A and B) [27]. In unbiased MD simulations, taking the surface area occupied by the lipids into consideration, the SecA N-terminal tail preferentially interacts with DOPG and POPG lipid head groups mainly through its basic residues (Figs. 6C and D), with a higher contribution from residues 13 to 20 within the C-terminal half of the polypeptide. Deletion of the N-terminal tail abolishes the protein translocation [28]. Since the activity can be restored *in vitro* once the tagged SecA is artificially anchored to proteoliposomes, the primary role of the N terminus is to facilitate SecA binding to the membrane.

To test whether the UFA content and the altered lipid packing affect the SecA : membrane interaction, binding of SecA to liposomes was examined. Once bound to the lipid leaflet, SecA can float with liposomes through a sucrose density gradient, thus allowing to estimate the binding efficiency (Fig. 7A). SecA readily interacted with PG-containing liposomes, while the binding was nearly abolished for SecA mutant lacking the N-terminal 20 amino acids (Fig. 7B). In agreement with earlier results, the mutant could not support preprotein translocation. Increasing the salt concentration from 50 to 500 mM reduced SecA binding to POPC : POPG liposomes by ~ 80% (Fig. 7C), so SecA : lipid binding was salt-sensitive, as expected for the electrostatics-driven interaction. Notably, for DOPC : DOPG liposomes, the reduction was limited
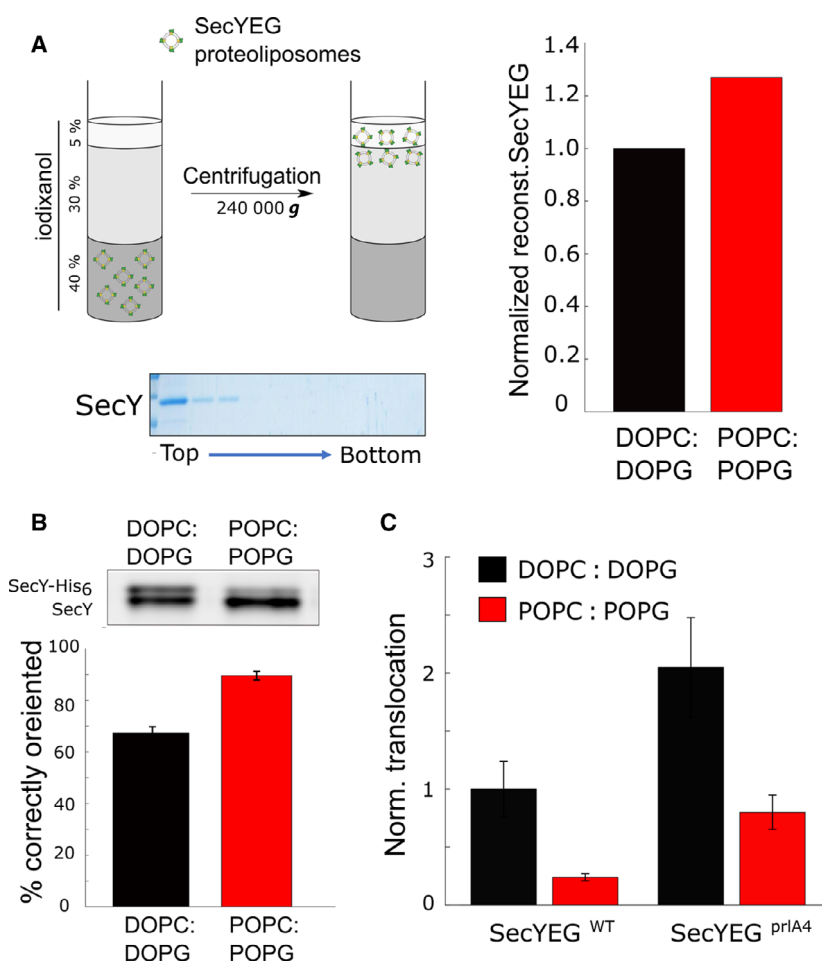
Fig. 4. (A) Flotation assay in iodixanol density gradient using SecYEG proteoliposomes demonstrated nearly equal reconstitution efficiency of the translocon for DOPC : DOPG or POPC : POPG lipids. The example SDS/PAGE shows the distribution of SecY reconstituted into DOPC : DOPG liposomes. (B) Site-specific cleavage of the N-terminal poly-histidine tag of SecY subunit by enterokinase reports on the accessibility of the tag in liposomes, and so reveals the orientation of reconstituted SecYEG. In POPC : POPG liposomes nearly 80% of the translocons were exposed to the protease, and so acquired the functionally relevant orientation. (C) The activity of the up-regulated translocon mutant SecYEG^{prlA4} is equally sensitive to the UFA content as the wild-type translocon (SecYEG^{WT}), suggesting that UFAs play a SecYEG-independent role in the translocation. Error bars show SD values, as measured in duplicates. The uniform molar ratio of PC : PG lipids of 7 : 3 was used for all samples.

to 40% only, and the amount of SecA bound to DOPC : DOPG liposomes exceeded that bound to POPC : POPG over the whole range of tested salt concentrations. The difference reached fivefold at 500 mM

KCl, thus confirming the effect of the lipid packing on SecA : membrane interaction and highlighting the role of hydrophobic interactions at the loosely packed interface.

Fig. 5. Fatty acid structure determines the biophysical properties of lipid bilayers. (A) General polarization of the laurdan dye suggests a looser packing of the lipid head groups in *cis*-UFA-enriched lipid bilayers (DOPC : DOPG). Error bars show SD values, as measured in triplicates. (B) Electron density profiles of POPC : POPG (top) and DOPC : DOPG (bottom) bilayers. The profiles provide information regarding the location of the membrane components along the plane normal. PC: phosphatidylcholine headgroup; PG: phosphatidylglycerol headgroup; OL: oleate acyl chain; PA: palmitate acyl chain. (C) Lateral pressure profile (Π) of the simulated bilayers, showing the characteristic negative component associated with the membrane : solvent interface (see the water density drop in B) and a central positive pressure component in the POPC : POPG system (top) that is absent in the DOPC : DOPG bilayer [24]. P_L and P_N are lateral and normal components of the pressure tensor. (D) Distributions of the area per lipid in the simulated bilayers. The area per lipid is significantly higher ($P < 0.001$; Tukey HSD test, Table 1) in the bilayer composed of DOPC : DOPG, despite overall similar electron density profiles. (E) 2D number density of lipids on the x z plane of the POPC : POPG bilayer and the difference of the x z densities and lateral pressure profiles of (POPC : POPG–DOPC : DOPG). In the DOPC : DOPG bilayer, the density is higher in the membrane centre and in the region of the ester bonds, but lower in the region of the fatty acid unsaturation and the polar head groups. In the pressure profile, two UFAs cause a higher repulsive component in the head group region (1), a more attractive pressure close to the ester bonds (2), a higher repulsive component in the region corresponding to the double bonds (3), and a lower repulsion in the centre of the membrane bilayer (4). The regions with a more attractive component in the DOPC : DOPG system (2,4) relate to a relatively higher density of lipids. 'Δ9' indicates the region where the unsaturated bonds in the upper leaflet of the lipid bilayer are located (see B, green curves). All values from B to E were calculated from all-atom MD simulations based on five independent replicas. The uniform molar ratio of PC : PG lipids of 7 : 3 was used for all experiments.

M. Kamel *et al.*

Unsaturated fatty acids enhance protein transport
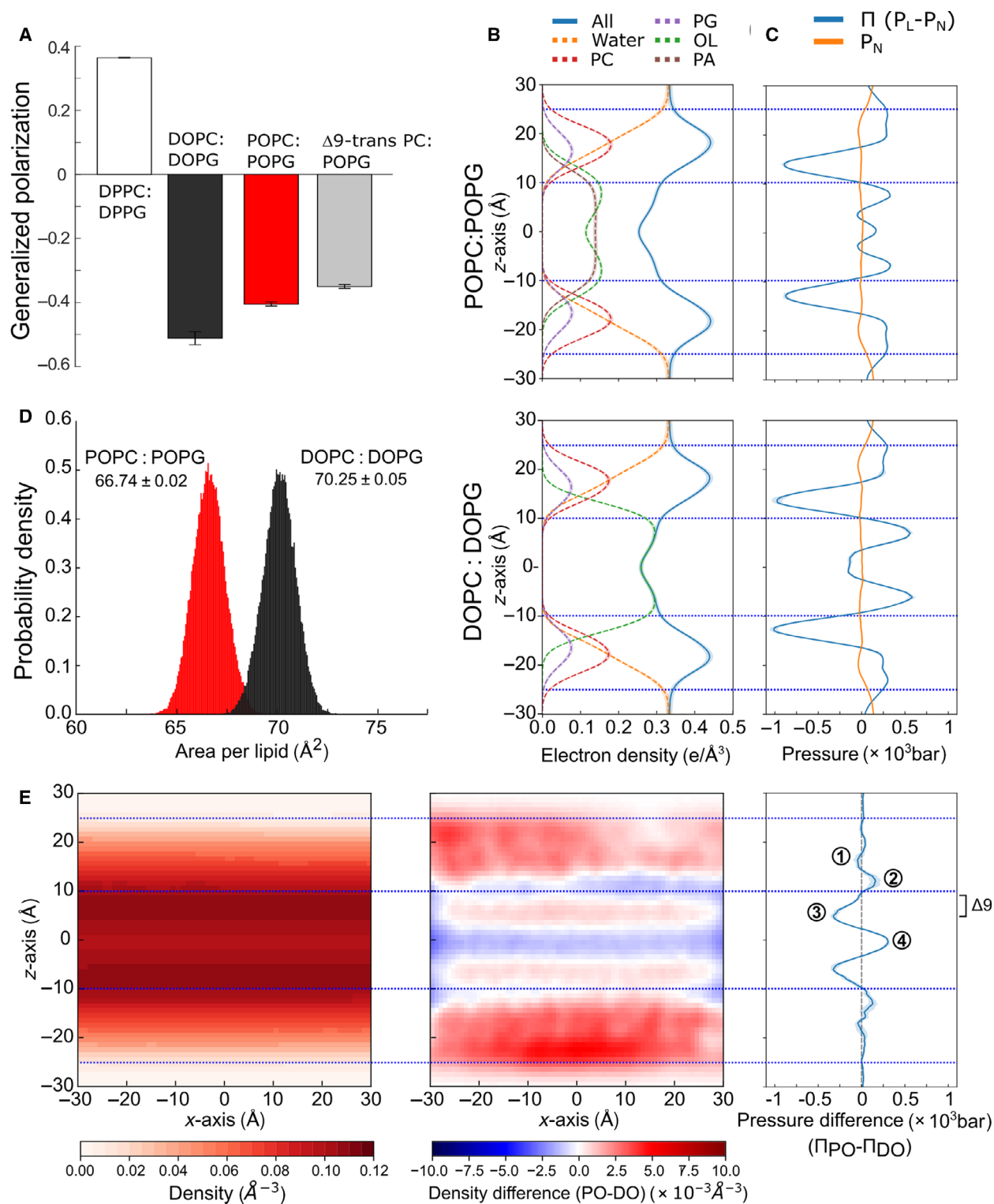
Notably, when POPC was substituted with DOPC in a stepwise manner, both SecA binding and the pre-protein translocation in SecYEG proteoliposomes continuously increased, and introducing DOPG instead of POPG had a similar effect (Figs 8A and B). This clear correlation supported the hypothesis that

the UFA-enhanced SecA : lipid interactions promote SecA : SecYEG translocation. We questioned then whether the configuration of the double bond within the UFA affects SecA : membrane interactions. Introducing a *trans*-bond in position Δ9 in both fatty acids of PC had a pronounced effect on the membrane properties : although the lipid bilayer resided in the fluid phase (phase transition temperature ~ 12 °C), the laurdan fluorescence indicated tight packing within the head group region similar to UFA-poor POPC : POPG membranes (Fig. 5A). The increase in the lipid packing led to suppressed binding of SecA and finally caused approx. 7-fold reduction in SecA : SecYEG-mediated translocation (Figs 8C and D). Alike, binding of SecA to gel-phase membranes DPPC : DPPG was suppressed three- to fourfold even at the low salt concentration (50 mM KCl; Fig. 8C), despite the presence of the anionic lipids, and correlated with the loss of SecA : SecYEG activity (Fig. 1C).

Aiming for quantitative characterization of SecA : lipid interactions, surface Plasmon resonance (SPR) experiments were carried out. The steady-state response upon binding of SecA to the chip-anchored liposomes was strongly enhanced in UFA-based DOPC : DOPG membranes (Fig. 9A). The measurements over a range of SecA concentrations provided an estimate of the apparent dissociation constant K_D for SecA : lipid interactions (Fig. 9B). In the presence of 150 mM KCl and 5 mM MgCl$_2$, SecA showed a 1.7-fold higher affinity to DOPC : DOPG membranes (125 ± 5 nM) than to POPC : POPG membranes (210 ± 45 nM). In agreement with the flotation assay (Fig. 7C), SecA : lipid binding was suppressed at elevated salt concentration of 300 mM KCl for both DOPC : DOPG and POPC:POPG, where the apparent K_D decreased to $\simeq 1.2$ µM and 2.4 µM, respectively (Fig. 9B). Notably, while the determined change in the affinity was small, the SPR response signal was nearly twofold higher upon SecA binding to DOPC : DOPG liposomes, even at the saturation level (1050 vs. 600

response units, Fig. 9A). As the amounts of immobilized unilamellar liposomes did not vary between samples, the differences in the SPR response signal cannot be related to the available SecA binding sites at the liposome surface. Instead, it seems feasible that the DOPC : DOPG membranes promote binding of SecA dimers, previously described in the cellular membranes [29,30].

To exclude that binding was affected by the non-physiological positive curvature of the liposomes, a complementary experiment was carried out using planar supported lipid bilayers (SLBs) deposited on a quartz crystal microbalance (QCM) chip [31]. Liposomes were noncovalently adsorbed on the quartz chip surface and fused to form continuous SLBs (Fig. 10A and B). Subsequent SecA binding increased the mass adsorbed on the quartz chip, which affected its resonance frequency (Fig. 10C and D). Depending on SecA concentration, the ATPase binding to DOPC : DOPG membranes measured in 150 mM KCl and 5 mM MgCl$_2$ was 25 to 50% higher than to POPC : POPG membranes, pointing to the higher mass of the protein accumulated at the membrane interface, also upon reaching the saturation of binding (Fig. 10D and E). The apparent K_D values were 91 nM and 161 nM, respectively (Fig. 10F), in good agreement with the SPR data. Thus, biochemical and biophysical assays confirmed the differential binding of SecA to lipid bilayers depending on the UFA content and the associated lipid head group packing, and the binding efficiency correlated with the translocation activity of the SecA : SecYEG complex.

Tetraoleoyl-cardiolipin stimulates SecA binding and preprotein transport

The inner membranes of *E. coli* and other Gram-negative bacteria commonly contain a minor fraction of cardiolipin (CL) molecules [13], and a recent mass spectrometry analysis revealed that the most abundant

Table 1. Area per lipid and membrane thickness measured in MD simulations of the investigated systems.[a]

Head group	POPC : POPG 70 : 30	DOPC : DOPG 70 : 30	POPC : bis(PO)CL 85 : 15	POPC : TOCL 85 : 15
PC APL[b,*]	67.14 (0.05)	70.68 (0.07)	73.05 (0.12)	74.13 (0.12)
PG APL[b,*]	65.86 (0.19)	69.28 (0.18)	-	-
CL APL[b,*]	-	-	79.23 (0.65)	80.38 (0.23)
Average APL[c,*]	66.74 (0.02)	70.25 (0.05)	73.97 (0.09)	75.06 (0.07)
Thickness[d]	37.38 (0.01)	37.06 (0.02)	38.71 (0.04)	38.64 (0.04)

[a]All measurements were done over the last 800 ns of five 1 µs replicas and are shown as the mean of replica means (standard error of the mean); [b]Area per lipid (Å²) as measured by APL@Voro [70]; [c]Area per lipid (Å²) measured as the xy-sectional area of the average simulation box used per lipid; [d]Membrane thickness (Å) measured as the distance between the z-coordinates of the centres of mass of the phosphorous atoms of each leaflet; [*]The pairwise difference of the mean across all systems is statistically significant ($P < 0.001$, Tukey HSD).

Fig. 6. SecA : membrane association is mediated by unsaturated fatty acids. (A) Helix wheel projection of the N-terminal end of *E. coli* SecA of the putative amphipathic helix (via heliquest.ipmc.cnrs.fr). The hydrophobic moment (~ 0.4) is indicated with the arrow. (B) A binding pose of the N-terminal amphipathic helix of SecA at the interface of the lipid bilayer after 1 μs of MD simulation (DOPC : DOPG, replica 4). Basic residues that show pronounced interactions with the head groups are highlighted. (C) Interactions of the SecA N-terminal helix (residues 1 to 25) with DOPC : DOPG lipids over MD simulations of 1 μs length. Per-residue contacts with membrane headgroups in each replica are shown. Cationic residues are highlighted in red. (D) Mean per-residue contacts of the N-terminal SecA peptide with head groups in DOPC : DOPG and POPC : POPG membranes over MD simulations of 1 μs length, with the coloured background showing the standard error of the mean over 5 replicas, as exemplary shown in C. When the absolute contacts are measured (top), comparable results are obtained irrespective of the head group considered. If the surface area occupied by the lipid types is taken into account (bottom, where R_{LIP} represents the ratio factor and APL_{LIP} the area per lipid for each lipid type reported in Table 1), negatively charged PG lipids show a higher propensity to interact with positively charged residues than the neutral PC head groups. The uniform molar ratio of PC : PG lipids of 7 : 3 was used for all simulations.

Fig. 7. SecA : membrane association is mediated by unsaturated fatty acids (A) Scheme of the flotation assay to probe SecA : lipid interactions. Upon the centrifugation, the liposomes loaded with aqueous buffer migrate to the top of the sucrose density gradient. Liposome-bound SecA is found in the top layer of the gradient, while free SecA remains in the bottom fraction. (B) Deletion of SecA N-terminal helix abolishes lipid binding as tested via the flotation assay and eliminates SecA : SecYEG translocation activity in DOPC : DOPG liposomes. (C) The flotation assay reveals UFA-dependent and salt-sensitive binding of SecA to the liposomes. Error bars show SD values, as measured in triplicates. The uniform molar ratio of PC : PG lipids of 7 : 3 was used for preparing the liposomes.

Fig. 8. UFA-dependent SecA : lipid binding correlates with the SecA : SecYEG activity. (A) Upon the gradual increase of the UFA content, the SecA : lipid binding (flotation assay) correlates with the translocation activity of SecA : SecYEG complex (B). (C) SecA binding is hindered in the presence of Δ9-*trans* UFA, that leads to the inhibition of the preprotein translocation by SecA : SecYEG (D). Thus, the configuration of the unsaturated fatty acid determines the functionality of SecA : SecYEG complex. All liposomes contained 30 mol % DOPG and 70 mol % indicated 18 : 1 PC lipids. Alike, SecA binding to gel-phase liposomes composed of DPPC : DPPG lipids is strongly suppressed in comparison to fluid-phase liposomes (DOPC : DOPG). Error bars show SD values, as measured either in triplicates (SecA binding) or duplicates (translocation).
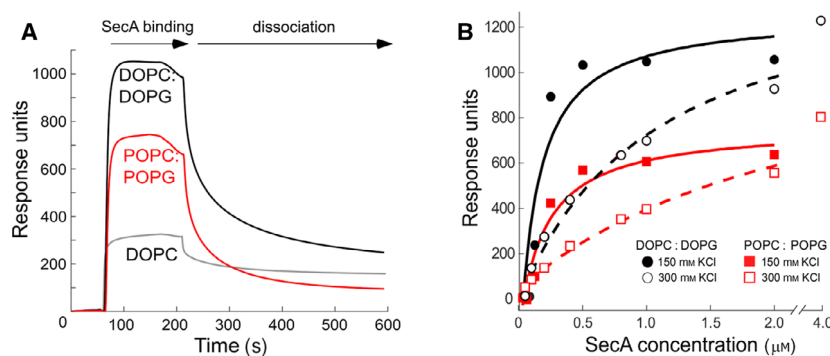
Fig. 9. Unsaturated fatty acids enhance the affinity of SecA : liposome interactions. (A) Surface Plasmon resonance (SPR) sensograms of SecA (concentration 500 nM) binding to immobilized liposomes, followed by the dissociation phase. Charge-neutral membranes composed of pure DOPC were used as a negative control. (B) Analysis of the steady-state SPR response over a range of SecA concentrations (31 nM to 2 µM) reveals enhanced binding to DOPC : DOPG membranes. SecA : lipid interactions are sensitive to the ionic strength, being weakened at the elevated salt concentration. The uniform molar ratio of PC : PG lipids of 7 : 3 was used for preparing the liposomes.

CL species in the *E. coli* membrane contain four mono-UFAs [17]. CL molecules are enriched two- to threefold in the proximity of the translocon [17,18], and it has been suggested that CL facilitates SecYEG homo-dimerization, but may also serve as an acceptor

for protons to contribute to the proton motive force [18]. However, the functional translocon *in vitro* and *in vivo* is built of monomeric SecYEG, and no stimulatory effect of CL on SecA : SecYEG activity in the UFA-enriched membranes was observed [15,32]. Thus,
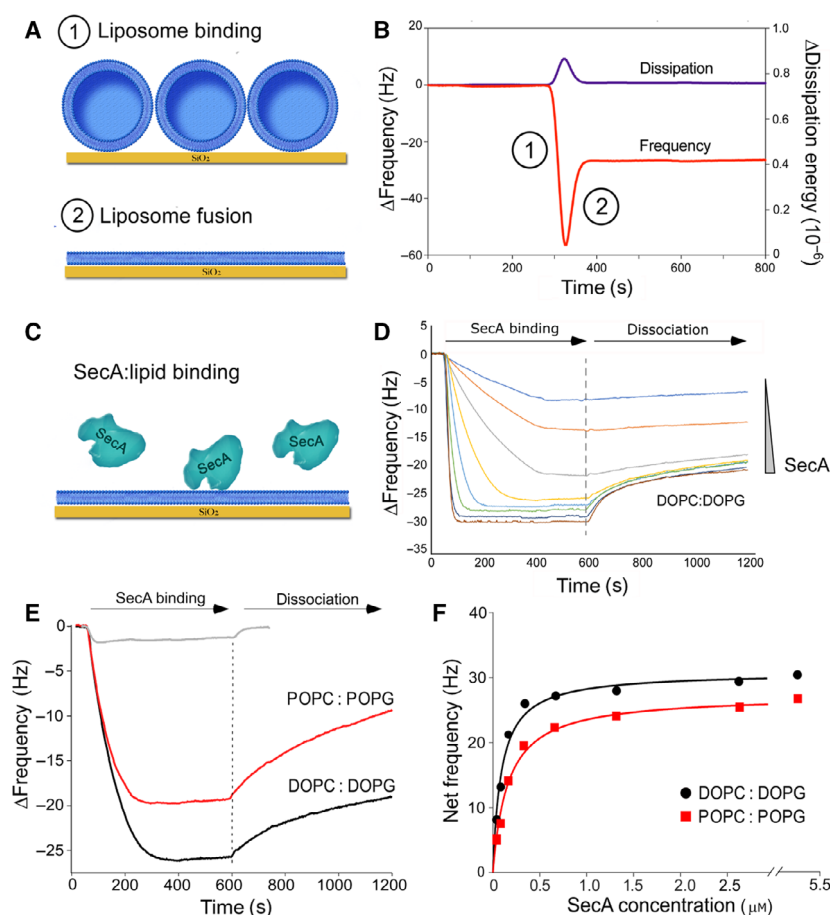
Fig. 10. Unsaturated fatty acids enhance SecA binding to the planar lipid bilayers (A) Formation of the lipid bilayer on the quartz crystal microbalance (QCM) chip surface. Liposomes are bound to the surface at high density, and their fusion in the presence of calcium leads to the formation of the supported lipid bilayer. (B) The attachment and the fusion of liposomes are observed as changes in the oscillation frequency of the chip (stages 1 and 2). An increase in the energy dissipation upon the liposome attachment is due to the large volume of encapsulated water, which is further released upon fusion (stage 2). (C, D) Measuring SecA binding to the lipid bilayer via changes in the oscillation frequency. SecA was injected in the buffer flow over DOPC : DOPG bilayer to monitor the association and dissociation stages. SecA concentration ranged from 40 nM to 5.25 μM (twofold dilution per titration step). (E) QCM sensograms of 800 nM SecA binding to planar lipid bilayers, followed by the dissociation phase. Charge-neutral membranes composed of pure DOPC were used as a negative control. (F) Analysis of the steady-state frequency change over a range of SecA concentrations (40 nM to 5.25 μM) reveals enhanced binding of SecA to DOPC : DOPG membranes. The uniform molar ratio of PC : PG lipids of 7 : 3 was used for all samples.

the role of CL in SecA : SecYEG activity has remained intensively disputed [7,33].

In light of the discovered effect of UFAs on Sec-mediated translocation, we questioned whether UFA-enriched CL, such as tetraoleoyl-CL (TOCL), may recruit SecA to the lipid membrane and to enhance the preprotein transport. To test this hypothesis, SecYEG was reconstituted in POPC : POPG : TOCL membranes with a variable amount of TOCL. To keep the net negative charge at the membrane interface constant, the variations in the CL content were compensated by tuning the POPG fraction. Changing the CL fraction from 0 to 15 mol % increased the

translocation activity up to 10-fold, indicating that TOCL is indeed a potent stimulator of protein translocation (Fig. 11A). To exclude potential dimerization of SecYEG in the presence of CL, the translocons were reconstituted into nanodiscs as monomers, and the translocation efficiency in the presence of TOCL was determined using the FRET-based assay [34,35]. The dimensions of nanodiscs (outer diameter ~ 15 nm) and the lipid : protein ratio used upon the reconstitution ensured that ~ 200 lipid molecules were embedded in each nanodisc [36]. TOCL strongly stimulated the translocation efficiency and kinetics, despite the nanodisc boundaries physically prevented dimerization of
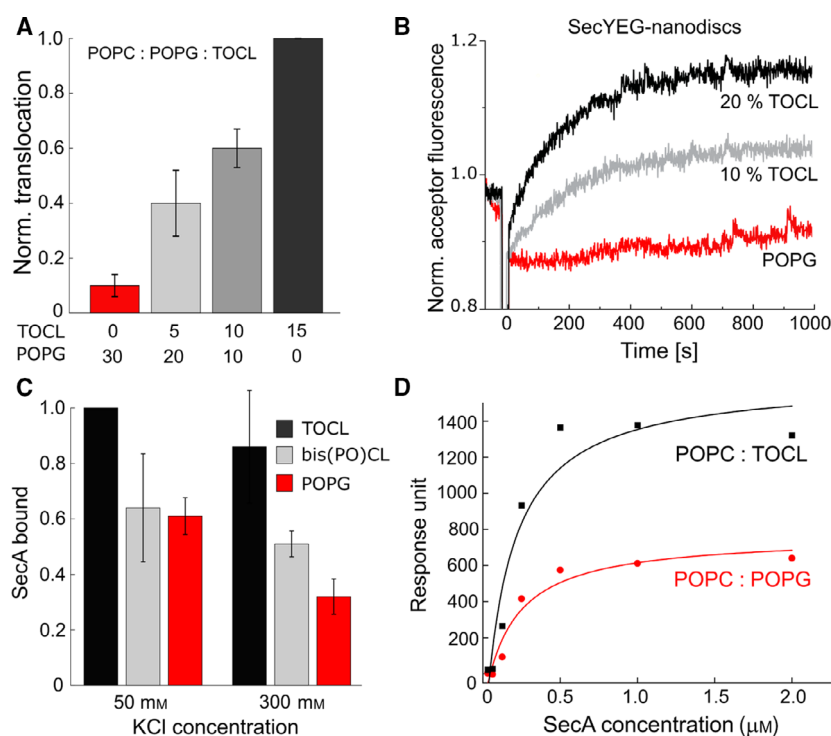
Fig. 11. UFA-enriched cardiolipin stimulates Sec-mediated translocation. (A) Elevated concentrations of tetraoleoyl-cardiolipin (TOCL) stimulate preprotein transport into liposomes. SecYEG-containing liposomes consisted of POPC and POPG/TOCL mixture at the indicated molar ratios to maintain the uniform electrostatic interactions at the interface. The error bars correspond to SD values based on measurements in duplicates. (B) FRET-based translocation assay shows increased activity of monomeric SecYEG in nanodiscs in presence of TOCL. The stimulated activity is achieved without oligomerization of the translocon. POPG : TOCL ratios were identical to those in panel (A). (C) Flotation assay confirms the preferential interactions of SecA with UFA-enriched TOCL. Binding to TOCL-containing membranes is the least affected by the elevated ionic strength, so the interactions with UFAs promote the membrane-bound form of SecA. Lipid membranes were composed of either 70 mol % POPC and 30 mol % POPG or 85 mol % POPC and 15 mol % CL. The error bars correspond to SD values based on measurements in duplicates. (D) SPR experiments show enhanced binding of SecA to liposomes containing POPC and 15 mol % TOCL in comparison to liposomes with POPC and 30 mol % POPG, despite the identical charge density at the interface.

SecYEG (Fig. 11B). While TOCL did not affect the stability of SecYEG (T_m ~ 66 °C, Fig. 3C), binding of SecA to TOCL-containing liposomes was enhanced compared to POPC : POPG, as tested by flotation assay and SPR (Fig. 11C and D). Although additional effects of interactions of TOCL with the active SecA : SecYEG complex are possible, our data demonstrate that even in the absence of the proton motive force, TOCL favours SecA : lipid interactions at the membrane interface and stimulates the translocation.

Effect of cardiolipin on translocation depends on the fatty acid structure

Does the CL-mediated stimulation originate from the UFA content, or may it be determined by the high charge density within the CL head group? To address this question, two CL variants, TOCL (four UFAs) and bis(palmitoyloleoyl)-CL (bis(PO)CL, two UFAs),

were examined with MD simulations and in model liposomes. Exchanging POPG with either TOCL or bis (PO)CL in the simulated bilayer (POPC : CL molar ratio 85 : 15) caused significant increases in the overall and lipid type-specific area per lipid with respect to the POPC : POPG system, and the change was the most pronounced for the POPC : TOCL bilayer (Table 1). Given the larger size of cardiolipins, an increase in the average area per lipid was to be expected, but, notably, the effect also comprised the other lipid types in the bilayer. As such, the area per POPC molecule increased by 10%, from 67 Å^2 (POPC : POPG bilayer) to 74 Å^2 (POPC : TOCL bilayer). The pressure profiles (Fig. 12A) and the particle density difference of the simulated bilayers with TOCL or bis(PO)CL indicate that TOCL causes a shift of the repulsive pressure from the acyl chain region towards the water interface, with a higher particle density in the ester bond region and lower density in the head group region (Fig. 12B),

Fig. 12. UFA-enriched cardiolipin stimulates Sec-mediated translocation. (A, B) The difference in 2D density profile and lateral pressure obtained by MD simulations for POPC : CL lipid bilayers (bis(PO)CL-TOCL) reveal a qualitatively similar trend as that observed for the POPC : POPG – DOPC : DOPG case (Figure 5). (C, D) The translocation efficiency and the translocation rate probed in the FRET-based assay using liposome-reconstituted SecYEG demonstrate the stimulatory effect of TOCL that agrees with the enhanced SecA binding (Figure 11C). Lipid membranes were composed of either 70 mol % POPC and 30 mol % POPG or 85 mol % POPC and 15 mol % CL. The error bars correspond to SD values based on measurements in duplicates.
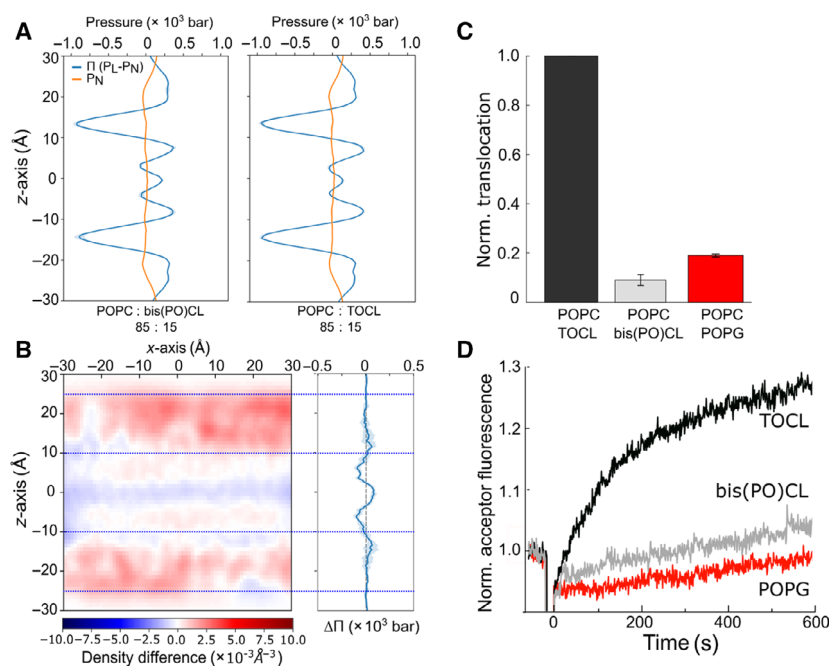
in a qualitative agreement with the results acquired from the simulated DOPC : DOPG and POPC : POPG bilayers (Fig. 3). Thus, both CL types caused substantial restructuring of the lipid bilayer compared to the POPC : POPG system, as indicated by the change in the lipid packing and the transmembrane distribution of the pressure density.

Notably, the density difference calculated between the bilayers with TOCL and bis(PO)CL is smaller in magnitude than the value determined for pure DOPC : DOPG and POPC : POPG membranes. In agreement with the computed predictions, the laurdan fluorescence in CL-containing liposomes manifested a modest, although significant, change in the polarization value upon variations in the UFA content : the general polarization increased from -0.389 ± 0.005 (15 mol % TOCL) to -0.335 ± 0.012 (15 mol % bis(PO)CL). To probe the effect of different CLs on SecA : SecYEG activity, functional tests were carried out using POPC : CL liposomes. SecA : lipid interactions were enhanced by TOCL, but not bis(PO)CL species in comparison to pure POPC : POPG membranes, suggesting that the UFA abundance, but not the charge density within the CL, affect the ATPase binding (Fig. 11C). Furthermore, the UFA-dependent binding of SecA converted into the differential effect of CLs on preprotein transport : while no stimulation was provided by bis(PO)CL, 15 mol % TOCL stimulated the activity of SecA : SecYEG (Fig. 12C). The FRET-based translocation assay in SecYEG-containing proteoliposomes further confirmed a prominent effect of TOCL, but not bis(PO)CL on the

translocon activity (Fig. 12D), so the composition of the membrane core influenced the transport rate of a polypeptide chain.

Discussion

The diversity of lipids found in prokaryotic and eukaryotic cellular membranes greatly determines physicochemical properties of the bulk membrane, but also promotes formation of functional membrane domains and mediates specific interactions with the membrane-associated proteins [37,38]. Both bulk and specific local properties of the lipid bilayer may regulate the functionality of membrane-embedded complexes, being crucial for cellular pathways, such as energy metabolism, signal transduction and the broad repertoire of transport processes. Protein translocation via the essential Sec machinery is a well-known example, where the naturally abundant anionic lipids are required for the assembly of the functional SecA : SecYEG complex [3,7,26]. While the contribution of electrostatic interactions at the interface has been extensively examined, here we reveal that the protein translocation is sensitive to changes in the fatty acid composition of the phospholipids. The protein translocation is augmented fivefold upon increasing the content of dioleoyl fatty acids in the range from 50 to 100 mol %, although the fluidity of the bilayer is not changed. While neither stability nor topology of the translocon SecYEG is affected by the lipid composition, the elevated translocation correlates with the

increased binding of the ATPase SecA to the UFA-enriched lipid bilayer. The stimulatory effect of UFAs on SecA binding is well-pronounced at the elevated salt concentrations, pointing to the previously not appreciated role of hydrophobic interactions.

While it was generally believed that SecA is equally distributed between the inner membrane interface and the cytoplasm, as determined by subcellular fractionation studies [27,29], the most recent results based on SecA imaging *in vivo* revealed that approx. 90% of the ATPase pool is found at the membrane, either interacting with the translocon or being bound to the lipid leaflet [30]. SecA localization at the cellular membrane appears to be sensitive to physiological factors, such as proton motive force and mechanical stress induced upon the cell lysis [30], and the recruitment of SecA to the membrane is essential for the translocation [26,28,39]. SecA : lipid binding is largely mediated by the N-terminal amphipathic helix of the ATPase : The helix is essential for interactions with the membrane, where it extensively binds anionic lipids via lysine and arginine residues at the polar side [28,40,41]. Further partitioning of the helix into the lipid leaflet, however, must rely on interactions with the hydrophobic fatty acids. Our all-atom MD simulations together with biophysical analysis of the lipid bilayer structure suggest that UFAs induce irregularities and looser head group packing at the membrane : solvent interface. A similar effect must have been observed in the early study on SecA : SecYEG, when DOPE was described as a potent stimulator of the translocon machinery [5]. The small PE head group combined with two UFA chains results in extensive packing defects at the membrane interface [10]. In the simplest scenario, those interfacial features allow the amphipathic helix of SecA to access the transiently exposed hydrophobic regions and facilitate partitioning of the helix into the bilayer [10,25,41]. At the elevated salt concentrations, the electrostatic coupling of the protein to the anionic lipids largely deteriorates, and the membrane-bound state of SecA depends on nonpolar contacts with the membrane interior. In combination with the previous studies, our data suggest that the hydrophobic interactions enhance the propensity of SecA to bind to the lipid membrane over a broad range of conditions, and the affinity is jointly determined by the electrostatic and apolar interactions at the interface.

Once bound to the lipid interface, SecA undergoes two-dimensional diffusion within the lipid leaflet prior docking on the SecYEG translocon [26,30]. Thus, the elevated concentration of the membrane-bound SecA favours the downstream assembly of the SecA : SecYEG complex and stimulates the preprotein transport, as observed in our experiments. Notably, the

quantitative analysis of SecA : lipid interactions via SPR and QCM reveals a modest 2- to 3-fold increase in the affinity, while the translocation activity increased up to ten-fold (POPC : POPG vs. POPC : TOCL). This may indicate that the preprotein translocation involves multiple SecA molecules, which diffuse at the membrane interface and transiently bind the translocon, as either dimers or monomers, to perform cycles of translocation. Despite the extensive research, neither the quaternary state and dynamics of SecA nor its processivity in translocation have been clarified [42–44]. Recent reports have suggested that the oligomeric state of the membrane-bound SecA depends on the membrane lipid composition, with monomers being prevalent for PO-type lipids [40,45], although the dimeric form of SecA has been described at the intact cellular membrane [27,30]. Notably, both SPR and QCM experiments showed changes in the net signal, that is Plasmon resonance response and the quartz resonance frequency upon binding saturation. The difference between SecA binding to POPC : POPG or DOPC : DOPG reached nearly 100%, as measured by SPR. The observed response levels likely reflect different amounts of SecA bound at the examined lipid interfaces, as could be related to different oligomeric states of the ATPase, that is dimers at DOPC : DOPG and monomers at POPC : POPG bilayers. Thus, it deserves further evaluation whether the membrane structure, including the UFA-mediated lipid packing, influences SecA quaternary dynamics.

The requirement of CL for SecA : SecYEG-mediated translocation has been intensively debated, and specific SecYEG : CL and SecA : CL contacts and CL-induced protein dimerization, which promote the preprotein transport, have been proposed [33,46,47]. Lately, the stimulatory effect of CL has been described in the presence of the proton motive force [18]. Here, we demonstrate that the UFA-enriched TOCL, but not bis(PO)CL, contributes to SecA binding and enhances the translocation up to 10-fold. Furthermore, the translocation experiments in nanodiscs allowed to rule out the translocon dimerization upon the translocation. Thus, UFA-mediated SecA binding does not depend on lipid species, but strongly correlates with the bulkhead group packing at the membrane interface. Interestingly though, MD simulations and measurements of the laurdan fluorescence reveal relatively small differences between lipid membranes containing TOCL or bis(PO)CL, while only TOCL is potent to stimulate the translocation. It suggests that more intricate mechanisms should be considered to interpret the effect of UFAs on SecA binding and translocation, for example formation of CL-specific domains within the otherwise miscible lipid membrane [48], restructuring

of the annular lipids upon SecA binding, or UFA-dependent dynamics of the SecA : SecYEG complex.

The experiments presented here are based on a reconstituted system that contains the core components of the Sec translocation pathway, that is SecB as a targeting factor, SecA motor protein and membrane-embedded translocation channel SecYEG, while a number of physiological factors, such as proton motive force and the translocation chaperone SecDFYajC, were omitted. The employed minimalistic approach was essential to discriminate the effect of the lipid-constituting UFAs on SecA recruitment and SecA : SecYEG activity, while maintaining the key physiologically relevant characteristics of the membrane, such as fluidity, the abundance of anionic lipids and the thickness of the hydrophobic core. A follow-up analysis may be conducted in more complex environments, such as membrane extracts and living cells. The demonstrated role of UFAs as mediators of SecA binding and protein translocation may be a critical factor for the reaction in living cells. Bacteria tune their membrane lipid composition in response to environmental factors and growth conditions, so the fraction of mono-UFAs and related cyclopropane-containing fatty acids in mesophilic bacteria, such as *E. coli* and *Pseudomonas aeruginosa*, increases up to 70 mol % at low temperatures [8,9,49]. Our data suggest that the modification of the lipid membrane within this range, as well as the presence of cardiolipins at the physiological concentrations of 5-10 mol %, will favour the membrane-bound state of SecA and thus promote protein transport to compensate for the temperature-dependent kinetics decay. Complementary, under conditions of hyperosmotic shock and increased intracellular salt concentration or dissipation of the proton motive force, the hydrophobic interactions of SecA with unsaturated lipids will prevent dissociation of the ATPase from the membrane. Likewise, it is to expect that SecA homologs from extremophile species are evolutionary tuned for interactions with UFA-depleted membranes, for example via the strong hydrophobic dipole at the N-terminal domain. Comparative functional analysis of SecA homologs from those species, and potentially the reconstituted SecA : SecYEG machinery, may further advance the understanding of the molecular adaptation mechanisms.

Materials and methods

Protein purification

Overexpression of SecYEG with the N-terminal deca-histidine tag in *E. coli* C41(DE3) cells was induced with 0.5 mM IPTG and carried out for 2 h at 37 °C. Cells were harvested by centrifugation and resuspended in buffer R (50 mM KOAc, 20 mM Hepes/KOH pH 7.4, 5 mM Mg(OAc)₂, 5% glycerol, 1 mM DTT and cOmplete Protease inhibitor cocktail (Roche, Mannheim, Germany)). Cells were lysed (Microfluidizer, M-110P, Microfluidics Corp., Westwood, MA, USA), and the debris was removed by centrifugation. Crude membranes were pelleted by centrifugation for 1 h at 40 000 r.p.m. (45 Ti rotor, Beckman Coulter, Brea, CA, USA) and then resuspended in buffer R. The membranes were solubilized using 1% DDM in presence of 500 mM KCl, 50 mM Hepes/KOH pH 7.4, 5% glycerol, 200 μM TCEP and the protease inhibitor cocktail. His$_{10}$-tagged SecYEG was isolated using Ni^{2+}-NTA agarose resin (Qiagen, Hilden, Germany). Once bound to Ni^{2+}-NTA beads, the single-cysteine SecY^{C148}EG variant was optionally labelled with ATTO 643-maleimide (ATTO-Tec GmbH) upon incubation with 100-200 μM dye for 2 h at 4 °C [15]. SecYEG-loaded resin was extensively washed with 50 mM Hepes/KOH pH 7.4, 500 mM KCl, 5% glycerol, 10 mM imidazole, 200 μM TCEP, 0.1% DDM and the protein was eluted with the buffer containing 300 mM imidazole. The protein was transferred to 50 mM Hepes/KOH pH 7.4, 150 mM KCl, 5% glycerol, 0.05% DDM, 200 μM TCEP using PD MidiTrap G-25 column (Cytiva/GE Life Sciences, Freiburg, Germany). Optionally, size-exclusion chromatography (SEC) was carried out using Superdex 200 30/10 GL Increase column (Cytiva/GE Life Sciences) to control the homogeneity of the sample (elution peak at 12.5 mL corresponds to SecYEG in a DDM micelle, total mass of approx. 145 kDa). Protein concentration was determined spectrophotometrically (extinction coefficient 72 000 M^{-1} cm^{-1}). The expression and purification steps were controlled with SDS/PAGE (Quick Coomassie stain, Serva), and in-gel fluorescence of the SecY-conjugated ATTO 643 dye was visualized (Amersham Imager 680RGB, GE Healthcare Life Sciences).

SecA gene was cloned into pET21a plasmid to carry the C-terminal His$_6$-tag. SecA overexpression in *E. coli* BL21 (DE3) cells was induced with 0.5 mM IPTG and carried out for 2 h at 30 °C. Cells were then harvested by centrifugation and resuspended in 50 mM KOAc, 20 mM Tris/HCL pH 7.5, 5 mM Mg(OAc)₂, 20% glycerol, 1 mM DTT and cOmplete protease inhibitor cocktail. Cells were lysed, and the lysate was clarified by centrifugation for 1 h at 100 000 g (45 Ti rotor, Beckman Coulter). The clarified lysate was incubated with Ni^{2+}-NTA agarose resin for 1 h at 4 °C, and the resin was then washed with 500 mM KOAc, 20 mM Tris/HCL pH 7.5, 5 mM Mg(OAc)₂, 20% glycerol, 20 mM imidazole and 1 mM DTT. SecA was eluted with the buffer containing 300 mM imidazole. The eluted fractions were concentrated using Amicon Ultra-4 filtering device, cut-off size 50 kDa (Millipore, Darmstadt, Germany) and SecA was subject to SEC using Superose 6 Increase 10/300 GL column (Cytiva/GE Life Sciences) in 50 mM KOAc, 20 mM Tris/HCL pH 7.5, 5 mM Mg(OAc)₂,

20% glycerol, 1 mM DTT, resulting in a peak at ~ 15.5 mL elution volume. Peak fractions were pooled together, and the protein concentration was determined spectrophotometrically (extinction coefficient 75 000 M^{-1} cm^{-1}). Precursor proteins proOmpA and proOmpA-DHFR were overexpressed in inclusion bodies as previously described elsewhere [50,51] and stored in 8 M urea.

Liposomes preparation

Synthetic lipids and *E. coli* polar lipid extract were purchased from Avanti Polar Lipids, Inc. as stocks in chloroform. The lipids were mixed in desired ratios, and chloroform was evaporated under vacuum conditions at 40 °C using a rotary evaporator (IKA). The dried lipid film was then rehydrated in 50 mM KCl, 50 mM Hepes/KOH pH 7.4 to achieve the lipid concentration of 5 mM. To form large unilamellar vesicles, the crude liposomes were manually extruded through the porous polycarbonate membranes (Nuclepore, Whatman) using the Mini-Extruder set (Avanti Polar Lipids, Inc.). The membrane pore size was decreased stepwise from 400 nm to 200 nm, and vesicle sizes were controlled by dynamic light scattering (Nicomp 3000, Entegris, Inc., Billerica, MA, USA).

SecYEG reconstitution

SecYEG variants were reconstituted in liposomes with different composition at 1 : 1000 protein : lipid ratio as follows. Liposomes were swelled by adding 0.2% DDM followed by incubation for 10 min at 40 °C and then mixed with SecYEG in 0.05% DDM. The reconstitution mixture was incubated for 30 min on ice. The detergent was then removed upon incubation with Bio-Beads SM-2 sorbent (Bio-Rad Laboratories, Feldkirchen, Germany) overnight at 4 °C. Formed proteoliposomes were pelleted upon centrifugation at 80 000 r.p.m. for 30 min (S120-AT3 rotor, Thermo Fisher/Sorvall) and resuspended in 50 mM KCl, 50 mM Hepes/KOH pH 7.4 to achieve the final translocon concentration of 5 μM. To examine the reconstitution efficiency, the proteoliposomes were subjected to centrifugation in the density gradient. 100 μL of proteoliposomes were diluted and mixed with 54% iodixanol-based medium (Optiprep™, Merck/Sigma) to achieve the final iodixanol concentration of 40%. 30% iodixanol was then layered on top followed by 15% and 5%. Samples were centrifuged for 3 h at 200 000 g (TST 60.4 swingout rotor, Thermo Fisher/Sorvall). The gradients were manually fractionated, and the contents were precipitated with trichloroacetic acid (TCA) and analysed on SDS/PAGE.

SecYEG topology in the formed proteoliposomes was analysed by probing the accessibility of the SecY cytoplasmic side. The recombinant SecYEG bears the N-terminal histidine tag on SecY subunit followed by an enterokinase cleavage site [5]. By cleaving the tag from SecYEG reconstituted in liposomes, the amount of correctly oriented SecYEG could be determined due to difference in migration on SDS/PAGE. 5 μL proteoliposomes were mixed with 8 units of enterokinase light chain (New England Biolabs) and diluted to 20 μL, then samples were incubated at 25 °C overnight.

Reconstitution of SecYEG into MSP2N2 nanodiscs was carried out following the previously established protocol [6,34,36]. To achieve the monomeric state of the translocon, a large excess of lipids and the scaffold protein MSP was supplied into the reconstitution reaction (SecYEG : MSP : lipid ratio of 1 : 10 : 1000). SecYEG-loaded and empty nanodiscs were separated via size exclusion chromatography using Superdex 200 10/300 Increase GL column (Cytiva/GE Life Sciences).

In vitro translocation assay

The previously described protocol for the fluorescently labelled preprotein translocation *in vitro* was followed with minor modifications [15,52]. 10 μL of proteoliposomes was mixed with 1 μM SecA (concentration for monomer), 0.5 μM SecB (concentration for tetramer), energy mix (0.05 mg·mL^{-1} phosphocreatine kinase, 10 mM phosphocreatine), 0.1 mg·mL^{-1} BSA, 10 mM DTT, 10 mM MgCl$_2$ and 1 μM proOmpA labelled with fluorescein-maleimide (proOmpA-FM). The total volume was adjusted to 50 μL with buffer (50 mM KCl, 50 mM Hepes/KOH pH 7.4), and samples were equilibrated at 37 °C for 5 min. The translocation was triggered by the addition of 6 mM ATP and left to proceed for 15 min. Afterwards, 10% volume was withdrawn as a reference for the input of proOmpA-FM, and 0.2 mg·mL^{-1} proteinase K was added to the remaining sample to degrade the nontranslocated preprotein. After incubation for 15 min, 150 μL 20% TCA was added, and the aggregated samples were pelleted via centrifugation at 20 000 g for 10 min (Eppendorf 5417 R table-top centrifuge). The pellets were washed with 500 μL ice-cold acetone and centrifuged for 5 min. Acetone was discarded, and the dried pellets were resuspended in 15 μL 2.5x SDS/PAGE sample buffer, incubated for 5 min at 95 °C and then loaded on SDS/PAGE. In-gel fluorescence of the protease-protected proOmpA-FM was recorded and quantified (IMAGEQUANT TL, Cytiva/GE Life Sciences). The background signal was subtracted using the implemented Local average algorithm. The amount of the transported proOmpA-FM was determined based on the available reference sample. At least two independent tests were carried out for each experiment.

FRET-based real-time kinetics assay

FRET-based analysis of the preprotein translocation was carried out following the previously established protocol [15,26]. Briefly, proOmpA^{C292}-DHFR fusion protein was labelled with Cyanine3-maleimide (donor) at the unique cysteine at position 292 of proOmpA domain, and SecY^{C148}EG was labelled with ATTO 643-maleimide

(acceptor) at the periplasmic side. To record the acceptor fluorescence, the monochromators of the thermostated spectrofluorometer (Fluorolog-3, Horiba™ Scientific) were set to the excitation wavelength of 510 nm (slit width 3 nm) and the emission wavelength of 690 nm (3 nm slit width). Prior the translocation, the DHFR domain was stably folded in presence of the cofactors methotrexate and NADPH, as previously described [15]. 100 nм proOmpA-DHFR was mixed with 5 µL proteoliposomes (400 nм SecYEG, dual orientation) in presence of 1 µм SecA and completed to 60 µL of buffer (150 mм KCl, 5 mм MgCl₂, 50 mм Hepes/KOH pH 7.4). The quartz cuvette (Hellma Analytics) was incubated at 37 °C for 150 s, and the translocation reaction was triggered by the addition of 5 mм ATP. The acceptor fluorescence was recorded for 20 min. Rate constants for FRET-dependent fluorescence were extracted using Origin software by fitting the curves to a one-phase association exponential function:

$$Y = Y_b + A\left(1 - e^{-kt}\right)$$ Eq (1).

where Y_b is baseline, A is the amplitude, k is the rate constant, and t is time. At least two independent tests were carried out for each experiment.

ATPase assay

SecA ATPase activity assay was done using malachite green kit (MAK307, Merck/Sigma, Darmstadt, Germany). Briefly, 25 nм or 0.5 µM SecA was mixed with 0.5 µM SecB, 1 µM proOmpA and 10 mм DTT, 5 mм MgCl₂ in the presence of 50 mм Hepes/KOH pH 7.4 and 150 mм KCl. 0.125 or 1 mм SecYEG proteoliposomes (or 1 µм SecYEG) were added; the reaction was started by the addition of ATP and incubated for 15 or 30 min at 37 °C. The reaction was diluted 10 times when necessary. Afterwards, the reaction was stopped by the addition of 20 µL working reagent supplied with the kit. The colour was allowed to develop for 30 min at the ambient temperature, and the absorbance was measured at 590 nm. The data were fitted to Michaelis–Menten equation:

$$V = V_{max} \frac{[S]}{K_m + [S]}$$ Eq (2).

where V is the reaction velocity, V_{max} is the maximum reaction velocity, [S] is the ATP concentration, and K_m is the Michaelis's constant. At least two independent tests were carried out for each experiment.

SecA flotation assay

SecA was mixed with liposomes in protein : lipid molar ratio of 1 : 5000, and the volume was completed to 100 µL with the buffer (50 mм KCl, 50 mм Hepes/KOH pH 7.4, 5 mм MgCl₂). When mentioned, elevated concentrations of KCl

were used. Samples were incubated 30 min at 25 °C and then mixed with 60% sucrose (w/v) to achieve final sucrose concentration of 30%. The samples were loaded in the centrifugation tube (S12-AT3 rotor, Thermo Fisher/Sorvall), followed by 20% sucrose solution (250 µL) and the sucrose-free buffer (50 µL). Samples were centrifuged for 1 h at 80 000 r.p.m. (AT3 rotor). Samples were then fractionated into 3 fractions, top (125 µL), middle (125 µL) and bottom (250 µL), and then precipitated by the addition of 200 µL of 20% TCA. The pellets were resuspended in the sample buffer and loaded on SDS/PAGE. The intensity of Coomassie-stained bands was quantified (IMAGEQUANT TL, Cytiva/GE Life Sciences), and the amount of SecA bound to liposomes was determined by dividing the intensity of the floating fraction (top) by the integral intensity of all fractions. At least two independent tests were carried out for each experiment.

Surface Plasmon resonance

SecA : lipid binding experiments were performed using L1 sensor chip on two-channel Biacore X100 instrument (GE Healthcare Life Sciences). SPR relies on changes in the evanescence wave within a short distance, typically ~ 100 nm, above the sensor surface, so the liposomes were additionally pre-extruded to the diameter of 50 nm. Prior the experiment, the chip surface was cleaned with 20 mм CHAPS (2 injections for 30 s each) and conditioned using SPR running buffer (150 mм KCl, 5 mм MgCl₂, 50 mм Hepes/KOH pH 7,4). The unilamellar liposomes were immobilized at the flow rate of 5 µL·min⁻¹ for 600 s to achieve 7000 to 10 000 response units. DOPC-only liposomes lacking SecA interaction were immobilized in the reference channel. Afterwards, 2 injections of 100 mм NaOH were performed to remove loosely attached material. SecA was transferred into the SPR running buffer and was injected for 150 s at the flow rate of 10 µL·min⁻¹. When indicated, 300 mм KCl was used instead of 150 mм KCl in SPR running buffer to probe SecA binding at higher ionic strength. After each measurement, the chip surface was regenerated (2 injections of 20 mм CHAPS), so the immobilized liposomes were removed. Data were fitted by nonlinear regression analysis of response levels at the steady state to one-site binding model:

$$Req = \frac{KaCR_{max}}{KaC + 1} + offset$$ Eq (3).

where Ka is the association constant, C is the concentration of SecA, R_{max} is the maximum response unit, and offset is the intercept of the fitted curve on the y-axis. Due to extensive binding of SecA to liposome surfaces and potential dissociation/re-binding events known as mass transfer effect, a detailed analysis on binding/dissociation kinetics was omitted. Notably, though, the binding/dissociation recordings were not altered upon increasing the flow rate to 30 µL·min⁻¹, as would be expected under the conditions of the mass transfer effect.

Quartz crystal microbalance

Quartz crystal microbalance (QCM) measurements were carried using Q-Sense Omega Auto instrument (Biolin Scientific, Gothenburg, Sweden). This technique allows the real-time monitoring of SecA interactions with planar supported lipid bilayers (SLBs) by measuring the shifts in the resonance frequency and dissipation energy, which proportionally depend on the mass changes and changes in viscoelastic properties on the surface of the chip, respectively. The formation of SLBs on the QCM-D sensor chip (QSX 303 SiO$_2$) was performed as follows. The surface of the plasma-treated sensor chip was equilibrated with aqueous buffer (50 mM Tris/HCL pH 7.4, 150 mM KCl) for 3 min to stabilize the frequency and dissipation energy baselines. Freshly extruded liposome suspension (extrusion via 100 nm membrane) was injected over the chip surface at flow rate of 50 μL·min^{-1} for 5 min in 50 mM Tris/HCl pH 7.4, 150 mM KCl, 10 mM CaCl$_2$. The liposomes could adsorb on the chip surface and underwent spontaneous collapse, which resulted in formation of SLBs. To remove loosely bound material from the chip surface, the surface was subsequently washed with the buffer (50 mM Tris/HCL pH 7.4 and 150 mM KCl). SLB formation resulted in a frequency shift of -27 ± 1 Hz and the energy dissipation of 0.7 ± 0.1, which is in excellent agreement with previously published data [53]. To probe SecA interaction with the SLBs, the ATPase was transferred into the running buffer (50 mM Tris/HCL pH 7.4, 150 mM KCl, 5 mM MgCl$_2$) and the protein solution was then injected over the SLBs at flow rate of 50 μL·min^{-1}. To determine the affinity of SecA to lipids, the concentration of the ATPase was varied in dilution series from 40 nM to 5.25 μM concentration, and the maximum change in the chip oscillation frequency was measured. Prior each cycle, the surface of the SLB was washed with the high-salt buffer (1 M NaCl, 20 mM Tris/HCL pH 7.4) and then with the running buffer to remove the bound SecA and equilibrate the SLB surface for the next round. The equilibrium dissociation constant (K_d) for this measurement was determined by plotting steady-state net-frequency signal responses prior to dissociation phase (R_{max}) against the corresponding SecA concentration (C). Data were fitted using GraphPad Prism 9 based on one-site binding model:

$$R_{eq} = \frac{R_{max}*C}{K_d+C} \qquad \text{Eq (4).}$$

Membrane fluidity analysis

Liposomes were mixed with 0.1 μM 1,6-diphenyl-1,3,5-hexatriene (DPH) to achieve dye : lipid ratio of 1 : 1000. Samples were incubated for 1 h at 25 °C in the dark. DPH fluorescence was recorded at 428 nm (slit width 5 nm) with the excitation wavelength of 350 nm (slit width 5 nm) using Fluorolog-3 fluorometer. Steady-state anisotropy (r) was calculated as:

$$r = \frac{I_{vv}-GI_{vh}}{I_{vv}+2GI_{vh}} \qquad \text{Eq (5).}$$

where I is the fluorescence intensity, and v and h denote the vertical and horizontal setting for the excitation and emission polarizers, respectively, G is the instrumental correction factor which is provided by the instrument for each measurement. At least two independent tests were carried out for each experiment.

Lipid packing analysis

Liposomes (lipid concentration 100 μM) were mixed with 0.3 μM laurdan to achieve dye : lipid ratio of 1 : 333. Samples were incubated at 37 °C for 1 h in the dark in presence of 50 mM KCl, 5 mM MgCl$_2$, 50 mM Hepes/KOH pH 7.4. Laurdan emission spectrum was recorded from 400 to 600 nm (slit width 3 nm) with the excitation wavelength of 350 nm (slit width 3 nm) using Fluorolog-3 fluorometer. Generalized polarization value (GP) was calculated as a ratio of integrated intensities from 400 nm to 460 nm (I_1) and from 470 nm to 550 nm (I_2):

$$GP = \frac{I1-I2}{I1+I2} \qquad \text{Eq (6).}$$

At least two independent tests were carried out for each experiment.

Cardiolipin head group parametrization

The parameters for the cardiolipin head group were obtained following the linings established in Lipid11 [54] and Lipid14 [55]. Briefly, multiple conformations of the methyl-capped headgroup were generated with Balloon, using an RMSD cutoff of 1 Å. The resulting 21 independent structures were optimized, and the electrostatic potential (ESP) was computed, using Gaussian 09 at the HF/6-31G* theory level, with parameters as given by antechamber [56]. The resulting ESP for all conformations was combined into a multiconformational fit, fixing the capping methyl group charges as established in Lipid11 [54] and using a standard two-step RESP procedure [56]. The obtained partial atomic charges were used together with Lipid17 atom types to generate an AMBER force field library file with LEaP. As the head group has four positions where acyl chains have to be attached (compared to the standard two attachment points per residue in AMBER), explicit bonds have to be set for two positions per cardiolipin when parametrizing a membrane system in LEaP. The parameters have been included in PACKMOL-Memgen [57] of AMBER20, where all combinations of the headgroup with every possible acyl chain in Lipid17 have been considered.

MD simulations

Systems for molecular dynamics simulations were prepared with PACKMOL-Memgen [57], using a length of the

membrane in x and y direction of 100 Å and default options otherwise. To mimic the experimental conditions, compositions of DOPC : DOPG 70 : 30, POPC : POPG 70 : 30, POPC : bis(PO)CL 85 : 15 and POPC : TOCL 85 : 15 were prepared. In addition, systems of DOPC : DOPG 70 : 30 and POPC : POPG 70 : 30 including the 25 N-terminal residues of SecA with an N-methyl amide cap in the C terminus at 25 Å of the membrane surface were prepared. The peptide structure was modelled with TopModel [58], using as main templates *E. coli* SecA (PDB ID : 3BXZ) and *B. subtilis* SecA (PDB ID : 3DL8). In all cases, potassium ions were added to neutralize the charges introduced by the negatively charged headgroups. To ensure independent starting configurations, all systems were packed five times with a different random seed.

From the packed systems, independent replicas were energy-minimized using the pmemd implementation included in AMBER18 [59], using ff14SB [60], TIP3P [61] and Lipid17 [55,62] parameters for the protein, water and membrane lipids, respectively. To relax the system stepwise, alternating steepest descent/conjugate gradient energy minimizations with a maximum of 20 000 steps each were performed. Initially, the positions of the membrane were restrained during minimization; the final round of minimization was performed without restraints. To thermalize the systems, a Langevin thermostat [63] with a friction coefficient of 1 ps^{-1} was used. The pressure, when required, was maintained using a semi-isotropic Berendsen barostat [64] with a relaxation time of 1 ps, coupling the membrane (xy) plane. The system was heated by gradually increasing the temperature from 10 to 100 K for 5 ps under NVT conditions, and from 100 to 300 K for 115 ps under NPT conditions at 1 bar. The thermalization process was continued for 5 ns under NPT conditions, after which production runs of 1 μs length were performed using the same conditions with the pmemd GPU implementation [65], constraining covalent bonds to hydrogens with the SHAKE algorithm [66] and using a time step of 2 fs.

The trajectories were analysed with cpptraj [67] as to lipid order parameters and electron density profiles. The lipid order parameter describes the level of order imposed on the lipid molecules in a bilayer arrangement and relates with deuterium-NMR measurements [68]. The electron density profile describes the probability of finding electron-rich regions along the membrane normal and can be related to X-ray scattering experiments [69]. As the membrane has an anisotropic, that is planar arrangement, it gives information regarding the bilayer arrangement, which in simulations can be additionally decomposed according to the contribution of each system component, obtaining information of its location along the membrane normal. In all cases, the profiles describe well-behaved membrane bilayers. The contacts of the SecA N-terminal peptide with the membrane headgroups were evaluated as the sum of the per-residue contributions as obtained from the native contacts routine, using

a cut-off of 4.5 Å. The average area per lipid of each system was calculate with cpptraj from the area of the xy plane and the number of lipids on each leaflet. To measure the per-lipid type contribution to the area per lipid, the APL@Voro software was used [70]. For this, the trajectories were centred and imaged on the bilayer, and transformed into the GROMACS XTC format with cpptraj. Afterwards, the trajectories were processed with the software, assigning the phosphorous atoms (or the central carbon of the glycerol moiety of cardiolipins) to the area by tessellation. The average xz particle density was calculated using the volmap function of cpptraj, which represents each atom as a Gaussian with a standard deviation equal to the atomic radius, similarly to what has been described previously [11]. Briefly, a 80x80x80 Å grid centred in the membrane centre, with a 1 Å spacing in every dimension, and the average density was calculated along the 1 μs simulation of each system. To obtain the xz profile, the density along the y dimension was averaged.

To calculate the lateral pressure of the equilibrated systems after 1 μs of simulation time as a function of the z-coordinate, all replicas were extended for additional 100 ns, recording the coordinates and velocities every 5 ps. The obtained trajectory was centred on the bilayer, transformed to GROMACS TRR format with cpptraj and postprocessed with GROMACS-LS to obtain the stress tensors [71]. For this, a nonbonded cut-off of 20 Å and otherwise equivalent conditions to the production run were used, processing each ns of simulation independently and calculating the average stress tensor with the provided tensortools script. The lateral pressure was calculated according to equation Eq. 7

$$\Pi(z) = \frac{P_{xx}(z) + P_{yy}(z)}{2} - P_N(z) \qquad \text{Eq (7).}$$

where the first term corresponds to the average lateral term (P_L), and P_N corresponds to the normal component.

Acknowledgements

Conflict of interest

The authors declare no conflict of interest in relation to the presented work.

Author contributions

MK performed biochemical and fluorescence-based analysis; MK and ML carried out SPR and DSF measurements; ML carried out QCM experiments; MK, ML and AK analysed and interpreted the data; SSV and HG carried out the computational simulations and interpreted the data in cooperation with MK and AK; all authors contributed to writing and editing the manuscript.

References

1 Tsirigotaki A, De Geyter J, Šoštarić N, Economou A & Karamanou S (2017) Protein export through the bacterial Sec pathway. *Nat Rev Microbiol* **15**, 21–36.

2 Kusters I & Driessen AJM (2011) SecA, a remarkable nanomachine. *Cell Mol Life Sci* **68**, 2053–2066.

3 Breukink E, Demel RA, de Korte-Kool G & de Kruijff B (1992) SecA insertion into phospholipids is stimulated by negatively charged lipids and inhibited by ATP: A monolayer study. *Biochemistry* **31**, 1119–1124.

4 Wu ZC, De Keyzer J, Kedrov A & Driessen AJ (2012) Competitive binding of the SecA ATPase and ribosomes to the SecYEG translocon. *J Biol Chem* **287**, 7885–7895.

5 Van Der Does C, Swaving J, Van Klompenburg W & Driessen AJM (2000) Non-bilayer lipids stimulate the activity of the reconstituted bacterial protein translocase. *J Biol Chem* **275**, 2472–2478.

6 Kater L, Frieg B, Berninghausen O, Gohlke H, Beckmann R & Kedrov A (2019) Partially inserted nascent chain unzips the lateral gate of the Sec translocon. *EMBO Rep* **20**, e48191.

7 Koch S, Exterkate M, López CA, Patro M, Marrink SJ & Driessen AJM (2019) Two distinct anionic phospholipid-dependent events involved in SecA-mediated protein translocation. *Biochim Biophys Acta - Biomembr* **1861**, 183035.

8 Morein S, Andersson A & Rilfors L (1996) Wild-type Escherichia coli cells regulate the membrane lipid composition in a "window" between gel and non-lamellar structures. *J Biol Chem* **271**, 6801–6809.

9 Siliakus MF, van der Oost J & Kengen SWM (2017) Adaptations of archaeal and bacterial membranes to variations in temperature, pH and pressure. *Extremophiles* **21**, 651–670.

10 Vanni S, Hirose H, Gautier R & Antonny B (2014) A sub-nanometre view of how membrane curvature and

composition modulate lipid packing and protein recruitment. *Nat Commun* **5**, 4916.

11 Ballweg S, Sezgin E, Doktorova M, Covino R, Reinhard J, Wunnicke D, Hänelt I, Levental I, Hummer G & Ernst R (2020) Regulation of lipid saturation without sensing membrane fluidity. *Nat Commun* **11**, e756.

12 Drin G & Antonny B (2010) Amphipathic helices and membrane curvature. *FEBS Lett* **584**, 1840–1847.

13 Sohlenkamp C & Geiger O (2016) Bacterial membrane lipids: Diversity in structures and pathways. *FEMS Microbiol Rev* **40**, 133–159.

14 Lentz BR (1989) Membrane "fluidity" as detected by diphenylhexatriene probes. *Chem Phys Lipids* **50**, 171–190.

15 Kedrov A, Kusters I, Krasnikov VV & Driessen AJM (2011) A single copy of SecYEG is sufficient for preprotein translocation. *EMBO J* **30**, 4387–4397.

16 Roussel G, Lindner E & White SH (2019) Stabilization of SecA ATPase by the primary cytoplasmic salt of Escherichia coli. *Protein Sci* **28**, 984–989.

17 Prabudiansyah I, Kusters I, Caforio A & Driessen AJM (2015) Characterization of the annular lipid shell of the Sec translocon. *Biochim Biophys Acta - Biomembr* **1848**, 2050–2056.

18 Corey RA, Pyle E, Allen WJ, Watkins DW, Casiraghi M, Miroux B, Arechaga I, Politis A & Collinson I (2018) Specific cardiolipin–SecY interactions are required for proton-motive force stimulation of protein secretion. *Proc Natl Acad Sci* **115**, 7967–7972.

19 Koch S, Seinen A-B, Kamel M, Kuckla D, Monzel C, Kedrov A & Driessen AJM (2021) Single-molecule analysis of dynamics and interactions of the SecYEG translocon. *FEBS J* **288**, 2203–2221.

20 Kotov V, Bartels K, Veith K, Josts I, Subhramanyam UKT, Günther C, Labahn J, Marlovits TC, Moraes I, Tidow H *et al.* (2019) High-throughput stability screening for detergent-solubilized membrane proteins. *Sci Rep* **9**, 10379.

21 De Keyzer J, Van der Does C, Swaving J & Driessen AJM (2002) The F286Y mutation of PrlA4 tempers the signal sequence suppressor phenotype by reducing the SecA binding affinity. *FEBS Lett* **510**, 17–21.

22 Harris FM, Best KB & Bell JD (2002) Use of laurdan fluorescence intensity and polarization to distinguish between changes in membrane fluidity and phospholipid order. *Biochim Biophys Acta - Biomembr* **1565**, 123–128.

23 Cantor RS (1999) Lipid composition and the lateral pressure profile in bilayers. *Biophys J* **76**, 2625–2639.

24 Ollila OHS & Vattulainen I (2010) Lateral Pressure Profiles in Lipid Membranes: Dependence on Molecular Composition. Molecular Simulations and Biomembranes: From Biophysics to Function, pp. 26–55. The Royal Society of Chemistry.

25 Findik BT, Smith VF & Randall LL (2018) Penetration into membrane of amino- terminal region of SecA when associated with SecYEG in active complexes. *Protein Sci* **27**, 681–691.

26 Koch S, De Wit JG, Vos I, Birkner JP, Gordiichuk P, Herrmann A, Van Oijen AM & Driessen AJM (2016) Lipids activate SecA for high affinity binding to the SecYEG complex. *J Biol Chem* **291**, 22534–22543.

27 Jilaveanu LB, Zito CR & Oliver D (2005) Dimeric SecA is essential for protein translocation. *Proc Natl Acad Sci USA* **102**, 7511–7516.

28 Bauer BW, Shemesh T, Chen Y & Rapoport TA (2014) A "push and slide" mechanism allows sequence-insensitive translocation of secretory proteins by the SecA ATPase. *Cell* **157**, 1416–1429.

29 Cabelli RJ, Dolan KM, Qian L & Oliver DB (1991) Characterization of membrane-associated and soluble states of SecA protein from wild-type and secA51(Ts) mutant strains of *Escherichia coli*. *J Biol Chem* **266**, 24420–24427.

30 Seinen A-B, Spakman D, van Oijen AM & Driessen AJM (2021) Cellular dynamics of the SecA ATPase at the single molecule level. *Sci Rep* **11**, 1433.

31 Nielsen SB & Otzen DE (2019) Quartz crystal microbalances as tools for probing protein-membrane interactions. *Methods Mol Biol* **2003**, 31–52.

32 Park E & Rapoport TA (2012) Bacterial protein translocation requires only one copy of the SecY complex in vivo. *J Cell Biol* **198**, 881–893.

33 Ryabichko S, Ferreira VDM, Heidi V, Kiyamova R, Dowhan W & Bogdanov M (2020) Cardiolipin is required in vivo for the stability of bacterial translocon and optimal membrane protein translocation and insertion. *Sci Rep* **10**, 6296.

34 Taufik I, Kedrov A, Exterkate M & Driessen AJM (2013) Monitoring the activity of single translocons. *J Mol Biol* **425**, 4145–4153.

35 Koch S, Driessen AJM & Kedrov A (2018) Biophysical analysis of sec-mediated protein translocation in nanodiscs. *Adv Biomembr Lipid Self-Assembly* **28**, 41–85.

36 Ritchie TK, Grinkova YV, Bayburt TH, Denisov IG, Zolnerciks JK, Atkins WM & Sligar SG (2009) Reconstitution of membrane proteins in phospholipid bilayer nanodiscs. *Methods Enzymol* **464**, 211–231.

37 Harayama T & Riezman H (2018) Understanding the diversity of membrane lipid composition. *Nat Rev Mol Cell Biol* **19**, 281–296.

38 Strahl H & Errington J (2017) Bacterial membranes : structure, domains, and function. *Annu Rev Microbiol* **71**, 519–538.

39 Das S, Stivison E, Folta-Stogniew E & Oliver D (2008) Reexamination of the role of the amino terminus of SecA in promoting its dimerization and functional state. *J Bacteriol* **190**, 7302–7307.

40 Roussel G & White SH (2020) Binding of SecA ATPase monomers and dimers to lipid vesicles. *Biochim Biophys Acta - Biomembr* **1862**, 183112.

41 Matin TR, Sigdel KP, Utjesanovic M, Marsh BP, Gallazzi F, Smith VF, Kosztin I & King GM (2017) Single-molecule peptide–lipid affinity assay reveals interplay between solution structure and partitioning. *Langmuir* **33**, 4057–4065.

42 Kusters I, Van Den Bogaart G, Kedrov A, Krasnikov VV, Fulyani F, Poolman B & Driessen AJM (2011) Quaternary structure of SecA in solution and bound to SecYEG probed at the single molecule level. *Structure* **19**, 430–439.

43 Sardis MF & Economou A (2010) SecA: A tale of two protomers: MicroReview. *Mol Microbiol* **76**, 1070–1081.

44 Gold VAM, Robson A, Bao H, Romantsov T, Duong F & Collinson I (2010) The action of cardiolipin on the bacterial translocon. *Proc Natl Acad Sci* **107**, 10044–10049.

45 Roussel G & White SH (2020) The SecA ATPase motor protein binds to Escherichia coli liposomes only as monomers. *Biochim Biophys Acta - Biomembr* **1862**, 183358.

46 Gold VAM, Robson A, Clarke AR & Collinson I (2007) Allosteric regulation of SecA: Magnesium-mediated control of conformation and activity. *J Biol Chem* **282**, 17424–17432.

47 Deville K, Gold VAM, Robson A, Whitehouse S, Sessions RB, Baldwin SA, Radford SE & Collinson I (2011) The oligomeric state and arrangement of the active bacterial translocon. *J Biol Chem* **286**, 4659–4669.

48 Unsay JD, Cosentino K, Subburaj Y & García-Sáez AJ (2013) Cardiolipin effects on membrane structure and dynamics. *Langmuir* **29**, 15878–15887.

49 Kropinski AMB, Lewis V & Berry D (1987) Effect of growth temperature on the lipids, outer membrane proteins, and lipopolysaccharides of Pseudomonas aeruginosa PAO. *J Bacteriol* **169**, 1960–1966.

50 Kusters I, van den Bogaart G, de Wit J, Krasnikov V, Poolman B & Driessen A (2010) Purification and Functional Reconstitution of the Bacterial Protein Translocation Pore, the SecYEG Complex. *Methods Mol Biol* **619**, 131–143.

51 Bol R, De Wit JG & Driessen AJM (2007) The active protein-conducting channel of Escherichia coli contains an apolar patch. *J Biol Chem* **282**, 29785–29793.

52 De Keyzer J, Van der Does C & Driessen AJM (2002) Kinetic analysis of the translocation of fluorescent precursor proteins into Escherichia coli membrane vesicles. *J Biol Chem* **277**, 46059–46065.

53 Wang L, Biswas KH, Yoon BK, Kawakami LM, Park S, Groves JT, Li L, Huang W & Cho N-J (2018) Membrane reconstitution of monoamine oxidase

80

enzymes on supported lipid bilayers. *Langmuir* **34**, 10764–10773.

54 Skjevik ÅA, Madej BD, Walker RC & Teigen K (2012) LIPID11: a modular framework for lipid simulations using amber. *J Phys Chem B* **116**, 11124–11136.

55 Dickson CJ, Madej BD, Skjevik ÅA, Betz RM, Teigen K, Gould IR & Walker RC (2014) Lipid14: the amber lipid force field. *J Chem Theory Comput* **10**, 865–879.

56 Wang J, Wang W, Kollman PA & Case DA (2006) Automatic atom type and bond type perception in molecular mechanical calculations. *J Mol Graph Model* **25**, 247–260.

57 Schott-Verdugo S & Gohlke H (2019) PACKMOL-Memgen: A simple-to-use, generalized workflow for membrane-protein–lipid-bilayer system building. *J Chem Inf Model* **59**, 2522–2528.

58 Mulnaes D, Porta N, Clemens R, Apanasenko I, Reiners J, Gremer L, Neudecker P, Smits SHJ & Gohlke H (2020) TopModel: template-based protein structure prediction at low sequence identity using top-down consensus and deep neural networks. *J Chem Theory Comput* **16**, 1953–1967.

59 Darden T, York DM & Pedersen LG (1993) Particle mesh Ewald: An N*log(N) method for Ewald sums in large systems. *J Chem Phys* **98**, 10089–10092.

60 Maier JA, Martinez C, Kasavajhala K, Wickstrom L, Hauser KE & Simmerling C (2015) ff14SB: Improving the Accuracy of Protein Side Chain and Backbone Parameters from ff99SB. *J Chem Theory Comput* **11**, 3696–3713.

61 Jorgensen WL, Chandrasekhar J, Madura JD, Impey RW & Klein ML (1983) Comparison of simple potential functions for simulating liquid water. *J Chem Phys* **79**, 926–935.

62 Case DA, Cerutti DS, Cheatham TE III, Darden TA, Duke RE, Giese TJ, Gohlke H, Goetz AW, Greene D,

Homeyer N *et al.* (2017) Amber17. University of California San Francisco.

63 Quigley D & Probert MI (2004) Langevin dynamics in constant pressure extended systems. *J Chem Phys* **120**, 11432.

64 Berendsen HJC, Postma JPM, van Gunsteren WF, Di Nola A & Haak JR (1984) Molecular dynamics with coupling to an external bath. *J Chem Phys* **81**, 3684–3690.

65 Le Grand S, Götz AW & Walker RC (2013) SPFP: Speed without compromise—A mixed precision model for GPU accelerated molecular dynamics simulations. *Comput Phys Commun* **184**, 374–380.

66 Ryckaert J-P, Ciccotti G & Berendsen HJC (1977) Numerical integration of the cartesian equations of motion of a system with constraints: molecular dynamics of n-alkanes. *J Comput Phys* **23**, 327–341.

67 Roe DR & Cheatham TE III (2013) PTRAJ and CPPTRAJ: Software for Processing and Analysis of Molecular Dynamics Trajectory Data. *J Chem Theory Comput* **9**, 3084–3095.

68 Piggot TJ, Allison JR, Sessions RB & Essex JW (2017) On the Calculation of acyl chain order parameters from lipid simulations. *J Chem Theory Comput* **13**, 5683–5696.

69 Liu Y & Nagle JF (2004) Diffuse scattering provides material parameters and electron density profiles of biomembranes. *Phys Rev E* **69**, 40901.

70 Lukat G, Krüger J & Sommer B (2013) APL@Voro: a voronoi-based membrane analysis tool for GROMACS trajectories. *J Chem Inf Model* **53**, 2908–2925.

71 Vanegas JM, Torres-Sánchez A & Arroyo M (2014) Importance of force decomposition for local stress calculations in biomembrane molecular simulations. *J Chem Theory Comput* **10**, 691–702.

Chapter 4

Characterization of SecA: membrane interaction and its role in protein transport

Authors:	Michael Kamel, Jennifer Loschwitz, Wieland Steinchen, Gerd Bange, Birgit Strodel, Alexej Kedrov.
Published:	In preparation.
Impact factor:	
Own work:	70%.
Contribution:	Michael Kamel wrote the manuscript.
	Michael Kamel performed biochemical, fluorescence-based analysis and SPR.
	Jennifer Loschwitz performed MD simulations.
	Wieland Steinchen performed HDX MS experiments.
	Michael Kamel and Alexej Kedrov analyzed and interpreted the data.

Abstract

SecA is a peripheral membrane motor protein that interacts with the membrane and the membrane-embedded channel, SecYEG, to transport unfolded pre-proteins across the cytoplasmic membrane of bacteria using ATP hydrolysis as an energy source. The membrane composition has a substantial effect on the protein transport activity of the SecYEG: SecA translocon. Anionic lipids have been shown to be essential for protein transport, which has been attributed to the electrostatic interaction with positive residues on the N-terminal helix of SecA. Additionally, it has been shown that SecA interacts preferentially with mono-unsaturated fatty acids-rich membranes, however, the underlying mechanism is still not clear.

Here, two different sites within SecA have been identified to interact with the membrane based on HDX-MS analysis: the N-terminal helix of SecA, as previously established, and the second half of the HSD of SecA. An AlphaFold2 model shows that the N-terminal helix of SecA is split into a small helix, a short linker, and a long helix. Mutational analysis shows that electrostatic interaction with the membrane is mediated through the long helix, while the short helix mediates hydrophobic interaction and SecA insertion into the membrane. Disturbing both interactions decreases membrane binding, while disturbing only hydrophobic interactions has an effect on the translocating ATPase activity of SecA. Moreover, this study provides evidence that the N-terminal helices of SecA homologs are tuned to provide efficient interaction with the different membranes across different bacterial species.

4.1   Introduction

The transport of secretory, periplasmic, and outer membrane proteins across the cytoplasmic membrane occurs mainly through the Sec translocon. The core components of the Sec translocon are the membrane-embedded channel, SecYEG, and the ATPase motor protein, SecA. After complete synthesis by the ribosomes, substrates with N-terminal cleavable signal peptides are picked up by cytoplasmic chaperones like the holdases SecB. SecB keeps the substrates in their unfolded secretion-competent state and delivers the client proteins to the Sec machinery, where they get transported across the cytoplasmic membrane. SecA bound to SecYEG provides the energy for transport through ATP hydrolysis coupled to conformational changes [1].

SecA is a peripheral membrane protein that is composed of multiple domains (Figure 4.1). It has two nucleotide-binding domains, NBD1 and NBD2, which are responsible for the binding and hydrolysis of ATP [2, 3], followed by the polypeptide crosslinking domain (PPXD) responsible for the binding of the pre-proteins [4, 5]. The C-domain of SecA is composed of four subdomains, the helical scaffold domain (HSD), the helical wing domain (HWD), the two helix finger (THF) [6], and finally the C-terminal linker domain (CTD) [7, 8]. SecA has an N-terminal amphipathic helix that has been shown to be essential for the membrane binding of SecA [9].
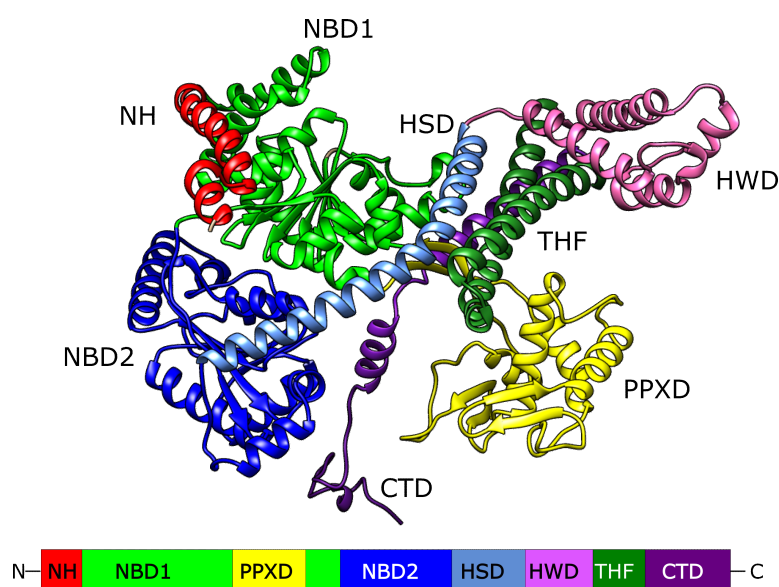
Figure 4.1: The structure and the domains of the peripheral membrane motor protein, SecA. Top: AlphaFold2 model of *E.coli* SecA with colored domains. Bottom: The different domains of SecA are arranged according to its primary sequence. NH: N terminal helix; NBD1, and NBD2: nucleotide-binding domain 1 and 2; PPXD: polypeptides crosslinking domain; HSD: helical scaffold domain; HWD: helical wing domain; THF: two helix finger and CTD; C-terminal linker domain.

The lipid composition of the cytoplasmic membrane has been shown to have a crucial effect on the Sec machinery. Anionic lipids, phosphatidyl glycerol, and cardiolipin are essential for protein transport via the SecYEG: SecA translocon [10–12]. This has been attributed to the interaction between the anionic lipids and the positively charged residues on the N-terminal amphipathic helix of SecA. This helps anchoring of SecA on the membrane interface and facilitates the assembly of the SecYEG: SecA complex. Absence of the anionic lipids or deletion of the N-

terminal helix of SecA abolishes the protein transport activity of the Sec machinery [13–16]. Our recent work has revealed that the acyl chain composition of the membrane has a crucial effect on the activity of the SecYEG: SecA translocon. Membranes which are rich in saturated acyl chains cause the membrane to exist in the gel phase within the physiological temperature. This leads to the complete abolishment of transport activity, highlighting the necessity of a fluid-phase membrane. Interestingly, increasing the content of the mono-unsaturated fatty acids (UFAs) within the membrane without changing the membrane fluidity leads to the stimulation of protein transport [17]. One possible explanation is that mono-UFAs introduce lipid packing disorder within the lipid head groups that allows a tighter interaction of the amphipathic helix of SecA with the membrane. However, the exact underlying mechanism is not clear.

Earlier studies have shown that SecA exists *in vivo* in two states, a soluble cytoplasmic state, and a membrane-bound state [18]. However, a new single molecule study based on super-resolution microscopy showed that SecA exists predominantly in the membrane-bound state [19]. There is a general agreement that the N-terminal helix of SecA is a crucial component of SecA: membrane interaction [15, 16]. Another study has shown that the C-terminus is also involved in membrane binding [9]. Nevertheless, the exact binding interface of SecA to the membrane has not been completely identified. Moreover, it has been shown that once the N-terminal helix of SecA stimulates membrane binding of SecA, conformational changes are followed that prime SecA for high affinity binding to SecYEG [16]. However, the exact mechanism and the role of the N-terminal helix in regulating protein transport are not yet understood.

The aim of this work is to determine the membrane contact sites of SecA and to understand the role of the N-terminal helix in regulating both membrane binding and protein transport. HDX-MS experiments suggested that the N-terminal helix of SecA and the second half of the HSD contact the membrane. Mutational analysis showed that decreasing the positive charge on the N-terminal helix of SecA decreases membrane binding but has little effect on SecA ATPase activity and protein transport. Notably decreasing the hydrophobicity of the first part of the helix or increasing its polarity impacts both SecA membrane binding and its ATPase activity. Additionally, this study provides evidence that the N-terminal helices of different SecA homologs show a preference for mono-UFAs-rich membranes and are evolutionarily tuned to interact with the different membrane compositions across the different bacterial species.

4.2 Material and methods

4.2.1 SecA expression and purification

The genes of *E. coli* SecA wild-type and mutants, and homologs from *P. aeruginosa, B. subtilis, and T. maritma* were cloned in pET21a plasmid with a C terminal hexahistidine tag and were transformed to *E.coli* BL21 (DE3). Overexpression was induced with 0.5 mM IPTG and carried out for 3 h at 37°C. Cells were harvested by centrifugation for 15 minutes at 5000 g, then resuspended in 20 mM Tris/HCl, pH 7.5, 50 mM KOAc, 5 mM Mg(OAc)$_2$, 200 μM TCEP, 20% glycerol, cOmplete protease inhibitor cocktail (Roche, Mannheim, Germany). Cells were then lysed (Microfluidizer, M-110P, Microfluidics Corp., Westwood, MA, USA) and the lysate was clarified by ultracentrifugation for 30 minutes at 40000 rpm (45 Ti rotor, Beckman Coulter, Brea, CA, USA). The supernatant was loaded on HisTrap^{TM} FF column (Cytiva Life Sciences), and the column was washed with 25 ml of 20 mM Tris/HCl, pH 7.5, 500 mM KOAc, 5 mM Mg(OAc)$_2$, 200 μM TCEP, 20 % glycerol, and 20 mM imidazole. The protein was then eluted with 20 mM Tris/HCl, pH 7.5, 50 mM KOAc, 5 mM Mg(OAc)$_2$, 200 μM TCEP, 20 % glycerol, and 300 mM imidazole. The elution fractions were then loaded on Superose 6 Increase 10/300 GL, and size excluded in 20 mM Tris/HCl, pH 7.5, 50 mM KOAc, 5 mM Mg(OAc)$_2$, 200 μM TCEP, 20 % glycerol, peak fractions were pooled together, protein concentration was then determined using an extinction coefficient of 77240 M^{-1}cm^{-1} using UV-Vis spectrophotometer (Neodot, NeoBiotech, Nanterre, France). Protein was then frozen and stored at -80°C.

4.2.2 SecYEG expression and purification

SecYEG was overexpressed in *E.coli* C41 (DE3) with an N-terminal deca-histidine tag on the SecY subunit. Overexpression was induced with 0.5 mM IPTG and then performed for 3 h at 37°C. Cells were then harvested by centrifugation for 15 minutes at 5000 g and resuspended in 20 mM Hepes/ KOH pH 7.5, 50 mM KOAc, 5 mM Mg(OAc)$_2$, 5 % glycerol, 1 mM DTT and cOmplete protease inhibitor cocktail. Cells were lysed and debris was then removed by centrifugation for 10 min at 10000 g in Sorvall SS34 rotor (Thermo Scientific). Membranes were isolated by ultracentrifugation for 1 h at 40000 rpm (45 Ti rotor, Beckman Coulter, Brea, CA, USA). Membranes were then solubilized for 1 h at 4°C in solubilization buffer (50 mM Hepes/KOH, pH 7.4, 500 mM KCl, 5 % glycerol, 200 μM TCEP, 1% N-dodecyl-β-D-maltoside (DDM) (Glycon Biochemicals GmbH, Luckenwalde, Germany)). The solubilized membranes were centrifuged for 10 minutes at a tabletop centrifuge and the supernatant was then incubated with Ni^{2+} NTA agarose beads (Qiagen, Hilden, Germany) for 1 h at 4°C. In case labeling was required for single cysteine SecY^{L148C}EG, the beads were incubated for 2 h at 4°C with 100 - 200 μM ATTO 647N maleimide (ATTO-Tec GmbH). The beads were washed with 50 mM Hepes/KOH, pH 7.4, 500 mM KCl, 5 % glycerol, 200 μM TCEP, 0.05% DDM, 20 mM imidazole, then eluted with 50 mM Hepes/KOH, pH 7.4, 150 mM KCl, 5 % glycerol, 200 μM TCEP, 0.05% DDM, 300 mM imidazole. The protein was then buffer exchanged using PD 10 column (Cytiva Life Sciences) in 50 mM Hepes/KOH, pH 7.4, 150 mM KCl, 5 % glycerol, 200 μM TCEP, 0.05% DDM. Protein concentration was then determined spectrophotometrically based on an extinction coefficient of 72000 M^{-1}cm^{-1}.

4.2.3 Liposomes preparation

All lipids were purchased from Avanti Polar Lipids, Inc in chloroform stocks. Lipids were mixed in the required ratios and then chloroform was evaporated under vacuum conditions at 40 °C using a rotary evaporator (IKA, IKA-Werke GmbH & Co. KG). The lipid film was then resuspended in 50 mM KCl, 50 mM Hepes/ KOH, pH 7.4. Liposomes were extruded using polycarbonate membranes (Nuclepore, Whatman) using the Mini-Extruder set (Avanti Polar Lipids, Inc.). For flotation assays and reconstitution of SecYEG, liposomes were extruded to 200 nm. For SPR experiments, liposomes were extruded first to 200 nm, then to 50 nm.

4.2.4 Liposomes flotation assay

SecA wild-type, mutants and homologs were mixed with liposomes to achieve a 5000-fold molar excess of lipids unless indicated otherwise, the volume was completed to 100 μl and incubated for 15 minutes at room temperature. The reaction was then mixed with 100 μl 60 % sucrose solution in flotation assay buffer (50 mM KCl, 50 mM Hepes/KOH pH 7.4, 5 mM MgCl$_2$). 250 of μl 20% sucrose was then layered on top followed by 50 μl flotation assay buffer. For experiments with different salt conditions, the required salt concentration was added to the flotation assay buffer and in all sucrose solutions. Samples were ultracentrifuged for 1 h at 80000 rpm (S12-AT3 rotor, Thermo Fisher/Sorvall). Afterward, the gradient was fractionated in 3 fractions from bottom to top, the bottom fraction with 250 μl, then the middle fraction with 125 μl, and the top fraction with 125 μl. 300 μl 20 % TCA was then added to each fraction, and samples were incubated for 30 minutes on ice, followed by 15 minutes of centrifugation in a tabletop centrifuge (Eppendorf 5417 R) at full speed at 4°C. The supernatant was discarded, and 500 μl ice-cold acetone was added followed by centrifugation for 5 minutes in a tabletop centrifuge at full speed. The pellets were dried at 37°C and resuspended in 30 μl of 2X SDS PAGE sample buffer and analyzed using SDS/PAGE. The intensities of SecA bands were quantified (IMAGEQUANT TL, Cytiva/GE Life Sciences), and the amount of SecA bound to liposomes was determined by dividing the SecA band intensity of the top fraction by the sum of all SecA bands of all fractions.

4.2.5 SecYEG reconstitution into proteoliposomes

Pre-extruded liposomes were solubilized using 0.5 % Triton X-100 for 10 minutes at 40°C. Afterward, SecYEG was mixed with solubilized liposomes in a 1:1000 protein-to-lipid ratio. The mixture was incubated for 30 minutes on ice. The detergent was removed by incubation with Bio-Beads SM-2 sorbent (Bio-Rad Laboratories, Feldkirchen, Germany) overnight at 4°C. The mixture was then ultracentrifuged for 30 minutes at 80000 rpm (S12-AT3 rotor, Thermo Fisher/Sorvall). Proteoliposomes were then resuspended in 50 mM Hepes/KOH, pH 7.4, and 150 mM KCl.

4.2.6 *In vitro* translocation assay

1 μM of dual orientation SecYEG reconstituted in proteoliposomes were mixed with 0.5 μM SecB (tetramer concentration), energy mix (0.05 mg/ml phosphocreatine kinase, 10 mM phosphocreatine), 0.1 mg/ml BSA, 5 mM MgCl$_2$, 10 mM DTT, 0.5 μM proOmpA labeled with fluorescein-5-maleimide (Cayman Chemical Company), 6 mM ATP and volume was completed

to 45 μl. The reactions were incubated for 5 minutes at 37°C, 5 μl of SecA that was diluted accordingly to reach a final concentration of (200 or 1000 nM) was added, and the reactions were incubated for 15 minutes. Reaction without SecA was included as a negative control. The reactions were placed on ice and 5 μl were withdrawn to represent 10 % of the total proOmpA added. 1 μl of 10 mg.ml^{-1} of proteinase K was added to the reaction, and they were incubated for 15 minutes at room temperature. 150 μl of 10 % TCA was added followed by incubation for 30 minutes on ice. The reactions were then centrifuged using a tabletop centrifuge (Eppendorf 5417 R) at full speed for 15 minutes at 4°C. The supernatant was discarded and 500 μl ice-cold acetone was added, and the samples were centrifuged for 5 more minutes in a tabletop centrifuge. Acetone was discarded and pellets were dried at 37°C, then resuspended in 15 μl of 2X SDS/PAGE sample buffer and loaded on SDS/PAGE. The In-gel fluorescence of the proteinase K-protected proOmpA band was quantified (IMAGEQUANT TL, Cytiva/GE Life Sciences), and the percent of transported proOmpA was calculated using the signal from the 10 % input sample as a reference.

4.2.7 FRET-based real-time translocation assay

FRET-based analysis of the pre-protein translocation was performed using Cyanine 3- maleimide (LumiProbe) labeled proOmpA^{C292}-DHFR fusion protein and ATTO 647N maleimide-labeled SecY^{C148}EG. Acceptor fluorescence was recorded as a function of time by setting the monochromators of the thermostated (37°C) spectrofluorometer (Fluorolog-3, Horiba™ Scientific) to the excitation wavelength of 510 nm (slit width 3 nm) and the emission wavelength of 690 nm (3 nm slit width). Prior to the reaction, the DHFR domain was folded by incubating 5 uM proOmpA-DHFR with 10 μM SecB, 10 mM NADPH, and 10 μM methotrexate in folding buffer (150 mM KCl, 50 mM Hepes/KOH, pH 7.4 and 5 mM TCEP) for 10 minutes at 37°C. 250 nM proOmpA-DHFR was mixed with proteoliposomes that are equivalent to 250 nM SecYEG (dual orientation) in the presence of 50 nM SecA and completed to 100 μL of buffer (150 mM KCl, 5 mM MgCl2, 50 mM Hepes/KOH pH 7.4). The quartz cuvette (Hellma Analytics) was incubated at 37 °C for 150 s, and the translocation reaction was started by the addition of 5 mM ATP. The acceptor fluorescence was recorded for 20 min.

4.2.8 ATPase assay

The ATPase activity of SecA was determined using the Malachite green phosphate assay kit (MAK307, Sigma Aldrich). Briefly, 10 nM of SecA wild-type or mutants were mixed with 10 molar excess of SecYEG proteoliposomes and the substrate proOmpA in ATPase buffer (150 mM KCl, 50 mM Hepes/KOH, pH 7.4 and 5 mM MgCl$_2$). 250 μM of ATP was then added in case of single point measurement or ATP was titrated from 3.125 to 250 μM in case of kinetics measurements. The reaction was carried out at 37°C for 15 minutes and then stopped by 20 μl of working reagent. The color was developed for 20 minutes at room temperature, subsequently, the absorbance was measured at 620 nm. Kinetic data were fitted to the Michelis-Menten equation.

$$V = V_{max} \frac{[S]}{K_m + [S]}$$

where V is the reaction velocity, V_{max} is the maximum reaction velocity, [S] is the ATP concentration and K_m is the Michaelis's constant.

4.2.9 Surface plasmon resonance

SPR measurements were carried out on a two-channel 2SPR system (SR7500DC, Reichert Inc.). Liposomes were immobilized on a chip with hydrophobic anchors (LP, XanTec Bioanalytics GmbH, Düsseldorf, Germany). Briefly, the surface of the chip was cleaned using a mixture of isopropanol and 50 mM NaOH (2:3) followed by an injection of 0.5 mM liposomes resulting in a signal of approximately 8000 response units (RU) in case of DOPC liposomes and 5000 RU in case of DOPC: DOPG (70:30) liposomes. Serial dilutions of SecA were prepared in the running buffer (150 mM KCl, 50 mM Hepes/KOH, pH 7.4, and 5 mM $MgCl_2$) and then injected for 5 minutes at the flow rate of 25 μL/min to allow SecA: liposome binding followed by a dissociation phase of 15 min with the running buffer. At the end of each association/dissociation cycle, the chip surface was cleaned by the injection of a mixture of isopropanol and 50 mM NaOH (2:3). The cleaning/regeneration step was required due to the incomplete dissociation of SecA. Kinetic analysis was performed using TraceDrawer 1.9 (Ridgeview Instruments AB, Uppsala, Sweden) and sensorgrams were fitted to a 1:1 two-state kinetic model, while affinity analysis was fitted to a one-site binding model. All sensorgrams were corrected by the subtraction of the reference channel and a buffer injection (blank).

4.2.10 Mass photometry

SecA wild-type or mutants were diluted to 10 nM in a buffer containing 150 mM KCl, 50 mM Hepes/KOH, pH 7.4, and 5 mM $MgCl_2$. The samples were measured using Refeyn one^{MP}(Refeyn Ltd, Oxford, United Kingdom). Data acquisition was performed using AcquireMP (Refeyn Ltd, v1.1.3) and data analysis was performed using DiscoverMP (Refeyn Ltd, v1.2.3).

4.2.11 *In vivo* complementation assay

The *E.coli* strain Bl21.19 was transformed with plasmids carrying the genes for wild-type SecA or mutants. Cells were plated on agar plates with ampicillin and chloramphenicol and grown at 30°C overnight. Overnight cultures were then prepared and grown at 30°C overnight. On the second day, the cultures were diluted 25 times to a new media and grown till OD reached 0.5. Afterward, a 5-dilution series were prepared from each culture with 10-fold dilution in each series and then plated on an agar plate and grown either on 42°C or 30°C. 10 μM IPTG was added when induction was required.

4.3 Results

4.3.1 The membrane contact sites of SecA

The presence of anionic lipids in the membrane is crucial for efficient SecA: membrane binding. SecA is also sensitive to the unsaturated fatty acids (UFAs) content of the membrane [17]. To understand the binding mechanism, the exact domains of SecA that contact the membrane have to be determined. To that aim, hydrogen-deuterium exchange mass spectrometry (HDX-MS) was employed. Among multiple applications, HDX-MS is a very powerful method to elucidate the binding sites of proteins to their ligands, by monitoring the difference in hydrogen-deuterium exchange between the protein alone and in the presence of an interacting partner [20]. Thus, it was assumed that SecA binding interface may be identified based on its accessibility. First, the minimum amount of lipids that are required to achieve an efficient SecA binding had to be determined. Therefore, using liposomes flotation assay (Figure 4.2 A), SecA was tested for liposome binding by incubating with an increasing molar ratio of DOPC: DOPG (70:30) liposomes starting from 1:250 to 1:5000 protein to lipids ratio. Subsequently, the mixture was placed on the bottom of a sucrose gradient and centrifuged. The efficiency of SecA binding was determined by quantifying the amount of SecA that floated with the liposomes relative to the total amount of SecA added. Efficient SecA binding was achieved at a protein-to-lipid molar ratio of 1:2000 (Figure 4.2 B). HDX MS was then performed on SecA alone and in the presence of 2000 fold molar excess of DOPC: DOPG (70:30) and POPC: TOCL (70:15), which is the lipid composition that was previously shown to achieve maximum SecA membrane binding [17]. By analyzing the difference in deuterium incorporation between liposomes bound SecA and SecA alone, two membrane contact sites of SecA were identified (Figure 4.2 C-E). The first site includes residues 7 to 29, which is the N-terminal helix of SecA as expected. As this domain is known to interact with the membrane, its appearance validated the applicability of HDX-MS. The second site comprises the residues 649 to 667, these residues represent the second half of the HSD domain of SecA.
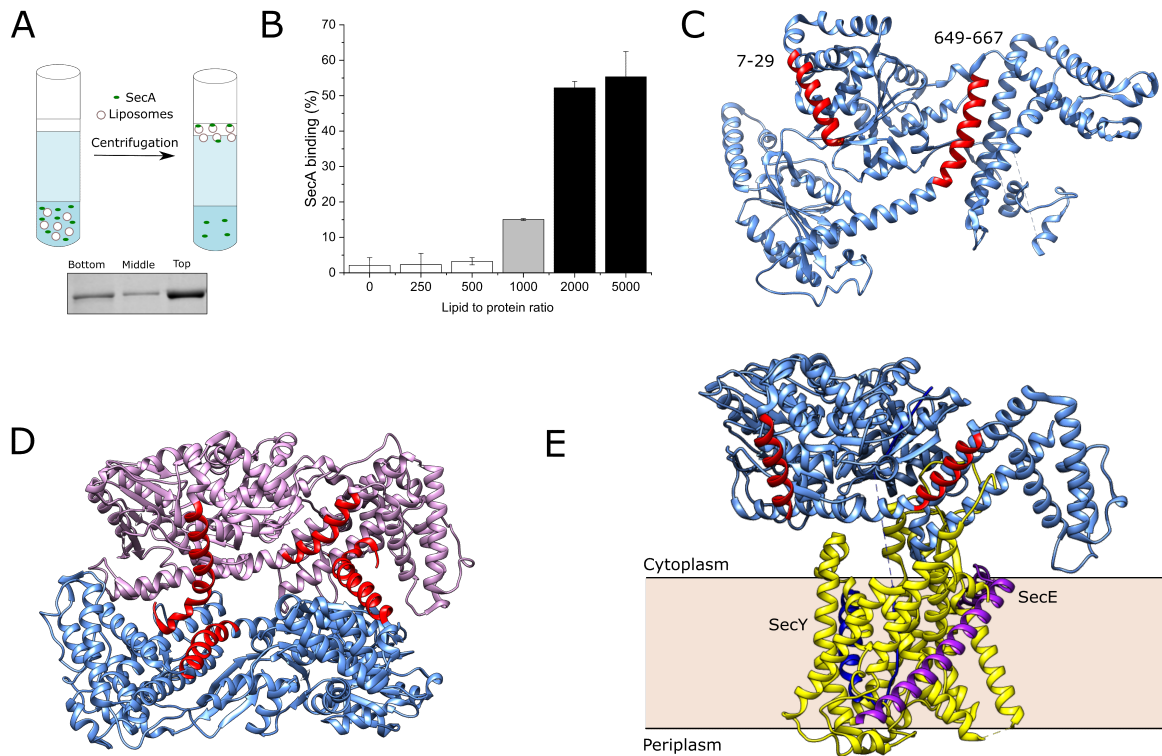
Figure 4.2: The membrane contact sites of SecA. A) SecA: liposomes flotation assay. B) A protein-to-lipid ratio of 1:2000 is sufficient to achieve efficient SecA binding to DOPC: DOPG liposomes. C) Residues 7 to 29 of the N-terminal helix and residues 649 to 667 of the HSD contact the membrane as determined by HDX-MS. D) The position of the two lipid-binding sites of SecA marked in red in the *B. subtilis* dimer, the probable physiological dimer (PDB: 1M6N). E) The position of the two lipid-binding sites of SecA in the cryo-EM structure of SecYEG: SecA translocon (PDB: 6ITC).

4.3.2 Characterization of the first membrane contact site: the N-terminal helix of SecA

The N-terminal helix of SecA has been previously shown to be essential for SecA membrane binding. Deleting the helix abolishes membrane binding and causes loss of activity. Bauer et al 2014 [15] showed that replacing the first 20 amino acids with a histidine tag restored membrane binding and protein transport activity when liposomes made of Ni $^{2+}$ containing lipids 18:1 DGS NTA were used. Helical wheel projection of the N-terminal helix of the *E. coli* SecA shows an amphipathic helix that has a highly polar face with a net charge of $+7$ and an opposite hydrophobic face. AlphaFold2 model of *E.coli* SecA (Figure 4.1 and 4.3 A) shows that the N-terminal helix is broken into a small helix ($\alpha 0$) from residues 2 to 10 and a long helix ($\alpha 1$) from residues 13 to 30 (Figure 4.3 A). In the available structures of the *E. coli* SecA (PDB: 2FSF, 2VDA, 3BXZ and 6GOX), the N-terminal helix was never completely resolved. To characterize the necessity of the helix and its amphipathic profile for SecA: membrane interaction, mutations were introduced to disturb the charge distribution over the helix and its hydrophobic property. Five different mutants were constructed. Firstly, the first mutant ΔN10 involves the deletion of the first 10 amino acids, hence deleting the $\alpha 0$ helix, while the second mutant, ΔN20, involves the deletion of the first 20 amino acids, which has been previously shown to abolish the membrane

binding and the activity of SecA [15, 16]. The mutant H1 involves the exchange of residues K4 and K9 with their preceding amino acids I3 and T8. These mutations cause the movement of the positive charges to the hydrophobic side of the $\alpha 0$ helix. The mutant H2 involves the exchange of R19 with L18 and V24 with K23. These exchanges cause the removal of 2 positive charges from the hydrophilic side of $\alpha 1$ helix reducing the total positive charge in the positively charged face and reducing the hydrophobic moment in the hydrophobic face of the helix. The mutant H3 includes both the mutations of H1 and H2 mutants (Figure 4.3 A). These mutants allow the characterization of which part of the helix is essential for membrane binding and whether the accumulation of the positive charges on one face of the helix is essential for both membrane binding and activity.

SecA exists as a dimer in solution with a dissociation constant that ranges from 1 nM to 3 μM that strongly depends on ionic strength [21, 22]. However, the oligomeric state of the membrane-bound SecA has been strongly disputed. Recent reports proposed that SecA monomerizes once it binds the membrane [23–26]. The oligomeric state of the designed mutants was determined using mass photometry, a method that can accurately measure the mass of molecules based on their light scattering properties [27]. Most SecA wild-type molecules existed as dimers (Figure 4.3 B), while SecA ΔN10 and ΔN20 existed mainly as monomers (Figure 4.3 C). This is in good agreement with previous results that reported that a ΔN11 mutant is mostly monomeric. [28, 29]. Additionally, these results fit well with the fact that the *B. subtilis* (PDB:1M6N) is the probable physiological dimer where the N-terminal helix of SecA is positioned exactly at the dimer interface (Figure 4.2 D). Therefore, it is expected that deleting the helix causes SecA monomerization. SecA H1, H2, and H3 mutants were mostly dimeric but to a lesser extent than the SecA wild type (Figure 4.3 C). The stability of the H1 and H3 variants was measured using differential scanning fluorimetry and found to be similar to the wild-type SecA indicating that these mutations did not affect the protein stability (Figure 4.3 D).

Next, the designed mutants were tested for membrane binding using liposomes flotation assay. Both the ΔN10 and ΔN20 mutants lost the ability to bind DOPC: DOPG liposomes. H1 showed a slight decrease in membrane binding as compared to the wild-type SecA. On the other hand, H2 and H3 mutants showed a dramatic decrease in binding to DOPC: DOPG. This shows that indeed the accumulation of positive charges on one face of the helix is essential for membrane binding (Figure 4.4 A).

The designed mutants were then tested for protein transport activity using the *in vitro* translocation assay. The aim was to examine the effect of reducing membrane binding on protein transport activity. As expected, the activity of SecA ΔN20 was lost as previously reported [15, 16], while the SecA ΔN10 mutant showed a dramatic decrease in activity as compared to the wild type SecA (Figure 4.4 B and C), in good agreement with earlier reports [28, 29]. Interestingly, SecA H1 and H3 mutants showed similar activity as the wild-type SecA, when a high concentration of SecA was used (1 μM) was used, despite the dramatic decrease in lipid binding that was observed for the H3 mutant (Figure 4.4 B). When a lower concentration of SecA was used (200 nM), the H3 mutant showed a slight decrease in transport activity, while the H2 mutant showed similar activity to wild-type SecA (Figure 4.4 C).
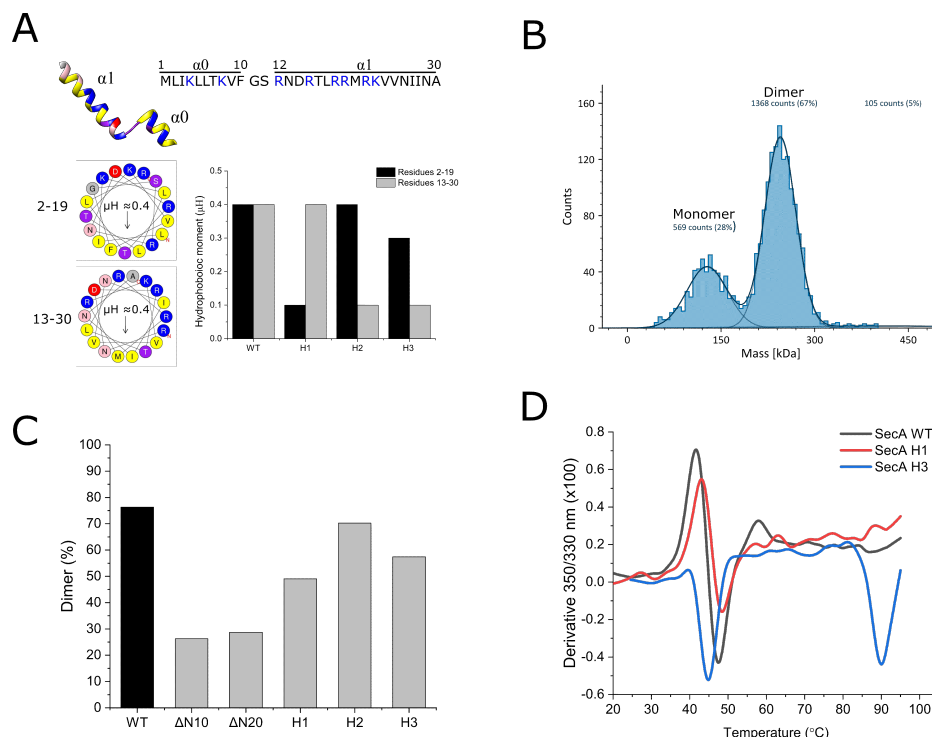
Figure 4.3: Characterization of the N-terminal helix of SecA mutants. A) The N-terminal helix of SecA is split into a small helix ($\alpha0$) and a large helix ($\alpha0$). Helical wheel projection shows that the helix has a positively charged face (blue) and a hydrophobic face (yellow). The designed mutants (H1, H2, and H3) affect the hydrophobic moment across both helices. B) Mass photometry shows that wild-type SecA exists mostly as a dimer. C) The fraction of dimeric SecA in wild-type SecA and the designed N-terminal helix mutants measured by mass photometry. D) The mutations that were introduced into the H1 and H3 mutant did not affect the protein stability as determined by differential scanning fluorimetry. Tm are $\approx$ 42°C, 43°C and 39°C for wild-type SecA, H1 and H3 mutant respectively.

This result was confirmed using a FRET-based real-time translocation assay (Figure 4.4 D) [17, 30]. Here, the assembly of the translocation complex SecYEG: SecA is monitored over time. The model substrate proOmpA fused at its C-terminus to the protein dihydrofolate reductase was used. The DHFR domain becomes folded in the presence of its ligands methotrexate and NADPH, consequently it becomes too bulky to enter the SecY channel during the translocation process. This causes clogging of the channel and trapping the SecYEG: SecA complex forming a stable intermediate. Using a Cyanine 3-labeled proOmpA-DHFR at a cysteine placed at residue 292, FRET signal is established once this donor fluorophore crosses the SecY channel and comes near to the FRET acceptor ATTO 647N positioned at a periplasmic loop of a labeled SecY at position C148, that was reconstituted beforehand in proteoliposomes. Here, DOPC: DOPG membranes were used, which allow for the highly efficient transport activity [17]. SecA H1 and H3 mutants showed a similar rise in the acceptor fluorescence as compared to wild-type SecA (Figure 4.4 E).
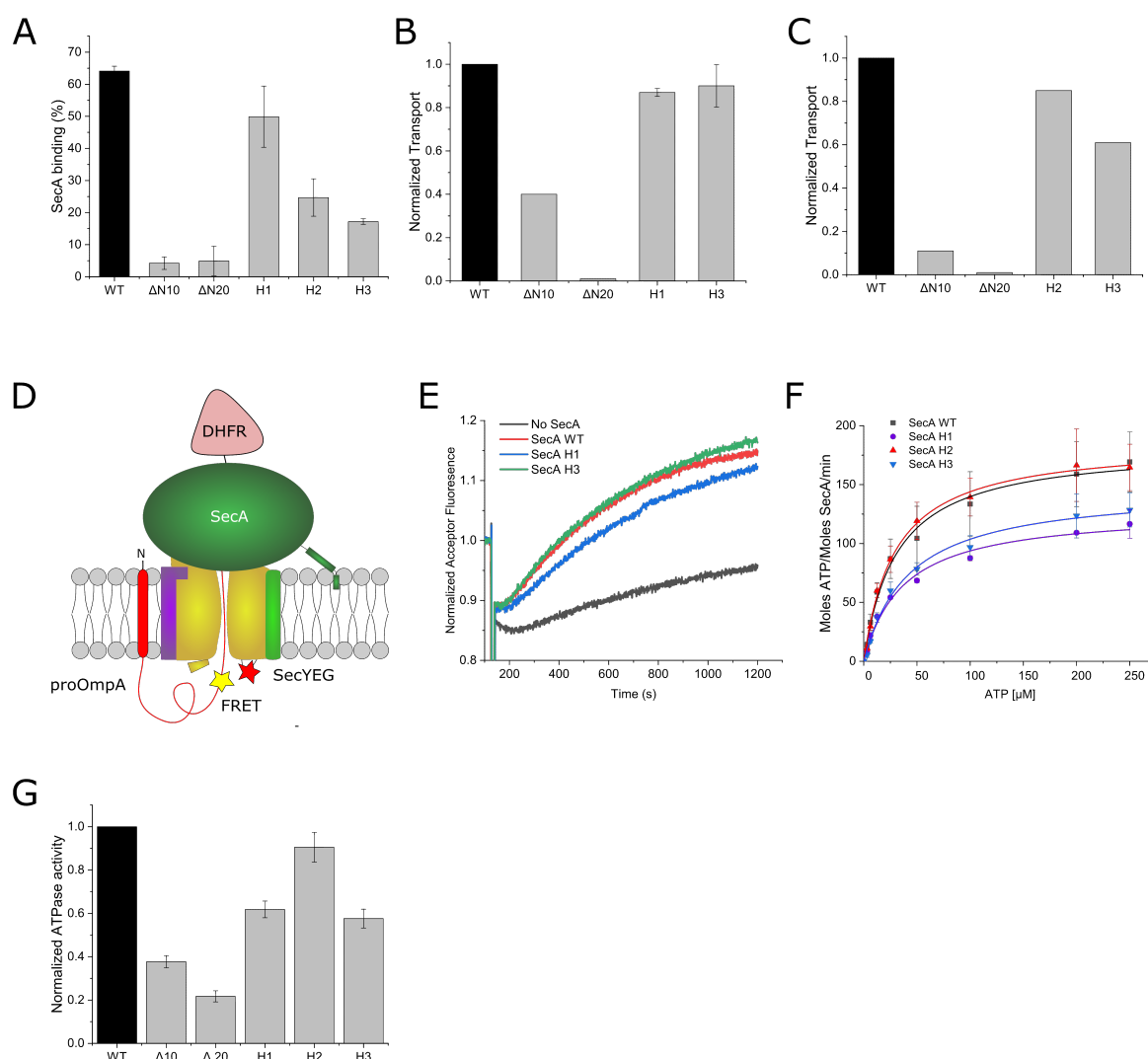
Figure 4.4: Characterization of the necessity of the N-terminal helix of SecA for membrane binding and protein transport. A) Liposomes flotation assay shows that the ΔN10 and N20 mutants lost their ability to bind the membrane, while the membrane binding of H2 and H3 mutants was dramatically decreased as compared to wild-type SecA. B) *In vitro* translocation assay shows that the transport activity of ΔN10 mutant was reduced, and abolished for ΔN20 mutant. H1 and H3 mutants show comparable transport activity to wild-type SecA at high SecA concentration (1 μM). C) *In vitro* translocation assay shows that the transport activity of the H2 mutant is not affected. The transport activity of the ΔN10 was strongly reduced, while that of the H3 mutant was slightly decreased as compared to wild-type SecA at lower SecA concentration (200 nM). D) FRET-based real-time translocation assay. E) FRET-based real-time translocation assay shows no change in the amount of assembled SecYEG: SecA complexes in the case of H1 and H3 mutants as compared to wild-type SecA. J) H1 and H3 mutants have a lower ATPase activity as compared to wild-type SecA, while the H2 mutant has a similar activity to wild-type SecA. F) ΔN10 and ΔN20 mutants have a dramatically lower translocating ATPase activity compared to wild-type SecA.

The translocating ATPase activity was then measured for these mutants. The translocating ATPase activity of the ΔN10 and ΔN20 mutants was dramatically reduced compared to the wild-type SecA. The H2 mutant showed a similar ATPase activity to the wild-type SecA, while H1 and H3 mutants showed a lower ATPase activity than the wild-type SecA (Figure 4.4 F and

G). This indicates that disturbing the charge and hydrophobicity of the $\alpha 1$ did not affect the ATPase activity of SecA. On the other hand, increasing the polarity of the hydrophobic face of the $\alpha 0$ helix decreased the translocating ATPase activity of SecA. These results suggest that the $\alpha 0$ helix plays an important role in stimulating the translocating ATPase activity of SecA, possibly by mediating hydrophobic interactions with the membrane.

To understand the physiological relevance of these results, these mutants were tested for their ability to complement the growth of an *E.coli* strain, BL21.19. This strain contains a secA temperature-sensitive mutation, it can grow normally at 30°C, but it is not viable at the non-permissive temperature 42°C unless supplemented with a plasmid carrying the secA gene [29]. Plasmids containing all the mutants were transformed into the BL21.19 strain. All the mutants were able to complement the growth of the strain at the non-permissive temperature when the expression of the *secA* gene was induced by the addition of IPTG except for the plasmid coding for SecA ΔN20 (Table 4.1). However, when no IPTG was added to the plates, ΔN10 only weekly complemented the growth in good agreement with the measured translocating ATPase activity of this mutant (Figure 4.5 B). Plasmids carrying the genes for H1 and H3 mutants complemented the growth in the presence and absence of IPTG. Surprisingly, the plasmid carrying the gene for H2 mutant only slightly complemented the growth when no IPTG was added, which is contradictory to its high translocating ATPase activity (Table 4.1). However, this mutant might have a lower expression level compared to wild-type SecA or the other mutants, which could explain this result. This behavior has been previously observed and reported for other SecA mutants [29].
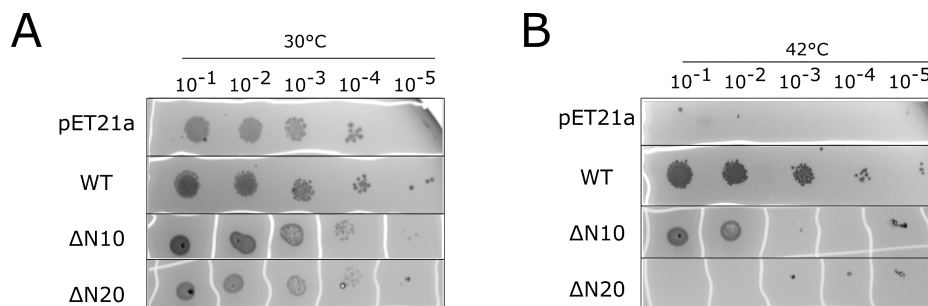
Figure 4.5: In vivo complementation assay. A) The SecA temperature sensitve strain, *E. coli* BL21.19 can grow normally at 30°C either in the absence (pET21a) or the presence of a plasmid coding for SecA (WT). B) A plasmid carrying the gene for wild-type SecA can complement the growth at the non-permissive temperature (42°C) of the SecA temperature-sensitive *E. coli* strain, BL21.19. While a plasmid coding for the ΔN10 mutant only slightly complemented the growth, and no growth was observed when a plasmid coding for ΔN20 mutant was used. Here, the assay was performed without induction.

4.3.3 SecA binds to the membrane in two states

To better understand SecA: membrane interaction, SecA binding to DOPC: DOPG liposomes were analyzed using SPR (Figure 4.6 A). DOPC: DOPG liposomes were immobilized on the surface of one channel of an LP chip, while DOPC was immobilized in the reference channel to subtract unspecific binding to the surface. SecA wild-type or H3 mutant was injected from 50 nM to 1000 nM. The H3 mutant was chosen since it shows the lowest membrane binding

propensity. A dramatic decrease in the response units of the H3 mutant was observed compared to wild-type SecA (Figure 4.6 B). Nevertheless, a steady state analysis showed no difference in the equilibrium dissociation constant ($\approx$ 350 and 210 nM for wild-type SecA and H3 mutant respectively). Therefore, a kinetic analysis of the SPR sensorgrams was performed. A one-to-one two-state kinetic model provided a reasonable fit to the association and dissociation phases of the obtained curves (Figure 4.6 C). Despite having similar association rates (Figure 4.6 D), the first dissociation rate was slightly higher for the H3 mutant (Figure 4.6 E).
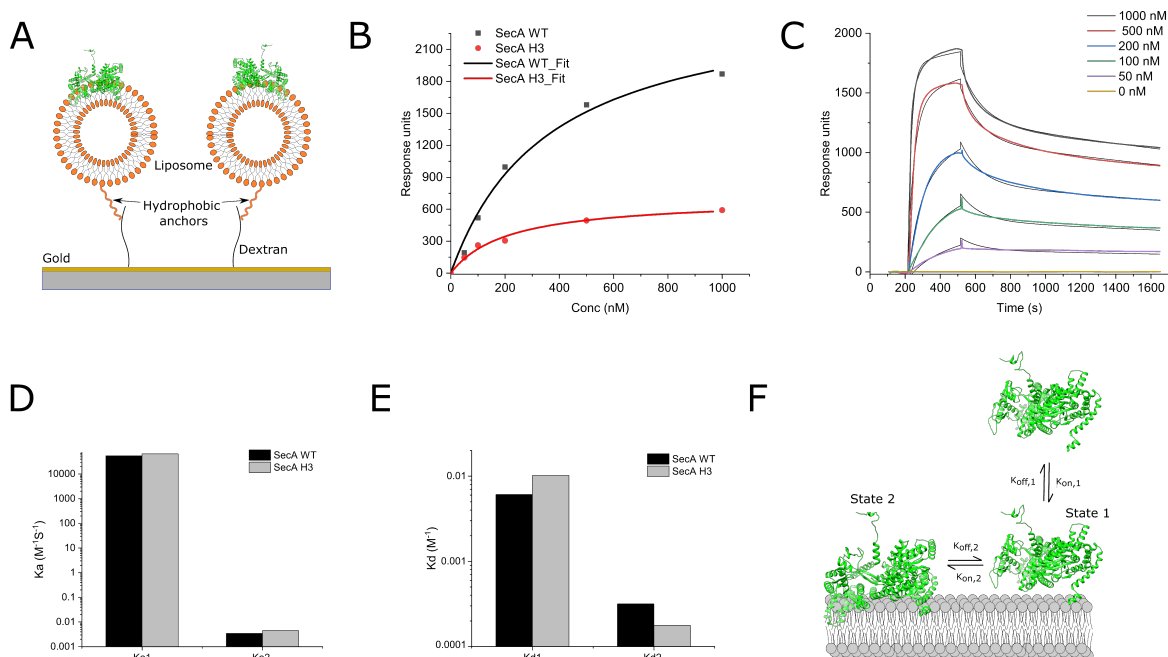
Figure 4.6: Characterization of the kinetics of SecA: membrane interactions using surface plasmon resonance. A) SecA binds to liposomes immobilized on the surface of the LB chip. B) Steady-state analysis of the sensorgrams of SecA wild-type and H3 mutants show a similar equilibrium dissociation constant ($\approx$ 350 and 210 nM for wild-type SecA and H3 mutant respectively) despite the dramatic difference in the response units. C) Surface plasmon resonance sensorgrams of SecA binding, followed by dissociation of different SecA concentrations (50 nM to 1000 nM). A one-to-one two-state binding model provided a reasonable fit for the obtained SecA sensorgrams. D) No change was observed in the association rate constants between wild-type SecA and the H3 mutant as determined by the kinetic fit. E) The first dissociation rate constant (Kd1) increased for the H3 mutant compared to wild-type SecA. F) A one-to-one two-state binding model shows that SecA undergoes a conformational change on the membrane surface after initial binding to the membrane.

This result suggests that SecA binds to the membrane first, then it changes its conformation on the surface of the membrane (Figure 4.6 F). This model is in good agreement with a recent publication [31] that showed similar kinetic behavior with liposomes made from *E. coli* polar lipids. Previously, it was reported that SecA binds to the membrane first, then it gets partially inserted in the membrane and the inserted SecA provides the translocating state [32, 33]. Therefore, based on these results, it is attractive to speculate that SecA initially binds the membrane using electrostatic interactions between the positively charged $\alpha 1$ helix and the anionic lipid in the membrane (State 1). On the other hand, the hydrophobic face of the $\alpha 0$ helix promotes hydrophobic interaction and insertion into the membrane (State 2). Here, decreasing the positive

charge on the positively charged face of the $\alpha 1$ helix of the H3 mutant affected the first state as indicated by the higher dissociation rate. However, the second state was not affected, which is supported by the preserved hydrophobic moment on its $\alpha 0$ helix (Figure 4.3 A).

4.3.4 Hydrophobic interaction between the N-terminal helix of SecA plays an important role for SecA activity

In order to test the proposed 2-state model of SecA: membrane interactions, coarse-grained MD simulation was performed on SecA in the presence of DOPC: DOPG membranes. Interestingly, the simulations showed that the $\alpha 0$ helix inserts deeply into the membrane, while $\alpha 1$ helix remains on the surface of the membrane (Figure 4.7 A). Examining the primary sequence of the $\alpha 0$ helix, a phenylalanine residue was found in position 10. Therefore, it is very attractive to speculate that this residue might be important for the hydrophobic interaction with the membrane and mediate SecA membrane insertion [34]. Three point mutations were designed, F10A to decrease the hydrophobicity, F10W to increase the hydrophobicity, and F10N to increase the polarity of the $\alpha 0$ helix. Interestingly, the F10A and F10N mutants dramatically lost their ability to bind DOPC: DOPG liposomes, while the membrane binding of the F10W mutant was only slightly affected (Figure 4.7 B). Measuring the translocating ATPase activity of these mutants showed that F10W was not affected, while F10A and F10N showed lower ATPase activity compared to wild-type SecA (Figure 4.7 D), with almost a two-fold decrease in the K_{cat} for the F10N mutant (Figure 4.7 C and Table 4.2). The *in-vivo* complementation assay showed that a plasmid coding for the SecA F10A and F10W mutants complemented the growth at the non-permissive temperature with and without induction. On the other hand, a plasmid coding for the F10N mutant slightly complemented the growth when no IPTG was added, in good agreement with the lower translocating ATPase activity of this mutant (Table 4.1).

Combined, these results shed light on the importance of the $\alpha 0$ helix. It strongly suggests that the $\alpha 0$ helix promotes hydrophobic interactions of SecA with the membrane, promotes its membrane insertion, and stimulates its translocating ATPase activity.

Table 4.1: *In vivo* complementation assay at 42°C

Mutant	With induction					Without induction				
	10^{-1}	10^{-2}	10^{-3}	10^{-4}	10^{-5}	10^{-1}	10^{-2}	10^{-3}	10^{-4}	10^{-5}
pET21a	-	-	-	-	-	-	-	-	-	-
SecA wild-type	+	+	+	+	+	+	+	+	+	+
SecA ΔN10	+	+	+	+	+	+	+	-	-	-
SecA ΔN20	+	-	-	-	-	-	-	-	-	-
SecA H1	+	+	+	+	+	+	+	+	+	+
SecA H2	+	+	+	+	+	+	+	-	-	-
SecA H3	+	+	+	+	+	+	+	+	+	+
SecA F10A	+	+	+	+	+	+	+	+	+	+
SecA F10W	+	+	+	+	+	+	+	+	+	+
SecA F10N	+	+	+	+	+	+	+	+	-	-

A

| 0.5 µs | 0.7 µs | 3.8 µs | 6.1 µs |
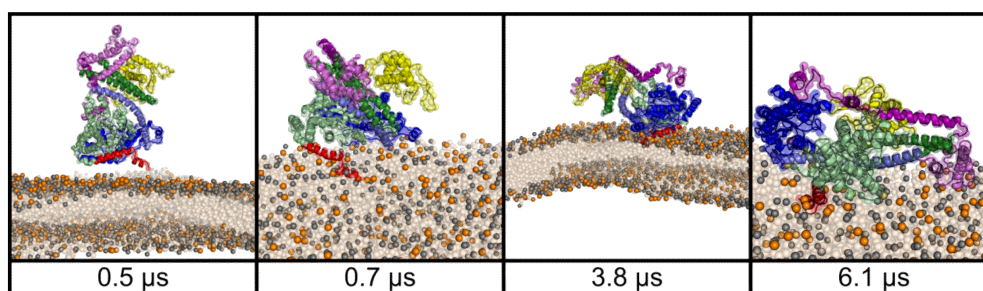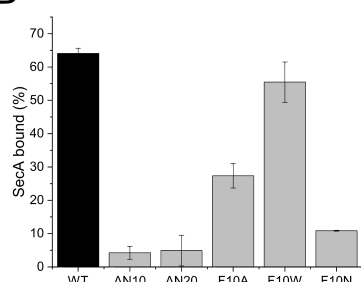
B   C   D

Figure 4.7: Characterization of the role of the hydrophobic interaction of the N-terminal helix of SecA with the membrane. A) Coarse-grained MD simulation snapshots show that the $\alpha 0$ helix of SecA inserts deeply into the membrane. B) Liposome flotation assay shows that F10A and F10N dramatically lost their ability to bind DOPC: DOPG membranes. C) F10N mutants have a lower ATPase activity as compared to wild-type SecA. D) F10W mutant has a similar translocating ATPase activity to wild-type SecA, while F10A and F10N mutants have a lower translocating ATPase activity with the F10N mutant showing almost a two-fold decrease in the translocating ATPase activity compared to the wild-type SecA.

Table 4.2: ATPase activity kinetic parameters of SecA wild-type, H1, H2, H3 and F10N mutants

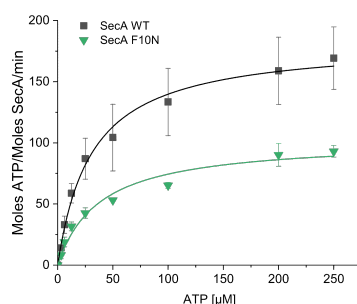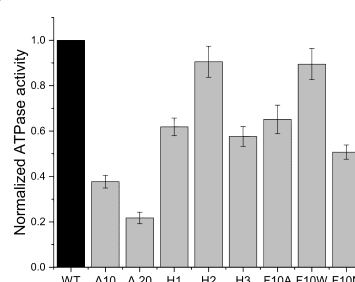| SecA	K_m (μM)	K_{cat} (Moles ATP/moles SecA/min)
SecA wild-type	30.7 ± 3.4 (SE)	182.7 ± 5.9
SecA H1	36.8 ± 4.7	128.2 ± 5
SecA H2	29.3 ± 2.2	186 ± 4.1
SecA H3	41.9 ± 4.6	147.1 ± 5.1
SecA F10N	37.8 ± 7.4	102.6 ± 6.2

4.3.5   Characterization of the second membrane contact site: HSD[649-667]

Next to the N-terminal helix, HDX-MS revealed the second membrane contact site is the residues 649 to 667 of the HSD of SecA. To characterize the necessity of the second membrane-binding site in SecA: membrane interactions, multiple sequence alignments of 10 SecA homologs that cover different gram-positive, negative, and extremophilic bacteria were performed. Four residues were observed to be conserved over the investigated SecA homologs, Q655, R656, Y660, and R663 (Figure 4.8 A). These residues were individually mutated to alanines. Mutant R663A couldn't be expressed in enough amounts to be tested, therefore it was omitted from the study.

The mutants were checked for their oligomeric state using mass photometry. All mutants existed mostly as dimers but to a lesser extent than the wild-type SecA (Figure 4.8 B).

Afterward, the mutants were checked for lipid binding using both DOPC: DOPG and POPC: POPG membranes (Figure 4.8 C). All the mutants showed a slight decrease in the membrane binding ability as compared to the wild-type SecA confirming the HDX-MS result that this domain is involved in membrane binding. Nevertheless, since these mutations did not dramatically impact the membrane binding, it is expected that this domain contacts the membrane after initial membrane binding mediated by the N-terminal helix. Moreover, the mutants were also tested for translocation activity using *in vitro* translocation assay in both SecYEG proteoliposomes and inner membrane vesicles with overexpressed SecYEG and they showed similar activity to the wild-type SecA (Figure 4.8 D and E). The FRET-based translocation assay also showed a similar rise in the acceptor fluorescence to the wild-type SecA (Figure 4.8 F).

Figure 4.8: Characterization of the necessity of the second membrane contact site for SecA: membrane interaction and protein transport. A) Multiple sequence alignment shows four conserved residues with the second membrane contact site (Q655, R656, Y660, and R653). B) The fraction of the dimeric SecA in the designed HSD mutants as determined by mass photometry. C) The HSD mutants show slightly lower binding to DOPC: DOPG and POPC: POPG liposomes compared to wild-type SecA. D) *In vitro* translocation assay of HSD mutants in DOPC: DOPG SecYEG proteoliposomes (upper) and inner membrane vesicles (lower). E) HSD mutants show similar transport activity to wild-type SecA in both DOPC: DOPG SecYEG proteoliposomes and inner membrane vesicles. G) HSD mutants show a similar rise in the acceptor fluorescence to wild-type SecA as measured by the FRET-based real-time translocation assay.

4.3.6 Characterization of the membrane binding of SecA homologs

The phospholipid composition of the inner membrane differs substantially among gram-positive, gram-negative, and extremophilic bacteria. For instance, gram-negative bacteria have approximately 70% phosphatidylethanolamine (PE) and 30% anionic lipids (phosphatidylglycerol and

cardiolipin) (Figure 4.9 A) [35]. Gram-positive bacteria *Bacillus subtilis* has around 45% anionic lipids, 25% PE, 4.5% lysyl phosphatidylglycerol, and 30% neutral lipids. It also has a high content of branched-chain fatty acids in its acyl chains (Figure 4.9 B) [36]. Thermophile *Thermotoga maritima* also has a high content of anionic lipids and contains a high content of membrane-spanning diabolic acids (Figure 4.9 C) [37]. Consequently, it is very reasonable to speculate that the N-terminal helices of SecA homologs might be evolutionarily tuned to interact with different membrane compositions across different bacterial species. The helical wheel projections of the N-terminal helices of different SecA homologs were examined to address those interactions. The results showed that these helices differ in both the hydrophobic moment and the total charge on the helix (Figure 4.9 D- F).
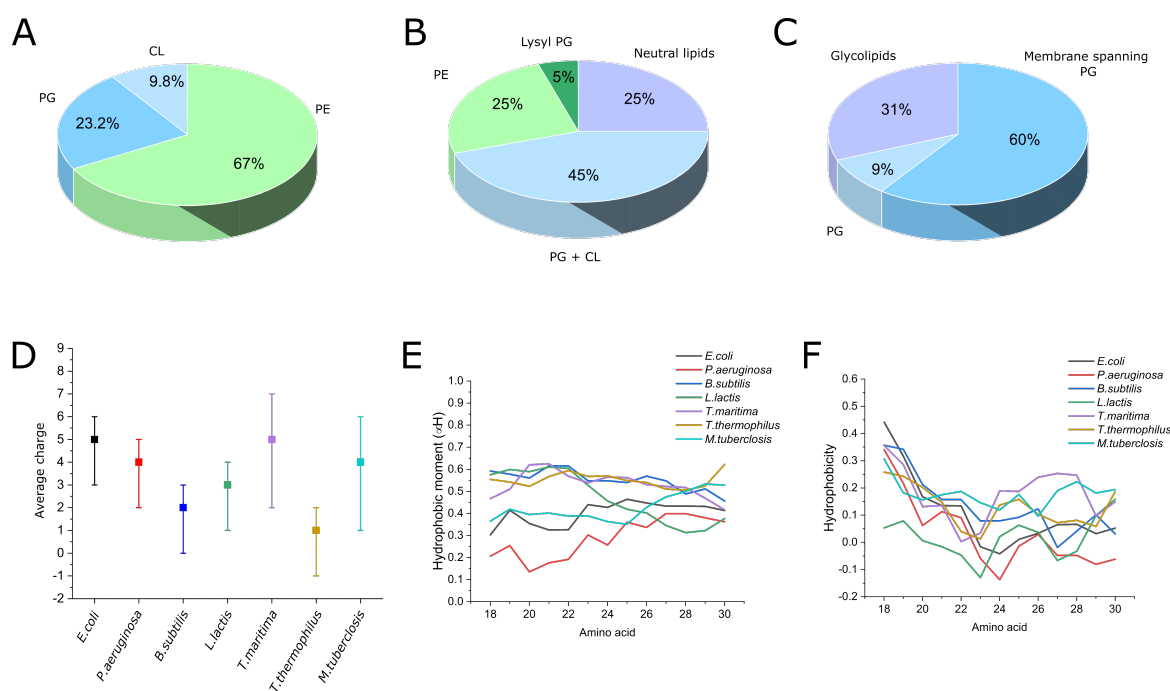
Figure 4.9: The membrane composition and the properties of the N-terminal helices of SecA homologs from different bacterial species. A, B, and C) The lipid composition of the membranes from *E.coli*, *B. subtilis* and *T. maritima* respectively. D) The average positive charge over the first 30 amino acids of the N-terminal helices of 7 SecA homologs, the error bar indicates the minimum and maximum charge over each 18 amino acids along the helix. E and F) Hydrophobic moment, and hydrophobicity of the N-terminal helices of 7 SecA homologs from gram-negative, gram-positive, and extremophilic bacteria respectively across the first 30 amino acids of the N-terminal helix.

First, SecA homolog from the gram-negative bacteria, *Pseudomonas aeruginosa* was studied. *P. aeruginosa* should have a similar anionic lipid content to *E. coli* in its cytoplasmic membrane [38]. The N-terminal helix of the *P. aeruginosa* SecA (PaSecA) has a less charged polar face with a net charge of +5 and the hydrophobic face is slightly less hydrophobic compared to the *E. coli* SecA. Interestingly, the PaSecA showed substantially less binding to DOPC: DOPG (70:30) membranes compared to *E.coli* SecA, and almost no binding was observed for POPC: POPG (70:30) membrane (Figure 4.10 B).

Afterward, the membrane binding of SecA homolog from *B. subtilis* (BsSecA) was checked.

The N-terminal helix of the BsSecA is substantially less charged compared to *E.coli* SecA with a net charge of $+2$. Interestingly, BsSecA only showed efficient lipid binding when 50 % PG content was present which nicely matches the anionic content of the *B. subtilis* membranes (Figure 4.9 B) and correlated with the weaker electrostatic charge on the N-terminal helix. Therefore, BsSecA was tested for membrane binding using liposomes made of DOPC: DOPG (50:50) and the same molar ratio for POPC: POPG liposomes. BsSecA showed very weak binding to POPC: POPG as compared to DOPC: DOPG liposomes, indicating the lipid packing disorder might play an important role in efficient BsSecA: membrane binding (Figure 4.10 C).

The binding of the SecA from the thermophilic bacteria *Thermotoga maritima* (TmSecA) was also tested. This bacteria has the ability to survive at high temperatures ranging from 60°C to 90°C [39]. The N-terminal helix of TmSecA is highly positively charged, and it has a more hydrophobic face than the *E. coli* SecA. It also required 50 % PG content to achieve efficient membrane binding. TmSecA also showed better binding to the mono-UFAs-rich membranes, DOPC: DOPG, compared to POPC: POPG membranes (Figure 4.10 D). These experiments show that the preferential binding of SecA to mono UFAs-rich membranes is conserved with different SecA homologs and that the net charge on the N-terminal helix alongside its hydrophobicity plays an important in determining SecA: membrane interaction.

Furthermore, the effect of salt concentration on the membrane binding ability of SecA was tested. The idea was to disturb the electrostatic interactions between the positively charged residues on the helix and the anionic lipids in the membrane. Interestingly, BsSecA retained membrane binding when the salt concentration was increased from 50 mM to 300 mM, while TmSecA dramatically lost membrane binding (Figure 4.10 E). These results indicate that the main driving force for membrane interaction of *B. subtilis* is hydrophobic interactions, while electrostatic interactions are responsible for the interaction of *T. maritima* with the membrane. The stability of all SecA homologs was measured using differential scanning fluorimetry, and all the mutants were found to be stable at the conditions, in which the binding experiments were performed (Figure 4.10 F and Table 4.3). The denaturation temperature of *T. maritima* SecA was around 88°C, which correlates with the growth temperature of this bacteria [39].

Table 4.3: Denaturation temperatures (Tm) of SecA homologs.

SecA homolog	Tm ($^\circ$C)
SecA *E. coli*	≈ 42
SecA *P. aeruginosa*	≈ 40.3
SecA *B. subtilis*	≈ 41.2 and 56
SecA *T. maritima*	≈ 87.7
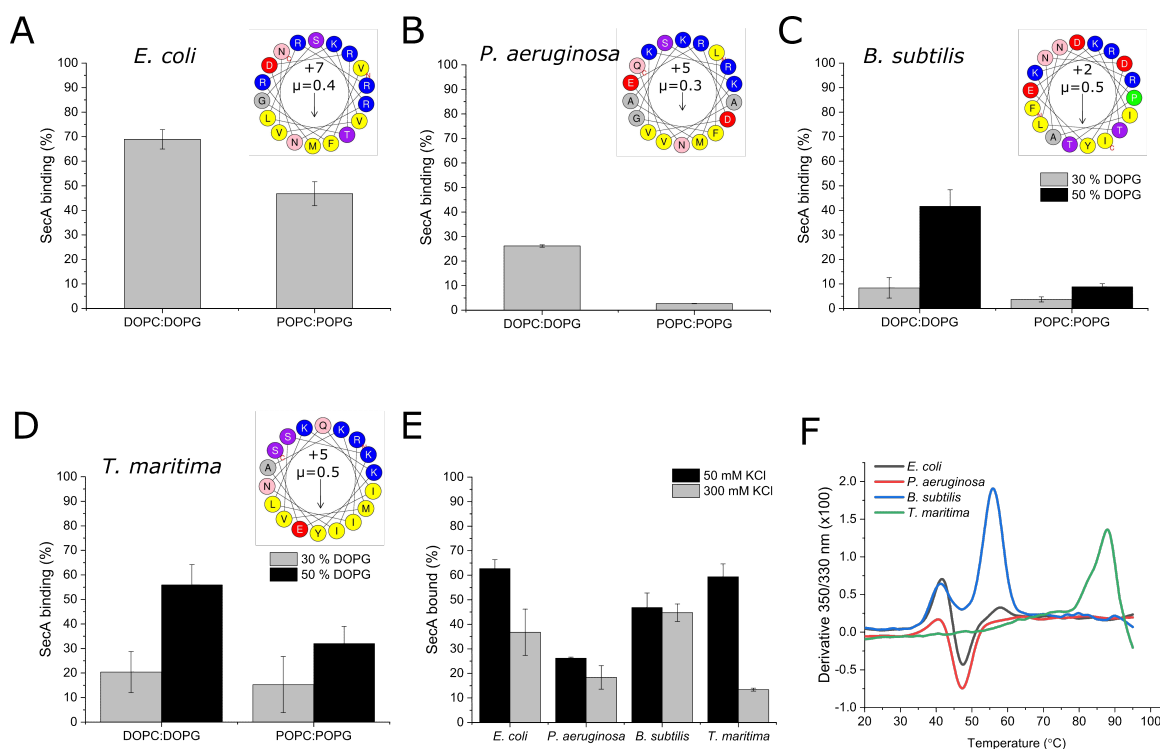
Figure 4.10: The membrane binding of SecA homologs. A, B) SecA homologs from the gram-negative bacteria *E. coli* (A) and *P. aeruginosa* (B) bind better to the mono-UFAs rich membranes DOPC: DOPG. C) SecA from the gram-positive bacteria *B. subtilis* requires 50% PG content for efficient binding and shows a preference for DOPC: DOPG membranes. D) Similarly, SecA from *T. maritima* binds preferentially to the mono-UFAs-rich membranes when 50% PG content is present. E) Increasing the salt concentration in the liposomes flotation assay slightly decreases the binding of *E. coli* and *P. aeruginosa* SecA, has no effect on *B. subtilis* SecA and almost abolishes the membrane binding of *T. maritima* SecA. F) Thermal denaturation profiles of SecA homologs based on differential scanning fluorimetry measurements.

In the next step, the N-terminal helix of the *E. coli* SecA was exchanged with the N-terminal helices of the SecA homologs tested above. The idea was to examine whether the N-terminal helices of SecA homologs will modulate the membrane binding behavior of the *E. coli* SecA. The membrane binding of all designed chimeric *E. coli* SecA proteins were dramatically decreased in comparison to *E. coli* SecA and the binding was only restored when 50% anionic lipids were present in the membrane (Figure 4.11 A-C). On the other hand, the membrane binding of ΔN20 mutant was not improved when 50% PG content was used (Figure 4.11 D), suggesting that the enhanced membrane binding at 50% PG is caused by the introduced helices. These results are nicely correlated with the requirement for anionic content for the efficient membrane binding of the SecA homologs from which the N-terminal helices were obtained. This suggests that the N-terminal helix of SecA modulates SecA: membrane interaction to different membrane compositions.
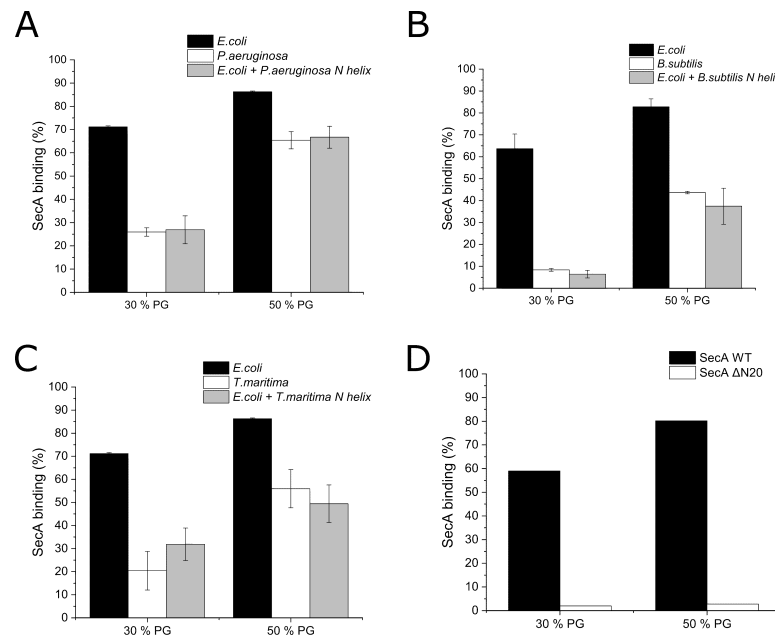
Figure 4.11: Exchanging the N-terminal helix between E. coli SecA and other homologs.
Exchanging the N-terminal helix of *E. coli* SecA with that of *P. aeruginosa* (A) , *B, subtilis* (B)
and *T. maritima* (C) helices dramatically decrease the membrane binding at 30% PG content
and enhance it at 50% PG content in the membrane. D) The membrane binding of the ΔN20
mutant is not improved when 50% PG is present.

4.4   Discussion

The Sec translocon is responsible for the export of periplasmic, secretory, and outer membrane proteins across the cytoplasmic membrane in bacteria. To perform its function, the peripheral membrane protein SecA has to interact with the SecYEG channel, which binds the unfolded and secretion-competent substrates and translocates them through the SecY channel using ATP hydrolysis as an energy source [1, 40]. The membrane composition has been shown to be very crucial for the activity of the SecYEG: SecA translocon. Anionic lipids have been reported to be essential for protein transport [10–12]. The N-terminal helix of SecA has positive residues that interact with the anionic lipids of the membrane. Several recent studies highlighted the role of SecA: membrane interaction. It was proposed that SecA can only have access to SecY through a membrane-bound intermediate [13, 14]. Deleting the N-terminal helix leads to the complete loss of membrane binding and transport activity [15, 16]. Moreover, we have recently reported that protein transport is sensitive to the content of mono-UFAs in the membrane, where the highest transport efficiency is achieved at membranes rich with mono-UFAs (see chapter 3) [17]. Based on biophysical analysis and MD simulations, it was proposed that the N-terminal amphipathic helix of SecA is able to sense the lipid packing disorder introduced by mono-UFAs-rich membranes. Consequently, SecA can form tighter binding to the exposed hydrophobic groove in the membrane via the hydrophobic face of its amphipathic N-terminal helix.

This phenomenon was previously reported for other proteins with amphipathic helices [41]. For instance, Arf1, a protein involved in intracellular vesicle trafficking is able to bind fluid membranes but not to membranes with liquid ordered domains [42]. Also, the amphipathic helix lipid packing sensor (ALPS) motif of some proteins like GMAP210 has the ability to bind membranes with higher content of mono-UFAs and highly curved membranes [43]. Furthermore, Opi1, a transcriptional repressor from yeast that controls the expression of lipid biosynthesis genes, is sensitive to the content of mono-UFAs, where it binds better to dioleoyl-based membranes with 100% mono-UFAs compared to palmitoyl-oleoyl based membranes with 50% mono-UFAs [44].

The aim of this work was to characterize the membrane-binding domains of SecA and elucidate the mechanism of membrane binding and how it influences protein transport. Using HDX MS, two membrane contact sites were identified. The N-terminal helix of SecA as previously reported, and the second half of the HSD of SecA. In a recent cryo-EM structure of SecA: SecYEG, the second half of the HSD domain was found to be facing the membrane [45]. Therefore, it is not unexpected for this site to contact the membrane (Figure 4.2 E). A recent study has identified three membrane-binding domains of SecA [46]. Their findings were based on the change of fluorescence of the environment-sensitive dye NBD once SecA is bound to liposomes. The dye was coupled to cysteines that were introduced in different positions all over the SecA primary sequence. The first domain was the N-terminal helix of SecA in good agreement with the results of this study. Conversely, they found two different lipid binding domains that were not observed in this study. The first was a loop that connect NBD2 to the HSD of SecA. In the cryo-EM structure of the SecA: SecYEG complex, this domain was also facing the membrane, but from the opposite side of second half of the HSD. The second domain was the CTD of SecA, which was previously reported to be involved in membrane binding [9]. A possible explanation for why the latter domain was not observed in the HDX-MS analysis is the presence of a histidine tag

in the C-terminus of the SecA used that might have interfered with the membrane binding. It is noteworthy to mention that in their studies, White and coworkers have used liposomes made of *E. coli* polar lipids, while liposomes made of either DOPC: DOPG or POPC/TOCL were used in this study which might also explain the discrepancy in the results.

To elucidate the exact mechanism of SecA: membrane interactions, several N-terminal helix mutants were designed. The first 10 amino acids of the N-terminal helix of SecA are not resolved in the available *E. coli* SecA structures. By investigating the AlphaFold2 model of the *E. coli* SecA, it was observed that the helix is distorted in that region forming a small helix ($\alpha 0$) from residues 1 to 10 followed by a small loop, then a long helix ($\alpha 1$). This predicted structural feature agrees with the available structure of *B. subtilis* SecA (PDB: 1M6N). Mutational analysis showed that deleting the first 10 amino acids, thereby deleting the $\alpha 0$ helix is enough to abolish membrane binding. Shifting the positive charges from one side of the $\alpha 0$ helix to the other did not have an effect on the membrane binding of SecA. However, decreasing the total positive charge on the hydrophilic side of the $\alpha 1$ helix dramatically decreased the membrane binding.

The SecA ΔN20 lost its activity for protein transport as expected and as previously reported. Interestingly, SecA ΔN10 retained partial activity and SecA H3 mutant showed comparable activity to the wild-type SecA. Koch et al 2016 suggested that SecA can only access the SecYEG channel through a membrane-bound intermediate, where SecA first binds the membrane, then undergoes a conformational change to acquire a high affinity for SecY [16]. Why did decreasing the membrane binding of SecA fail to decrease the activity of the SecA H3 mutant? Previous reports proposed that SecA can insert into the membrane, where it becomes primed and exhibits a high affinity to the SecY channel and that primed state is the translocating state [32, 33]. Using SPR to characterize SecA: membrane interaction, a one-to-one two-state kinetic model described the interaction the best similar to what was previously reported [31]. Consequently, the first state would be the initial binding based on electrostatic interactions, where SecA subsequently changes its conformation into the membrane-inserted state which will represent the second state. Therefore, it was speculated based on these results that SecA targeting to the membrane is mediated by the electrostatic interactions between the $\alpha 1$ helix and the anionic lipids in the membrane. Then SecA $\alpha 0$ helix gets inserted into the membrane due to the hydrophobic interactions between the hydrophobic face of the helix with the hydrophobic groove exposed due to the lipid packing disorder introduced by mono-UFAs in the membrane.

Here, decreasing the total charge on the N-terminal helix in the H3 mutant strongly reduced the total membrane binding of the protein, however, the remaining bound protein might have still been inserted into the membrane and primed to perform the protein transport function. Looking at the helical wheel projection of the SecA H3 mutant, it was noticed that hydrophobic moment was still present in the first 20 amino acids of the helix (Figure 4.3 A), which would support the insertion into the membrane. To test this hypothesis, the *in vitro* translocation assay was performed using the wild-type SecA in an increasing salt concentration to disturb the electrostatic interactions between the N-terminal helix of SecA and the membrane. Although the membrane binding was decreased (see Chapter 3, Figure 7 C), the transport activity was only slightly decreased at high salt concentrations. Only in the case of POPC: POPG membrane, where it is expected that the hydrophobic interactions are lower than that of DOPC: DOPG,

due to the smaller lipid packing disorder, was the transport activity substantially affected (Figure 4.12). This shows that even though the electrostatic interactions were decreased, the hydrophobic interaction was sufficient to stimulate protein transport.
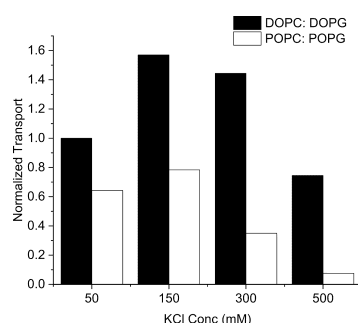
Figure 4.12: The effect of salt on the transport activity of wild-type SecA. Increasing the concentration of salt in the *in vitro* translocation assay slightly decreases protein transport in the case of DOPC: DOPG SecYEG proteoliposomes, while substantially affecting protein transport in POPC: POPG SecYEG proteoliposomes.

Our most recent coarse-grained MD simulations and ongoing cooperation with Jennifer Loschwitz and Birgit Strodel provided more insights on SecA: membrane interactions. Remarkably, the $\alpha 0$ helix was observed to insert deeply into the membrane, while the $\alpha 1$ helix remained on the surface of the membrane. It was previously reported using electron paramagnetic resonance spectroscopy that the residue F10 of the $\alpha 0$ helix penetrates deeply into the membrane [34]. Mutating the phenylalanine to a polar residue aspargine (F10N) caused a substantial decrease in the membrane binding of SecA coupled with a two-fold decrease in the translocating ATPase activity. Moreover, the F10N mutant weakly complemented the growth of the secA Ts strain, BL21.19 similarly to the ΔN10 mutant. Therefore, these result combined with the observation that the H1 and H3 mutants have lower translocating ATPase activity than the H2 mutant, allows two conclusions: firstly, the $\alpha 0$ helix is responsible for the hydrophobic interaction with the membrane and hence the membrane insertion of SecA, while the $\alpha 1$ helix mediates electrostatic interactions with the membrane. Secondly, it is rather the hydrophobic, not the electrostatic interaction with the membrane that has an effect on the ATPase and protein transport activity of SecA.

In both the crystal and cryo-EM structure of the SecYEG: SecA complex, $\alpha 0$ helix was never resolved, while $\alpha 1$ helix position would be facing the membrane though not forming a contact [45, 47]. The position of $\alpha 1$ helix in the structure matches well with its position in the MD simulation of SecA with the membrane. Therefore, the membrane-inserted position of the $\alpha 0$ helix observed in the MD simulation would fit well with both the crystal and the cryo-EM structures. Furthermore, it was reported that the $\alpha 0$ helix mediates hydrophobic interactions between the SecA protomers in a dimeric SecA [33]. Therefore, it is reasonable to speculate that once SecA binds the membrane and monomerizes, the $\alpha 0$ helix mediates the hydrophobic interactions with the membrane. The $\alpha 0$ helix might also act as a sensor for the lipid packing defects within mono-UFAs-rich membranes, explaining why the SecYEG: SecA translocon shows higher transport activity in these membranes. This statement is supported by the fact that the SecYEG: SecA translocon is still highly active in DOPC: DOPG membranes, while it loses

its activity in the case of POPC: POPG membranes at high salt conditions when electrostatic interactions are disturbed (Figure 4.12).

Examining the oligomeric state of the SecA variants showed that the SecA ΔN10 and ΔN20 existed mainly as monomers, while the wild-type, H1, H2, and H3 mutants manifested largely dimeric states. It can not be neglected that a possible explanation of the weak and loss of activity of the SecA ΔN10 and ΔN20 respectively could be because of the loss of dimerization. Indeed, earlier reports suggested that the dimeric SecA is essential for protein transport [21, 48]. More recently a model was published that both the dimer and monomer of SecA are essential at different steps of the translocation pathway [33]. Multiple reports show that SecA monomerizes once it binds the membrane [23, 25, 26, 31, 49, 50]. Furthermore, the *B. subtilis* dimer has been repeatedly reported to be the probable physiologically relevant dimer [22, 33, 51–53]. In this dimer, the N-terminal helix of SecA contributes to the dimeric interface, therefore, it can only bind the membrane if SecA monomerizes. Consequently, the loss of the dimerization of the SecA ΔN10 and ΔN20 might have contributed to the loss of activity, but it is rather the loss of membrane binding that is the responsible factor. As introducing a histidine tag in the N-terminus of SecA ΔN20 restored both membrane binding and transport activity of Ni-NTA-containing membranes [15].

Mutational analysis of conserved residues within the second half of the HSD showed a minor decrease in membrane binding and no change in protein transport activity. This confirms the result of the HDX-MS experiment that indeed this domain is involved in lipid binding. However, it is expected this domain interact with the membrane after initial binding via the N-terminal helix. This is supported by our MD simulations and the fact that deleting the N-terminal helix abolished membrane binding. The SecA R663A mutant could not be expressed in good quantities indicating that this mutation impacts the stability and/or the folding of the protein. The HSD could not be deleted due to its essential role in connecting the motor part and the translocase part of SecA. However, to make a conclusive statement about the role of this domain in membrane binding, a more in-depth characterization needs to be carried out. For instance, examining the effect of mutating all mentioned residues at the same time or mutating the arginines to negatively charged amino acids on both membrane binding and protein transport. Interestingly, the hydrophobicity of residue I659 in the *E. coli* SecA seem to be conserved across SecA homologs (Figure 4.8 A), this residue might provide additional hydrophobic interaction with the membrane. Therefore, mutational analysis of this residue might support the necessity of this domain in SecA: membrane interaction.

The composition of the cytoplasmic membranes of different bacterial species can vary substantially in both the headgroup content and the acyl chain composition [38]. Therefore, it is tempting to speculate that the N-terminal helices of SecA homologs from different bacterial species might have been evolutionarily tuned to be able to interact with the membrane of the respective species [54]. The N-terminal helices of different SecA homologs were examined to test this hypothesis. Several interesting patterns were observed. The N-terminal helices of gram-negative bacteria are highly charged and have less hydrophobic moment compared to gram-positive bacteria. Thermophilic bacteria also have strong hydrophobic moments but vary in the total charge of the helix from highly charged to weakly charged helices. Three different

SecA homologs were checked for membrane binding. All the tested homologs showed a higher preference to bind mono-UFA-rich membranes. This is in good agreement that all the examined helices show an amphipathic profile with a hydrophobic face that can preferentially bind to the hydrophobic groove exposed by the lipid packing disorder of mono-UFAs-rich membrane. Interestingly, both BsSecA and TmSecA could only efficiently bind the membrane when 50% of anionic lipid was present. This matches well with the content of anionic lipids in the membranes of both bacteria.

Exchanging the N-terminal helix of the *E. coli* SecA with that of the SecA homologs caused a substantial decrease in the membrane binding that could be restored by increasing the content of anionic lipids. The increase in binding at 50 % PG content was not observed when only the N-terminal helix of *E. coli* SecA was deleted. All of these results combined further suggest that indeed the N-terminal helix of SecA is responsible for modulating SecA interaction with different membranes. However, when the N-terminal helix of BsSecA or PaSecA was replaced with the *E. coli* N-terminal helix, unstable mutants were produced that could not be expressed in enough amounts to be tested. Optimizing the expression and purification of these mutants may provide valuable insights, as increasing the membrane binding ability of these mutants by the *E. coli* N-terminal helix would further support this hypothesis.

When the salt concentration was increased, the membrane binding of BsSecA was not affected, while the membrane binding of TmSecA was almost abolished. The N-terminal helix of BsSecA is substantially less charged than *E. coli* SecA and TmSecA. Accordingly, the low positive charge would be enough to target the protein to the membrane with high anionic lipids content, nonetheless, the main interactions might be mediated by hydrophobic interactions with the membrane. The N-terminal helix of TmSecA is highly charged. Comparing the crystal structure of BsSecA and TmSecA, it was interesting to observe that the TmSecA does not have the $\alpha 0$ helix (Figure 4.13). This nicely explains why the TmSecA loses its membrane binding in high salt conditions. Additionally, this observation fits very well with the argument that $\alpha 0$ helix mediates hydrophobic interaction with the membrane. This indicates that electrostatic interactions with the membrane might play a rather more important role than hydrophobic interactions for TmSecA. *T. maitima* has a high content of membrane-spanning diabolic acids which makes the membrane more rigid and highly ordered, which might explain the necessity for a highly charged helix to bias the membrane-bound state of SecA [37].

This work identified that both the N-terminal helix and the second half of HSD of SecA interact with the membrane. It shed light on the importance of the small $\alpha 0$ helix of the N-terminal helix of SecA, the hydrophobic interaction between this helix and the membrane, and its effect on the translocating ATPase activity of SecA. Moreover, it provides evidence that N-terminal helices of SecA homologs are tuned to interact with different membrane compositions across different species. More bioinformatic analysis is needed to characterize the properties of N-terminal helices of different SecA homologs across the bacterial species, and correlating that with the membrane content of these species can further support this hypothesis.
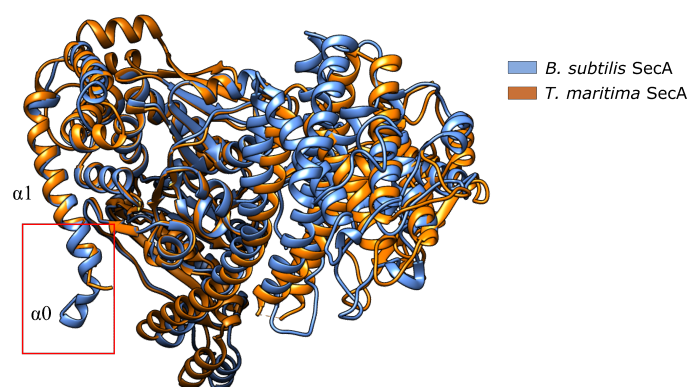
Figure 4.13: T. maritima SecA does not have the α0 helix. Structural alignment of the crystal structure of *B. subtilis* SecA (PDB: 1M6N) in blue and that of *T. maritima* SecA (PDB: 4YS0) in orange. The red box indicates the absence of the α0 helix for *T. maritima* SecA.

This study showed that α0 helix might act as a lipid packing sensor, however, a complete explanation of the underlying mechanism for the stimulated transport in mono-UFA is still lacking. Further studies are still required, for instance, measuring the diffusion coefficient of SecA in giant unilamellar vesicles made of DOPC: DOPG and POPC: POPG GUVs may further support this hypothesis, and are currently in progress in collaboration with Prof. Dr. Salvatore Chiantia, University of Potsdam. A slower diffusion of SecA in DOPC: DOPG membranes would indicate the stabilization of the membrane inserted state and the translocating state of SecA in these membranes. The potential effect of mono-UFA on the dynamics of the membrane channel SecYEG should not be neglected, which might also contribute to the stimulated protein transport in this membrane. Measuring the lateral gate dynamics and plug domain movement using electron paramagnetic resonance spectroscopy may provide valuable insights.

References

[1] A. G. Komarudin and A. J. Driessen, "SecA-mediated protein translocation through the SecYEG Channel," *Microbiology Spectrum*, vol. 7, no. 4, pp. 7–4, 2019.

[2] K. Sato, H. Mori, M. Yoshida, and S. Mizushima, "Characterization of a potential catalytic residue, Asp-133, in the high affinity ATP-binding site of Escherichia coli SecA, translocation ATPase," *Journal of Biological Chemistry*, vol. 271, no. 29, pp. 17439–17444, 1996.

[3] J. F. Hunt, S. Weinkauf, L. Henry, J. J. Fak, P. McNicholas, D. B. Oliver, and J. Deisenhofer, "Nucleotide control of interdomain interactions in the conformational reaction cycle of SecA," *Science*, vol. 297, no. 5589, pp. 2018–2026, 2002.

[4] H. Ding, I. Mukerji, and D. Oliver, "Nucleotide and phospholipid-dependent control of PPXD and C-domain association for SecA ATPase," *Biochemistry*, vol. 42, no. 46, pp. 13468–13475, 2003.

[5] N. Chada, K. Chattrakun, B. P. Marsh, C. Mao, P. Bariya, and G. M. King, "Single-molecule observation of nucleotide induced conformational changes in basal SecA-ATP hydrolysis," *Science advances*, vol. 4, no. 10, p. eaat8797, 2018.

[6] K. J. Erlandson, S. Miller, Y. Nam, A. R. Osborne, J. Zimmer, and T. A. Rapoport, "A role for the two-helix finger of the SecA ATPase in protein translocation," *Nature*, vol. 455, no. 7215, pp. 984–987, 2008.

[7] P. Fekkes, C. van der Does, and A. J. Driessen, "The molecular chaperone SecB is released from the carboxy-terminus of SecA during initiation of precursor protein translocation," *The EMBO journal*, vol. 16, no. 20, pp. 6105–6113, 1997.

[8] P. Fekkes and A. J. Driessen, "Protein targeting to the bacterial cytoplasmic membrane," *Microbiology and Molecular Biology Reviews*, vol. 63, no. 1, pp. 161–173, 1999.

[9] E. Breukink, N. Nouwen, A. van Raalte, S. Mizushima, J. Tommassen, and B. de Kruijff, "The C terminus of SecA is involved in both lipid binding and SecB binding," *Journal of Biological Chemistry*, vol. 270, no. 14, pp. 7902–7907, 1995.

[10] T. De Vrije, R. De Swart, W. Dowhan, J. Tommassen, and B. De Kruijff, "Phosphatidylglycerol is involved in protein translocation across Escherichia coli inner membranes," *Nature*, vol. 334, no. 6178, pp. 173–175, 1988.

[11] R. Lill, W. Dowhan, and W. Wickner, "The ATPase activity of SecA is regulated by acidic phospholipids, SecY, and the leader and mature domains of precursor proteins," *Cell*, vol. 60, no. 2, pp. 271–280, 1990.

[12] E. Breukink, R. A. Demel, G. De Korte-Kool, and B. De Kruijff, "SecA insertion into phospholipids is stimulated by negatively charged lipids and inhibited by ATP: a monolayer study," *Biochemistry*, vol. 31, no. 4, pp. 1119–1124, 1992.

[13] J. Hendrick and W. Wickner, "SecA protein needs both acidic phospholipids and SecY/E protein for functional high-affinity binding to the Escherichia coli plasma membrane.," *Journal of Biological Chemistry*, vol. 266, no. 36, pp. 24596–24600, 1991.

[14] J. H. Floyd, Z. You, Y.-H. Hsieh, Y. Ma, H. Yang, and P. C. Tai, "The dispensability and requirement of SecA N-terminal aminoacyl residues for complementation, membrane binding, lipid-specific domains and channel activities," *Biochemical and biophysical research communications*, vol. 453, no. 1, pp. 138–142, 2014.

[15] B. W. Bauer, T. Shemesh, Y. Chen, and T. A. Rapoport, "A "push and slide" mechanism allows sequence-insensitive translocation of secretory proteins by the SecA ATPase," *Cell*, vol. 157, no. 6, pp. 1416–1429, 2014.

[16] S. Koch, J. G. de Wit, I. Vos, J. P. Birkner, P. Gordiichuk, A. Herrmann, A. M. van Oijen, and A. J. Driessen, "Lipids activate SecA for high affinity binding to the SecYEG complex," *Journal of Biological Chemistry*, vol. 291, no. 43, pp. 22534–22543, 2016.

[17] M. Kamel, M. Löwe, S. Schott-Verdugo, H. Gohlke, and A. Kedrov, "Unsaturated fatty acids augment protein transport via the SecA: SecYEG translocon," *The FEBS journal*, vol. 289, no. 1, pp. 140–162, 2022.

[18] R. Cabelli, K. M. Dolan, L. Qian, and D. B. Oliver, "Characterization of membrane-associated and soluble states of SecA protein from wild-type and SecA51 (ts) mutant strains of Escherichia coli.," *Journal of Biological Chemistry*, vol. 266, no. 36, pp. 24420–24427, 1991.

[19] A.-B. Seinen, D. Spakman, A. M. van Oijen, and A. J. Driessen, "Cellular dynamics of the SecA ATPase at the single molecule level," *Scientific reports*, vol. 11, no. 1, pp. 1–16, 2021.

[20] O. Vadas, M. Jenkins, G. Dornan, and J. Burke, "Using hydrogen–deuterium exchange mass spectrometry to examine protein–membrane interactions," *Methods in enzymology*, vol. 583, pp. 143–172, 2017.

[21] I. Kusters, G. van den Bogaart, A. Kedrov, V. Krasnikov, F. Fulyani, B. Poolman, and A. J. Driessen, "Quaternary structure of SecA in solution and bound to SecYEG probed at the single molecule level," *Structure*, vol. 19, no. 3, pp. 430–439, 2011.

[22] A. J. Wowor, D. Yu, D. A. Kendall, and J. L. Cole, "Energetics of SecA dimerization," *Journal of molecular biology*, vol. 408, no. 1, pp. 87–98, 2011.

[23] E. Or, A. Navon, and T. Rapoport, "Dissociation of the dimeric SecA ATPase during protein translocation across the bacterial membrane," *The EMBO journal*, vol. 21, no. 17, pp. 4470–4479, 2002.

[24] E. Or and T. Rapoport, "Cross-linked SecA dimers are not functional in protein translocation," *FEBS letters*, vol. 581, no. 14, pp. 2616–2620, 2007.

[25] G. Roussel and S. H. White, "The SecA ATPase motor protein binds to Escherichia coli liposomes only as monomers," *Biochimica et Biophysica Acta (BBA)-Biomembranes*, vol. 1862, no. 9, p. 183358, 2020.

[26] G. Roussel and S. H. White, "Binding of SecA ATPase monomers and dimers to lipid vesicles," *Biochimica et Biophysica Acta (BBA)-Biomembranes*, vol. 1862, no. 2, p. 183112, 2020.

[27] D. Wu and G. Piszczek, "Standard protocol for mass photometry experiments," *European Biophysics Journal*, vol. 50, no. 3-4, pp. 403–409, 2021.

[28] L. B. Jilaveanu, C. R. Zito, and D. Oliver, "Dimeric SecA is essential for protein translocation," *Proceedings of the National Academy of Sciences*, vol. 102, no. 21, pp. 7511–7516, 2005.

[29] S. Das, E. Stivison, E. Folta-Stogniew, and D. Oliver, "Reexamination of the role of the amino terminus of SecA in promoting its dimerization and functional state," *Journal of bacteriology*, vol. 190, no. 21, pp. 7302–7307, 2008.

[30] A. Kedrov, I. Kusters, V. V. Krasnikov, and A. J. Driessen, "A single copy of SecYEG is sufficient for preprotein translocation," *The EMBO journal*, vol. 30, no. 21, pp. 4387–4397, 2011.

[31] K. Winkler, A. Karner, A. Horner, C. Hannesschlaeger, D. Knyazev, C. Siligan, M. Zimmermann, R. Kuttner, P. Pohl, and J. Preiner, "Interaction of the motor protein SecA and the bacterial protein translocation channel SecYEG in the absence of ATP," *Nanoscale Advances*, vol. 2, no. 8, pp. 3431–3443, 2020.

[32] A. Economou and W. Wickner, "SecA promotes preprotein translocation by undergoing ATP-driven cycles of membrane insertion and deinsertion," *Cell*, vol. 78, no. 5, pp. 835–843, 1994.

[33] G. Gouridis, S. Karamanou, M. F. Sardis, M. A. Schärer, G. Capitani, and A. Economou, "Quaternary dynamics of the SecA motor drive translocase catalysis," *Molecular cell*, vol. 52, no. 5, pp. 655–666, 2013.

[34] B. T. Findik, V. F. Smith, and L. L. Randall, "Penetration into membrane of amino-terminal region of SecA when associated with SecYEG in active complexes," *Protein Science*, vol. 27, no. 3, pp. 681–691, 2018.

[35] I. Prabudiansyah, I. Kusters, A. Caforio, and A. J. Driessen, "Characterization of the annular lipid shell of the Sec translocon," *Biochimica et Biophysica Acta (BBA)-Biomembranes*, vol. 1848, no. 10, pp. 2050–2056, 2015.

[36] D. Bishop, L. Rutberg, and B. Samuelsson, "The chemical composition of the cytoplasmic membrane of Bacillus subtilis," *European journal of biochemistry*, vol. 2, no. 4, pp. 448–453, 1967.

[37] D. X. Sahonero-Canavesi, L. Villanueva, N. J. Bale, J. Bosviel, M. Koenen, E. C. Hopmans, and J. S. Sinninghe Damsté, "Changes in the distribution of membrane lipids during growth of Thermotoga maritima at different temperatures: Indications for the potential mechanism of biosynthesis of ether-bound diabolic acid (membrane-spanning) lipids," *Applied and Environmental Microbiology*, vol. 88, no. 2, pp. e01763–21, 2022.

[38] C. Sohlenkamp and O. Geiger, "Bacterial membrane lipids: diversity in structures and pathways," *FEMS microbiology reviews*, vol. 40, no. 1, pp. 133–159, 2016.

[39] R. Huber, T. A. Langworthy, H. König, M. Thomm, C. R. Woese, U. B. Sleytr, and K. O. Stetter, "Thermotoga maritima sp. nov. represents a new genus of unique extremely thermophilic eubacteria growing up to 90 C," *Archives of Microbiology*, vol. 144, pp. 324–333, 1986.

[40] T. Cranford-Smith and D. Huber, "The way is the goal: how SecA transports proteins across the cytoplasmic membrane in bacteria," *FEMS microbiology letters*, vol. 365, no. 11, p. fny093, 2018.

[41] M. Giménez-Andrés, A. Čopič, and B. Antonny, "The many faces of amphipathic helices," *Biomolecules*, vol. 8, no. 3, p. 45, 2018.

[42] J.-B. Manneville, J.-F. Casella, E. Ambroggio, P. Gounon, J. Bertherat, P. Bassereau, J. Cartaud, B. Antonny, and B. Goud, "COPI coat assembly occurs on liquid-disordered domains and the associated membrane deformations are limited by membrane tension," *Proceedings of the National Academy of Sciences*, vol. 105, no. 44, pp. 16946–16951, 2008.

[43] M. Magdeleine, R. Gautier, P. Gounon, H. Barelli, S. Vanni, and B. Antonny, "A filter at the entrance of the Golgi that selects vesicles according to size and bulk lipid composition," *Elife*, vol. 5, p. e16988, 2016.

[44] H. F. Hofbauer, M. Gecht, S. C. Fischer, A. Seybert, A. S. Frangakis, E. H. Stelzer, R. Covino, G. Hummer, and R. Ernst, "The molecular recognition of phosphatidic acid by an amphipathic helix in Opi1," *Journal of Cell Biology*, vol. 217, no. 9, pp. 3109–3126, 2018.

[45] C. Ma, X. Wu, D. Sun, E. Park, M. A. Catipovic, T. A. Rapoport, N. Gao, and L. Li, "Structure of the substrate-engaged SecA-SecY protein translocation machine," *Nature communications*, vol. 10, no. 1, pp. 1–9, 2019.

[46] G. Roussel, E. Lindner, and S. H. White, "Topology of the SecA ATPase Bound to Large Unilamellar Vesicles," *Journal of Molecular Biology*, vol. 434, no. 12, p. 167607, 2022.

[47] J. Zimmer, Y. Nam, and T. A. Rapoport, "Structure of a complex of the ATPase SecA and the protein-translocation channel," *Nature*, vol. 455, no. 7215, pp. 936–943, 2008.

[48] A. J. Driessen, "SecA, the peripheral subunit of the Escherichia coli precursor protein translocase, is functional as a dimer," *Biochemistry*, vol. 32, no. 48, pp. 13190–13197, 1993.

[49] M. Alami, K. Dalal, B. Lelj-Garolla, S. G. Sligar, and F. Duong, "Nanodiscs unravel the interaction between the SecYEG channel and its cytosolic partner SecA," *The EMBO journal*, vol. 26, no. 8, pp. 1995–2004, 2007.

[50] E. Or, D. Boyd, S. Gon, J. Beckwith, and T. Rapoport, "The bacterial ATPase SecA functions as a monomer in protein translocation," *Journal of Biological Chemistry*, vol. 280, no. 10, pp. 9097–9105, 2005.

[51] S. M. Auclair, D. B. Oliver, and I. Mukerji, "Defining the solution state dimer structure of Escherichia coli SecA using Forster resonance energy transfer," *Biochemistry*, vol. 52, no. 14, pp. 2388–2401, 2013.

[52] A. J. Wowor, Y. Yan, S. M. Auclair, D. Yu, J. Zhang, E. R. May, M. L. Gross, D. A. Kendall, and J. L. Cole, "Analysis of SecA dimerization in solution," *Biochemistry*, vol. 53, no. 19, pp. 3248–3260, 2014.

[53] T. Banerjee, C. Lindenthal, and D. Oliver, "SecA functions in vivo as a discrete anti-parallel dimer to promote protein transport," *Molecular microbiology*, vol. 103, no. 3, pp. 439–451, 2017.

[54] C. Del Val and A.-N. Bondar, "Diversity and sequence motifs of the bacterial SecA protein motor," *Biochimica et Biophysica Acta (BBA)-Biomembranes*, vol. 1862, no. 10, p. 183319, 2020.

Chapter 5

Single-molecule analysis of the dynamics and interactions of the SecYEG translocon

Authors: Sabrina Koch, Anne-Bart Seinen, Michael Kamel, Daniel Kuckla,
                  Cornelia Monzel, Alexej Kedrov and Arnold J.M Driessen

Single-molecule analysis of dynamics and interactions of the SecYEG translocon

Sabrina Koch[1], Anne-Bart Seinen[1,2] (iD), Michael Kamel[3], Daniel Kuckla[4], Cornelia Monzel[4] (iD), Alexej Kedrov[3] (iD) and Arnold J.M. Driessen[1] (iD)

1 Molecular Microbiology, Groningen Biomolecular Sciences and Biotechnology Institute, Zernike Institute for Advanced Materials, University of Groningen, The Netherlands
2 Biophysics, AMOLF, Amsterdam, The Netherlands
3 Synthetic Membrane Systems, Institute of Biochemistry, Heinrich Heine University Düsseldorf, Germany
4 Experimental Medical Physics, Department of Physics, Heinrich Heine University Düsseldorf, Germany

Protein translocation and insertion into the bacterial cytoplasmic membrane are the essential processes mediated by the Sec machinery. The core machinery is composed of the membrane-embedded translocon SecYEG that interacts with the secretion-dedicated ATPase SecA and translating ribosomes. Despite the simplicity and the available structural insights on the system, diverse molecular mechanisms and functional dynamics have been proposed. Here, we employ total internal reflection fluorescence microscopy to study the oligomeric state and diffusion of SecYEG translocons in supported lipid bilayers at the single-molecule level. Silane-based coating ensured the mobility of lipids and reconstituted translocons within the bilayer. Brightness analysis suggested that approx. 70% of the translocons were monomeric. The translocons remained in a monomeric form upon ribosome binding, but partial oligomerization occurred in the presence of nucleotide-free SecA. Individual trajectories of SecYEG in the lipid bilayer revealed dynamic heterogeneity of diffusion, as translocons commonly switched between slow and fast mobility modes with corresponding diffusion coefficients of 0.03 and 0.7 $\mu m^2 \cdot s^{-1}$. Interactions with SecA ATPase had a minor effect on the lateral mobility, while bound ribosome:nascent chain complexes substantially hindered the diffusion of single translocons. Notably, the mobility of the translocon:ribosome complexes was not affected by the solvent viscosity or macromolecular crowding modulated by Ficoll PM 70, so it was largely determined by interactions within the lipid bilayer and at the interface. We suggest that the complex mobility of SecYEG arises from the conformational dynamics of the translocon and protein:lipid interactions.

Introduction

About 25–30% of the total bacterial proteins carry out their metabolic and structural function in compartments outside the cytoplasm. The major route for exporting these proteins beyond the cytoplasmic membrane is provided by the essential and universally conserved secretory (Sec) pathway (Fig. 1) [1,2]. The bacterial Sec pathway includes two major targeting routes, which merge at the membrane-embedded protein-conducting channel, or translocon, SecYEG (Fig. 1A). Targeting of membrane proteins commonly occurs co-translationally, and their recognition is based on the presence of a highly hydrophobic N-terminal domain, either a signal sequence or the first transmembrane α-helix (TMH) [3]. Once this signal emerges from the ribosomal exit tunnel, it is recognized and bound by the signal recognition particle (SRP) that facilitates targeting of the ribosome:nascent chain complex (RNC) to the membrane-localized SRP receptor FtsY and then SecYEG translocon [4]. After SRP:FtsY dissociation, the nascent chain is inserted into the SecYEG translocon, and membrane partitioning is facilitated by translation forces of the ribosomes, as well as pulling forces originating from interactions of the nascent chain with the translocon and lipids [5]. Another route is followed by moderately hydrophobic secretory and outer membrane protein precursors (preproteins), which are targeted and translocated post-translationally (Fig. 1B). During preprotein synthesis, the polypeptide emerging from a ribosome is recognized and bound by the ribosome-associated chaperone trigger factor and, possibly, the motor protein SecA [6,7]. Once the synthesis is completed, the preprotein is carried over to the secretion-dedicated chaperone SecB that keeps it in an unfolded, secretion-competent state [8]. In the next step, the preprotein is targeted and transferred to SecA, which is bound to the translocon SecYEG via the cytoplasm-exposed loops 6/7 and 8/9 of the subunit SecY (Fig. 1A), and translocation is initiated [9]. SecA and/or proton motive force may also be required for the translocation of large and polar periplasmic loops within membrane proteins, thus suggesting a dynamic interaction between the translocon and cytosolic components of the targeting pathways [7,10,11].

The majority of translocon structures, as well as many functional studies, have been based on detergent-solubilized proteins, although detergents are known to alter structural and functional properties of proteins [12,13]. Therefore, there is a great demand to perform structural, biochemical and biophysical analysis in physiologically relevant and well-defined systems.

Reconstitution of isolated proteins into proteoliposomes remains the most common approach to study membrane proteins, including those of the Sec machinery [14,15], and more recent studies have also used translocons reconstituted in lipid-based nanodiscs [16–20]. Complementary, free-standing and supported lipid bilayers (SLB) offer robust model systems to investigate protein dynamics [21]. SLBs can be formed by fusing lipid vesicles on solid surfaces, such as mica or glass, and can be employed to probe protein:lipid interactions via surface plasmon resonance or quartz crystal microbalance measurements [22], or to carry out surface imaging down to the single-molecule level via atomic force microscopy (AFM) and total internal reflection fluorescence microscopy (TIRFm) [23,24]. Recently, AFM imaging of SecYEG complexes allowed to assign local height increases to the cytoplasm-exposed loops of individual translocons, and to visualize SecYEG:SecA and SecYEG:SecYEG interactions [25]. In an alternative approach, two-dimensional streptavidin crystals were used as a support to form SLBs and to investigate the lateral diffusion of SecYEG using high-speed AFM [26]. This provided insights into conformational changes at the single-molecule level, but the method was not sufficiently fast to analyze the naturally occurring lateral diffusion of proteins, so additional treatment with glutaraldehyde was employed to artificially decrease the diffusion rate of translocons.

Differently to AFM, fluorescence microscopy does not involve mechanical interaction with the examined sample, but also offers single-molecule resolution to monitor the temporal dynamics of membrane proteins [27,28]. Here, we employ TIRFm to study interactions of *Escherichia coli* SecYEG with the cytoplasmic ligands, the ATPase SecA and ribosomes, and to probe their effects on the translocon dynamics and the long-disputed oligomeric state. Single-molecule brightness analysis of SLB-reconstituted translocons suggested that SecYEG complexes remained largely monomeric in their freely diffusing state and when bound to ribosomes, while the assembly of oligomers was stimulated in the presence of SecA. Statistical analysis of single-particle trajectories revealed two distinct diffusion modes of SecYEG within the membrane, and individual translocons could switch between fast and slow diffusion, either in their free state or when bound to ribosomes or SecA, while binding of RNCs drastically suppressed the fast diffusion mode. As the interactions between the SLB and the supporting surface were largely excluded, the nonuniform diffusion pattern in SLBs has been
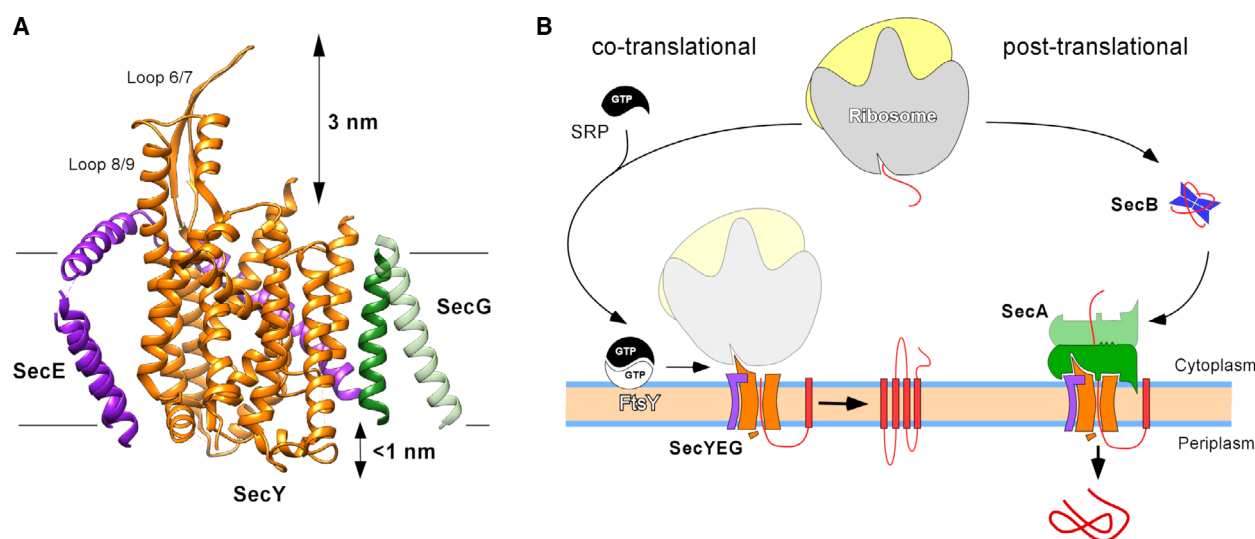
Fig. 1. SecYEG as a hub for protein translocation. (A) Structure of the *Escherichia coli* SecYEG in the lipid bilayer (PDB ID: 6R7L, Ref. [18]). The translocon subunits as well as the approximate heights of the cytoplasmic and periplasmic loops are indicated. The putative position of SecG TMH 1 is shown in light green (PDB ID: 5AWW, Ref. [9]). SecYEG structure is rendered with UCSF Chimera v. 1.13 [72]. (B) Scheme of the co- and post-translational protein targeting to the inner membrane of *E. coli*. The membrane-embedded SecYEG translocon conducts insertion of the nascent membrane proteins delivered in a tertiary complex of the ribosome, SRP, and the membrane-associated receptor FtsY. Secretory and cell wall proteins are delivered to the SecYEG as nonfolded precursors with the help of the dedicated chaperone SecB. The translocation is mediated by the translocon-associated ATPase SecA.

attributed to the conformational dynamics of SecYEG and associated protein:lipid interactions.

Results

Supported lipid bilayers provide the physiologically relevant membrane environment, where dynamics of individual reconstituted translocons, such as association and mobility, can be monitored. However, the setup-specific interactions of proteins and lipids with the supporting surface may hinder their lateral diffusion and so influence the experimental outcome. Direct deposition of SLBs on the solid support would likely result in an intermediate aqueous layer, which may be as thin as 5 Å [29,30]. Indeed, when the SLBs were formed on the bare glass surface, the mobility of lipids was severely suppressed. This was shown by continuous photobleaching (CPB) experiments using dye-conjugated lipids 1,2-dioleoyl-sn-glycero-3-phosphoethanolamine (DOPE)-NBD and recording of diffusion-based signal recovery. On glass surfaces, no signal recovery was recorded even after 20 min (Fig. 2). In contrast, when the glass surface was pre-coated with a short aminosilane (3-aminopropyl)triethoxysilane (APTES, length below 1 nm) [31], the fluorescence within the bleached areas rapidly recovered due to lipid diffusion. Based on the CPB

experiments, a lipid diffusion coefficient of $3.2 \pm 0.4 \ \mu m^2 \cdot s^{-1}$ was determined (Fig. 3). This is in a good agreement with previous studies on membrane fluidity [32]. Thus, the short silane spacer reduced the interaction with the solid surface and served to recover the dynamics of the lipids within the bilayer. Importantly, a large mobile fraction of reconstituted translocons was observed within the APTES-supported bilayer (see below), so a relatively small spacing was sufficient to prevent the protein:surface interaction.

To investigate SecYEG dynamics within SLBs and its interactions with SecA ATPase and ribosomes, a TIRFm setup with a mounted flow cell was employed. The flow cell was built from a silane-coated coverslip and an object slide connected via a spacer containing the flow channel. The continuous system allowed the addition of buffer and binding partners to the pre-formed SLBs, as well as washing off unbound material. To reduce interactions of the periplasmic interface of SecYEG with the glass surface, the glass surface was coated with an elongated aminosilane, *N*-(2-aminoethyl)-3-aminoisobutyldimethylmethoxysilane, of approx. 1.5 nm in length (Fig. 4A). Proteoliposomes bearing SecYEG-Atto 647N translocons were mixed 1 : 250 with protein-free liposomes [14,33], and the mixture was loaded into the flow cell. In presence of 150 mм KCl the liposomes could bind to and spread
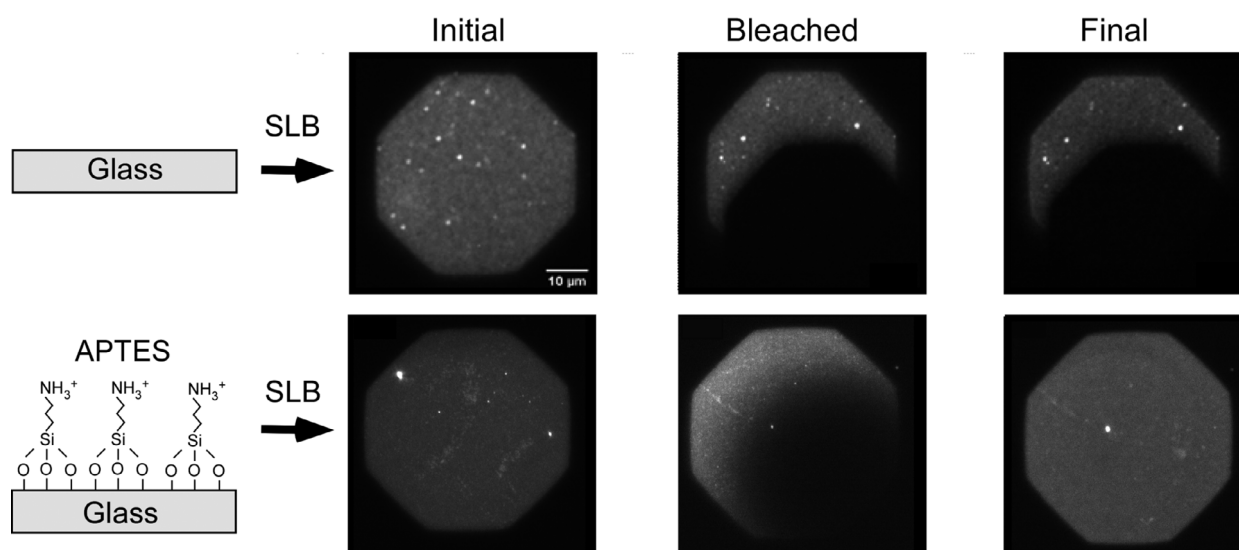
Fig. 2. Silane cushion ensures lipid mobility within the deposited SLB. DOPE-NBD fluorescence recovery after photobleaching was recorded in SLBs deposited on unfunctionalized cleaned glass (top row) and APTES-coated glass surface (bottom row). The 'Initial' image of the formed SLB was recorded before photobleaching and another image was recorded with a lateral shift to differentiate between photobleached and nonphotobleached area ('Bleached'). The fluorescence was allowed to recover over 15–20 min by switching off the lamp, and then, another image was recorded ('Final'). No recovery was detected for SLBs on the bare glass surface indicating an immobile lipid bilayer. Complete recovery of the fluorescence after 20 min was observed for APTES-supported SLBs indicating the mobile bilayer.

over the coverslip due to electrostatic interactions of anionic lipids with positively charged amine group of the silane coat. To verify the proper formation of a lipid bilayer, simultaneous dual-color TIRFm of octadecyl rhodamine B chloride (R18) and SecYEG-Atto 647N was performed (Fig. 4B). R18 is a fluorescent probe, which spontaneously immerses with its alkyl tail into a lipid bilayer, while its polar fluorophore moiety faces the hydrophilic exterior. After the liposomes containing R18 were added to the flow cell, they fused with the deposited SLB, whereupon R18 molecules diffused freely throughout the field of view (Fig. 4C), indicating proper bilayer formation without exclusion zones as a prerequisite for the diffusion analysis.

Site-specific labeling of SecYEG with a small fluorescence dye, such as Atto 647N-maleimide, at the periplasmic interface did not affect the protein activity (Fig. 5A), as the dye did not interfere with SecA and ribosome binding at the cytoplasmic side [33]. The dual topology of reconstituted translocons within the proteoliposomes was confirmed via probing the translocon accessibility for the limited specific proteolysis (Fig. 5B), so two distinct SecYEG populations were expected to be present within SLBs. The brightness distribution of individual particles detected within the SLB was employed to analyze the translocon oligomeric state. Previous biochemical and structural

studies have shown that SecYEG complexes may assemble into oligomers in detergent micelles and lipid bilayers [34,35], but a single copy of SecYEG is sufficient to form a functional translocon [16,33,36,37]. To probe the oligomeric state of SecYEG in our experimental setup, the fluorescence intensity of individual foci was analyzed over time to determine the number of translocons per foci (Fig. 5C). SecYEG was predominantly present as a monomer, which built a fraction of approx. 70% of analyzed translocons. Dimers and occasional monomers bearing two fluorophores constituted about 20%, and higher oligomers constituted below 10% of molecules, and the distribution remained stable over the measurement time.

Individual translocons could be detected in consecutively recorded frames, and their trajectories within the SLB were reconstructed (Fig. 6A). About 25% of proteins were mobile, which constituted around 100 proteins per movie, while the rest remained motionless (Fig. 6B). The population of the immobile particles was primarily attributed to the inversely oriented SecYEG, which statistically represented 40–60% of reconstituted translocons within the SLB (Fig. 5B) [14,33]. The inversely oriented translocons exposed their long cytoplasmic loops toward the solid support, so their diffusion could be hindered despite the silane coating (Fig. 1A). Furthermore, occasional protein aggregates and the fluorophore contaminations could
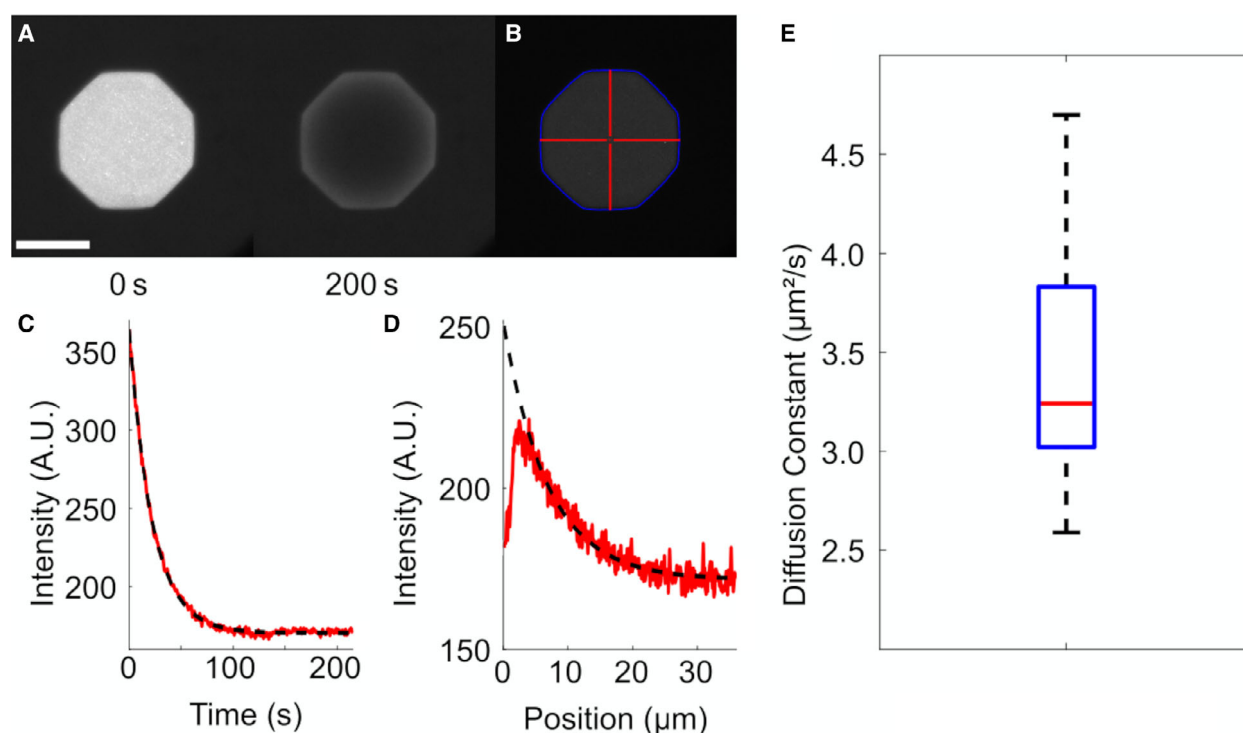
Fig. 3. Verification of SLB mobility utilizing CPB. (A) Fluorescence of DOPE-NBD within SLB deposited on the APTES-coated glass before and after 200 s of bleaching. Scale bar 40 µm. (B) SLB before bleaching with lines indicating the analyzed intensities. From the central point where the lines would intersect, the bleaching constant is determined. Scale as in (A). (C) Mean fluorescence intensity measured at the center spot shown in (B) during the bleaching process. Dashed line: Fit according to Eqn (1), as described in Methods. (D) Mean fluorescence intensity averaged over 5 neighboring pixels along one of the radial lines. Dashed line: Fit according to Eqn (2), as described in Methods. (E) The overall diffusion constant determined for DOPE-DBD lipid amounted to (3.2 ± 0.4) µm²·s⁻¹. Two different samples with a total of $N = 14$ measurements were evaluated. Values represent the median and median absolute deviation $\Delta D = \text{median}(D(i) - \text{median}(D))$.

contribute to the immobile fraction that was excluded from further analysis. The trajectories of the mobile translocons, which contained 5000–10 000 steps per movie, were used to estimate the diffusion coefficients using the cumulative probability distribution (CPD) of step sizes. CPD refers to the probability that a particle stays within a given area around it, thus decreasing the radius r around a moving particle increases the probability that the particle will leave the area determined by r^2. Fitting of the experimentally derived CPD with the cumulative probability function (CPF) provides the number of diffusive species, their fractions and the corresponding diffusion coefficients. Interestingly, the SLB-reconstituted translocons did not diffuse uniformly, but demonstrated clear dynamic heterogeneity (Fig. 6A). SecYEG diffusion could occur in equally distributed short and long step sizes (slow and fast diffusion modes), and individual translocons could switch between these modes. Accordingly, no adequate fitting of the experimental CPD data to a single-component CPF could be achieved, as the

goodness of fit indicated by the residual sum of squares (RSS) was larger compared to the two-component CPF fit (Fig. 6C). CPD was best described by the two-component model, and increasing the terms led to overfitting, yielding erroneous fitting parameters, such as equal diffusion coefficients for different components. The median diffusion coefficient of the slow mode was found at 0.029 µm² s⁻¹, while the fast mode had a median diffusion coefficient of 0.7 µm²·s⁻¹ (Fig. 6D). Notably, two modes with diffusion coefficients of 0.08 and 0.77 µm²·s⁻¹ were also observed for SLB-reconstituted translocons when the short silane APTES was used for coating the glass surface (Fig. 7). Thus, the variations in distance between the SLB and the supporting surface had little effect on the mobility of the translocons, suggesting that the dynamic heterogeneity in SecYEG diffusion was largely determined by the intrinsic interactions within the lipid bilayer.

During translocation of polar polypeptide chains, such as preproteins or periplasmic domains of membrane proteins, SecYEG binds the cytosolic motor
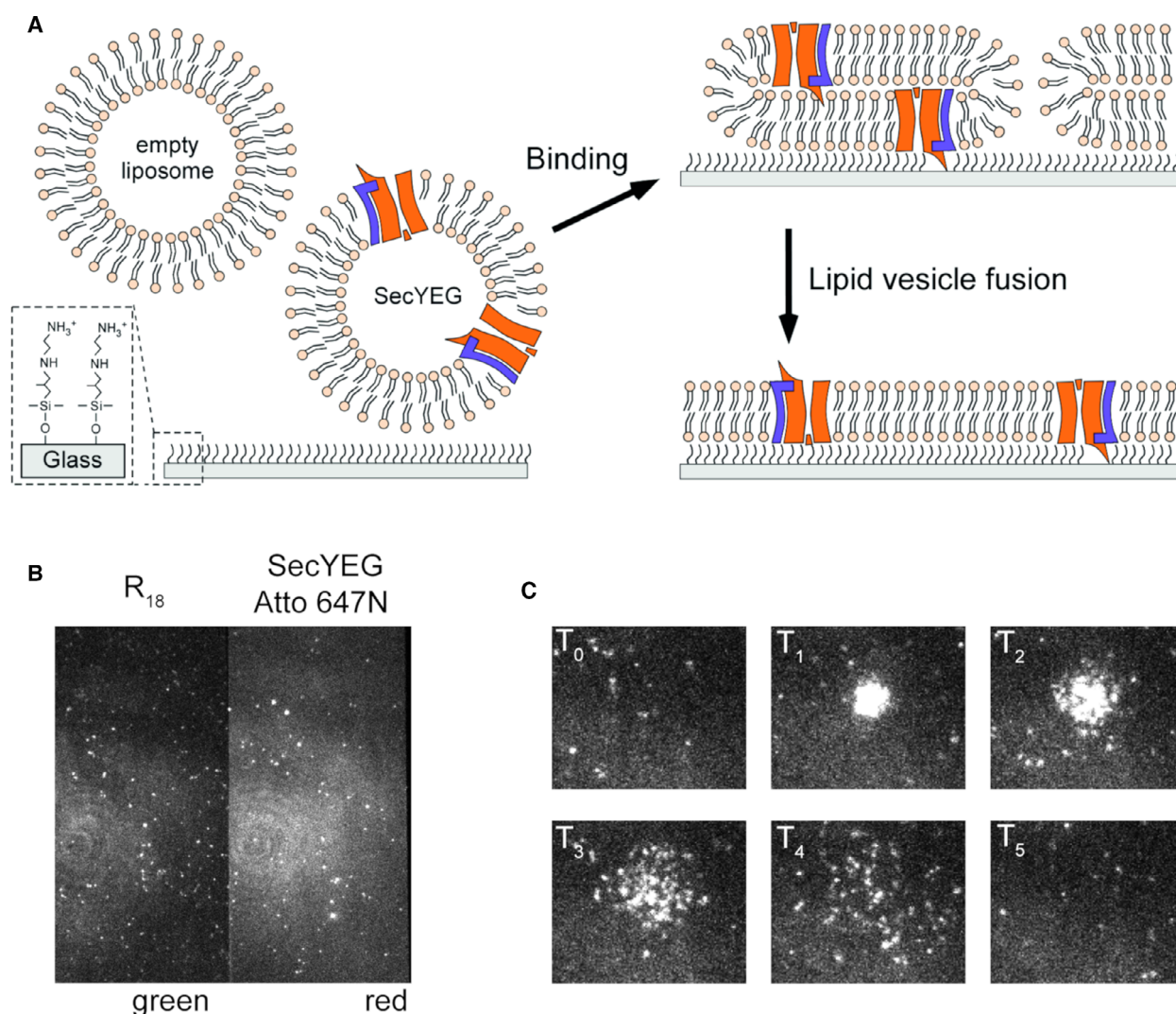
Fig. 4. Preparation of SecYEG-containing SLBs. (A) Scheme of the SLB formation via fusion of SecYEG proteoliposomes and liposomes on the silane-functionalized glass surface. The vesicles bound to the glass-silane surface undergo flattening and fusion to form a continuous lipid bilayer with incorporated translocons. (B) Example frame of the dual-view data acquisition with a beam splitter for green and red channel, detecting R18 and SecYEG-Atto 647N molecules, respectively. (C) Fusion of R18 molecules with the SLB validates the formation of the bilayer. T_0, prior to R18 vesicle fusion. T_1, first contact, R18 vesicle enters the focal plane. T_2, R18 vesicle fusion with the SLB, releasing the R18 molecules into the SLB showing a radial Brownian diffusion pattern. T_3, 66 ms after initial vesicle fusion with the SLB still showing a radial diffusion pattern without exclusion zones. T_4, 99 ms after initial vesicle fusion, R18 molecules start to diffuse out of the imaging boundaries, still in a radial diffusion pattern and without indications of an improper SLB. T_5, diffusion out of the imaging boundaries and bleaching of the R18 molecules resulted in a state similar to T_0, where no local accumulation or exclusion of the dye was observed.

protein SecA. To investigate the effect of SecA binding on the oligomeric state and the diffusion dynamics of SecYEG, the ATPase was introduced to the translocon-containing SLBs. SecA binds SecYEG with high affinity even in the absence of a preprotein [11,17]. The effect of SecA binding could be recognized in raw individual trajectories of SecYEG (Fig. 8A), and CPD analysis revealed a significant change for both slow

and fast diffusion modes. The fast diffusion mode revealed a decrease in the diffusion coefficient, from 0.78 to 0.68 $\mu m^2 \cdot s^{-1}$, while the slow-diffusion coefficient increased to 0.033 $\mu m^2 \cdot s^{-1}$ upon SecA addition (Fig. 8B). The brightness analysis suggested that a fraction of the SecYEG underwent dimerization in presence of SecA, as the monomer population reduced to 61% (Fig. 8C).
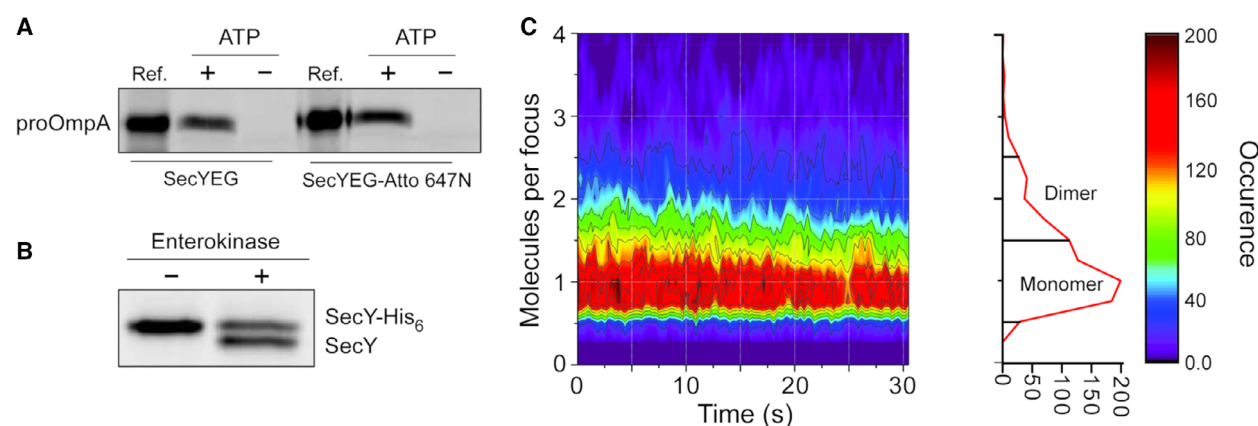
Fig. 5. Characterization of the reconstituted SecYEG translocon. (A) Fluorescent labeling does not affect SecYEG activity. Translocation activities of unlabeled cysteine-free SecYEG translocon and the fluorescently labeled single-cysteine variant SecY^{C148}EG-Atto 647N were nearly identical, as comparable amounts of the fluorescently labeled preprotein proOmpA were translocated into proteoliposomes in presence of ATP. 'Ref.' indicates the reference (10% of proOmpA input). (B) Reconstituted translocons acquire alternating orientations in lipid bilayers. Accessibility of SecY N-terminal end for enterokinase cleavage revealed the dual topology of the reconstituted SecYEG. In-gel fluorescence imaging shows a shift of SecY-Atto 647N band upon incubation with the protease. 65% $\pm$ 9% of the reconstituted SecYEG exposed the cytoplasmic side the outside of the liposomes ($N = 3$). (C) SecYEG oligomeric state within SLB examined via single-particle brightness analysis. The distribution shows the calculated number of molecules per focus over time. The distribution is largely spread around a single molecule per focus, indicating that the SecYEG translocon in a native-like environment is predominantly monomeric. The ratio of monomers vs dimers was approx. 3 : 1 (15 792 monomeric vs 5663 dimers, based on the full movie). The distribution remained stable over the experimental time span (30 s).

To study the translocon dynamics upon interactions with translating ribosomes and co-translational insertion of a membrane protein, trajectories of SecYEG-Atto 647N were further recorded in the absence and presence of ribosomes. Empty 70S ribosomes did not cause substantial changes in SecYEG diffusion: The individual trajectories showed an unaltered even distribution of short and long step sizes and the diffusion coefficients for two observed modes were weakly affected by ribosomes (Fig. 9A,B), indicating low-affinity transient binding events to SecYEG. Similarly, minor changes in SecYEG diffusion were observed in the presence of RNCs bearing a highly polar nascent chain of the cytoplasmic protein GatD (Fig. 9C). The low affinity of the translocon to GatD-RNC was validated in an independent assay using nanodisc-reconstituted SecYEG. SecYEG was incubated with RNCs containing GatD nascent chain and then centrifuged in continuous density gradient of sucrose (Fig. 9D). While RNCs were found in the center of the gradient (~ 25% sucrose), SecYEG remained in the upper fraction, suggesting that no stable complexes were assembled.

A very different behavior was observed for SecYEG in the presence of FtsQ-RNCs. In this construct, a single TMH of FtsQ was fused at its C-terminal end to the regulatory TnaC sequence, which allowed the stalling of ribosomal translation [38]. The complete FtsQ TMH exposed from the ribosomal exit tunnel allowed for an interaction with the Sec translocon even in the absence of cellular targeting factors, as validated by the centrifugation in the sucrose density gradient (Fig. 9D) [11,18]. The complex assembly was then probed via single particle tracking in SLBs. While the ribosome-free SecYEG manifested the switch between diffusion modes (diffusion coefficients 0.025 and 0.70 $\mu m^2 \cdot s^{-1}$), in the presence of 50 nM FtsQ-RNCs, the coefficient of the fast diffusion decreased by ~ 30% to 0.48 $\mu m^2 \cdot s^{-1}$, while the slow-diffusion coefficient rose to 0.034 $\mu m^2 \cdot s^{-1}$ (Fig. 10A). Importantly, upon adding FtsQ-RNCs, the long step sizes, which largely contributed to the fast diffusion mode, also became less abundant and the decrease of the diffusional mobility of SecYEG upon RNC binding could be directly seen in individual trajectories (Fig. 10B). Thus, we concluded that stable nascent chain-specific assembly of SecYEG : RNC led to pronounced differences in the translocon mobility. As no changes in the brightness of the observed foci were detected (Fig. 10 C), the translocons remained monomeric also in complex with RNCs, in agreement with the available structural data [18].

The prominent effect of FtsQ-RNC on SecYEG diffusion could potentially originate from the increased
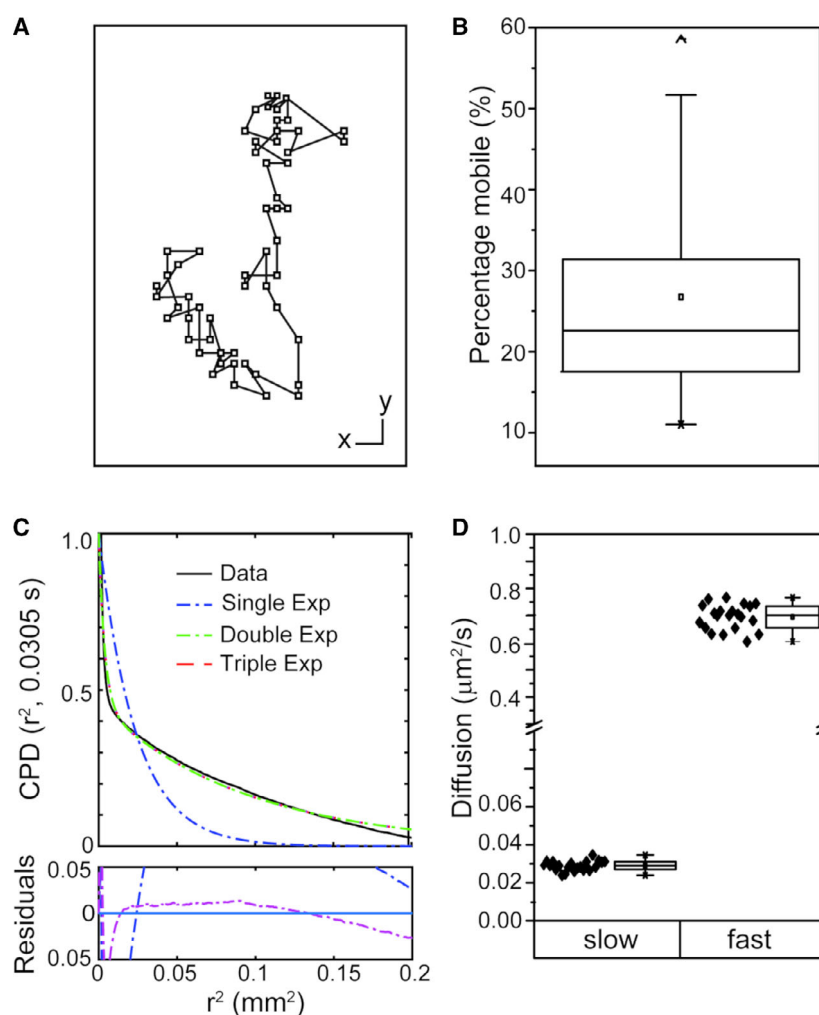
Fig. 6. Tracking of single SecYEG translocons in SLBs. (A) A representative diffusion trajectory of a single SecYEG-Atto 647N molecule. Heterogeneous step sizes are observed. Scale bars for the lateral displacements (*x*, *y*) correspond to 0.5 μm. (B) Percentage of mobile SecYEG particles within the silane-supported SLB. Box plot was created from 40 independent movies, the median was found at 22.6%. The immobile fraction was assigned to the inverted translocons, but also occasional aggregates and fluorescent contaminations. (C) CPD analysis of SecYEG diffusion included fitting of the data to different CPFs containing either one, two, or three components. The corresponding residuals (panel below) indicate that the single-component CPF cannot be applied to analyze SecYEG diffusion. (D) Two diffusion modes of translocons with median diffusion coefficients of 0.03 and 0.7 $\mu m \cdot s^{-2}$ were revealed. Each dot corresponds to a value acquired from an individual movie.

mass and the large solvent-exposed volume of the assembled complex, or from interactions within the SLB, such as distortion of the lipid bilayer or the translocon conformation. According to Saffman-Delbrück model, diffusion of the membrane-embedded translocon is determined by the viscosity of the lipid bilayer and, to a less extent, the viscosity of the aqueous phase [39]. Thus, changing the viscosity of the aqueous phase would reveal the contribution of the peripherally bound ribosome. The buffer viscosity may be tuned by Ficoll, a chemically inert hydrophilic polysaccharide commonly employed to mimic the intracellular crowding [40]. Ficoll PM 70 did not hinder SecYEG:RNC interactions, as it was validated using nanodisc-reconstituted translocons (Fig. 11A). To probe the effect of the buffer viscosity on SecYEG diffusion in SLBs, tracking experiments were repeated in the presence of 40 % (w/v) Ficoll PM 70. The high concentration of Ficoll PM 70 in solution did not

affect the diffusion of free SecYEG in SLBs, so the solvent-exposed loops did not influence the mobility of the integral membrane protein (Fig. 11B). Importantly, the elevated viscosity in solution did not affect the lateral diffusion of SecYEG:RNC complexes assembled at the SLB interface. Thus, the solvent:ribosome interactions had a weak effect on the lateral mobility of the SecYEG:ribosome complex within the SLB, and the hindered diffusion was likely determined by protein:lipid interactions and the conformation of the membrane-embedded translocon.

Discussion

Despite the extensive biochemical, biophysical and structural analysis, functional dynamics of the universally conserved Sec translocon in the lipid membrane environment remain challenging to understand. Aiming for physiologically relevant insights on the
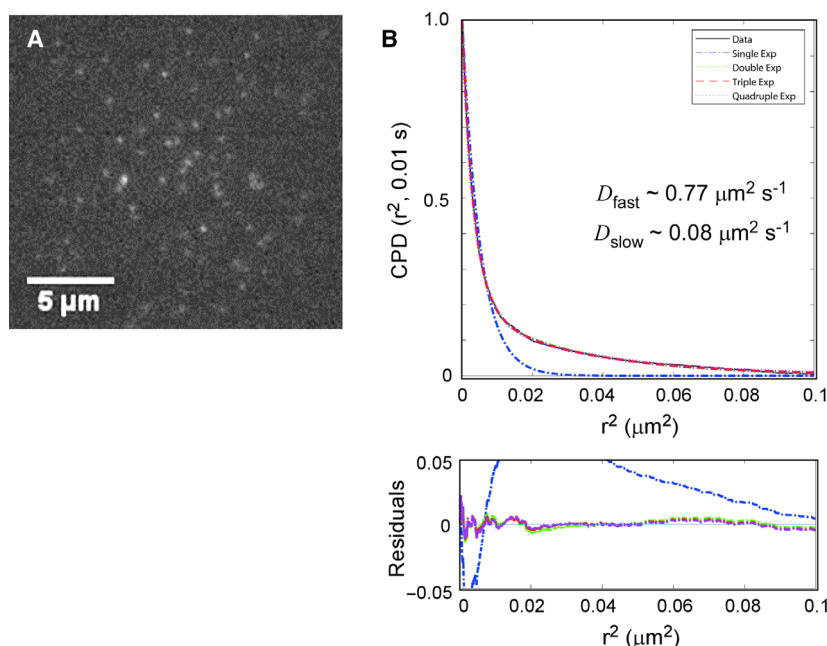
Fig. 7. Mobility of SecYEG in APTES-SLBs. (A) Observation of individual SecYEG-Atto 647N translocons in wide-field microscopy experiments. (B) CPD analysis of SecYEG diffusion suggests two distinct modes (slow and fast) with approx. 10-fold different diffusion coefficients, which match closely those observed for SLBs formed on longer silane variant *N*-(2-aminoethyl)-3-aminoisobutyldimethylmethoxysilane.

translocon dynamics, fluorescence correlation spectroscopy (FCS) and cryo-electron microscopy have been previously employed to probe SecYEG:ribosome and SecYEG:SecA interactions in lipid-based nanodiscs and giant unilamellar vesicles (GUVs) [11,16,18,33,41]. Complementary to those highly sensitive methods, single-molecule detection of translocons should allow probing the properties of individual molecules within the ensemble and potentially revealing the heterogeneity in molecular dynamics [25,26]. With this goal, we have established the fluorescence-based tracking approach to investigate SecYEG diffusion and the oligomeric state at the single-molecule level and to investigate how interactions with SecA and ribosomes modulate the translocon.

In contrast to GUVs, SLBs are easier to prepare and they are not sensitive to axial movement of the membrane caused by membrane undulations [42] and translocation activity of SecYEG within mica-deposited SLBs has been recently reported [25]. To reproduce the native fluidity of both leaflets of the bilayer, SLBs should allow lateral mobility of lipids and embedded translocons [43]. Interactions of SLBs with the solid support cannot be excluded once the lipid membrane is deposited directly on glass. Our data show that the thin aqueous layer of ~ 5 Å formed between the lipid bilayer and the supporting surface [29,30,44,45] was not sufficient to ensure lateral diffusion within the SLB, in agreement with previous reports for DOPE-containing SLBs [46]. Introducing a short silane coating APTES recovered the lateral

mobility of lipids and reconstituted translocons, wherefore sufficient spacing was provided to avoid the interaction of SLBs with the surface underneath. The elongated silane-derivate coating was then implemented to prevent contacts between the surface and the short periplasmic loops of SecYEG [9,26], while the cytoplasmic interface of the translocon was exposed to the aqueous solvent, being accessible for interactions with ribosomes and SecA. Inversely oriented and so inactive translocons may contact the surface with the long structured cytoplasmic loops 6/7 and 8/9 of SecY. These loops extend up to 3 nm beyond the membrane interface, so their lateral diffusion may be hindered even in presence of the silane spacer. We believe that these inversely oriented SecYEG largely determined the fraction of the immobile particles observed within SLBs, as they constitute approx. 50% of translocons within the bilayer due to the stochastic orientation of the reconstituted proteins [14,33]. Under this feasible assumption, the performed SLB-based mobility analysis allowed segregating translocons in the nonrelevant membrane topology, as well as occasional aggregates, at the single-molecule level and focusing on the properties of the functionally oriented proteins.

Tracking individual translocons within the SLB revealed the dynamic heterogeneity in their diffusion, as the protein displacement could occur either in short (~ 50 nm) or long (200–300 nm) steps, making the conventional mean square displacement analysis (MSD) challenging [47]. Instead, a multicomponent
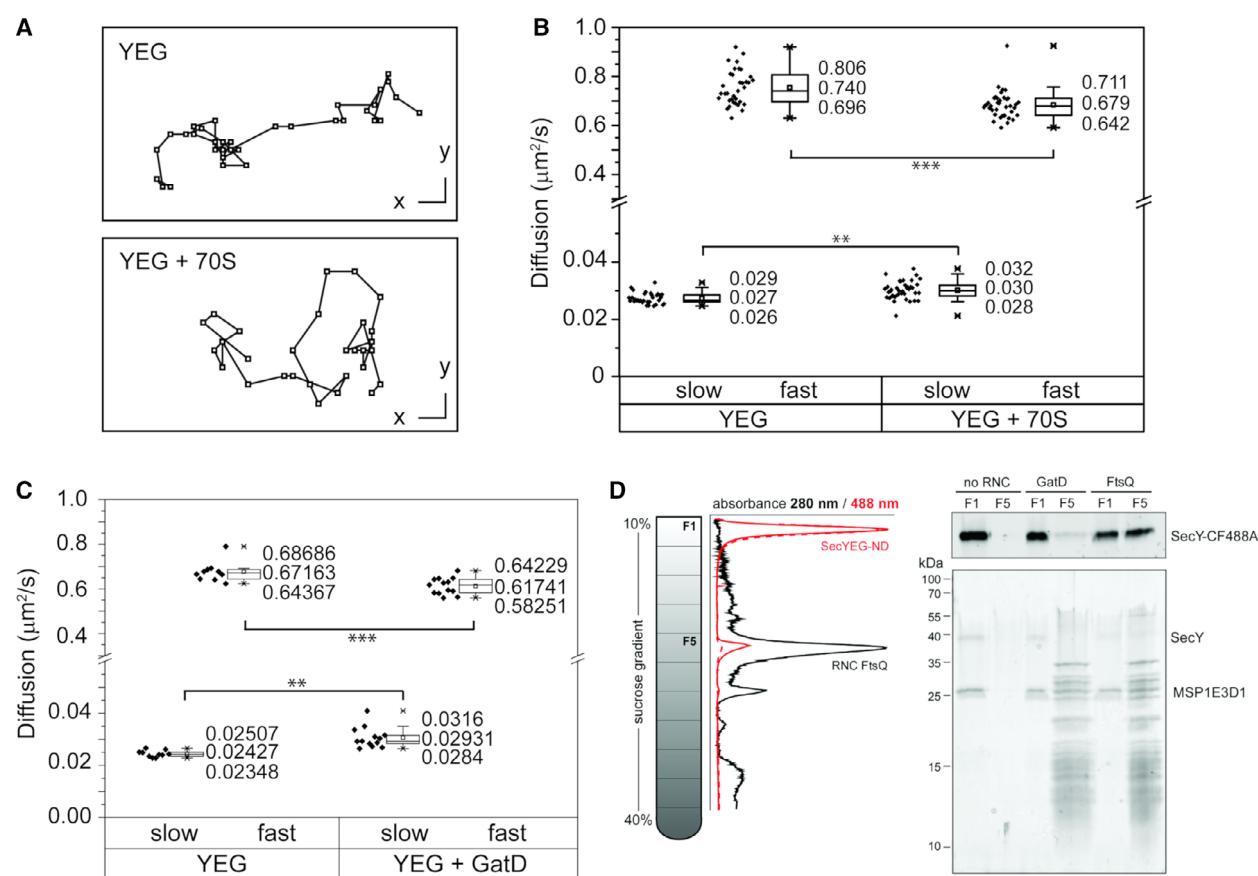
A

B

C
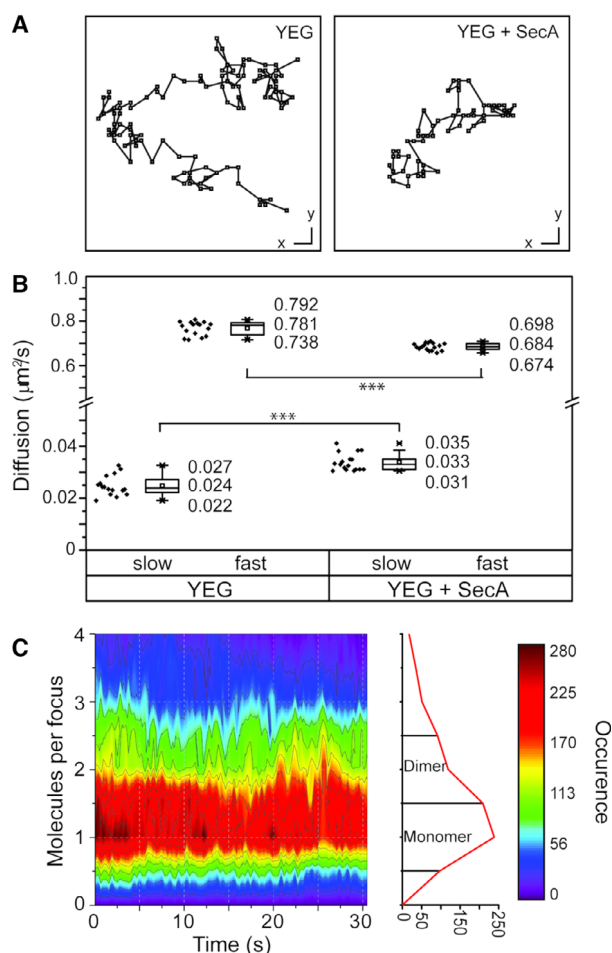
Fig. 8. SecYEG diffusion in the presence of SecA. (A) Representative trajectories of a single SecYEG-Atto 647N molecule alone and in the presence of SecA. Scale bars correspond to 0.5 μm. (B) In the presence of SecA SecYEG the slow-diffusion coefficient increased from 0.024 to 0.033 $\mu m \cdot s^{-2}$, while the fast diffusion coefficient decreased from 0.78 to 0.68 $\mu m \cdot s^{-2}$. ***indicates $P < 0.0005$ in a *t*-test. (C) Single-molecule analysis reveals higher heterogeneity in SecYEG brightness, which may indicate partial dimerization of translocons. The ratio of monomers vs dimers was approx. 2.5 : 1 (52 399 monomeric vs 21 545 dimers, based on the full movie).

CPD analysis suggested that two diffusion modes of SecYEG differed by their instant diffusion coefficients approx. 20-fold, 0.03 and 0.7 $\mu m^2 \cdot s^{-1}$. Recently, the AFM-based study demonstrated that the heterogeneity in SecYEG diffusion may occur in the presence of local confinements at the membrane interface, in agreement with the 'picket-fence model' [26,48]. However, the origin of the heterogeneity within the homogeneous SLB is less clear. The experiments performed with the silane coatings of different length suggested

that the supporting surface had minor effect on SecYEG mobility. One possible explanation for the nonuniform diffusion behavior might be provided by transient interactions within the SLB. Complex diffusion patterns within model membranes have been described for lipids and lipid analogues [43,49], but also transmembrane peptides [50], and assigned either to subdiffusion within specific lipid clusters or formation of protein : lipid assemblies with altered diffusional properties. Furthermore, the shape of the transmembrane protein and the occasional hydrophobic mismatch between a membrane protein and the lipid bilayer greatly affects the lateral mobility and causes deviations from Saffman-Delbrück model [51,52]. Specific interactions of SecYEG with anionic phospholipids have been recently described [18,53,54], and the designed SLBs contained 30 mol% 1,2-dioleoyl-sn-glycero-3-phosphoglycerol (DOPG) to mimic their naturally abundant content. While it is unlikely that DOPG lipids segregate within the formed SLBs, dynamic association/dissociation of lipids from the translocon interface may cause conformational changes within SecYEG and alter its lateral mobility. Structural rearrangements may involve peripheral and lipid-exposed domains, such as TMHs 1 and 2 of SecE and the complete SecG subunit, which are highly dynamic as judged from biochemical and structural data [9,18,55,56]. When being re-positioned within the translocon, those peripheral domains would cause a substantial change in the shape of the translocon or cause distortions in the lipid packing, which determine the lateral diffusion within the highly viscous lipid membrane [39,51,52].

Empty 70S ribosomes and ribosomes loaded with the highly polar nascent chain of GatD had modest effect on the translocon lateral diffusion, as it is readily explained by low affinity, transient binding events, and lack of ribosome : lipid interactions [11]. Upon addition of FtsQ-RNCs, the diffusion rate of SecYEG decreased by 30%, indicating that binding of FtsQ-RNCs reduces the lateral mobility of translocons. As diffusion of the SecYEG:FtsQ-RNC complex was not sensitive to the viscosity of the aqueous phase, it was rather determined by the interactions at the lipid interface and within the membrane, than by the shear imposed by the bound ribosome. Interestingly, the ribosome does not only bind to loops 6/7 and 8/9 of SecY, but may also interact with surrounding lipids near the translocon lateral gate. The rRNA helix H59 was observed in a direct contact with lipid head groups and was suggested to recruit anionic phospholipids and disorder the lipid bilayer to assist the insertion of nascent membrane proteins [57]. Those

S. Koch *et al.*   SecYEG mobility is affected by the ribosome binding
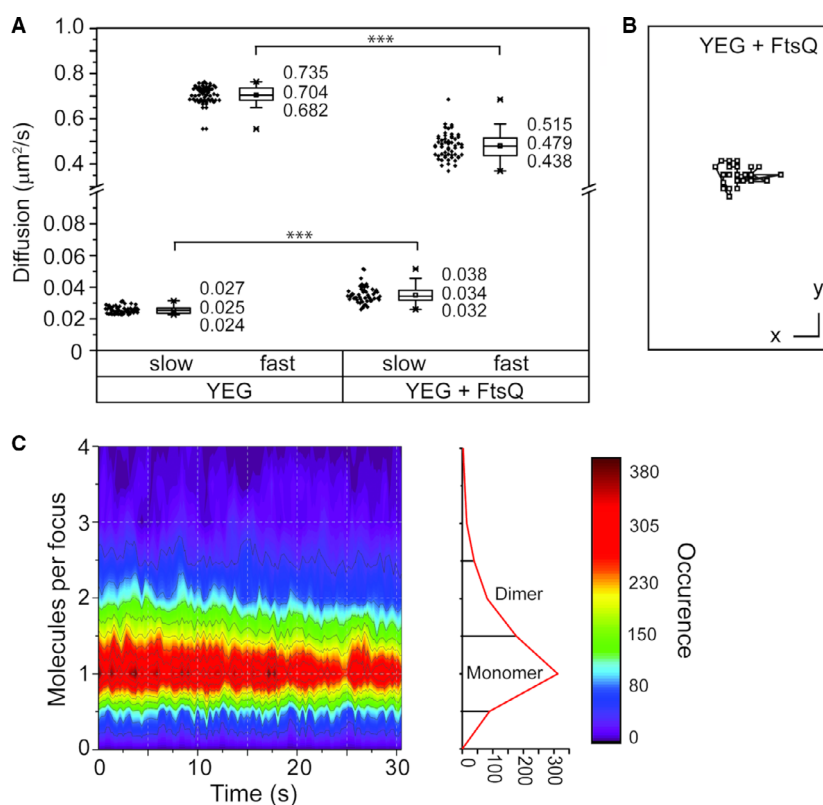

Fig. 9. SecYEG diffusion in the presence of ribosomes. (A) Representative trajectories of single SecYEG-Atto 647N molecules alone and in the presence of 70S ribosomes. Scale bars correspond to 0.5 μm. (B) In the presence of nontranslating 'empty' ribosomes ('70S') the fast diffusion coefficient reduces from 0.74 to 0.68 μm·s^{-2}. ** indicates $P < 0.005$, and *** indicates $P < 0.0005$ in a *t*-test. (C) In presence of polar GatD-RNCs the fast diffusion coefficient reduces from 0.67 to 0.61 μm·s^{-2}. Thus, both empty ribosomes and GatD-RNCs have minor effect on the lateral mobility of the translocons. (D) SecYEG : RNC assembly is sensitive to the nascent chain polarity. Nanodisc-reconstituted SecYEG was incubated with RNCs containing GatD (polar) or FtsQ (apolar) nascent chains. The complex assembly was probed via centrifugation in sucrose density gradients. Left: UV-Vis profiles and collected fractions of sucrose density gradients. For FtsQ-RNC sample, the absorbance of SecYEG-conjugated CF488A dye (solid red line) correlated with the strong UV absorbance of RNCs (black line), indicating that a fraction of SecYEG-nanodiscs was bound to these RNCs. No correlation was observed between GatD-RNC and SecYEG-nanodiscs (dashed red line), indicating weak or no binding. Right: SDS/PAGE of selected fractions F1 (no sucrose) and F5 (25% sucrose) collected for free SecYEG-nanodiscs ('no RNC') and SecYEG in presence of GatD and FtsQ-RNCs. In-gel fluorescence visualizes the distribution of SecY-CF488A (top). To avoid the fluorescence signal saturation, fraction F1 load was reduced to 10%. The nanodisc-forming protein MSP1E3D1 is indicated on Coomassie-stained SDS-PAGE (bottom).

ribosome:bilayer interactions, as well as conformational changes involving SecE and SecG subunits, would further affect the diffusion of the translocon.

A moderate decrease in the diffusion coefficient of SecYEG detected upon SecA binding correlates with previous results acquired by means of FCS on free-standing membranes of GUVs [33]. Crystal structures of the SecA:SecYEG complex reveal that SecA interacts with loop 6/7 and loop 8/9 of SecY, which are the same binding sites as for ribosome binding [11,57,58]. Additionally, SecA was shown to interact with lipids, in particular anionic phospholipids: The amphipathic

N-terminal helix of SecA anchors at the lipid bilayer interface, which activates SecA for high affinity binding to the translocon [17,59,60]. Despite these SecA: lipid interactions, binding of the motor protein did not affect the translocon diffusion as much as binding of FtsQ-RNC, which can be explained by a smaller surface area involved in SecA:SecYEG:lipid contact and minor structural rearrangements within SecYEG in absence of the substrate preprotein [58]. Also, the less pronounced effect on the translocon diffusion might be due to transient association and dissociation of SecYEG : SecA complex in the absence of nucleotides

Fig. 10. Tight docking of ribosomes affects the mobility of SecYEG. (A) In the presence of translation-stalled FtsQ-RNCs the fast diffusion coefficient of SecYEG drops from 0.7 to 0.48 $\mu m \cdot s^{-2}$. (B) A representative trajectory of single SecYEG in the presence of FtsQ-RNCs reflects the hindered diffusion of the ribosome-bound translocon. (C) Brightness distribution of single translocon foci reveals that SecYEG remains monomeric upon interactions with FtsQ-RNCs. The ratio of monomers vs dimers was approx. 4 : 1 (56 582 monomeric vs 14 290 dimers, based on the full movie).

[33,58]. As single-molecule analysis suggested a broader distribution of translocon brightness in presence of SecA, partial dimerization of SecYEG could occur under these conditions [16,33]. It should be noted, however, that the putative oligomeric assemblies contained multiple translocons and may contain a major fraction of SecYEG. The functional role of the dimerization is not clear, as monomers of SecYEG were shown to form active translocons *in vitro* and *in vivo* [16,33,41,61].

Single-molecule observations of biological processes allow describing complex molecular mechanisms in
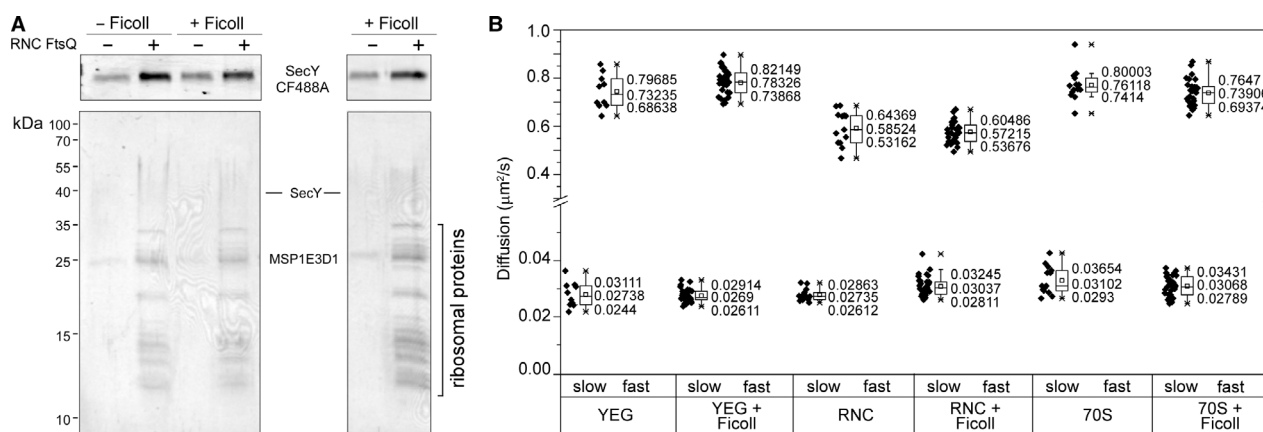
Fig. 11. The buffer viscosity does not affect diffusion of SecYEG and SecYEG : ribosome complexes. (A) The elevated viscosity and macromolecular crowding induced by polysaccharide Ficoll does not prevent SecYEG : ribosome interactions. FtsQ-RNCs bind nanodisc-reconstituted SecYEG in presence of 40% (w/v) Ficoll PM 70 and pellet as a complex through the sucrose cushion. Top: In-gel fluorescence of SecY-CF488A; bottom: Coomassie-stained SDS-PAGE showing SecYEG-ND bands and the pattern of ribosomal proteins. (B) Ficoll PM 70 at concentration 40% (w/v) does not affect the mobility of free or ribosome-bound SecYEG.

unprecedented details, revealing individual pathways and hidden intermediate states. Here, we describe the first fluorescence-based single-molecule analysis of the translocon SecYEG in SLBs and demonstrate its applicability to investigate not only diffusion, but also interactions of individual translocons with ribosomes and SecA in real-time. SLB-reconstituted SecYEG was found predominantly in monomeric form, and could also bind RNCs as a monomer, though a partial dimerization was observed in presence of SecA motor protein. Surprisingly, substantial dynamic heterogeneity was observed in diffusion trajectories of single SecYEG molecules that was attributed to transient translocon:lipid interactions and the conformations dynamics of SecYEG. Our data revealed a strong effect of RNC binding on the diffusional characteristics of the SecYEG complex, which is can be related to SecYEG:lipid and ribosome:lipid interactions, and/or conformational changes within the translocon. Further, the work provides benchmarking values of membrane diffusion rates of various complexes of SecYEG that will facilitate interpretation and analysis of the diffusion of the translocon, also in living cells.

Methods

Protein purification and labeling

SecA was overexpressed in *E. coli* BL21 (DE3) cells carrying the pTrc99A-SecA plasmid and purified as described [17,62]. $SecY_{C148}EG$ was overexpressed in *E. coli* SF100 and C41(DE3) cells carrying the pEK20-C148 plasmid [33] and isolated from crude membranes as described [14]. The translocon was labeled at the unique periplasmic cysteine in position 148 upon incubation with 100 μM Atto 647N-maleimide (Atto-Tec GmbH, Siegen, Germany) or CF488A-maleimide (Biotium Inc., Hayward, CA, USA) as described [17]. Protein concentrations and the labeling efficiency were determined spectrophotometrically using the corresponding extinction coefficients at 280 nm: SecA—75 750 $M^{-1}·cm^{-1}$, SecYEG—71 000 $M^{-1}·cm^{-1}$ at 280 nm, CF488A—70 000 $M^{-1}·cm^{-1}$ at 490 nm, and Atto 647N—150 000 $M^{-1}·cm^{-1}$ at 647 nm.

Lipid preparation

A mixture of chloroform-dissolved lipid DOPG:DOPE:1,2-dioleoyl-sn-glycero-3-phosphocholine (DOPC; Avanti Polar Lipids Inc., AL, USA) was prepared at the molar ratio 30:30:40 [33]. DOPG concentration of 30 mol % was used to mimic the anionic lipid content of the cytoplasmic membrane of *E. coli*, while the zwitterionic lipid DOPC facilitated the stability of the planar SLB. The chloroform was

evaporated under a nitrogen stream, after which chloroform remnants were extracted overnight under vacuum conditions using a desiccator. The resulting lipid film was resuspended in 20 mM HEPES/KOH pH 7.5, 2 mM DTT to obtain final lipid concentration of 10 mg·mL^{-1}.

Reconstitution of SecYEG into proteoliposomes

Liposomes were diluted to 4 mg·mL^{-1} using a buffer containing 20 mM HEPES/KOH pH 7.5, 50 mM KCl, 0.5% Triton X-100, and 0.05% *n*-dodecyl-β-D-maltoside (DDM). Lipids were incubated for 15 min at 37 °C and subsequently 15 min on ice. SecYEG-Atto 647N (final concentration 200 nM) was added to 1 mL of the lipid : detergent mixture (1 : 30 000 protein-to-lipid ratio) and incubated for 30 min at 4 °C. The detergent was removed in three steps of 1.5 h with 50, 75, and 100 mg Bio-Beads SM2 sorbent (Bio-Rad Laboratories GmbH, Düsseldorf, Germany), whereby the last incubation was performed overnight. Translocon functional activity was validated in translocation assay in proteoliposomes using preprotein proOmpA labeled with BDP-FL-maleimide (Lumiprobe GmbH, Hannover, Germany) as a substrate [63]. Topology of reconstituted SecYEG was probed based on the accessibility of the N-terminal cleavage site within SecY for the enterokinase [14]. Proteoliposomes were incubated with eight units of the enterokinase light chain (New England Biolabs GmbH, Frankfurt/Main, Germany) overnight at 25 °C. The cleavage efficiency was evaluated based on the shift of SecY band in SDS/PAGE.

Reconstitution of SecYEG into nanodiscs

The reconstitution was performed following the previously established protocols [16,18]. Briefly, purified and fluorescently labeled SecYEG translocons in DDM were mixed with MSP1E3D1 major scaffold proteins and detergent-solubilized DOPG:DOPE:DOPC lipids at the molar ratio 1:10:500. Spontaneous nanodisc formation was achieved upon the detergent removal with Bio-Beads SM2 sorbent. SecYEG-loaded nanodiscs were separated from empty nanodiscs via size-exclusion chromatography using Superdex 200 10/300 Increase column and AKTA Pure system (GE Healthcare Life Sciences, MA, USA) in 150 mM KOAc, 5 mM Mg(OAc)₂, 25 mM HEPES pH 7.4, and cOmplete protease inhibitor cocktail (Roche, Basel, Switzerland).

RNC isolation

TnaC-stalled RNCs were prepared *in vivo* and isolated as previously described [18,64]. Briefly, KC6Δ*ssrA*Δ*smpB* cells [65] were used to synthesize poly-histidine-tagged fragments of FtsQ and GatD proteins followed by the TnaC sequence that caused stalling of the ribosomal translation at elevated

tryptophan concentrations [38], so stable and well-defined RNCs could be formed. N-terminal poly-histidine tags of the nascent chains were employed for Ni-NTA-based purification of RNCs, and assembled RNCs were further isolated by centrifugation in continuous 10–40% sucrose gradients (Gradient station, Biocomp Instruments, Fredericton, Canada). Presence of the tRNA-linked nascent chains was validated via the tag-specific western blotting. For preparing empty ribosomes, a crude ribosome extract from nontransformed KC6 cells was incubated in presence 1 mM puromycin for 30 min on ice to release nascent chains, and fully assembled 70S ribosomes were isolated via sucrose gradient, as described above.

SecYEG : RNC binding in nanodiscs

Two-hundred nanomolar CF488A-labeled translocons reconstituted into nanodiscs were optionally incubated with 200 mM FtsQ- or GatD-RNC for 30 min at the ambient temperature, loaded on top of continuous 10–40% sucrose gradients in SW40-type tubes and centrifuged 160 000 g for 3 h at 4 °C. The gradients were fractionated from top to the bottom with Gradient station (Biocomp Instruments) in fractions of 1 mL, while continuously recording absorbance at 280 and 488 nm. Contents of individual fractions were precipitated in 15% (w/v) trichloracetic acid and analyzed on SDS-PAGE by recording in-gel fluorescence and Coomassie-stained proteins (AI680 RGB imager; GE Healthcare Life Sciences). To probe the effect of Ficoll PM 70 on SecYEG:RNC interactions, 200 nM nanodisc-reconstituted SecYEG-CF488A was prepared in 40% (w/v) Ficoll 70, and then, 200 nM FtsQ-RNC were added. The reaction was incubated for 30 min at the ambient temperature, then rapidly diluted twofold with the nanodisc buffer, loaded above the sucrose cushion [1 M sucrose, 150 mM KOAc, 5 mM Mg(OAc)$_2$, 25 mM HEPES pH 7.4, and protease inhibitor cocktail (Roche)] and centrifuged in S120-AT3 rotor (Sorvall/Thermo Fisher, Waltham, MA, USA) at 60 000 g for either 20 or 40 min, 4 °C. Pellets were collected and analyzed on SDS-PAGE.

Glass functionalization and flow cell preparation

For SLB formation several requirements are essential: Firstly, the surface has to be cleaned vigorously in order to eliminate organic adsorbents and other contaminants, such as dust [24]. Secondly, a critical concentration of vesicles has to be supplied to the surface to initiate vesicle rupture and subsequent SLB formation. Crowding most likely enhances the interaction between vesicles, which induces stress and rupture [66]. Thirdly, to support SLB formation for vesicles harboring negatively charged lipids, such as DOPG, high ionic strength buffers are necessary [67]. Glass for microscopy was sonicated in acetone at 30 °C for 30 min followed by rinsing the glass six times with

deionized water. Next, the coverslip surface was activated by sonicating for 45 min at 30 °C in 5 M KOH. Afterward, traces of KOH were removed by rinsing six times with deionized water, followed by drying the glass for 30 min at 110 °C. Glass surfaces were plasma cleaned for 10 min prior to the surface functionalization with 2% (v/v) *N*-(2-aminoethyl)-3-aminoisobutyldimethylmethoxysilane (abcr GmbH, Karlsruhe, Germany) for 1 hour at room temperature. Afterward, the coverslips were rinsed once with acetone and subsequently dried with pressurized air and stored overnight under vacuum. Prior to each microscopy experiment, a flow cell was constructed by cutting out a channel from a piece of double-sided tape (75 × 25 mm) and fixed to a cleaned object slide containing inlet and outlet holes. The flow cell was formed by placing the object slide on top of a functionalized cover slip. Tubing was inserted into the inlet and outlet openings and fixed with epoxy glue.

The glass functionalization procedure was slightly modified for coating with APTES. Briefly, APTES was dissolved in water to a final concentration of 2%, the pH was then adjusted to three using HCl. The functionalized glass cover slides were then immersed in the silane solution and incubated for 2 h at 75 °C. The glass cover slides were then washed with the deionized water and stored in water until used.

Supported lipid bilayer generation

Liposomes were diluted to 4 mg·mL^{-1} using a buffer containing 50 mM HEPES/KOH, pH 7.5, and 50 mM KCl and sonicated in an ultra-sonic bath (Sonorex Super; Bandelin, Berlin, Germany) for 15 cycles alternating between on/off stages, each of 15-s duration, to form small unilamellar liposomes. Protein-free liposomes were mixed with proteoliposomes containing SecYEG (final SecYEG concentration 50 pM, protein-to-lipid ratio below 1 : 5 000 000). The flow cell chamber was washed with 50 mM HEPES/KOH pH 7.5, 50 mM KCl at a flow rate of 10 μL·min^{-1} prior injecting the SecYEG proteoliposome/liposome mixture. The fusion of the SecYEG proteoliposomes/liposomes on the surface, which thereby form an SLB, was induced by elevated salt concentrations in a washing step using 50 mM HEPES/KOH pH 7.5 and 150 mM KCl. Unbound material was washed out of the flow cell chamber with 50 mM HEPES/KOH pH 7.5, 50 mM KCl. 2D diffusion of R18 was monitored for every experiment to validate reliable SLB formation and diffusion analysis. To investigate SecYEG binding, the concentration of added FtsQ-RNCs, SecA, 70S ribosomes and GatD was 50 nM.

Wide-field microscopy

For single-particle tracking and CPB an epifluorescence microscope (IX73 Olympus, Tokyo, Japan) in combination with an 100× oil-objective (Apochromat & TIRF, NA 1.45;

Olympus) was used. All images were captured with a back-illuminated sCMOS camera (Prime95B; Teledyne Photometrics, Tucson, AZ, USA). The microscope was controlled via CELLSENS DIMENSION software (Olympus). For wide-field laser excitation of SecYEG-Atto 647N, 638 nm laser was used (Cobolt MLD-06 638 nm; Cobolt AB, Solna, Sweden). This was combined with a multiband pass dichroic splitter for excitation (Di03-R405/488/561/635-t1-25 × 36, Semrock, IDEX Co., West Henrietta, NY, USA) and the emitted light was filtered by a 635-nm-long pass filter (BLP01-635R-25, Semrock, IDEX Co.). For illumination during CPB experiments with DOPE-NBD a solid-state white light source (Lumencor SOLA SE 2; Lumencor, Beaverton, OR, USA) was used together with a 482/18 nm single-band bandpass filter (FF02-482/18–25; Semrock, IDEX Co.). The reflected light was filtered by a 525/39 nm single-band bandpass filter (FF01-525/39–25; Semrock, IDEX Co.).

Measurement of SLB mobility with continuous photobleaching

Lipid mobility within the SLB was probed via CPB following a previously published protocol [68]. With this technique, the lateral diffusion constant of DOPE-NBD in the bilayer is measured. Photobleaching occurs during continuous observation of fluorescent labels. As long as lipids within the bilayer are mobile, bleached fluorophores coupled to lipids can be replaced by fresh ones due to diffusion. Quantitative evaluation of the bleaching rate of fluorophores and of the intensity profile at the rim of the illuminated area enables extraction of the diffusion constant. The illumination field stop was opened to about 100 μm, and the illuminated area was bleached after prolonged exposure. Depending on the lipid mobility a bright rim was visible at the edges. To determine the bleaching constant, B, the average intensity in a square area $(0.55 \times 0.55\ \mu m^2)$ in the center of the illuminated area was fitted with Eqn (1):

$$I(t) = I_0 e^{-\mathrm{B}t} + I_{\mathrm{Bg}}, \qquad (1)$$

where I_0 is the initial intensity, I_{Bg} is the background intensity, and B is the bleaching constant, which are fitting parameters. By knowing B, the diffusion constant D could be extracted from the spatial intensity distribution. To do this, a mean intensity curve $I(r)$ was calculated from the intensity distribution averaged over a five-pixel wide line drawn perpendicular to the edge of the field stop. This was then fitted with Eqn (2).

$$I(r) = I_0 e^{-\mathrm{x}A} + I_{\mathrm{Bg}}, \qquad (2)$$

where $A = \sqrt{B/D}$, I_0 and I_{Bg} as before. From each bleached area, along four radial lines the diffusion

constants were calculated from A and B. The images were taken at a rate of 1 Hz at exposure time of 0.5 s. The analysis was automated using self-written routines in Matlab (R2018a; MathWorks Inc., Natick, MA, USA).

Total internal reflection fluorescence microscopy

TIRFm measurements were performed at room temperature on an Olympus IX-71 microscope equipped a 100× oil-objective UApoN, NA 1.49 (Olympus) and set to TIRF-illumination ($\Theta < \Theta_c$) equipped with a DV2 multichannel imaging system (Teledyne Photometrics) with 537/29 and 610/75 ET band pass filters and a zt561RDC mirror (Chroma Technology Corp., Bellows Falls, VT, USA). SecYEG-Atto 647N were excited by 638 nm continuous-wave laser (Coherent Inc., Santa Carla, CA, USA) at approximately 1 kW·cm^{-2}. Images were captured using a 512×512 pixel electron multiplying charge coupled device camera C9100-13 (Hamamatsu Photonics) with EM-gain set to 254 at 33 frames·second^{-1} (temporal resolution 30 ms) and METAVUE imaging software (Molecular Devices LLC, San Jose, CA, USA).

Data acquired in TIRFm measurements were analyzed with IMAGEJ v1.48 using built-in and purpose-built plugins. Data were visualized using ORIGINPRO v9.1 (OriginLab Corp., Northampton, MA, USA) and MATLAB R2016b (MathWorks Inc.). To localize and track fluorescently labeled translocons, images were processed using a discoidal averaging filter with an inner and outer radius of one and four pixels, respectively [69]. Next, local fluorescence maxima which intensities exceeded either fixed or dynamic threshold (see below), and which were separated by at least four pixels, were selected. A two-dimensional Gaussian model was fitted to each point-spread functions (PSF) on the original unprocessed image by minimizing the RSS value by means of the Levenberg-Marquardt algorithm [70,71]. The resulting Gaussian model gave the amplitude, subpixel coordinates, symmetrical spread localization accuracy, and goodness of fit of the peak positions for each frame below the diffraction limit with an accuracy of 10–20 nm.

Oligomeric state of SecYEG

To investigate the oligomeric state of SecYEG particles in SLB, foci were detected using a fixed gray value threshold to minimize the dynamic threshold filtering artefacts caused by local background intensity changes. The fixed threshold value was based on the intensities of particles in the last recorded frames, where bleaching positively affected the background fluorescence, and where the remaining fluorescence represented an estimation of a single-molecule intensity. Signals passing the threshold were fitted to a two-

dimensional Gaussian model by minimizing the RSS value by means of the Levenberg-Marquardt algorithm. The obtained amplitude and PSF were used to calculate the Gaussian integral for each foci in the last 100 frames of multiple movies (Eqn 3). The obtained values were plotted in a histogram and fitted with a 2D Gaussian, of which the peak maximum represented the average integrated Gaussian intensity of a single molecule.

$$\int_{-\infty}^{\infty}\int_{-\infty}^{\infty} f(x,y)dxdy = 2\pi A\sigma_x\sigma_y. \qquad (3)$$

Subpixel coordinates were obtained from particles, upon which a selection with a radius of two pixels from the centroid was made. From this selection, the raw integrated density was calculated and divided by the integrated Gaussian intensity of a single molecule, resulting in the number of molecules per focus.

Membrane diffusion behavior of SecYEG

To study the diffusional behavior of SecYEG, particles were detected using a dynamic threshold. The dynamic threshold was defined as $-x + 6*\sigma$, where $-x$ and σ are the average and standard deviation of the background gray value, respectively. The peak location data were filtered to exclude poorly fitted peaks (adjusted RSS < 0.2), after which the remaining coordinates were used to create particle trajectories by linking particles located nearest to each other in consecutive frames. A maximum step size constraint of three pixels was used to prevent linkage of particles too far apart to be the same. The step sizes constituting these trajectories were filtered on a minimal displacement of $0.06~\mu\text{m}^2\cdot\text{s}^{-1}$ to filter out artefacts, for example false linkages and immobile molecules, and the trajectories were filtered on the fitting accuracy of at least 20 nm trajectory lengths, and the particle displacement. The resulting data set consisting out of approximately 5000–10 000 step sizes per movie, contained only the coordinates of moving particles, which were further used for calculation of the CPD of step sizes. In short, a probability density function was created from the step size data and normalized resulting in the CPD. To extract the SecYEG diffusion characteristics, the CPD was fitted to the multi-component CPD function (CPF, Eqn 4):

$$P(r^2,\tau) = 1 - \alpha e^{\left(\frac{-r^2}{\langle r_\alpha^2\rangle + 4\sigma^2}\right)} - \beta e^{\left(\frac{-r^2}{\langle r_\beta^2\rangle + 4\sigma^2}\right)} - \gamma e^{\left(\frac{-r^2}{\langle r_\gamma^2\rangle + 4\sigma^2}\right)}, \quad (4)$$

where α, β, and γ are the fraction of each population with the constraints that the sum of fractions cannot exceed 1. $\langle r_{\alpha,\beta,\gamma}^2\rangle$ give the MSD for each population at each time point (τ). The localization accuracy, σ, was determined from the mean error in the x and y parameters from the

Gaussian fit. The CPF goodness-of-fit was determined by calculating the RSS value. The MSD of the best fitting model (RSS close to 0) was used to calculate the diffusion coefficient from the slope by plotting the obtained MSD value as a function of time.

Acknowledgement

Conflicts of interest

The authors declare no conflict of interest.

Author contributions

All authors conceived the idea for the project and designed the experiments. SK and MK performed experiments including protein purification, lipid preparation, A-BS, SK, MK, and DK performed glass functionalization, microscopy experiments and data analysis. AK isolated RNCs and performed nanodisc-based experiments. CM, AJMD, and AK supervised the work. All authors contributed to writing and editing of the manuscript and approved the final version.

References

1 Park E & Rapoport TA (2012) Mechanisms of Sec61/SecY-mediated protein translocation across membranes. *Annu Rev Biophys* **41**, 21–40.

2 Plessis DJF, Nouwen N & Driessen AJM (2011) The Sec translocase. *Biochim Biophys Acta* **1808**, 851–865.

3 Hegde RS & Bernstein HD (2006) The surprising complexity of signal sequences. *Trends Biochem Sci* **31**, 563–571.

4 Akopian D, Shen K, Zhang X & Shan S (2013) Signal recognition particle: an essential protein-targeting machine. *Annu Rev Biochem* **82**, 693–721.

5 Niesen M, Muller-Lucks A, Hedman R, von Heijne G & Miller TFI (2018) Forces on nascent polypeptides

during membrane insertion and translocation via the Sec translocon. *Biophys J* **115**, 1885–1894.

6 Hoffmann A, Bukau B & Kramer G (2010) Structure and function of the molecular chaperone Trigger factor. *Biochim Biophys Acta Mol Cell Res* **1803**, 650–661.

7 Huber D, Jamshad M, Hanmer R, Schibich D, Döring K, Marcomini I, Kramer G & Bukau B (2017) SecA cotranslationally interacts with nascent substrate proteins *in vivo*. *J Bacteriol* **199**, e00622-16.

8 Sala A, Bordes P & Genevaux P (2014) Multitasking SecB chaperones in bacteria. *Front Microbiol* **5**, 666.

9 Tanaka Y, Sugano Y, Takemoto M, Mori T, Furukawa A, Kusakizako T, Kumazaki K, Kashima A, Ishitani R, Sugita Y *et al*, (2015) Crystal structures of SecYEG in lipidic cubic phase elucidate a precise resting and a peptide-bound state. *Cell Rep* **13**, 1561–1568.

10 Fröderberg L, Houben E, Samuelson JC, Chen M, Park S-K, Phillips GJ, Dalbey R, Luirink J & de Gier JWL (2003) Versatility of inner membrane protein biogenesis in *Escherichia coli*. *Mol Microbiol* **47**, 1015–1027.

11 Wu ZC, De Keyzer J, Kedrov A & Driessen AJM (2012) Competitive binding of the SecA ATPase and ribosomes to the SecYEG translocon. *J Biol Chem* **287**, 7885–7895.

12 Shen HH, Lithgow T & Martin LL (2013) Reconstitution of membrane proteins into model membranes: seeking better ways to retain protein activities. *Int J Mol Sci* **14**, 1589–1607.

13 Cross TA, Sharma M, Yi M & Zhou HX (2011) Influence of solubilizing environments on membrane protein structures. *Trends Biochem Sci* **36**, 117–125.

14 Van Der Does C, Swaving J, Van Klompenburg W & Driessen AJM (2000) Non-bilayer lipids stimulate the activity of the reconstituted bacterial protein translocase. *J Biol Chem* **275**, 2472–2478.

15 Van Der Laan M, Houben ENG, Nouwen N, Luirink J & Driessen AJM (2001) Reconstitution of Sec-dependent membrane protein insertion: nascent FtsQ interacts with YidC in a Sec YEG-dependent manner. *EMBO Rep* **2**, 519–523.

16 Taufik I, Kedrov A, Exterkate M & Driessen AJM (2013) Monitoring the activity of single translocons. *J Mol Biol* **425**, 4145–4153.

17 Koch S, De Wit JG, Vos I, Birkner JP, Gordiichuk P, Herrmann A, Van Oijen AM & Driessen AJM (2016) Lipids activate SecA for high affinity binding to the SecYEG complex. *J Biol Chem* **291**, 22534–22543.

18 Kater L, Frieg B, Berninghausen O, Gohlke H, Beckmann R & Kedrov A (2019) Partially inserted nascent chain unzips the lateral gate of the Sec translocon. *EMBO Rep* **20**, e48191.

19 Koch S, Driessen AJM & Kedrov A (2018) Biophysical analysis of Sec-mediated protein translocation in nanodiscs. In Advances in Biomembranes and Lipid Self-Assembly (Iglič A, Rappolt M & García-Sáez AJ, eds.), Vol. 28, pp. 41–85. Elsevier Science, Amsterdam.

20 Haruyama T, Sugano Y, Kodera N, Uchihashi T, Ando T, Tanaka Y, Konno H & Tsukazaki T (2019) Single-unit imaging of membrane protein-embedded nanodiscs from two oriented sides by high-speed atomic force microscopy. *Structure* **27**, 152–160.e3.

21 Brian AA & McConnell HM (1984) Allogeneic stimulation of cytotoxic T cells by supported planar membranes. *Proc Natl Acad Sci USA* **81**, 6159–6163.

22 Cho NJ, Frank CW, Kasemo B & Höök F (2010) Quartz crystal microbalance with dissipation monitoring of supported lipid bilayers on various substrates. *Nat Protoc* **5**, 1096–1106.

23 Matysik A & Kraut RS (2014) Preparation of mica supported lipid bilayers for high resolution optical microscopy imaging. *J Vis Exp* **88**, e52054.

24 Nguyen PA, Field CM, Groen AC, Mitchison TJ & Loose M (2015) Using supported bilayers to study the spatiotemporal organization of membrane-bound proteins. *Methods Cell Biol* **128**, 223–241.

25 Gari RRS, Chattrakun K, Marsh BP, Mao C, Chada N, Randall LL & King GM (2019) Direct visualization of the *E. coli* Sec translocase engaging precursor proteins in lipid bilayers. *Sci Adv* **5**, eaav9404.

26 Karner A, Nimmervoll B, Plochberger B, Klotzsch E, Horner A, Knyazev DG, Kuttner R, Winkler K, Winter L, Siligan C *et al*, (2017) Tuning membrane protein mobility by confinement into nanodomains. *Nat Nanotechnol* **12**, 260–266.

27 García-Sáez AJ & Schwille P (2010) Surface analysis of membrane dynamics. *Biochim. Biophys Acta Biomembr* **1798**, 766–776.

28 Bianchi F, Syga L, Moiset G, Spakman D, Schavemaker PE, Punter CM, Seinen AB, Van Oijen AM, Robinson A & Poolman B (2018) Steric exclusion and protein conformation determine the localization of plasma membrane transporters. *Nat. Commun* **9**, 501.

29 Kiessling V & Tamm LK (2003) Measuring distances in supported bilayers by fluorescence interference-contrast microscopy: polymer supports and SNARE proteins. *Biophys J* **84**, 408–418.

30 Nováková E, Giewekemeyer K & Salditt T (2006) Structure of two-component lipid membranes on solid support: an X-ray reflectivity study. *Phys Rev E Stat Nonlin Soft Matter Phys* **74**, 051911.

31 Zhu M, Lerum MZ & Chen W (2012) How to prepare reproducible, homogeneous, and hydrolytically stable aminosilane-derived layers on silica. *Langmuir* **28**, 416–423.

32 Machán R & Hof M (2010) Lipid diffusion in planar membranes investigated by fluorescence correlation spectroscopy. *Biochim Biophys Acta Biomembr* **1798**, 1377–1391.

33 Kedrov A, Kusters I, Krasnikov VV & Driessen AJM (2011) A single copy of SecYEG is sufficient for preprotein translocation. *EMBO J* **30**, 4387–4397.

34 Dalal K, Chan CS, Sligar SG & Duong F (2012) Two copies of the SecY channel and acidic lipids are necessary to activate the SecA translocation ATPase. *Proc Natl Acad Sci USA* **109**, 4104–4109.

35 Gold VAM, Robson A, Bao H, Romantsov T, Duong F & Collinson I (2010) The action of cardiolipin on the bacterial translocon. *Proc Natl Acad Sci USA* **107**, 10044–10049.

36 Becker T, Bhushan S, Jarasch A, Armache JP, Funes S, Jossinet F, Gumbart JC, Mielke T, Berninghausen O, Schulten K *et al*, (2009) Structure of monomeric yeast and mammalian Sec61 complexes interacting with the translating ribosome. *Science* **326**, 1369–1373.

37 Park E & Rapoport TA (2012) Bacterial protein translocation requires only one copy of the SecY complex *in vivo*. *J Cell Biol* **198**, 881–893.

38 Gong F & Yanofsky C (2002) Instruction of translating ribosome by nascent peptide. *Science* **297**, 1864–1867.

39 Saffman PG & Delbrück M (1975) Brownian motion in biological membranes. *Proc Natl Acad Sci USA* **72**, 3111–3113.

40 Kuznetsova IM, Turoverov KK & Uversky VN (2014) What macromolecular crowding can do to a protein. *Int J Mol Sci* **15**, 23090–23140.

41 Ma C, Wu X, Sun D, Park E, Catipovic MA, Rapoport TA, Gao N & Li L (2019) Structure of the substrate-engaged SecA-SecY protein translocation machine. *Nat Commun* **10**, 2872.

42 Milon S, Hovius R, Vogel H & Wohland T (2003) Factors influencing fluorescence correlation spectroscopy measurements on membranes: Simulations and experiments. *Chem Phys* **288**, 171–186.

43 Matysik A & Kraut RS (2014) TrackArt: The user friendly interface for single molecule tracking data analysis and simulation applied to complex diffusion in mica supported lipid bilayers. *BMC Res Notes* **7**, 274.

44 Miller CE, Majewski J, Gog T & Kuhl TL (2005) Characterization of biological thin films at the solid-liquid interface by X-ray reflectivity. *Phys Rev Lett* **94**, 238104.

45 Sackmann E (1996) Supported membranes: scientific and practical applications. *Science* **271**, 43–48.

46 Hamai C, Yang T, Kataoka S, Cremer PS & Musser SM (2006) Effect of average phospholipid curvature on supported bilayer formation on glass by vesicle fusion. *Biophys J* **90**, 1241–1248.

47 Michalet X (2010) Mean square displacement analysis of single-particle trajectories with localization error: Brownian motion in an isotropic medium. *Phys Rev E Stat Nonlin Soft Matter Phys* **82**, 041914.

48 Ritchie K, Iino R, Fujiwara T, Murase K, Kusumi A, Ritchie K, Iino R, Fujiwara T & Murase K (2003) The fence and picket structure of the plasma membrane of live cells as revealed by single molecule techniques. *Mol Membr Biol* **20**, 13–18.

49 Sarangi NK, Ayappa KG & Basu JK (2017) Complex dynamics at the nanoscale in simple biomembranes. *Sci Rep* **7**, 11173.

50 Ott M, Shai Y & Haran G (2013) Single-particle tracking reveals switching of the HIV fusion peptide between two diffusive modes in membranes. *J Phys Chem B* **117**, 13308–13321.

51 Quemeneur F, Sigurdsson JK, Renner M, Atzberger PJ, Bassereau P & Lacoste D (2014) Shape matters in protein mobility within membranes. *Proc Natl Acad Sci USA* **111**, 5083–5087.

52 Kreutzberger AJB, Ji M, Aaron J, Mihaljević L & Urban S (2019) Rhomboid distorts lipids to break the viscosity-imposed speed limit of membrane diffusion. *Science* **363**, eaao0076.

53 Prabudiansyah I, Kusters I, Caforio A & Driessen AJM (2015) Characterization of the annular lipid shell of the Sec translocon. *Biochim Biophys Acta Biomembr* **1848**, 2050–2056.

54 Koch S, Exterkate M, López CA, Patro M, Marrink SJ & Driessen AJM (2019) Two distinct anionic phospholipid-dependent events involved in SecA-mediated protein translocation. *Biochim Biophys Acta Biomembr* **1861**, 183035.

55 Bischoff L, Wickles S, Berninghausen O, Van Der Sluis EO & Beckmann R (2014) Visualization of a polytopic membrane protein during SecY-mediated membrane insertion. *Nat Commun* **5**, 4103.

56 Nagamori S, Nishiyama K-I & Tokuda H (2002) Membrane topology inversion of SecG detected by labeling with a membrane-impermeable sulfhydryl reagent that causes a close association of SecG with SecA. *J Biochem* **132**, 629–634.

57 Frauenfeld J, Gumbart J, van der Sluis EO, Funes S, Gartmann M, Beatrix B, Mielke T, Berninghausen O, Becker T, Schulten K *et al*, (2011) Cryo-EM structure of the ribosome–SecYE complex in the membrane environment. *Nat Struct Mol Biol* **18**, 614–621.

58 Zimmer J, Nam Y & Rapoport TA (2008) Structure of a complex of the ATPase SecA and the protein-translocation channel. *Nature* **455**, 936–943.

59 Lill R, Dowhan W & Wickner W (1990) The ATPase activity of SecA is regulated by acidic phospholipids, SecY, and the leader and mature domains of precursor proteins. *Cell* **60**, 271–280.

60 Breukink E, Demel RA, de Korte-Kool G & de Kruijff B (1992) SecA insertion into phospholipids is stimulated by negatively charged lipids and inhibited by ATP: a monolayer study. *Biochemistry* **31**, 1119–1124.

61 Corey RA, Pyle E, Allen WJ, Watkins DW, Casiraghi M, Miroux B, Arechaga I, Politis A & Collinson I

133

(2018) Specific cardiolipin–SecY interactions are required for proton-motive force stimulation of protein secretion. *Proc Natl Acad Sci USA* **115**, 7967–7972.

62 Prabudiansyah I, Kusters I & Driessen AJM (2015) *In vitro* interaction of the housekeeping SecA1 with the accessory SecA2 protein of Mycobacterium tuberculosis. *PLoS One* **10**, 0128788.

63 De Keyzer J, Van der Does C & Driessen AJM (2002) Kinetic analysis of the translocation of fluorescent precursor proteins into *Escherichia coli* membrane vesicles. *J Biol Chem* **277**, 46059–46065.

64 Kedrov A, Wickles S, Crevenna AH, van der Sluis EO, Buschauer R, Berninghausen O, Lamb DC & Beckmann R (2016) Structural dynamics of the YidC: ribosome complex during membrane protein biogenesis. *Cell Rep* **17**, 2943–2954.

65 Seidelt B, Innis CA, Wilson DN, Gartmann M, Armache JP, Villa E, Trabuco LG, Becker T, Mielke T, Schulten K *et al*, (2009) Structural insight into nascent polypeptide chain-mediated translational stalling. *Science* **326**, 1412–1415.

66 Allerbo O, Lundström A & Dimitrievski K (2011) Simulations of lipid vesicle rupture induced by an adjacent supported lipid bilayer patch. *Colloids Surfaces B Biointerfaces* **82**, 632–636.

67 Cremer PS & Boxer SG (1999) Formation and spreading of lipid bilayers on planar glass supports. *J Phys Chem B* **103**, 2554–2559.

68 Fenz SF, Merkel R & Sengupta K (2009) Diffusion and Intermembrane distance: case study of avidin and e-cadherin mediated adhesion. *Langmuir* **25**, 1074–1085.

69 Hedde PN, Fuchs J, Oswald F, Wiedenmann J & Nienhaus GU (2009) Online image analysis software for photoactivation localization microscopy. *Nat Methods* **6**, 689–690.

70 Levenberg K (1944) A method for the solution of certain non – linear problems in least squares. *Q Appl Math* **2**, 164–168.

71 Marquardt DW (1963) An algorithm for least-squares estimation of nonlinear parameters. *J Soc Ind Appl Math* **11**, 431–441.

72 Pettersen EF, Goddard TD, Huang CC, Couch GS, Greenblatt DM, Meng EC & Ferrin TE (2004) UCSF Chimera - a visualization system for exploratory research and analysis. *J Comput Chem* **25**, 1605–1612.

Chapter 6

Reconstitution of the bacterial membrane protein insertion pathway using cell-free protein synthesis for structural studies

Authors:	Michael Kamel, Yulia Schaumkessel, Cristian Rosales Hernandez, Hanna Kratzat, Roland Beckmann, Alexej Kedrov.
Published:	In preparation.
Impact factor:	
Own work:	70%.
Contribution:	Michael Kamel wrote the manuscript.
	Michael Kamel performed all biochemical experiments.
	Yulia Schaumkessel established the in-house cell-free protein synthesis.
	Crisitian Rosales Hernandez, Hanna Kratzat performed cryo-EM and single particle analysis.
	Michael Kamel and Alexej Kedrov analyzed and interpreted the data.

Abstract

The insertion of α-helical membrane proteins into the bacterial membrane and their folding occur mostly in a co-translational manner through the SecYEG translocon and/or the insertase, YidC. Some substrates require either SecYEG or YidC or both of them for proper insertion and folding. The exact selection mechanism for the insertion pathway is not clear. Structures of either SecYEG or YidC in complex with ribosome nascent chain complexes (RNCs) during insertion were previously reported. However, many of the structures were resolved in a detergent micelle which does not reflect the native environment and they have low to mid resolution. Some structures were reported in a lipid bilayer where SecYEG and YidC were reconstituted in nanodiscs, nevertheless, the complexes were assembled with pre-formed stalled RNCs. Additionally, they reported rather a late stage of the insertion pathway in which the transmembrane helix has been already inserted. Therefore, the path of the nascent chain from the ribosomal exit tunnel to the membrane is not clearly identified.

Here, the aim was to establish a platform to elucidate the structure and dynamics of membrane protein insertion. To that aim, constructs have been established composed of nascent chains fused at its C-terminus to an arrest peptide (SecM) to allow for efficient stalling of the ribosomes during translation. Different nascent chains were chosen, FtsQ, a model substrate for SecYEG-mediated insertion, while for YidC-mediated insertion, F_oc and MscL were chosen. Different lengths of the substrates were designed to allow probing of different stages of the insertion pathway. The constructs were supplied to cell-free protein synthesis reactions in the presence of SecYEG or YidC either reconstituted in MSP-based nanodiscs or directly isolated from the membrane using maleic acid copolymers. This approach allowed for the co-translational assembly of the complexes in a near-native state. Affinity purification and sucrose gradient centrifugation allowed for the isolation of the complexes to be further used in structural studies using cryo-EM. The assembly of the complexes was confirmed using western blot, co-migration of the nanodiscs with the insertion machinery with ribosomes and cryo-EM. This work provides a foundation that could be further expanded to investigate the mechanism of membrane protein insertion by using substrates of different lengths to get snapshots of the insertion pathway using cryo-EM. Moreover, it can be further employed to investigate the structure of the SecYEG-YidC complex using a nascent chain that requires both of them for proper insertion and folding.

6.1 Introduction

Around 20 -30 % of protein-coding genes within all organisms code for membrane proteins [1]. Being highly hydrophobic, these proteins are normally targeted co-translationally as ribosome nascent complexes to the cytoplasmic membrane in bacteria or archaea and the endoplasmic reticulum in eukaryotes to be inserted into the membrane via the protein conducting channel, the Sec translocon. In bacteria, another insertase has shown to be important for membrane protein insertion, YidC, which can work dependently or independently of SecYEG [2, 3].

The Sec translocon is a heterotrimeric complex that is composed of SecY/E/G subunits in bacteria and Sec61α /γ/β in eukaryotes. SecY forms the channel and is composed of ten transmembrane helices (TMHs) that are organized into two halves composed of TMH 1 to 5 and 6 to 10 respectively, forming a pseudosymmetric clamshell-like structure (Figure 6.1 A). A side section of SecY shows that it resembles an hourglass with two funnels separated by a central constriction called the pore ring. The pore ring comprises hydrophobic and bulky amino acids and is sealed from the periplasmic side with the TMH 2a, called the plug domain. A lateral gate is located between TMH 2b and 7 in front of SecY, it facilitates the entrance of the signal peptides and TMHs of the substrates into the lipid bilayer. Long cytosolic loops between TMH 6/7 and TMH 8/9 provide the binding site for ribosomes during co-translational insertion [4]. SecE has 3 TMHs and an amphipathic helix and has been shown to stabilize the two halves of SecY [4, 5]. SecG has 2 TMHs and has been shown to be non-essential, but it increases the efficiency of protein translocation [6].

YidC is an essential protein in bacteria, that has homologs in mitochondria (Oxa1), chloroplasts (Alb3), and in the endoplasmic reticulum (Get1 and EMC3). In *E. coli*, YidC is composed of six TMHs, a large periplasmic domain called the P1 domain between TMHs 1 and 2, and a coiled-coil region in the cytoplasmic side between TMHs 2 and 3, called the C1 region (Figure 6.1 B). Between the P1 domain and TMH 2, an amphipathic helix called EH1 is located. TMHs 3 and 5 form a transmembrane gap that can clamp an incoming substrate forming a hydrophobic slide mechanism. TMHs 2 to 6 form a globular bundle with a hydrophilic groove in the inner leaflet of the membrane and is open towards the cytoplasmic side and closed on the periplasmic side of the membrane. This groove has been proposed to host the substrate hydrophilic domains destined to be translocated to the periplasm. Another important domain of YidC is the C-terminal region, which is called the C2 loop, it is rich in positively charged amino acids that have been shown to form a binding site for translating ribosomes [7–9]. YidC has short TMHs that promote membrane thinning, it serves to decrease the energy barrier for the insertion of nascent chains [9, 10]. As clearly observed, SecYEG and YidC have different structural features, and therefore they have different mechanisms for membrane protein insertion.
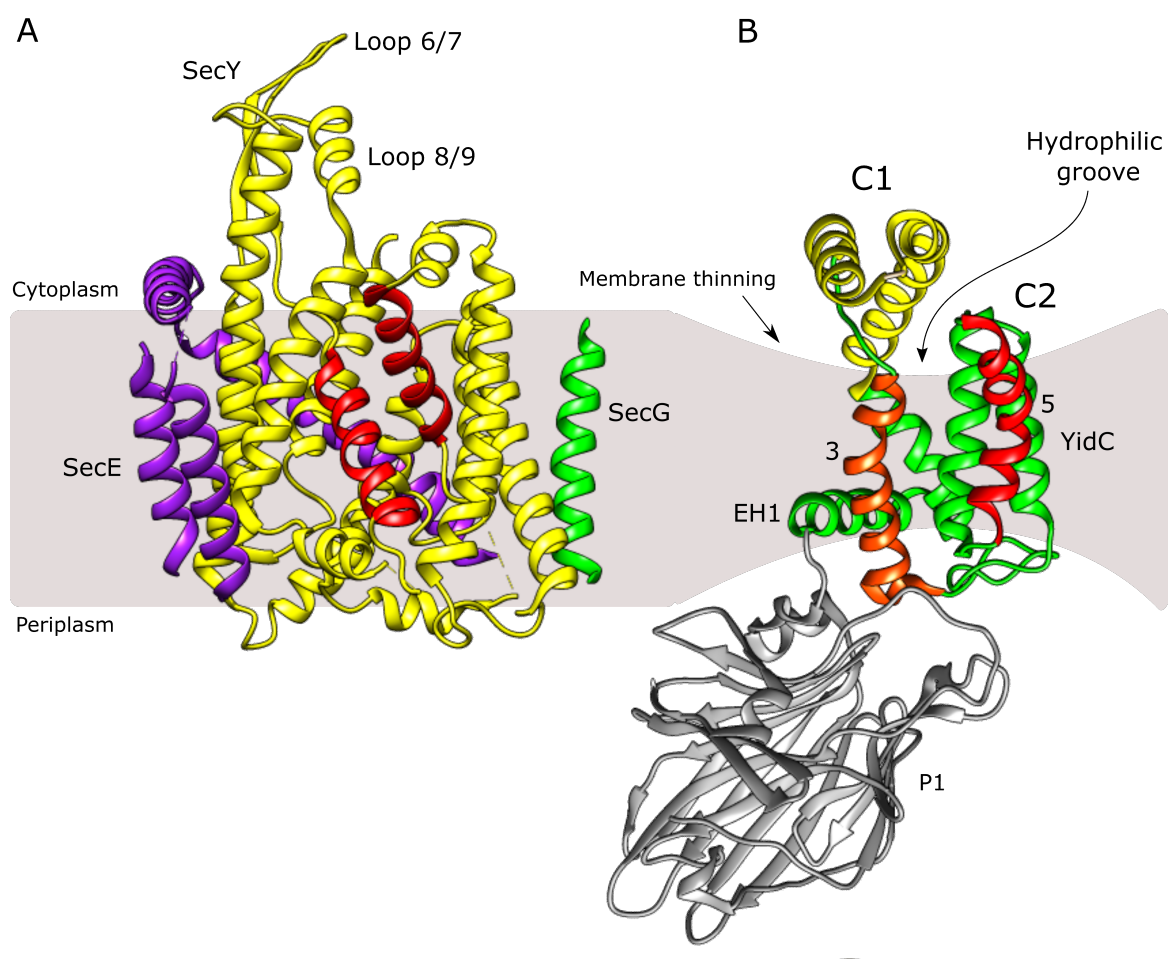
Figure 6.1: The structure of SecYEG and the insertase, YidC. A) Cryo-EM structure of SecYEG (PDB: 6R7L) showing SecY in yellow, SecE in purple and SecG in light green. Lateral gate is depicted in red. B) Crystal structure of the membrane protein insertase, YidC (PDB: 6AL2). TMH3 and 5 are depicted in orange and red respectively, they form a transmembrane gap that hosts an incoming nascent chain. YidC promotes membrane thinning that reduces energy barrier for nascent chain insertion.

Despite the numerous structures of ribosome nascent complexes (RNCs) bound to the membrane insertion machinery, the exact mechanism of membrane protein insertion remains unclear. First, many of the available structures report on a later stage of membrane protein insertion, where the TMH has already been inserted into the membrane. Second, most of the structures have been resolved in detergent micelles, which does not reflect the native environment of the nascent membrane protein and the translocon itself [11–18]. Few structures were obtained in a lipid bilayer where the insertion machinery was reconstituted in nanodiscs. Nevertheless, they either have a low resolution or constitute a complex that was formed artificially in a tube where the RNCs and the insertion machinery were independently purified [19–21]. A cryo-ET structure of the eukaryotic Sec61 in complex with ribosomes was reported in native membranes, but it revealed a non-inserting state of the translocon giving no information about protein insertion [22]. Moreover, different nascent chains require different insertion pathways: Some nascent chains require either SecYEG [23–25] or YidC alone [26–29], while other nascent chains require both SecYEG and YidC, either for proper membrane insertion or for correct folding [24, 30–34].

However, the exact selection mechanism for the insertion pathway still remains unclear.

To overcome the existing limitations, a cell-free protein synthesis (CFPS) platform was established that allows for the co-translational assembly of RNCs with either SecYEG or YidC that was reconstituted beforehand in MSP-based nanodiscs or maleic acid copolymer-based-lipid particles. The established platform can then be employed to provide more information about the different stages of the insertion pathways using cryo-EM when substrates with different lengths are used.

6.2 Material and methods

6.2.1 SecYEG expression and purification

SecYEG was overexpressed in *E.coli* C41(DE3) with an N-terminal deca-histidine tag, expression was induced with 0.5 mM IPTG and then performed for 3 h at 37 °C. Cells were then harvested by centrifugation for 15 minutes at 5000 g (FiberLite F8-6x1000y rotor, Piramoon Technologies Inc.), and resuspended in 20 mM Hepes/ KOH, pH 7.5, 50 mM KOAc, 5 mM $Mg(OAc)_2$, 5 % glycerol, 1 mM DTT and cOmplete protease inhibitor cocktail (Roche, Mannheim, Germany). Cells were lysed (Microfluidizer, M-110P, Microfluidics Corp., Westwood, MA, USA). Debris was then removed by centrifugation for 10 min at 10000 g (Sorvall SS34 rotor, Thermo Scientific). Membranes were isolated by ultracentrifugation for 1 h at 40000 rpm (45 Ti rotor, Beckman Coulter, Brea, CA, USA). Membranes were then solubilized for 1 h at 4 °C in solubilization buffer (50 mM Hepes/KOH, pH 7.4, 500 mM KCl, 5 % glycerol, 200 μM TCEP, 1% DDM (n-dodecyl β-maltoside; Glycon Biochemicals GmbH, Luckenwalde, Germany)). The solubilized membranes were centrifuged at full speed for 10 minutes at a tabletop centrifuge (Hermle Z 216 MK, Hermle Labortechnik GmbH) and the supernatant was then incubated with Ni^{2+} NTA agarose beads (Qiagen, Hilden, Germany) for 1 h at 4 °C. In case labeling was required for single cysteine SecYEG mutant $SecY^{L148C}EG$, the beads were incubated for 2 h at 4 °C with 100 - 200 μM ATTO 643 maleimide (ATTO-Tec GmbH), CF488A maleimide (Sigma Aldrich) or Fluorescein 5 maleimide (Cayman Chemical Company). The beads were washed with 50 mM Hepes/KOH, pH 7.4, 500 mM KCl, 5 % glycerol, 200 μM TCEP, 0.05% DDM, 10 mM imidazole, then the target protein was eluted with 50 mM Hepes/KOH, pH 7.4, 150 mM KCl, 5 % glycerol, 200 μM TCEP, 0.05% DDM, 300 mM imidazole. The protein was then buffer exchanged using PD 10 column (Cytiva Life Sciences) in 50 mM Hepes/KOH, pH 7.4, 150 mM KCl, 5 % glycerol, 200 μM TCEP, 0.05% DDM. Protein concentration was determined using an extinction coefficient of 72000 $M^{-1}cm^{-1}$ using UV-vis spectrophotometry (Neodot, NeoBiotech, Nanterre, France).

6.2.2 YidC expression and purification

YidC was overexpressed in *E.coli* C41(DE3) with an internal deca-histidine tag within P1 domain, expression was induced with 0.5 mM IPTG and then performed for 3 h at 37 °C. Cells were then harvested by centrifugation for 15 minutes at 5000 g (FiberLite F8-6x1000y rotor, Piramoon Technologies Inc.), and resuspended in 20 mM Hepes/ KOH. pH 7.5, 50 mM KOAc, 5 mM $Mg(OAc)_2$, 5 % glycerol, 1 mM DTT and cOmplete protease inhibitor cocktail (Roche,

Mannheim, Germany). Cells were lysed (Microfluidizer, M-110P, Microfluidics Corp., Westwood, MA, USA), Debris was then removed by centrifugation for 10 min at 10000 g (Sorvall SS34 rotor, Thermo Scientific). Membranes were isolated by ultracentrifugation for 1 h at 40000 rpm (45 Ti rotor, Beckman Coulter, Brea, CA, USA). Membranes were then solubilized for 1 h at 4 °C in solubilization buffer (50 mM Hepes/KOH, pH 7.4, 500 mM KCl, 5 % glycerol, 200 μM TCEP, 1% Cymal6 (Anatrace, Maumee, Ohio, United States)). The solubilized membranes were centrifuged at full speed for 10 minutes at tabletop centrifuge (Hermle Z 216 MK, Hermle Labortechnik GmbH) and the supernatant was then incubated with Ni^{2+} NTA agarose beads (Qiagen, Hilden, Germany) for 1 h at 4 °C. In case labeling was required for single cysteine YidC^{D269C} mutant, the beads were incubated for 2 h at 4°C with 100 - 200 μM Fluorescein-5-Maleimide (Cayman Chemical Company). The beads were washed with 50 mM Hepes/KOH, pH 7.4, 500 mM KCl, 5 % glycerol, 200 μM TCEP, 0.1% Cymal-6, 10 mM imidazole, the protein was eluted with 50 mM Hepes/KOH, pH 7.4, 150 mM KCl, 5 % glycerol, 200 μM TCEP, 0.1%Cymal-6, 300 mM imidazole. The protein was then buffer exchanged using PD 10 column (Cytiva Life Sciences) in 50 mM Hepes/KOH, pH 7.4, 150 mM KCl, 5 % glycerol, 200 μM TCEP, 0.1% Cymal-6. Protein concentration was determined using an extinction coefficient of 62000 $M^{-1}cm^{-1}$ using UV-vis spectrophotometry.

6.2.3 SecYEG-YidC fusion expression and purification

A construct was used that is composed of an N-terminal deca-histidine-tagged SecY, SecG, and a fusion of residues 1-535 of YidC with the first cytoplasmic loop of SecE followed by its third transmembrane domain (Figure 6.2 C inset). The fusion protein was produced in *E.coli* ER2566 strain, expression was induced by 0.5 mM IPTG and then performed for 3 h at 37 °C. Cells were then harvested by centrifugation for 15 minutes at 5000 g (FiberLite F8-6x1000y rotor, Piramoon Technologies Inc.), and resuspended in 20 mM Hepes/ KOH. pH 7.5, 50 mM KOAc, 5 mM Mg(OAc)$_2$, 5 % glycerol, 1 mM DTT and cOmplete protease inhibitor cocktail (Roche, Mannheim, Germany). Cells were lysed (Microfluidizer, M-110P, Microfluidics Corp., Westwood, MA, USA), debris was then removed by centrifugation for 10 min at 10000 g (Sorvall SS34 rotor, Thermo Scientific). Membranes were isolated by ultracentrifugation for 1 h at 40000 rpm (45 Ti rotor, Beckman Coulter, Brea, CA, USA). Membranes were then solubilized for 1 h at 4 °C in solubilization buffer (50 mM Hepes/KOH, pH 7.4, 500 mM KCl, 5 % glycerol, 200 μM TCEP, 1% DDM (Glycon Biochemicals GmbH, Luckenwalde, Germany)). The solubilized membranes were centrifuged at full speed for 10 minutes at tabletop centrifuge (Hermle Z 216 MK, Hermle Labortechnik GmbH) and the supernatant was then incubated with Ni^{2+} NTA agarose beads (Qiagen, Hilden, Germany) for 1 h at 4 °C. The beads were washed with 50 mM Hepes/KOH, pH 7.4, 500 mM KCl, 5 % glycerol, 200 μM TCEP, 0.1% DDM, 10 mM imidazole, the protein was eluted with 50 mM Hepes/KOH, pH 7.4, 150 mM KCl, 5 % glycerol, 200 μM TCEP, 0.1% DDM, 300 mM imidazole. The elution fractions were then pooled together, concentrated, and loaded on Superdex 200 Increase 10/300 GL (Cytiva Life Sciences) for size exclusion in 50 mM Hepes/KOH, pH 7.4, 150 mM KCl, 5% glycerol, 200 μM TCEP, 0.05 % DDM. Peak fractions were collected and protein concentration was then determined using an extinction coefficient of 134000 $M^{-1}cm^{-1}$ using UV-vis spectrophotometry (Neodot NeoBiotech, Nanterre, France).

6.2.4 Preparation of liposomes

Two different liposomes were prepared composed of either 70% 1,2-dioleoyl-sn-glycero-3- phosphocholine (DOPC) and 30% 1,2-dioleoyl-sn-glycero-3-phospho-(1-rac-glycerol) (DOPG) or 70% 1-palmitoyl-2-oleoyl-glycero-3-phosphocholine (POPC) and 30% 1-palmitoyl-2-oleoyl-sn-glycero-3-phospho-(1-rac-glycerol) (POPG). All lipids were purchased from Avanti Polar Lipids, Inc as chloroform stocks. Lipids were mixed from chloroform stocks to achieve the desired ratio. Subsequently, the chloroform was evaporated under vacuum conditions at 40 °C using a rotary evaporator (IKA, IKA-Werke GmbH & Co. KG). The lipid film was then resuspended in liposomes buffer (50 mM KCl, 50 mM Hepes/ KOH, pH 7,4) to achieve a 5 mM final concentration. Liposomes were extruded to 200 nm using polycarbonate membranes (Nuclepore, Whatman) using the Mini-Extruder set (Avanti Polar Lipids, Inc.).

6.2.5 Reconstitution of bacterial membrane protein insertion machinery in membrane scaffold protein-based nanodiscs

Detergent-purified SecYEG was reconstituted in MSP2N2 nanodiscs with DOPC: DOPG (70:30) lipids. First, liposomes were solubilized using 0.5% Triton X-100 at 40 °C, then the solubilized lipids were mixed with detergent-purified SecYEG and MSP2N2 to achieve a final protein: MSP: lipid molar ratio of 1:10:1000. The mixture was incubated on ice for 30 minutes then loaded on 100 mg of Bio-Beads SM-2 sorbent (Bio-Rad Laboratories, Feldkirchen, Germany) and incubated overnight at 4°C. The Bio-Beads were then discarded and the sample was transferred to a new tube and centrifuged at 30000 g for 30 minutes (TLA55 rotor, Beckman Coulter GmbH, Brea, CA, USA) in Optima Max-XP Ultracentrifuge (Beckman Coulter GmbH, Brea, CA, USA). The supernatant was subsequently loaded on Superose 6 Increase 10/300 GL (Cytiva) for size exclusion in nanodisc buffer (150 mM KCl, 50 mM Hepes/KOH, pH 7.4, 5% glycerol) to separate the loaded discs from empty nanodiscs. The peak fractions were collected and concentrated using an Amicon ®Ultra-4, Ultracel 30 K centrifugal filters (Merck Millipore Ltd. Tullagreen, Carrigtwohill, Co Cork, Ireland).

Detergent-purified YidC was reconstituted in MSP1D1 nanodiscs in POPC: POPG (70:30) lipids. Similarly, liposomes were solubilized using 0.5% Triton X-100, then the solubilized lipids were mixed with detergent-purified YidC and MSP1D1 to achieve a final protein: MSP: lipid molar ratio of 1:10:200. The reconstitution was then continued similarily to SecYEG. For SecYEG-YidC fusion, MSP2N2 and DOPC: DOPG (70:30) liposomes were used. The fusion protein was mixed with MSP2N2 and Triton X-100 solubilized liposomes to achieve the molar ratio of 1:10:1000 respectively. The reconstitution was performed similarly to the SecYEG reconstitution.

6.2.6 Isolation of bacterial membrane protein insertion machinery in maleic acid copolymers lipid particles

Membranes with overexpressed SecYEG, YidC, or SecYEG-YidC fusion were solubilized with 2.5 % styrene-maleic acid (SMA) or diisobytulene-maleic acid (DIBMA) in solubilization buffer (500 mM KCl, 50 mM Tris/HCl, pH 8.2, 5 % glycerol). For SMA, the solubilization mixtures were incubated in a roller shaker (RS TR05, Phoenix Instrument) for 2 h at room temperature, while

for DIBMA, they were incubated at 37°C for 3 h (Infors HT Ecotron Shaker Incubator, Infors HT). Subsequently, the solubilization mixture was ultracentrifuged at 100000 g for 30 minutes (TLA120.1 rotor) in Optima Max-XP Ultracentrifuge (Beckman Coulter GmbH, Brea, CA, USA). The supernatants were loaded on 250 μl Ni^{2+} NTA agarose beads (Qiagen, Hilden, Germany) and incubated overnight at 4°C. The beads were then washed with at least 20-column volumes of 500 mM KCl, 50 mM Hepes/KOH, pH 7.4, 5 % glycerol, 10 mM imidazole, then eluted with 150 mM KCl, 50 mM Hepes/KOH, pH 7.4, 5 % glycerol, 300 mM imidazole. Samples were then analyzed using SDS-PAGE and fractions showing the protein bands were collected and diluted, then concentrated using an Amicon ®Ultra-4, Ultracel 30 K centrifugal filters (Merck Millipore Ltd. Tullagreen, Carrigtwohill, Co Cork, Ireland). The concentrated samples were diluted at least 10 times and reconcentrated, this process was repeated at least 3 times to decrease the imidazole concentration in the samples to below 1 mM. The size of SecYEG-DIBMA lipid particles was measured using dynamic light scattering (Malvern Zetasizer Nano ZS, Malvern Panalytical Ltd, Enigma Business Park, Grovewood Road, United Kingdom).

6.2.7 Reconstitution of SecYEG in liposomes

To reconstitute SecYEG in DOPC: DOPG (70:30) liposomes, liposomes were solubilized using 0.5 % Triton X-100 for 10 minutes at 40 °C. Afterward, SecYEG was mixed with solubilized liposomes in a 1:1000 protein-to-lipid molar ratio. The mixture was incubated for 30 minutes on ice. The detergent was removed by incubation with 100 mg Bio-Beads SM-2 sorbent (Bio-Rad Laboratories, Feldkirchen, Germany) overnight at 4 °C. The Bio-Beads were then discarded and the mixture was transferred to a new tube, then ultracentrifuged for 30 minutes at 80000 rpm (S12-AT3 rotor, Thermo Fisher/Sorvall). Proteoliposomes were then resuspended in liposomes buffer (50 mM Hepes/KOH, pH 7.4 and 50 mM KCl).

6.2.8 Differential scanning fluorimetry

Detergent-solubilized SecYEG, SecYEG proteoliposomes, and SecYEG DIBMA lipid particles were loaded on Prometheus NT.48 capillaries (NanoTemper Technologies GmbH, Flößergasse 4, Munich, Germany). Their stability was measured within a temperature range of 20 to 80 °C and a ramp rate of 2°C per minute using Prometheus Panta nano DSF (NanoTemper Technologies GmbH).

6.2.9 Preparation of S30 lysate

E.coli BL21(DE3) or KC6 or KC6 δompT cells were transformed with TargoTron^{TM} pAR1219 plasmid (Sigma Aldrich) encoding for T7 RNA polymerase. 2 litres of 2x YPTG media was inoculated with 100 ml overnight cultures, and cells were grown to OD$_{600}$= 0.5 and induced with 1 mM IPTG, then left to grow to OD$_{600}$= 1. Cells were harvested at 7500 rpm for 15 min (FiberLite F8-6x1000y rotor, Piramoon Technologies Inc.). The cell pellet was washed three times with lysis buffer (10 mM Tris-acetate pH 8, 14 mM Mg(OAc)$_2$, 60 mM KOAc, 1 mM PMSF). The pellet was resuspended in lysis buffer (1 ml per gram pellet). Subsequently, cells were lysed by sonication (10 times, 15 s on, 30 s off, 50 % power, 5 pulsed cycles) (Sonopuls, Bandelin).

The lysate was centrifuged at 12000 g for 15 min (S120 AT6 rotor, Thermo Fisher/Sorvall). The supernatant was ultracentrifuged at 30000 g for 30 minutes (S120 AT6 rotor, Thermo Fisher/Sorvall). The supernatant was then aliquoted and stored at -80 °C. For more details on the optimization of the S30 lysate preparation (See Master thesis from Yulia Schaumkessel, *In vitro* biogenesis of membrane proteins, 2020)

6.2.10 Cell free protein synthesis reaction

The cell-free protein synthesis reaction (CFPS) was performed based on the previously established protocol (Master thesis from Yulia Schaumkessel, *In vitro* biogenesis of membrane proteins, 2020). The reaction is composed of 40% S30 lysate, 1X master mix (10 mM ammonium acetate, 130 mM potassium acetate, 33 mM sodium pyruvate, 1.5 mM spermidine, 1 mM putrescine, 4 mM sodium oxalate, 1.2 mM ATP, 0.85 mM of GTP, CTP and UTP, 34 μg/ml folinic acid, 170.6 μg/ml, *E.coli* tRNA MRE 600 (Roche Diagnostics GmbH, Mannheim, Germany), 0.33 mM NAD$^+$, 0.26 mM coenzyme A and 2 mM of each amino acid), at least 10 ng/μl plasmid DNA and 0-12 mM magnesium acetate. The optimum magnesium acetate concentration was screened for each new batch of lysate using either SecA N20-YFP or YFP-SecM constructs. The master mix was prepared as 2.6 X and then diluted to reach 1X in the reaction. Reactions were performed at 37 °C for 1 h unless mentioned otherwise. At least 100 nM of SecYEG or YidC reconstituted in MSP nanodiscs or in maleic acid copolymers lipid particles were added to the CFPS reaction in case of co-translational assembly of ribosome nascent chain (RNCs) with the bacterial membrane protein insertion machinery reactions.

6.2.11 Isolation of ribosomes from CFPS reactions

Ribosomes were isolated from CFPS reactions using different techniques. First, using multi-modal chromatography, after performing the CFPS reactions, the reactions were loaded on HiTrap Capto Core 700 in RNCs buffer (150 mM potassium acetate, 25 mM magnesium acetate, 50 mM Hepes/KOH, pH 7.4, 5% glycerol). The flow-through was collected as it contains the ribosomal fractions, then the column was washed with 1M NaOH in 30 % isopropanol solution to elute all bound material and regenerate the column. Subsequently, the flow-through fractions were analyzed using SDS-PAGE.

Second, ribosomes were also isolated using a sucrose cushion. Here, CFPS reactions (100 μl) were loaded on 300 μl of 1.1 M sucrose in RNCs buffer (150 mM potassium acetate, 25 mM magnesium acetate, 50 mM Hepes/KOH, pH 7.4). The samples were then centrifuged for 1 h at 110000 g (TLA55 rotor, Beckman Coulter GmbH, Brea, CA, USA) in Optima Max-XP Ultracentrifuge (Beckman Coulter GmbH, Brea, CA, USA). The supernatants were discarded and the pellets were resuspended in RNCs buffer in a similar volume to the reaction volume used and then analyzed using SDS-PAGE.

When high purity of ribosomes was required in the case of cryo-EM analysis, the ribosomes were isolated using a sucrose gradient. Briefly, the reactions were loaded on the top of a 10% to 40% linear sucrose gradient that was formed using the Gradient Station (BioComp Instruments, Fredericton, New Brunswick, Canada). The samples were centrifuged for 16 h at 16500 rpm (SW40 Ti rotor, Beckman Coulter GmbH, Brea, CA, USA). The gradients were fractionated

using the Gradient Fractionator of the Gradient Station (BioComp Instruments, Fredericton, New Brunswick, Canada). The peaks with the ribosomal fractions were collected together, buffer exchanged to remove the sucrose using PD Miditrap G25 columns (Cytiva Life Sciences), and then concentrated using an Amicon ®Ultra-4, Ultracel 30 K centrifugal filters (Merck Millipore Ltd. Tullagreen, Carrigtwohill, Co Cork, Ireland).

6.2.12   Cryo-EM

Cryo-EM experiments and single particle analysis were performed by Cristian Rosales Hernandez and Hanna Kratzat. Vitrification was carried out using a Vitrobot mark IV (FEI). For each grid, 3.5 μl of the sample was applied onto a glow-discharged Quantifoil holey carbon grid coated with 2 nm carbon. A dataset of 5000 micrographs with a total of approximately 1000000 particles was collected using Titan Krios 300 keV cryo-electron microscope with Falcon II direct electron detector.

6.3 Results

6.3.1 Reconstitution of the bacterial insertion machinery in nanodiscs

In order to study membrane protein biogenesis, different constructs containing the bacterial insertion machinery were employed. First, a construct coding for the heterotrimeric membrane channel, SecYEG with a 10X histidine tag at the N-terminus of SecY to allow for purification. Second, a construct coding for the bacterial membrane protein insertase, YidC with an internal 6X histidine tag in the P domain. Finally, a construct coding for SecY with an N-terminus 10X histidine tag, a fusion protein of YidC with SecE separated by a 3C protease cleavage sequence, and SecG was used. This construct allowed stabilizing the otherwise transient complex during the purification and reconstitution in nanodiscs steps. Eventually, the YidC-SecE could be separated using the 3C protease to allow for the natural arrangement of the complex in the lipid bilayer. All the proteins were expressed and purified using immobilized metal affinity and size exclusion chromatography to homogeneity.

The proteins were then reconstituted in membrane scaffold protein (MSP) nanodiscs. YidC was reconstituted in MSP1D1 nanodiscs with POPC: POPG (70:30) in a protein: MSP: lipids molar ratio of 1:10:200. This lipid composition was chosen to mimic the physiological fluid phase and anionic content of the membrane. SecYEG and SecYEG-YidC fusion proteins were reconstituted in MSP2N2 nanodiscs with DOPC: DOPG (70:30) with a protein: MSP: lipids molar ratio of 1:10:1000. Here, MSP2N2 was chosen since it can form a nanodisc which is sufficiently large (14.5 to 17 nm) [35] to accommodate the SecYEG- YidC complex and a dimer of SecYEG in case this is the preferred functional state of SecYEG. DOPC: DOPG lipids were chosen based on the recent report that showed that the SecYEG translocon is more efficient in protein translocation in DOPC: DOPG vesicles [36]. Figure 6.2 shows the size exclusion chromatograms, the coomassie stained SDS-PAGE, and the in-gel fluorescence of the formed nanodiscs. In the size exclusion chromatograms, the first peak contains the loaded nanodiscs and the second peak contains empty nanodiscs.
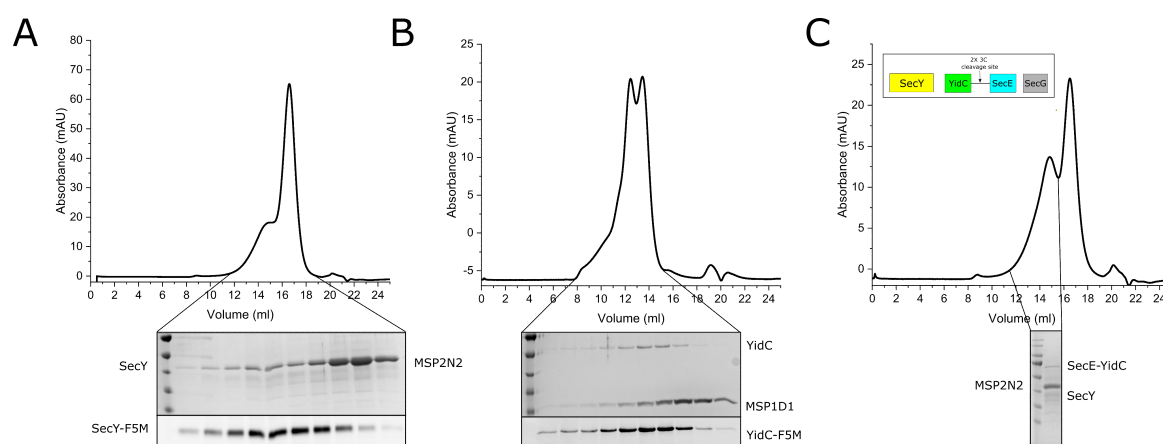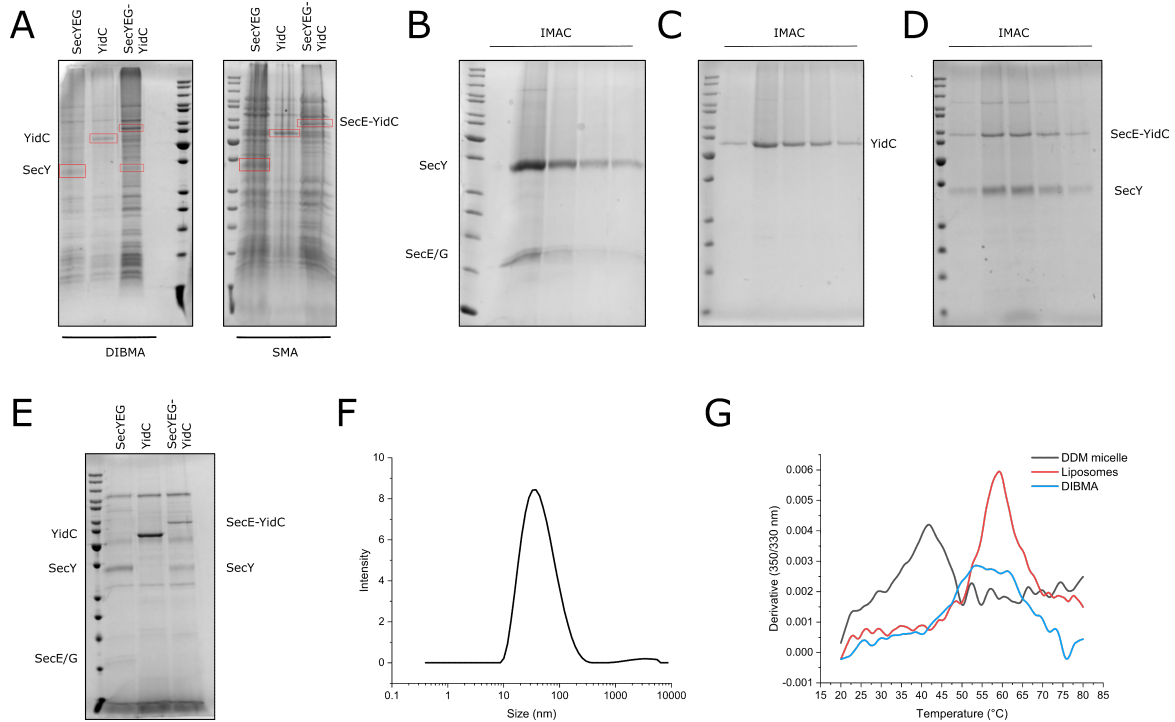
Figure 6.2: Reconstitution of bacterial membrane protein insertion machinery in MSP nanodiscs. Top: size exclusion chromatograms of SecYEG reconstituted in MSP2N2 nanodiscs (A), YidC reconstituted in MSP1D1 nanodisc (B), and SecYEG-YidC fusion protein reconstituted in MSP2N2 nanodiscs (C). The first peak shows loaded nanodiscs and the second peak represents empty nanodiscs. Bottom: coomassie staining and in-gel fluorescence confirm the co-migration of fluorescently labeled SecYEG with MSP2N2 (A), fluorescently-labeled YidC with MSP1D1 and SecY, YidC-SecE fusion protein with MSP2N2 nanodiscs indicating successful reconstitution in nanodiscs.

6.3.2 Isolation of the bacterial insertion machinery in maleic acid lipid particles

Complementry to MSP, maleic acid copolymers were also used to form lipid nanoparticles containing the insertion machinery. The advantage of using maleic acid copolymer is that it allows for the direct detergent-free reconstitution of the insertion machinery in nanodiscs from the native membranes and keeping the native lipids. This serves to preserve the native architecture and native environment of the proteins. Two different maleic acid copolymers were employed, styrene-maleic acid copolymer (SMA) and di-isobutylene maleic acid copolymer (DIBMA). Styrene maleic acid copolymers disintegrate lipid membranes and form lipid nanoparticles called (SMALPs) and has been shown to efficiently isolate different membrane proteins directly from the membrane within discs of around 10 nm [37]. However, it is quite difficult to estimate the protein concentration within SMALPs as the SMA polymer absorbs light at 280 nm, and it is also sensitive to divalent cations like (Ca^{2+} and Mg^{2+}), which it can chelate and become insoluble. This can impose problems when working with ribosome nascent chain complexes (RNCs) which need Mg^{2+} for the stability of the 70S ribosomes [38–40]. Therefore, DIBMA was also employed which has been shown to tolerate higher concentrations of divalent cations and it does not interfere with the UV absorption of proteins [41].

Therefore, isolated *E.coli* membranes with the overexpressed insertion machinery were incubated with either SMA or DIBMA, and after solubilization, the insoluble debris was pelleted, and the solubilized material was evaluated on SDS-PAGE (Figure 6.3 A). Bands matching the size of SecYEG, YidC, and SecYEG-YidC fusion could clearly be observed on the coomassie-stained gels indicating the successful isolation of the insertion machinery in maleic acid lipid particles when using either SMA or DIBMA copolymer. Consequently, the solubilized membranes were loaded on Ni-NTA agarose beads to purify the histidine-tagged proteins in SMALPS or DIBMALPs. All

the proteins were successfully purified in SMALPs and DIBMAPs as confirmed by SDS-PAGE (Figure 6.3 B-E).

Figure 6.3: Isolation of bacterial membrane protein insertion machinery in maleic acid copolymers lipid particles A) DIBMA and SMA solubilized membranes with overexpressed bacterial membrane protein insertion machinery. B, C, D) Elution fractions after immobilized metal affinity chromatography of SecYEG, YidC, SecYEG-YidC DIBMALPs respectively. E) Elution fraction after IMAC of SecYEG, YidC and SecYEG-YidC fusion SMALPS. F) Dynamic light scattering of SecYEG-DIBMA lipid particle showing an average size of 36 nm. G) Nano differential scanning fluorimetry shows higher stability of SecYEG in DIBMA lipid particles compared to SecYEG in DDM micelles and similar to SecYEG reconstituted in DOPC: DOPG liposomes.

Dynamic light scattering (DLS) analysis of the purified DIBMA lipid particles shows an average size of around 35 nm (Figure 6.3 F) in good agreement with the previously reported size of DIBMA lipid particles [42]. The stability of SecYEG in DIBMA lipid particles was also measured using differential scanning fluorimetry (nanoDSF). In nanoDSF, the intrinsic tryptophan fluorescence is measured as the protein is heated up. Once the protein loses its native fold, this leads to the exposure of tryptophans to the hydrophilic aqueous solution causing a red shift of its fluorescence. Consequently, the ratio between the tryptophan emission at 350 to 330 will increase with increasing temperature, which can be used to report on the transition temperature of protein unfolding. Here, a clear stabilization of SecYEG occurs when embedded in DIBMA lipid particles as compared to detergent-solubilized SecYEG and similar to that caused by SecYEG reconstitution in liposomes (Figure 6.3 G).

6.3.3 Co-translational assembly of RNCs -SecYEG complex

To prepare the CFPS platform, different components need to be present for an efficient reaction. Firstly, S30 lysate needs to be prepared which comprises an *E.coli* lysate centrifuged at 30000 g.

The lysate contains all the necessary components for successful protein synthesis. For instance, ribosomes, tRNA, an RNA polymerase for mRNA transcription, and the different proteins required for transcription and translation. Other essential components include amino acids, nucleotides (ATP, GTP, CTP, and UTP), an energy regeneration system to regenerate ATP in the reaction, and a plasmid containing the gene of interest. Here, the S30 lysate was prepared from *E.coli* BL21(DE3) cells containing the overexpressed T7 RNA polymerase. Therefore, the target gene was cloned into pRSET carrying the T7 promotor. Sodium pyruvate and sodium oxalate were included as an energy regeneration system. Sodium pyruvate activates the oxidative phosphorylation pathway which allows the regeneration of ATP in the reaction. While sodium oxalate inhibits the conversion of sodium pyruvate to phosphoenolpyruvate using the phosphoenolpyruvate synthetase [43]. The prepared lysate was tested for activity by supplying the reaction with a plasmid containing the gene for the fluorescent protein, YFP. Here, Mg acetate was titrated from 0 to 12 mM in the reaction, as it has been previously reported that Mg concentration needs to be optimized for every newly prepared lysate [44]. Mg is essential for the stabilization of the 70S ribosomes and for NTPs [44–46]. Here, YFP was successfully synthesized with an optimum synthesis at 4-6 mM Mg acetate (Figure 6.4 A top).

In order to resolve the different steps of the co-translational insertion pathway, we aimed to stall the ribosomes at defined stages of the translation and insertion of the membrane proteins of interest. To that end, a stalling sequence was employed to successfully stall the ribosomes during the translation and allow for the assembly of a ribosome nascent chain complex with the insertion machinery either in MSP or maleic acid copolymer nanodiscs. Here, a stalling sequence based on SecM was used. SecM is a 170 amino acid protein that acts to regulate the translation of the downstream gene *secA*. The SecM sequence has the ability to stall the translation due to its interaction with the entrance of the ribosomal tunnel through the amino acid arginine in its sequence. Furthermore, the presence of the amino acid proline at the end of the sequence has been shown to alter the geometry of the peptidyl transfer center slowing down the translation rate [47–50]. When SecA is present in sufficient amounts in the cell, it pulls the SecM sequence from the ribosomal exit tunnel and it translocates it to the periplasmic side of the membrane through the SecYEG channel, where it will get degraded. However, when all the SecYEG channels are jammed, or no sufficient SecA is present, the SecM sequence will stall the ribosomes, which allows for the resolving of the mRNA secondary structure elements downstream of the SecM sequence. This causes the exposure of the ribosome binding site upstream of secA and the initiation of the translation of the SecA protein [51–53]. Here, a modified SecM sequence (FSTPVWIWWWPRIRGPP) was used that allows for efficient stalling of the ribosomes as previously reported [54, 55]. First, in order to confirm the stalling efficiency of the sequence, it was fused to YFP which allows for easy detection using in-gel fluorescence. In case of successful stalling, the YFP band will migrate slower on the gel compared to the normal YFP protein as it should still be covalently bound with the proline tRNA, present in the P site of the ribosome. Indeed, two bands could be observed on the gel, a fast migrating band that indicates the release of YFP from the ribosome and a slower migrating band that has a higher intensity than the fast migrating band indicating successful stalling (Figure 6.4 A bottom).
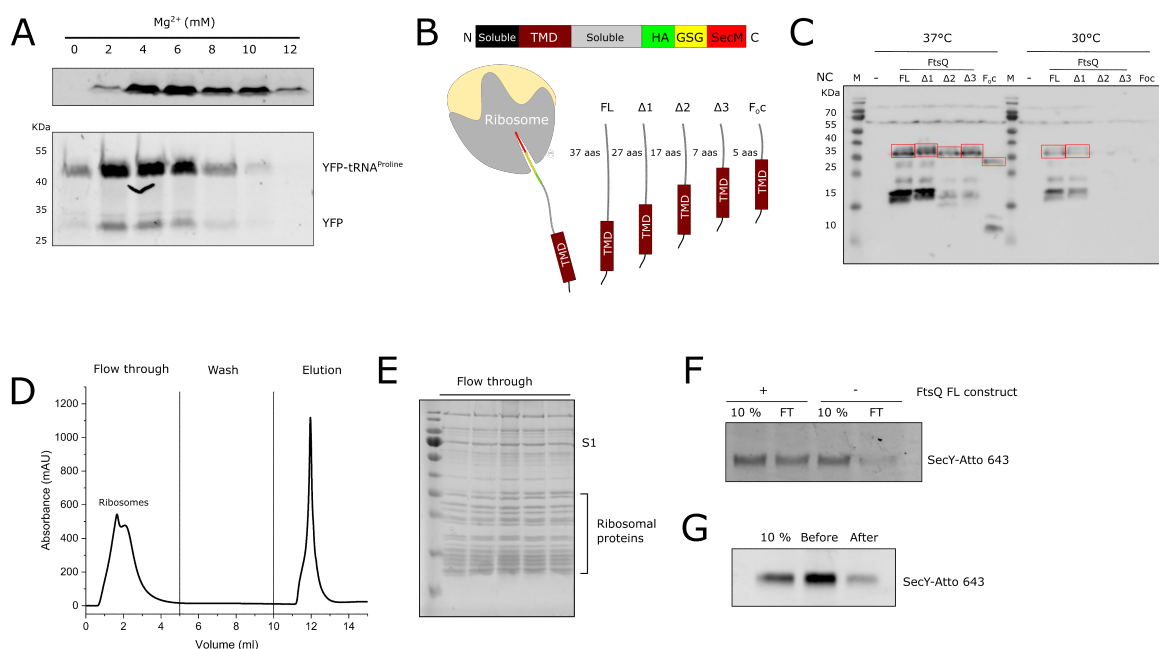
Figure 6.4: Cell-free protein synthesized RNCs interact with SecYEG nanodiscs. A) Top: magnesium titration for the optimization of the cell-free synthesis of the soluble protein YFP with optimum magnesium concentration at 4 - 6 mM. Bottom: successful ribosomal stalling of the translation of YFP-SecM with an optimum synthesis and stalling at 2-4 mM magnesium. B) The designed constructs to achieve ribosome stalling and assembly of RNCs-bacterial insertion machinery complex. C) Anti-HA tag blot shows the successful synthesis of all nascent chains tested and shows that optimum synthesis is achieved at 37 °C. The nascent chains covalently bound to proline tRNA are indicated with the red boxes. D) A chromatogram showing the Capto core 700-based isolation of ribosomes, the first peak shows the flow through that contains the ribosomal fractions followed by a short wash, then elution to regenerate the column. E) Coomassie-stained gel of the first peak in the chromatogram showing the typical ribosomal protein pattern. F) SecYEG MSP2N2 nanodiscs co-elutes with the ribosomal fractions when a plasmid with FtsQ FL construct is added to the CFPS reaction, while only a minimum amount of SecYEG nanodiscs co-elutes when no plasmid was added confirming a successful assembly of the complex (10 % indicates 10% of the initial reaction volume). G) Higher amount of SecYEG nanodiscs co-elutes with ribosomes when the SecYEG nanodiscs are added before the start of the reaction compared to when added after the reaction is completed. This suggests the co-translational assembly of the complex.

In the next step, several constructs were designed with the SecM sequence fused to FtsQ. FtsQ was used because it is a model substrate for SecYEG and/or SecYEG/YidC insertion pathway [24, 56]. The construct comprises the first TMH of FtsQ, followed by the hydrophilic polypeptide chain that is translocated to the periplasm, an HA tag for detection using a western blot, a multiple GSG linker (GSG$_6$), and the SecM sequence. Different lengths were designed for the periplasmic domain of FtsQ, this should serve to control how exposed will be the TMH of FtsQ from the ribosomal exit tunnel. Additionally, it might control the assembly of RNCs-insertion machinery complex offering different snapshots of the insertion pathway (Figure 6.4 B). It has also been reported that different lengths of the periplasmic domain of FtsQ can modulate the affinity towards SecYEG and YidC [16, 57].

All the constructed plasmids were supplied to the CFPS reaction. Here, two reaction temper-

atures were compared, 30 and 37°C. The higher yield was achieved at 37°C, though two bands were observed, fast and slow migrating bands, indicating released nascent chains and nascent chains bound to the proline tRNA respectively (Figure 6.4 C).

In the next steps, the CFPS reaction was carried out using FtsQ FL in the presence of fluorescently-labeled SecYEG reconstituted in MSP2N2 nanodiscs. Subsequently, the reaction was loaded on a Capto Core 700 resin. Capto Core is a resin that combines different modes of chromatography for the purification of the required macromolecule. The resin has a porous inactive shell that excludes any molecules that are bigger than 700 kDa from entering the core of the resin. The core is made of octylamine ligands that have both positive charges and hydrophobic properties, so the proteins will be separated based on electrostatic and hydrophobic properties. Using this resin allows for the isolation of the ribosomes from the rest of the components of the reactions as the ribosomes are too large to enter the core of the column. The octylamine ligand can capture other impurities from the reaction (Figure 6.4 D and E). SecYEG nanodisc should enter the core of the column, however, in case they co-elute with ribosomes, this would indicate a successful complex formation between the ribosomes translating FtsQ and SecYEG nanodiscs. Indeed, when SecYEG nanodiscs were added to a reaction supplied with the plasmid coding for FtsQ FL, SecYEG nanodiscs co-eluted with the ribosomes, while only a minor amount of SecYEG nanodiscs co-eluted with ribosomes when no plasmid was supplied to the reaction (Figure 6.4 F). Interestingly, when SecYEG nanodiscs were added after the reaction was completed, lower amounts of SecYEG nanodiscs co-eluted with ribosomes compared to the reactions where SecYEG nanodiscs were added at the beginning of the reaction. This suggests a more efficient assembly of the SecYEG nanodiscs-RNCs complex in a co-translational manner (Figure 6.4 G).

6.3.4   Isolation of RNCs-SecYEG complex

To efficiently purify the complex for structural studies using cryo-EM, CFPS reactions supplied with either SecYEG in DIBMA nanoparticles or MSP2N2 nanodiscs were loaded on the top of 10-40 % sucrose gradient. Here, FtsQ Δ2 and Δ3 were used, as theoretically, they should form tighter interactions with SecYEG. Using FtsQ FL might cause the ribosomes to detach from SecYEG, as in this case, the TMH could have already been fully inserted into the membrane. After centrifugation, all the components of the reaction should stay on the top of the gradient, while only ribosomes can penetrate the gradient allowing for efficient isolation of the ribosomes (Figure 6.5 A). Both SecYEG in MSP2N2 nanodiscs or DIBMALPs co-migrated with ribosomes through the sucrose gradient indicating complex assembly (Figure 6.5 B and C). The ribosomal fractions were pooled together and concentrated (Figure 6.5 D). The presence of the nascent chain with ribosomes was confirmed by a western blot against the HA tag (Figure 6.5 E). Here, only the stalled nascent chain was detected, since the released nascent chains could not enter the sucrose gradient due to their small weight. The concentration of ribosomes was then estimated by measuring the absorbance at 260 nm, while the concentration of SecYEG nanodiscs co-purified with ribosomes was estimated by generating a calibration curve from the in-gel fluorescence of different concentrations of SecYEG. Accordingly, it was estimated that around 20 % of the ribosomes have bound SecYEG nanodiscs. To further enhance the amount of SecYEG-bound ribosomes, the reaction was first incubated with Ni-NTA resin, where the histidine tag on SecYEG

and MSP2N2 can bind, subsequently, the elution fractions were loaded on a 10 - 40 % sucrose gradient. However, this enhanced the amount of SecYEG-bound ribosomes to only 28 and 40 % in the case of FtsQ $\Delta 2$ and $\Delta 3$, respectively (Figure 6.5 F).
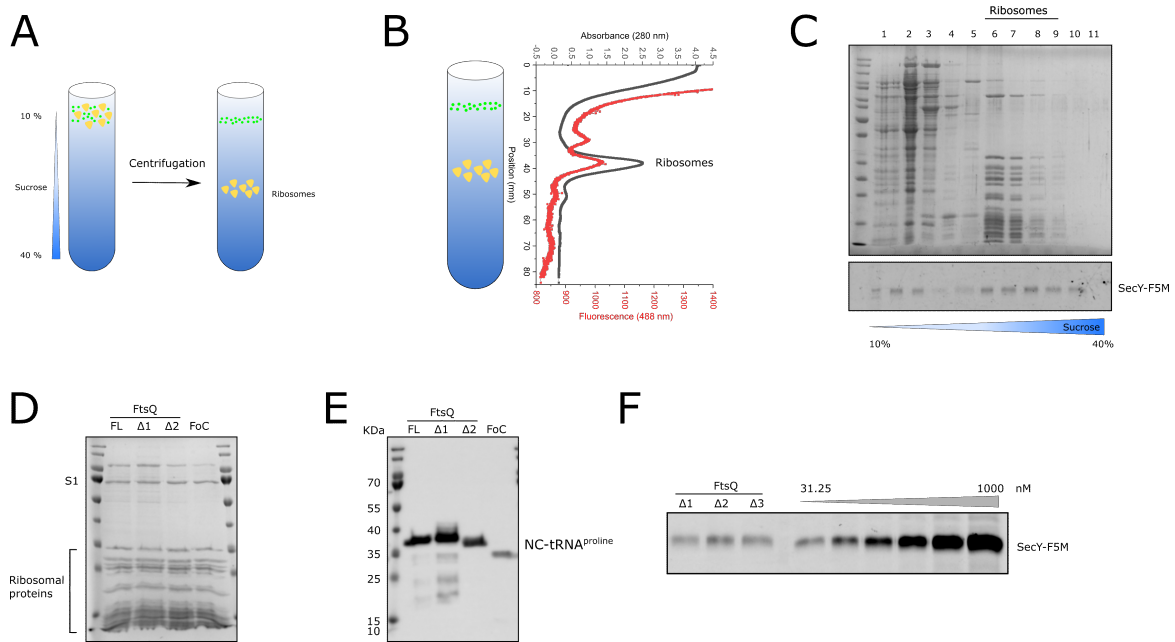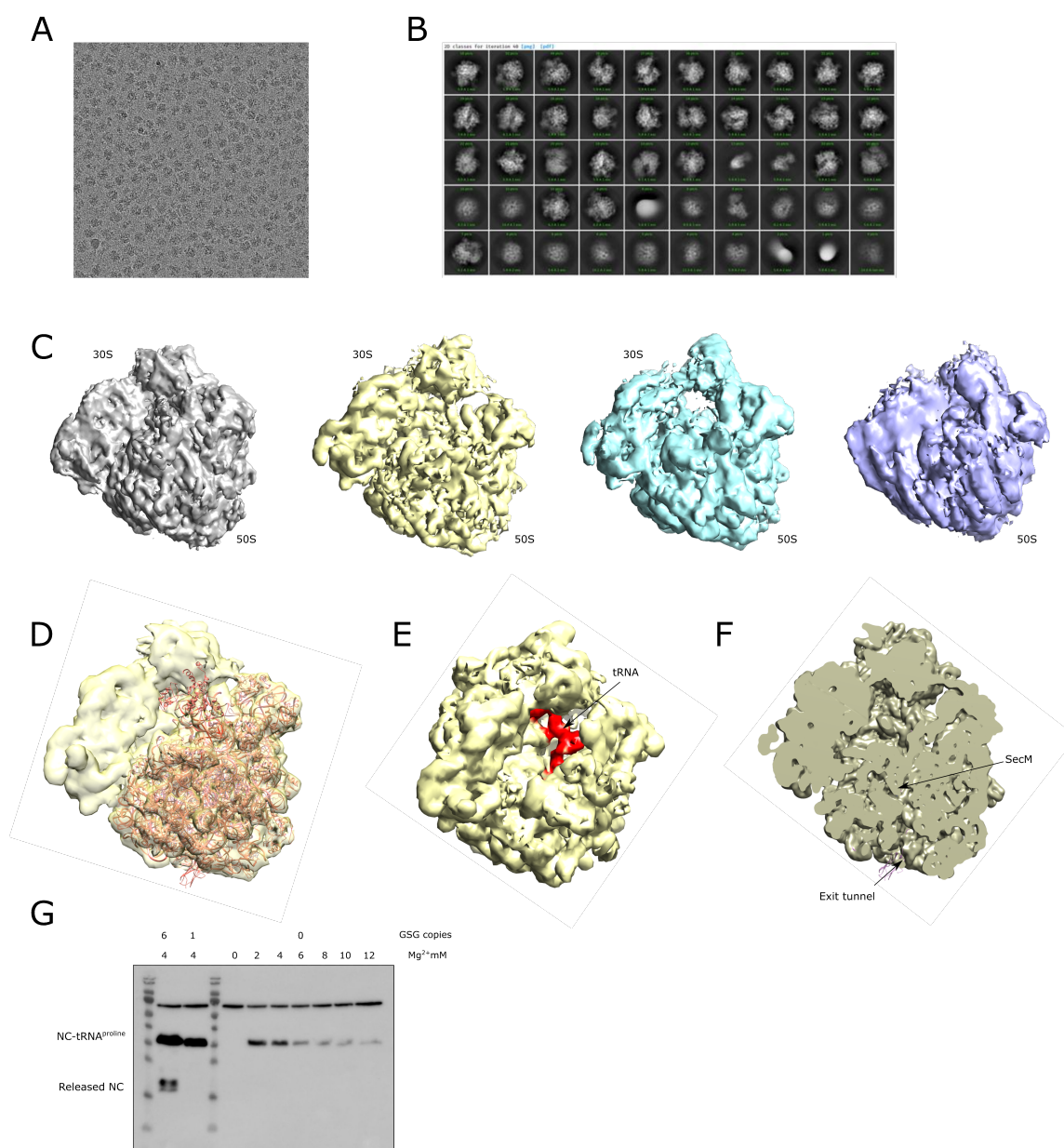

Figure 6.5: Purification of stalled RNCs in complex with SecYEG nanodiscs. A) Sucrose gradient centrifugation to isolate the ribosomes from the CFPS reaction. B) The gradient profile of CFPS reaction after sucrose gradient centrifugation. The ribosomes migrate as a defined peak in the middle of the gradient and fluorescently-labeled SecYEG DIBMA lipid particles co-migrate with the ribosomes as confirmed by the fluorescence peak that co-migrate with the ribosomal peak. C) Coomassie-stained gel of the fractions from the sucrose gradient in B showing the ribosomal protein pattern (fraction 6-9) and in-gel fluorescence (bottom) confirms the co-migration of fluorescently labeled SecYEG DIBMA lipid particles with the ribosomes. D) Purified ribosomes after sucrose gradient centrifugation and concentration from CFPS reaction supplied with FtsQ FL, FtsQ $\Delta 1$, FtsQ $\Delta 2$, and $F_o c$ constructs. E) Anti-HA tag blot showing the nascent chains in the stalled ribosomes after sucrose gradient centrifugation and concentration, the bands of the released nascent chains disappeared due to the successful separation of the ribosomes from the rest of the CFPS reaction. F) 15, 28, and 40 % of the isolated ribosomes contain bound SecYEG-MSP2N2 nanodiscs as estimated from the calibration curve established from the in-gel fluorescence of fluorescently-labeled SecYEG loaded in an increasing concentration when FtsQ $\Delta 1$, FtsQ $\Delta 2$, and FtsQ $\Delta 3$ constructs were used respectively.

6.3.5 Cryo-EM and single particle analysis of the RNCs-SecYEG complex

The sample with SecYEG MSP2N2 nanodiscs with FtsQ $\Delta 3$ RNCs was then provided for cryo-EM (Figure 6.6 A). Different 2D classes could be observed (Figure 6.6 B), which allowed the 3D reconstruction and sorting, where 4 classes could be identified (Figure 6.6 C). Two of these classes showed the volume of a 70S ribosome (Figure 6.6 D), and by further analysis, a tRNA was detected in the P-site of the ribosomes (Figure 6.6 E), and 15 residues of the SecM sequence could be detected in the ribosomal exit tunnel (Figure 6.6 F).

Figure 6.6: Cryo-EM for stalled RNCs in complex with SecYEG MSP2N2 nanodiscs with FtsQ Δ3 RNCs . A) A micrograph showing the ribosomes on the cryo-EM grid. B) 2D classification of the ribosomes on the grid. C) 3D classification shows 4 different classes, class 1 and 2 show fully assembled 70S ribosomes, class 3 shows a fully assembled 70S ribosome with no tRNA in the P site, and class 4 shows only the 50S subunit of the ribosome. D) A Fit of a published 50S subunit structure (PDB: 6I0Y) in the volume of class 2 from 3D classification. E) The red color indicates the presence of tRNA in the P site of the ribosomes. F) A density is observed in the ribosomal exit tunnel that correlated with the first 15 amino acids of the SecM sequence confirming successful ribosomal stalling. G) Anti-HA blot showing that reducing the copies of GSG from 6 to 1 in the FtsQ FL construct improved the stalling efficiency indicated by the absence of the released nascent chain. Mg^{2+} titration to optimize the synthesis of FtsQ FL with no GSG linker shows that the synthesis is dramatically lower for this construct compared to the constructs with a GSG linker.

Surprisingly, no SecYEG nanodiscs could be observed bound to the ribosome. A possible reason for that could be the disassembly of the complex due to freeze-thawing or during the vitrification process during the formation of the cryo-EM grids. Another possible explanation could be that the ribosome might have detached from SecYEG due to the completed insertion of the TMH of the nascent chain or weakened interaction due to the long GSG_6 linker. Furthermore, the long GSG linker in the construct used might have promoted the release of the nascent chain from the ribosomal exit tunnel. To overcome the drawback of these constructs, new constructs were designed lacking the GSG linker. However, these constructs showed a dramatic decrease in the yield of nascent chain synthesis in the CFPS reaction. Therefore, a new construct was designed that has only 1 copy of the GSG instead of the six copies in the previous construct. The new construct showed an acceptable nascent chain synthesis yield and enhanced the stalling efficiency and can be further used for structural characterization (Figure 6.6 G).

6.3.6 Assembly of YidC nanodiscs with F_oc and MscL RNCs

In order to study membrane protein insertion through YidC, two substrates were chosen that depend completely on YidC for insertion, F_oc, and MscL. These two substrates differ by their topologies in the membrane. MscL is a type II membrane protein with the N-terminus in the cytosol, while F_oc is a type III membrane protein where the N-terminus is located in the periplasm (Figure 6.7 A) [58]. For F_oc, the first TMH followed by a small part from the cytoplasmic loop was fused to an HA tag followed by a 1 copy of GSG and the SecM sequence. While for MscL, three different constructs were designed, all containing the first TMH. The FL, the TMH was followed by the whole periplasmic loop (30 amino acids). MscL Δ1 and Δ2 variants had a deletion of 10 and 20 amino acids from the periplasmic loop respectively (Figure 6.7 C).

Fluorescently labeled YidC in MSP1D1 nanodiscs was supplied to the CFPS reaction containing the F_oc construct. Anti-HA blot confirmed the successful synthesis of the nascent chain and ribosome stalling (Figure 6.4 C). The reaction was then loaded on a 10-40 % sucrose gradient. YidC co-migrated with the ribosomal fractions when the F_oc construct was present, while a little amount of YidC nanodiscs co-migrated with ribosomes when the construct was absent. This indicates the successful assembly of the YidC nanodiscs-F_oc RNCs complex (Figure 6.7 B). The reaction was also carried out in the presence of the MscL constructs and afterward, it was loaded on a sucrose cushion, which allow for faster separation of the ribosomes from the rest of the reaction components (Figure 6.7 D). Anti-HA blot confirmed the synthesis of the nascent chain, where a single band was observed between 25 and 35 KDa indicating the nascent chain was bound to the proline tRNA (Figure 6.7 E). YidC nanodiscs co-pelleted with the ribosomes in the case of all the constructs, and a minimum amount of YidC co-pelleted with ribosomes when no plasmid was included in the reaction. The maximum amount of YidC nanodiscs co-pelleted with ribosomes when the MscL FL construct was used (Figure 6.7 F). This indicates that this construct might form the most stable complex that can be further used for structural characterization. For the shortest construct, the synthesis yield was quite low which might explain the low amount of co-pelleted YidC nanodiscs.
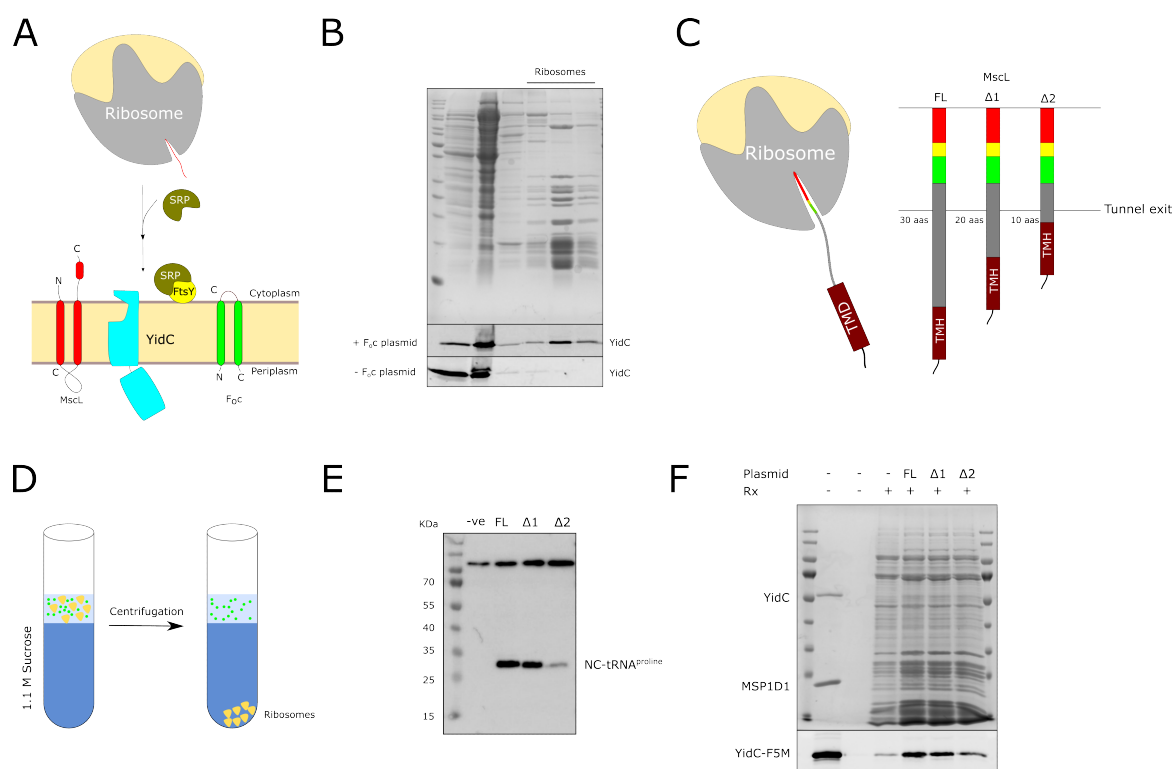
Figure 6.7: Assembly of F_oc and MscL RNCs in complex in YidC in MSP1D1 nanodiscs.
A) Membrane topology of MscL and F_oc after being inserted by YidC. B)YidC MSP1D1 co-migrates with ribosomes in a sucrose gradient when a plasmid with F_oc was supplied to the CFPS reaction. C) Three different constructs were used for the MscL nascent chain that differs in the length of the periplasmic domain. D) Sucrose cushion centrifugation to isolate ribosomes. E) Anti-HA blot indicating successful synthesis and ribosome stalling of MscL nascent chains. F) YidC MSP1D1 nanodiscs co-migrate better with MscL FL RNCs. R_X indicates if CPFS reaction was present and the first lane indicates 100 % YidC MSP1D1 nanodiscs that were added to the reactions.

6.4 Discusion

Membrane proteins are inserted into the cytoplasmic membrane of bacteria with the help of the SecYEG translocon, the insertase YidC, or both. Typically, the nascent chains are targeted to these insertion machineries co-translationally within the RNCs with the help of the SRP, which then binds to the SR receptor, FtsY. Afterward, the RNC is transferred to SecYEG or YidC, where they insert the protein into the membrane, while still being translated. However, the exact mechanism of membrane protein insertion through SecYEG or YidC, or both is still unclear. For instance, the selection mechanism for the insertion pathway is not clear and the exact path of the nascent chain from the ribosome exit tunnel to the membrane is not completely resolved.

Different structures already exist for SecYEG in a complex with ribosomes while inserting a nascent chain into the membrane. Mitra et al 2005 reported the structure of the *E.coli* SecYEG in a complex with stalled FtsQ ribosome nascent chain. The structure shows two copies of SecYEG interacting with the RNC. However, the complex was assembled *in vitro* with detergent-purified SecYEG and independently purified RNCs, which might not reflect the native complex and has a low resolution (14.9 Å) [12]. Menetret et al 2007 also reported a complex of SecYEG, however with a non-translating ribosome and they show that only one copy of SecY interacts with the ribosome. Nevertheless, this complex was assembled of independently purified ribosomes and detergent-solubilized SecYEG [13]. Frauenfeld et al 2011 reported the first structure of SecYEG embedded in the lipid environment of nanodiscs with FtsQ RNCs, but similarly, the complex was formed in a tube between SecYEG nanodiscs and independently purified RNCs. Moreover, it showed a late-stage of nascent chain insertion where the TMH was already inserted near the lateral gate and did not explain clearly how the nascent chain reached this position [19]. Bischoff et al 2014 reported the first structure of SecYEG inserting a polytopic membrane protein. One advantage of this structure is the *in vivo* assembly of the complex, nevertheless, it was also purified in detergent and provides a moderate resolution. It also shows the two TMH already in the membrane near the lateral gate of SecY, without a clear pathway of how the TMHs reached this position [16]. Recently, a new structure was reported by Kater et al 2019 where they revealed an early stage of insertion that provides insight into the lateral gate dynamics as partial unzipping was observed. The SecYEG-RNCs complex was resolved in MSP1E3D1 nanodiscs. Despite that it was the first structure that resolved an early stage of insertion, it was artificially assembled *in vitro* which might also not reflect the native state of the complex [20]. Similarly, the structure of YidC in a complex with RNCs was either investigated in a detergent-solubilized state [9], or in MSP1D1 nanodiscs with the complex formed by mixing the individually purified components in a tube [21].

Therefore, most of the available structures either provide a limited resolution or are resolved in a detergent-solubilized state which might not reflect the native conformation of the complex. Furthermore, many of the resolved complexes were assembled in a tube which does not imitate the co-translation nature of the complex formation. Moreover, no structure of SecYEG-YidC alone or in a complex with RNCs was resolved due to the transient nature of these complexes. A cryo-electron microscopy-based construction allowed modeling the architecture of the so-called holo-translocon, a complex that comprises SecYEG, YidC, and SecDFYajC but the structure had a very limited resolution [59]. Moreover, no RNCs were involved in this complex, therefore, its

relevance in membrane protein insertion is not clear.

Here, a different strategy was employed to obtain the structure of the co-translationally-assembled membrane protein insertion pathway. A CFPS platform supplemented with the insertion machinery reconstituted in nanodiscs was utilized for the co-translation assembly of the complex. During the synthesis of the nascent chain, it can directly engage with the supplied nanodiscs with the embedded SecYEG/YidC insertion machinery, and be inserted into the lipid bilayer provided by the nanodisc. This approach can closely imitate the continuous process and native conditions that happen inside the cell.

SecYEG, YidC, and SecYEG-YidC fusion were successfully reconstituted in MSP-based nanodiscs. A complementary approach was also employed using maleic acid copolymers. The advantage of maleic acid copolymers is that they can directly isolate the desired proteins from the native membrane into nanodiscs. This provides a more native state for the assembly of the complex by preserving the native lipids and may potentially preserve any interacting partners that might further promote the insertion [37, 41]. All the membrane protein insertion machineries were successfully isolated in DIBMALPs and SMALPs. Nevertheless, DIBMALPs were further used due to their ability to tolerate higher concentrations of magnesium which is necessary for the integrity of the ribosomes [41, 60]. It is noteworthy to mention that it was initially suggested to use DIBMA to isolate *in vivo* assembled RNCs-SecYEG/YidC complexes, yet it was observed that using DIBMA in the concentrations required for membrane solubilization caused the aggregation of ribosomes, possibly by chelating the magnesium required to keep the ribosomal subunits intact (Figure 6.8).
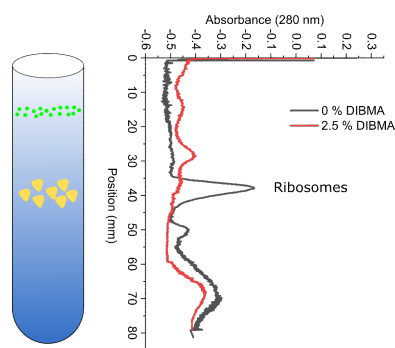
Figure 6.8: DIBMA causes the aggregation of the ribosomes when used in concentrations that are sufficient to solubilize the membrane.

CFPS has become a prominent approach to study membrane proteins. The synthesis and the co-translational insertion of several membrane proteins into nanodiscs have been established in the absence of SecYEG or YidC [61, 62]. Therefore, it is very reasonable to use CFPS to study co-translational insertion using SecYEG and/or YidC. Using CFPS reactions, stalled RNCs were successfully formed. Here, different nascent chains were designed that differ in the length of the hydrophilic domain following the first TMH. This should allow for probing different stages of the insertion pathway since this will control the position of the TMH relative to the ribosomal tunnel exit (Figure 6.9). Additionally, it has been shown previously that the length of the hydrophilic stretch after the TMH can control the affinity of the ribosome nascent chain to SecYEG or YidC [16, 21]. SecYEG reconstituted in MSP2N2 nanodiscs and DIBMALPs, supplied to CFPS

reactions successfully formed a complex with FtsQ RNCs. On the other hand, YidC reconstituted in MSP1D1 formed a complex with $F_o c$ as well as MscL RNCs.
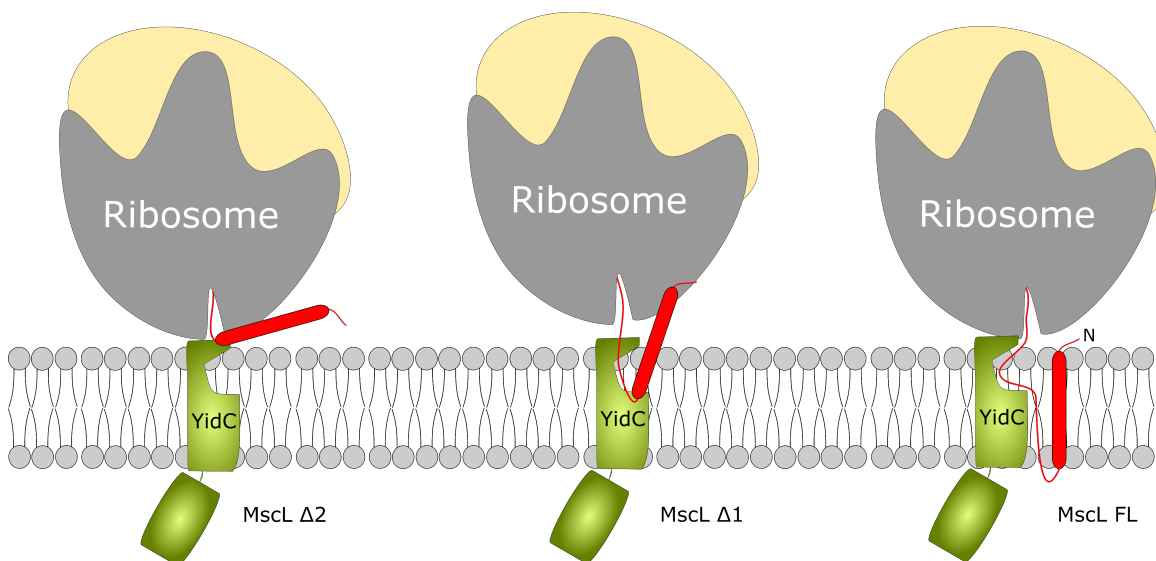
Figure 6.9: Different lengths of MscL nascent chains can be used to get different snapshots of the insertion pathway

In order to purify the assembled complexes, Ni-NTA beads were used, where histidine-tagged MSP2N2 and SecYEG can be pulled down. Sucrose gradient centrifugation was then performed to separate the RNCs-bound nanodiscs. Only 40 % of the eluted ribosomes after incubation of Ni-NTA beads had bound SecYEG nanodiscs possibly indicating nonspecific binding of ribosomes to the Ni-NTA beads. Therefore, further optimization of the purification strategy is required, for instance increasing the amount of imidazole during the washing steps. Another possibility is using a twin strep II tag variant of MSP, where the assembled complexes can be pulled down using Strep-Tactin resin. Strep II tags provide higher purity and efficiency compared to histidine tags [63].

When Ni-NTA purification was applied to SecYEG DIBMALPs, no SecYEG was observed in the elution fractions after Ni-NTA binding. A possible cause is that the histidine tag on SecY might be inaccessible when embedded in DIBMALPs. It was observed during the Ni-NTA-based purification of SecYEG- DIBMALPs after DIBMA-based membrane solubilization, that a long incubation period (overnight) is required to increase the yield. When shorter incubation was used, little amount of the protein was obtained after elution with imidazole. This effect has also been previously reported by other research groups [64]. Therefore, for the purification of the SecYEG-DIBMALPs- RNCs complex, further optimization of the purification procedure is required. A longer linker can be placed between SecY and the histidine tag to allow for better accessibility of the tag or a different tag like the Twin-Strep tag or FLAG tag may be used to achieve better enrichment of RNCs with bound SecYEG.

The sample with SecYEG MSP2N2 nanodiscs with FtsQ $\Delta 2$ and 3 were supplied for cryo-EM and single particle analysis. The stalling of the ribosome was confirmed by the presence of the tRNA in the P site of the ribosome and by the presence of a density in the ribosomal exit tunnel that would represent 15 amino acids of the SecM sequence. Nevertheless, no SecYEG

nanodisc was observed to be bound to the ribosome at the tunnel exit. Two possible reasons can explain that. First, it could be that the complex was disassembled, however, in-gel fluorescence, coomassie staining and western blot confirmed the presence of SecYEG nanodiscs and stalled nascent chains in the final samples provided for cryo-EM. Nevertheless, freeze-thawing of the sample or the vitrification process during the formation of the cryo-EM grids might have caused the disassembly of the complex. It was previously reported that the freeze-thawing might cause the release of the nascent chain from the stalled ribosome, subsequently, this will cause the disassembly of the complex [64]. To overcome this problem, the freshly assembled and purified complex can be directly supplied for grid preparation and cryo-EM analysis.

Second, the RNCs could have become loosely bound to SecYEG nanodiscs due to the completed insertion of the TMH, as a long hydrophilic stretch exists between the PTC (peptide transfer center) and the TMH. However, it was previously reported that a tight interaction between the SecYEG and RNCs occurs up to a 90 to 95-long hydrophilic stretch after the TMH [16]. In the constructs used, 52 and 62 amino acids for FtsQ $\Delta 2$ and 3, respectively exist between the TMH and the PTC, which should still allow for tight interaction of the ribosome with SecY. On the other hand, the presence of a long GSG linker in the construct might have weakened the interaction between ribosomes and SecY and facilitated the detachment of the ribosomes or it might promote the release of the nascent chain from the ribosome exit tunnel. Assuming that the ribosomal exit tunnel could accommodate 40 amino acids [65], the GSG linker will extend from inside the ribosomal tunnel making the whole SecYEG-RNCs complex very flexible, which could impact the stability of the complex. Therefore, to eliminate this problem, new constructs were designed which contain a single GSG repeat instead of the six GSG repeats in the original construct. The complete removal of the GSG linker caused a dramatic decrease in the synthesis yield of the nascent chain. The construct with a single GSG repeat dramatically decreased the amount of the released nascent chain and provided superior stalling efficiency supporting the notion that the long GSG linker promotes the nascent chain release. This new construct can be then used for the assembly of complex and structural studies using cryo-EM.

Recently, new samples were prepared using the constructs with FtsQ $\Delta 1$ and $\Delta 2$ with the 1 copy of GSG in the presence of SecYEG MSP2N2 nanodiscs. Assembled complexes were isolated using IMAC followed by sucrose gradient centrifugation. The purified complexes were directly supplied for vitrification and cryo-EM measurement. After initial single particle analysis, 3D reconstruction confirmed the presence of the SecYEG MSP2N2 nanodiscs at the ribosome exit tunnel confirming the reliability of the established platform (Figure 6.10). Careful sorting and refinement may allow building of a model where the SecYEG structure can be fitted, and the position of the nascent chain can be determined and compared between the two constructs.
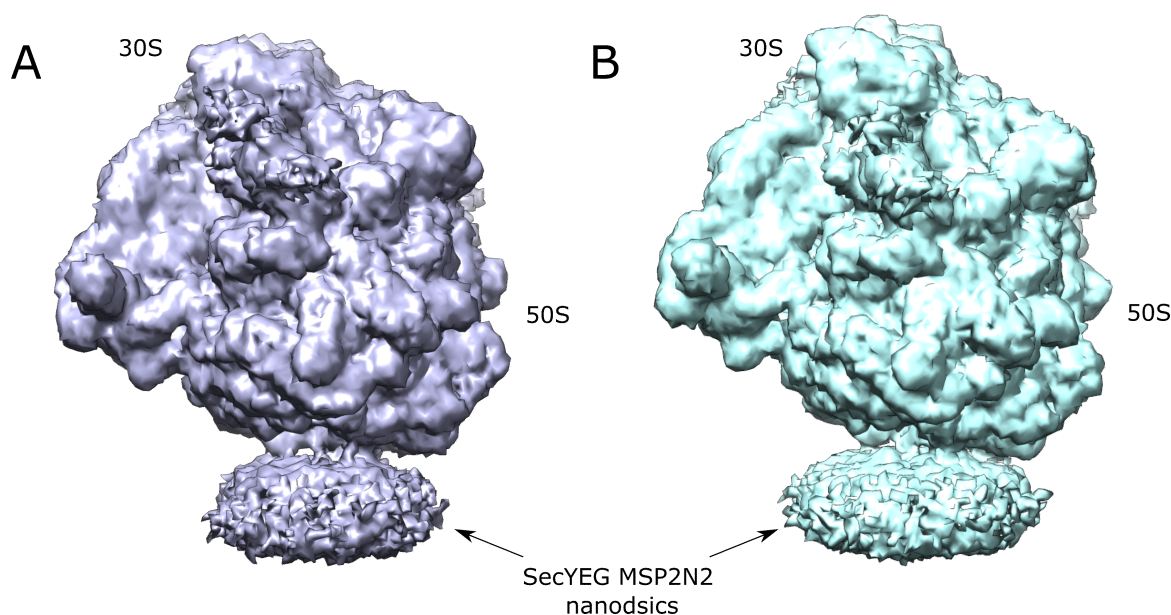
Figure 6.10: Cryo-EM confirms the assembly of FtsQ RNCs with SecYEG MSP2N2. 3D reconstruction confirms the presence of SecYEG MSP2N2 nanodiscs at the ribosome exit tunnel when the construct with FtsQ $\Delta 1$ (A) and $\Delta 2$ (B) with 1GSG copy were used.

In order to study SecYEG-YidC mediated insertion, FtsQ could also be used as the model substrate since crosslinking studies have reported that YidC contacts FtsQ TMHs during membrane insertion [24]. Other substrates like NuoK [31] and CyoA [30, 66] can also be used since it has been shown that they require both SecYEG and YidC for membrane insertion with a different order.

Different biophysical methods can be employed to probe the assembly of the complex when nascent chain with different lengths are used. For instance, fluorescence correlation spectroscopy (FCS) or microfluidic diffusional sizing (MDS) using fluorescently-labeled SecYEG/YidC can be used. FCS has been previously employed to measure YidC-RNCs interactions [21]. MDS (Fluidic Analytics) is a method that can measure the hydrodynamic radius of diffusing fluorescently-labeled particles based on their diffusion coefficient [67]. SecYEG/YidC nanodiscs have a smaller hydrodynamic radius than that of ribosomes. The bacterial ribosome has a diameter of 20 to 25 nm [68], consequently, once RNCs bind fluorescently labeled SecYEG/YidC nanodiscs, a change in the hydrodynamic radius will be detected confirming the complex integrity.

Crosslinking studies can also be performed utilizing the platform established here to get more insights into the exact pathway of the nascent chain during insertion. Introducing cystines at different positions in the nascent chain and the respective insertion machinery can provide information about the contact sites of the nascent chain as it passes from the ribosomal exit tunnel till it gets inserted into the membrane.

To sum up, a CFPS platform was established that allowed for the co-translational assembly of ribosome nascent chain complexes in a complex with the membrane protein insertion machinery embedded in nanodiscs. This platform can then be further employed to elucidate the mechanism and dynamic of membrane protein insertion and folding. Using substrates with different lengths will allow to get snapshots of the complex at the different stages of the insertion pathway.

Moreover, it can be used to elucidate and determine the full pathway of FtsQ insertion and the necessity to recruit YidC. It can possibly give more insight into the structure of the SecYEG-YidC complex and how they work together to orchestrate the insertion and folding of different substrates with different properties.

References

[1] G. Von Heijne, "The membrane protein universe: what's out there and why bother?," *Journal of internal medicine*, vol. 261, no. 6, pp. 543–557, 2007.

[2] K. Denks, A. Vogt, I. Sachelaru, N.-A. Petriman, R. Kudva, and H.-G. Koch, "The Sec translocon mediated protein transport in prokaryotes and eukaryotes," *Molecular membrane biology*, vol. 31, no. 2-3, pp. 58–84, 2014.

[3] A. Kuhn, H.-G. Koch, and R. E. Dalbey, "Targeting and insertion of membrane proteins," *EcoSal Plus*, vol. 7, no. 2, 2017.

[4] B. V. D. Berg, W. M. Clemons Jr, I. Collinson, Y. Modis, E. Hartmann, S. C. Harrison, and T. A. Rapoport, "X-ray structure of a protein-conducting channel," *Nature*, vol. 427, no. 6969, pp. 36–44, 2004.

[5] J. A. L. a Nijeholt, J. de Keyzer, I. Prabudiansyah, and A. J. Driessen, "Characterization of the supporting role of SecE in protein translocation," *FEBS letters*, vol. 587, no. 18, pp. 3083–3088, 2013.

[6] K.-i. Nishiyama, M. Hanada, and H. Tokuda, "Disruption of the gene encoding p12 (SecG) reveals the direct involvement and important function of SecG in the protein translocation of Escherichia coli at low temperature.," *The EMBO journal*, vol. 13, no. 14, pp. 3272–3277, 1994.

[7] F. Jiang, M. Chen, L. Yi, J.-W. de Gier, A. Kuhn, and R. E. Dalbey, "Defining the regions of Escherichia coli YidC that contribute to activity," *Journal of Biological Chemistry*, vol. 278, no. 49, pp. 48965–48972, 2003.

[8] K. Kumazaki, S. Chiba, M. Takemoto, A. Furukawa, K.-i. Nishiyama, Y. Sugano, T. Mori, N. Dohmae, K. Hirata, Y. Nakada-Nakura, *et al.*, "Structural basis of Sec-independent membrane protein insertion by YidC," *Nature*, vol. 509, no. 7501, pp. 516–520, 2014.

[9] S. Wickles, A. Singharoy, J. Andreani, S. Seemayer, L. Bischoff, O. Berninghausen, J. Soeding, K. Schulten, E. O. van der Sluis, and R. Beckmann, "A structural model of the active ribosome-bound membrane protein insertase YidC," *Elife*, vol. 3, p. e03035, 2014.

[10] Y. Chen, S. Capponi, L. Zhu, P. Gellenbeck, J. A. Freites, S. H. White, and R. E. Dalbey, "YidC insertase of Escherichia coli: water accessibility and membrane shaping," *Structure*, vol. 25, no. 9, pp. 1403–1414, 2017.

[11] R. Beckmann, C. M. Spahn, N. Eswar, J. Helmers, P. A. Penczek, A. Sali, J. Frank, and G. Blobel, "Architecture of the protein-conducting channel associated with the translating 80S ribosome," *Cell*, vol. 107, no. 3, pp. 361–372, 2001.

[12] K. Mitra, C. Schaffitzel, T. Shaikh, F. Tama, S. Jenni, C. L. Brooks III, N. Ban, and J. Frank, "Structure of the E. coli protein-conducting channel bound to a translating ribosome," *Nature*, vol. 438, no. 7066, pp. 318–324, 2005.

[13] J.-F. Ménétret, J. Schaletzky, W. M. Clemons Jr, A. R. Osborne, S. S. Skånland, C. Denison, S. P. Gygi, D. S. Kirkpatrick, E. Park, S. J. Ludtke, *et al.*, "Ribosome binding of a single copy of the SecY complex: implications for protein translocation," *Molecular cell*, vol. 28, no. 6, pp. 1083–1092, 2007.

[14] T. Becker, S. Bhushan, A. Jarasch, J.-P. Armache, S. Funes, F. Jossinet, J. Gumbart, T. Mielke, O. Berninghausen, K. Schulten, *et al.*, "Structure of monomeric yeast and mammalian Sec61 complexes interacting with the translating ribosome," *science*, vol. 326, no. 5958, pp. 1369–1373, 2009.

[15] E. Park, J.-F. Ménétret, J. C. Gumbart, S. J. Ludtke, W. Li, A. Whynot, T. A. Rapoport, and C. W. Akey, "Structure of the SecY channel during initiation of protein translocation," *Nature*, vol. 506, no. 7486, pp. 102–106, 2014.

[16] L. Bischoff, S. Wickles, O. Berninghausen, E. O. Van Der Sluis, and R. Beckmann, "Visualization of a polytopic membrane protein during SecY-mediated membrane insertion," *Nature communications*, vol. 5, no. 1, p. 4103, 2014.

[17] M. Gogala, T. Becker, B. Beatrix, J.-P. Armache, C. Barrio-Garcia, O. Berninghausen, and R. Beckmann, "Structures of the Sec61 complex engaged in nascent peptide translocation or membrane insertion," *Nature*, vol. 506, no. 7486, pp. 107–110, 2014.

[18] R. M. Voorhees, I. S. Fernández, S. H. Scheres, and R. S. Hegde, "Structure of the mammalian ribosome-Sec61 complex to 3.4 Å resolution," *Cell*, vol. 157, no. 7, pp. 1632–1643, 2014.

[19] J. Frauenfeld, J. Gumbart, E. O. v. d. Sluis, S. Funes, M. Gartmann, B. Beatrix, T. Mielke, O. Berninghausen, T. Becker, K. Schulten, *et al.*, "Cryo-EM structure of the ribosome–SecYE complex in the membrane environment," *Nature structural & molecular biology*, vol. 18, no. 5, pp. 614–621, 2011.

[20] L. Kater, B. Frieg, O. Berninghausen, H. Gohlke, R. Beckmann, and A. Kedrov, "Partially inserted nascent chain unzips the lateral gate of the Sec translocon," *EMBO reports*, vol. 20, no. 10, p. e48191, 2019.

[21] A. Kedrov, S. Wickles, A. H. Crevenna, E. O. van der Sluis, R. Buschauer, O. Berninghausen, D. C. Lamb, and R. Beckmann, "Structural dynamics of the YidC: ribosome complex during membrane protein biogenesis," *Cell reports*, vol. 17, no. 11, pp. 2943–2954, 2016.

[22] S. Pfeffer, L. Burbaum, P. Unverdorben, M. Pech, Y. Chen, R. Zimmermann, R. Beckmann, and F. Förster, "Structure of the native Sec61 protein-conducting channel," *Nature communications*, vol. 6, no. 1, p. 8403, 2015.

[23] P. B. Wolfe, M. Rice, and W. Wickner, "Effects of two sec genes on protein assembly into the plasma membrane of Escherichia coli.," *Journal of Biological Chemistry*, vol. 260, no. 3, pp. 1836–1841, 1985.

[24] M. L. Urbanus, P. A. Scotti, L. Fröderberg, A. Sääf, J.-W. L. de Gier, J. Brunner, J. C. Samuelson, R. E. Dalbey, B. Oudega, and J. Luirink, "Sec-dependent membrane protein insertion: sequential interaction of nascent FtsQ with SecY and YidC," *EMBO reports*, vol. 2, no. 6, pp. 524–529, 2001.

[25] T. Welte, R. Kudva, P. Kuhn, L. Sturm, D. Braig, M. Müller, B. Warscheid, F. Drepper, and H.-G. Koch, "Promiscuous targeting of polytopic membrane proteins to SecYEG or YidC by the Escherichia coli signal recognition particle," *Molecular biology of the cell*, vol. 23, no. 3, pp. 464–479, 2012.

[26] M. van der Laan, P. Bechtluft, S. Kol, N. Nouwen, and A. J. Driessen, "F1F0 ATP synthase subunit c is a substrate of the novel YidC pathway for membrane protein biogenesis," *The Journal of cell biology*, vol. 165, no. 2, pp. 213–222, 2004.

[27] S. A. Neugebauer, A. Baulig, A. Kuhn, and S. J. Facey, "Membrane protein insertion of variant MscL proteins occurs at YidC and SecYEG of Escherichia coli," *Journal of molecular biology*, vol. 417, no. 4, pp. 375–386, 2012.

[28] M. Chen, J. C. Samuelson, F. Jiang, M. Muller, A. Kuhn, and R. E. Dalbey, "Direct interaction of YidC with the Sec-independent Pf3 coat protein during its membrane protein insertion," *Journal of Biological Chemistry*, vol. 277, no. 10, pp. 7670–7675, 2002.

[29] A. Gallusser and A. Kuhn, "Initial steps in protein membrane insertion. Bacteriophage M13 procoat protein binds to the membrane surface by electrostatic interaction," *The EMBO journal*, vol. 9, no. 9, pp. 2723–2729, 1990.

[30] N. Celebi, L. Yi, S. J. Facey, A. Kuhn, and R. E. Dalbey, "Membrane biogenesis of subunit II of cytochrome bo oxidase: contrasting requirements for insertion of N-terminal and C-terminal domains," *Journal of molecular biology*, vol. 357, no. 5, pp. 1428–1436, 2006.

[31] C. E. Price and A. J. Driessen, "Conserved negative charges in the transmembrane segments of subunit K of the NADH: Ubiquinone Oxidoreductase determine its dependence on YidC for membrane insertion 2," *Journal of Biological Chemistry*, vol. 285, no. 6, pp. 3575–3581, 2010.

[32] S. Nagamori, I. N. Smirnova, and H. R. Kaback, "Role of YidC in folding of polytopic membrane proteins," *The Journal of cell biology*, vol. 165, no. 1, pp. 53–62, 2004.

[33] L. Zhu, H. R. Kaback, and R. E. Dalbey, "YidC protein, a molecular chaperone for LacY protein folding via the SecYEG protein machinery," *Journal of Biological Chemistry*, vol. 288, no. 39, pp. 28180–28194, 2013.

[34] S. Wagner, O. Pop, G.-J. Haan, L. Baars, G. Koningstein, M. M. Klepsch, P. Genevaux, J. Luirink, and J.-W. de Gier, "Biogenesis of MalF and the MalFGK2 maltose transport complex in Escherichia coli requires YidC," *Journal of Biological Chemistry*, vol. 283, no. 26, pp. 17881–17890, 2008.

[35] T. Ritchie, Y. Grinkova, T. Bayburt, I. Denisov, J. Zolnerciks, W. Atkins, and S. Sligar, "Reconstitution of membrane proteins in phospholipid bilayer nanodiscs," *Methods in enzymology*, vol. 464, pp. 211–231, 2009.

[36] M. Kamel, M. Löwe, S. Schott-Verdugo, H. Gohlke, and A. Kedrov, "Unsaturated fatty acids augment protein transport via the SecA: SecYEG translocon," *The FEBS journal*, vol. 289, no. 1, pp. 140–162, 2022.

[37] S. C. Lee, T. J. Knowles, V. L. Postis, M. Jamshad, R. A. Parslow, Y.-P. Lin, A. Goldman, P. Sridhar, M. Overduin, S. P. Muench, *et al.*, "A method for detergent-free isolation of membrane proteins in their local lipid environment," *Nature protocols*, vol. 11, no. 7, pp. 1149–1162, 2016.

[38] D. J. Klein, P. B. Moore, and T. A. Steitz, "The contribution of metal ions to the structural stability of the large ribosomal subunit," *Rna*, vol. 10, no. 9, pp. 1366–1379, 2004.

[39] A. S. Petrov, C. R. Bernier, C. Hsiao, C. D. Okafor, E. Tannenbaum, J. Stern, E. Gaucher, D. Schneider, N. V. Hud, S. C. Harvey, *et al.*, "RNA–magnesium–protein interactions in large ribosomal subunit," *The Journal of Physical Chemistry B*, vol. 116, no. 28, pp. 8113–8120, 2012.

[40] G. Akanuma, K. Yamazaki, Y. Yagishi, Y. Iizuka, M. Ishizuka, F. Kawamura, and Y. Kato-Yamada, "Magnesium suppresses defects in the formation of 70S ribosomes as well as in sporulation caused by lack of several individual ribosomal proteins," *Journal of Bacteriology*, vol. 200, no. 18, pp. e00212–18, 2018.

[41] A. O. Oluwole, B. Danielczak, A. Meister, J. O. Babalola, C. Vargas, and S. Keller, "Solubilization of membrane proteins into functional lipid-bilayer nanodiscs using a diisobutylene/maleic acid copolymer," *Angewandte Chemie International Edition*, vol. 56, no. 7, pp. 1919–1924, 2017.

[42] A. O. Oluwole, J. Klingler, B. Danielczak, J. O. Babalola, C. Vargas, G. Pabst, and S. Keller, "Formation of lipid-bilayer nanodiscs by diisobutylene/maleic acid (DIBMA) copolymer," *Langmuir*, vol. 33, no. 50, pp. 14378–14388, 2017.

[43] M. C. Jewett and J. R. Swartz, "Mimicking the Escherichia coli cytoplasmic environment activates long-lived and efficient cell-free protein synthesis," *Biotechnology and bioengineering*, vol. 86, no. 1, pp. 19–26, 2004.

[44] T. Kigawa, T. Yabuki, N. Matsuda, T. Matsuda, R. Nakajima, A. Tanaka, and S. Yokoyama, "Preparation of Escherichia coli cell extract for highly productive cell-free protein expression," *Journal of structural and functional genomics*, vol. 5, pp. 63–68, 2004.

[45] K. H. Nierhaus, "Mg2+, K+, and the ribosome," *Journal of bacteriology*, vol. 196, no. 22, pp. 3817–3819, 2014.

[46] E. Henrich, C. Hein, V. Dötsch, and F. Bernhard, "Membrane protein production in Escherichia coli cell-free lysates," *FEBS letters*, vol. 589, no. 15, pp. 1713–1722, 2015.

[47] S. Bhushan, T. Hoffmann, B. Seidelt, J. Frauenfeld, T. Mielke, O. Berninghausen, D. N. Wilson, and R. Beckmann, "SecM-stalled ribosomes adopt an altered geometry at the peptidyl transferase center," *PLoS biology*, vol. 9, no. 1, p. e1000581, 2011.

[48] H. Muto, H. Nakatogawa, and K. Ito, "Genetically encoded but nonpolypeptide prolyl-tRNA functions in the A site for SecM-mediated ribosomal stall," *Molecular cell*, vol. 22, no. 4, pp. 545–552, 2006.

[49] A. Tsai, G. Kornberg, M. Johansson, J. Chen, and J. D. Puglisi, "The dynamics of SecM-induced translational stalling," *Cell reports*, vol. 7, no. 5, pp. 1521–1533, 2014.

[50] J. Zhang, X. Pan, K. Yan, S. Sun, N. Gao, and S.-F. Sui, "Mechanisms of ribosome stalling by SecM at multiple elongation steps," *Elife*, vol. 4, p. e09684, 2015.

[51] P. McNicholas, R. Salavati, and D. Oliver, "Dual regulation of Escherichia coli secA translation by distinct upstream elements," *Journal of molecular biology*, vol. 265, no. 2, pp. 128–141, 1997.

[52] H. Nakatogawa and K. Ito, "Secretion monitor, SecM, undergoes self-translation arrest in the cytosol," *Molecular cell*, vol. 7, no. 1, pp. 185–192, 2001.

[53] M. E. Butkus, L. B. Prundeanu, and D. B. Oliver, "Translocon "pulling" of nascent SecM controls the duration of its translational pause and secretion-responsive secA regulation," *Journal of bacteriology*, vol. 185, no. 22, pp. 6719–6722, 2003.

[54] F. Cymer, R. Hedman, N. Ismail, and G. von Heijne, "Exploration of the arrest peptide sequence space reveals arrest-enhanced variants," *Journal of Biological Chemistry*, vol. 290, no. 16, pp. 10208–10215, 2015.

[55] N. Kempf, C. Remes, R. Ledesch, T. Züchner, H. Höfig, I. Ritter, A. Katranidis, and J. Fitter, "A novel method to evaluate ribosomal performance in cell-free protein synthesis systems," *Scientific reports*, vol. 7, no. 1, p. 46753, 2017.

[56] P. A. Scotti, Q. A. Valent, E. H. Manting, M. L. Urbanus, A. J. Driessen, B. Oudega, and J. Luirink, "SecA is not required for signal recognition particle-mediated targeting and initial membrane insertion of a nascent inner membrane protein," *Journal of Biological Chemistry*, vol. 274, no. 42, pp. 29883–29888, 1999.

[57] Z. C. Wu, J. de Keyzer, A. Kedrov, and A. J. Driessen, "Competitive binding of the SecA ATPase and ribosomes to the SecYEG translocon," *Journal of Biological Chemistry*, vol. 287, no. 11, pp. 7885–7895, 2012.

[58] R. S. Hegde and R. J. Keenan, "The mechanisms of integral membrane protein biogenesis," *Nature Reviews Molecular Cell Biology*, vol. 23, no. 2, pp. 107–124, 2022.

[59] M. Botte, N. R. Zaccai, J. L. À. Nijeholt, R. Martin, K. Knoops, G. Papai, J. Zou, A. Deniaud, M. Karuppasamy, Q. Jiang, *et al.*, "A central cavity within the holo-translocon suggests a mechanism for membrane protein insertion," *Scientific reports*, vol. 6, no. 1, p. 38399, 2016.

[60] S. C. Hall, C. Tognoloni, J. Charlton, É. C. Bragginton, A. J. Rothnie, P. Sridhar, M. Wheatley, T. J. Knowles, T. Arnold, K. J. Edler, *et al.*, "An acid-compatible co-polymer for the solubilization of membranes and proteins into lipid bilayer-containing nanoparticles," *Nanoscale*, vol. 10, no. 22, pp. 10609–10619, 2018.

[61] N. J. Harris, E. Reading, K. Ataka, L. Grzegorzewski, K. Charalambous, X. Liu, R. Schlesinger, J. Heberle, and P. J. Booth, "Structure formation during translocon-unassisted co-translational membrane protein folding," *Scientific reports*, vol. 7, no. 1, pp. 1–15, 2017.

[62] O. Peetz, E. Henrich, A. Laguerre, F. Löhr, C. Hein, V. Dötsch, F. Bernhard, and N. Morgner, "Insights into cotranslational membrane protein insertion by combined LILBID-mass spectrometry and NMR spectroscopy," *Analytical chemistry*, vol. 89, no. 22, pp. 12314–12318, 2017.

[63] J. J. Lichty, J. L. Malecki, H. D. Agnew, D. J. Michelson-Horowitz, and S. Tan, "Comparison of affinity tags for protein purification," *Protein expression and purification*, vol. 41, no. 1, pp. 98–105, 2005.

[64] G. A. Pellowe, H. E. Findlay, K. Lee, T. M. Gemeinhardt, L. R. Blackholly, E. Reading, and P. J. Booth, "Capturing membrane protein ribosome nascent chain complexes in a native-like environment for co-translational studies," *Biochemistry*, vol. 59, no. 30, pp. 2764–2775, 2020.

[65] K. Dao Duc, S. S. Batra, N. Bhattacharya, J. H. Cate, and Y. S. Song, "Differences in the path to exit the ribosome across the three domains of life," *Nucleic acids research*, vol. 47, no. 8, pp. 4198–4210, 2019.

[66] E. van Bloois, G.-J. Haan, J.-W. de Gier, B. Oudega, and J. Luirink, "Distinct requirements for translocation of the N-tail and C-tail of the Escherichia coli inner membrane protein CyoA," *Journal of Biological Chemistry*, vol. 281, no. 15, pp. 10002–10009, 2006.

[67] S. Fiedler, M. A. Piziorska, V. Denninger, A. S. Morgunov, A. Ilsley, A. Y. Malik, M. M. Schneider, S. R. Devenish, G. Meisl, V. Kosmoliaptsis, *et al.*, "Antibody affinity governs the inhibition of SARS-CoV-2 spike/ACE2 binding in patient serum," *ACS Infectious Diseases*, vol. 7, no. 8, pp. 2362–2369, 2021.

[68] K. Byrgazov, O. Vesper, and I. Moll, "Ribosome heterogeneity: another level of complexity in bacterial translation regulation," *Current opinion in microbiology*, vol. 16, no. 2, pp. 133–139, 2013.

Chapter 7

Discussion

The Sec translocon is a universal conserved system responsible for transporting proteins into and across the cytoplasmic membrane in bacteria, and the endoplasmic reticulum in eukaryotes. In a simple view, the Sec translocon performs these two functions in two different modes. Transport across the membrane occurs in a post-translational mode, while transport to the membrane for insertion occurs in a co-translational mode. The main component of the Sec translocon is the membrane-embedded channel, called SecYEG in bacteria and Sec$\alpha\gamma\beta$ in eukaryotes.

This work combined the use of different membrane mimetic systems with the biochemical and biophysical characterization of key important steps to gain more insight into both the post-translational and co-translational pathways of the Sec translocon.

7.1 The effect of the membrane on the SecYEG: SecA translocon

7.1.1 Unsaturated fatty acids stimulate protein transport

In bacteria, the post-translational transport of protein across the cytoplasmic membrane is mediated by the peripheral membrane protein, SecA. SecA is an ATPase motor protein that hydrolyzes ATP to provide energy for protein transport. It is mainly composed of two major domains, the motor part, and the translocase part. SecA needs to bind the membrane to perform its function, where it undergoes two-dimensional diffusion to find the SecYEG channel [1]. Earlier reports showed that half of the SecA is localized in the cytoplasm, while the other half is localized in the membrane [2], however, a new single-molecule microscopy study showed that most of the cellular pool of SecA exists in the membrane [3].

The physicochemical properties of the membrane are determined by the diversity of lipids that form the membrane. Lipids can also form functional membrane domains, and promote specific interactions with membrane-associated proteins. The function of different membrane-associated proteins and complexes can be regulated by the bulk and local properties of the surrounding membrane [4]. The membrane lipids have been shown to play an essential role in protein transport across the SecYEG: SecA translocon. Anionic lipids like phosphatidylglycerol and cardiolipin are essential for protein transport [5–7]. An accepted reason for the necessity of anionic lipids is their role in mediating the membrane binding of SecA via its N terminal amphipathic helix which contains positive residues [1, 8–10]. In contrast, the effect of the acyl chain composition of the membrane has never been investigated, even though bacteria change their acyl chain composition in response to different environmental and growth conditions. For instance, at lower temperatures bacteria show a high content of unsaturated fatty acids to maintain the fluid state of the membrane, while at higher temperatures, bacteria contain a higher content of saturated fatty acids that help to withstand these temperatures [11–13].

The first aim of this work was to investigate how the acyl chain composition of the membrane affects protein transport through the SecYEG: SecA translocon. Additionally, it aimed to determine the specific role of the different anionic lipids in the membrane. Different reports have explained the role of cardiolipin, where some reports show that cardiolipin is essential and stimulate protein transport [14], while other shows that cardiolipin has no further role compared to phosphatidylglycerol [15, 16]. In this work, the protein transport experiments were performed

in an *in vitro* minimalistic system in the absence of the proton motive force and other auxiliary components like SecDFYajC which has been shown to stimulate protein transport [17–19]. The minimalistic system allowed for the resolution of the stimulatory effect of UFAs, which might have been difficult to resolve based on an *in vivo* complex system. Using an *in vitro* reconstituted system based on proteoliposomes, first the SecA: SecYEG translocon has been shown to be not functional in a gel phase membrane, and second the protein transport activity is sensitive to the content of monounsaturated fatty acids (UFAs) in the membrane. Protein transport is substantially higher (up to fivefold) in membranes with 100 % UFAs compared to membranes containing 50 % UFAs. Moreover, cardiolipin stimulates protein transport but only when a UFA-rich variant is used.

Though in the membranes of gram-negative bacteria, the content of UFAs never riches 100 %. However, it is noteworthy to mention that bacteria adapt to low temperatures by increasing the content of UFAs, branched-chain fatty acids, and short-chain fatty acids [13]. Earlier reports showed *E.coli* inner membrane has approximately 65% mono-UFAs when grown at 17°C compared to 49% when grown at 37°C [20]. Similar behavior was observed for the gram-negative bacteria *P. aeruginosa* which showed approximately 60% mono-UFAs at 15°C compared to 37% at 45 °C growth temperature [12]. Our data showed that the transport activity of the SecYEG: SecA translocon was already stimulated when the content of mono-UFA content increased from 50 % to 60 and 70% which correlates well with the physiological content of UFAs at the low growth temperature. Additionally, it has been reported that the mono-UFAs rich cardiolipin is the most abundant cardiolipin in *E. coli* membranes [21]. It is also noteworthy to mention local enrichment of mono-UFAs around the translocon could also occur. This is supported by the fact that both PG and CL have been reported to have specific contacts with the SecY: SecA translocon by MD simulations [22, 23]. Therefore, it is reasonable to assume that stimulatory effect of mono-UFAs might play an important role *in vivo*. For instance, they will promote the membrane-bound state of SecA at low temperature, thus promoting protein transport to compensate for kinetic decay.

It is quite challenging to resolve the exact role of UFAs *in vivo*. Nevertheless, one can purify lipid extracts from bacteria that were grown at low and high temperatures. Reconstituting the translocon in these native membrane extracts and performing the *in vitro* transport assay can further confirm the results complemented by mass spectrometry analysis of the membrane extracts.

7.1.2 SecA binds preferentially to mono-UFAs rich membranes

The membrane-embedded channel SecYEG or the motor protein SecA or both can contribute to the sensitivity to UFAs content in the membrane. The initial results showed that the stability and folding of SecYEG was not affected when reconstituted in membranes with different content of mono-UFAs. A more thorough investigation would need to be performed to exclude SecYEG as a possible sensitive component for the UFAs content in the membrane. For instance, monitoring the dynamics of the lateral gate might provide valuable insights. The lateral gate needs to be opened during protein translocation to allow for the insertion of the signal peptide of the substrate into the membrane [24, 25]. Possible experiments are monitoring the lateral gate dynamics using

electron paramagnetic resonance spectroscopy, single-molecule FRET, and MD simulations. Allen et al 2016 showed placing a FRET pair on the residues A103 and V353 of SecY can monitor the opening and the closing of the lateral gate [26]. Taufik et al 2013 also showed that a FRET pair on positions L148 and G313 can also report on the lateral gate dynamics [27].

On the other hand, it has been previously shown that SecA membrane binding is crucial for protein transport [1, 8–10]. Therefore, it was tempting to speculate that SecA might be the sensitive component for the content of UFAs in the membrane via its N-terminal amphipathic helix. The role of amphipathic helices for modulating membrane binding has been reported in many proteins [28]. Pex11 is a peroxisomal protein that can regulate the number of peroxisomes in a cell and induces the tubulation of peroxisomal membranes. Peroxisomes are endoplasmic reticulum-derived organelles that perform key functions in lipid metabolism. Peroxisome division includes several events; peroxisome elongation, membrane constriction, and peroxisome fission. Pex11 mediates the elongation step of peroxisomal division [29]. It has an amphipathic helix that has a positively charged face and a hydrophobic face. It binds strongly to membranes with anionic lipids that mimic the content of peroxisomal membranes, but not to neutral lipids. Both electrostatic and hydrophobic interactions have been shown to play an important role in membrane binding [30]. Some proteins have the so-called, amphipathic helix lipid packing sensor (ALPS) motif, like Arfgap1 and GMAP-210. Arfgap1 is a GTPase activating protein for the small G protein Arf1. Arf1 regulates the formation of transport vesicles by promoting the formation of the COPI coat once in the GTP-bound conformation [31]. GMAP-210 belongs to the family of Golgi-associated proteins, called Golgins. Golgins have been proposed to be responsible for tethering transport vesicles in the vicinity of Golgi cisternae [32]. The binding of the ALPS motif to the membrane is characterized by the ability to sense lipid packing defects caused by either positive membrane curvature or the conical shape of lipids, and it has no dependence on the charge of the lipids. Therefore, it has the ability to bind membranes with higher content of mono-UFAs and highly curved membranes [33, 34]. Opi1, a transcription factor in *Saccaromyces cervisiae* that control the expression of lipid biosynthetic genes has an amphipathic helix that possesses a hydrophilic positively charged face and a hydrophobic face. It has been shown that the membrane binding is improved *in vitro* when the content of UFAs in the membrane is increased from 50 % to 100 % [35].
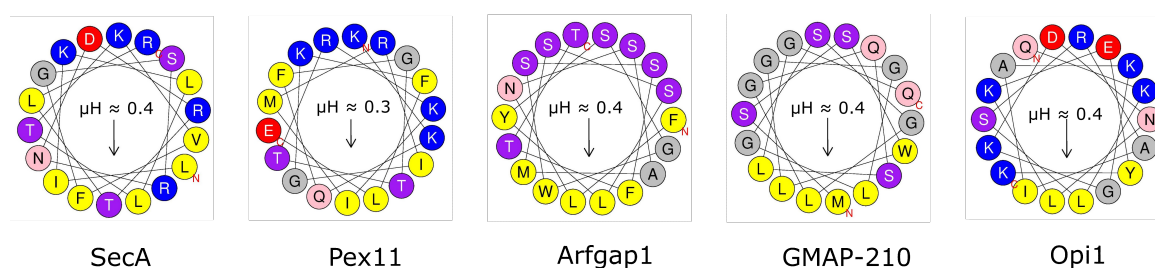
Figure 7.1: Helical wheel projection showing the hydrophilic and hydrophobic faces of different amphipathic helices.

Therefore, by comparing the properties of the N-terminal helix of SecA with the amphipathic helices of these proteins (Figure 7.1), it was expected that similar behavior could be exhibited by SecA. Indeed, this was proven using liposome flotation assay, SPR, and QCM, that SecA binds

preferentially to mono-UFAs-rich membranes. Moreover, this effect becomes more pronounced at higher salt concentrations where the electrostatic interactions between the positively charged residues in the N-terminal helix of SecA and anionic lipids in the membranes are disturbed. Consequently, it was speculated that the N-terminal helix can sense lipid packing defects, and enhances SecA binding to mono-UFAs rich membrane.

To further understand the underlying mechanism for the preference of SecA to mono-UFAs rich membranes, the exact membrane binding domains of SecA were determined. Using HDX-MS, it was discovered that the N-terminal helix and the second half of the helical scaffold domain of SecA interact with the membrane. Both these domains should be facing the membrane based on previously reported structures of SecYEG: SecA complex [36, 37]. The HSD scaffold is expected to interact with the membrane in a later stage after the initial interaction using the N-terminal helix. This is supported by the fact that completely deleting the N-terminal helix abolished membrane binding and that single mutations within this domain only slightly affect membrane binding. However, more thorough investigations need to be performed to elucidate the exact role of the HSD of SecA on membrane binding and protein transport.

7.1.3 Hydrophobic interaction between SecA and the membrane affects protein transport

The N-terminal helix of SecA is split into two helices as predicted by the AlphaFold2 model of SecA, supported by the crystal structure of *B. subtilis* SecA (PDB: 1M6N) [38]. A small helix ($\alpha0$) is followed by a small flexible linker and then a long helix ($\alpha1$). Deleting the $\alpha0$ helix was enough to abolish membrane binding and dramatically reduced protein transport activity which was completely abolished when half of the $\alpha1$ helix was also deleted (first 20 residues). Decreasing the positive charge on the $\alpha1$ helix helix reduced membrane binding, but had little effect on the translocating ATPase activity and protein transport via SecYEG: SecA translocon. Decreasing the hydrophobicity or increasing the polarity of the $\alpha0$ helix reduced both membrane binding and the translocating ATPase activity of SecA. It has been previously shown that SecA inserts into the membrane, with the inserted state being the active translocating state of SecA [39].

Consequently, it is reasonable to conclude that the $\alpha0$ helix mediates hydrophobic interactions with the membrane, promoting SecA insertion and stimulating its translocating ATPase activity. This is also endorsed by an earlier study that showed using protease protection assay that the amount of membrane inserted SecA is drastically reduced by deleting the first helix [39, 40]. While the electrostatic interaction between the helix and the membrane might only be required for the initial membrane recruitment of SecA. Here, one might also speculate that the $\alpha0$ helix might act as a lipid packing sensor that might enhance SecA binding to mono-UFAs-rich membranes. This might explain the stimulatory effect of mono-UFAs on protein transport via the SecYEG: SecA translocon.
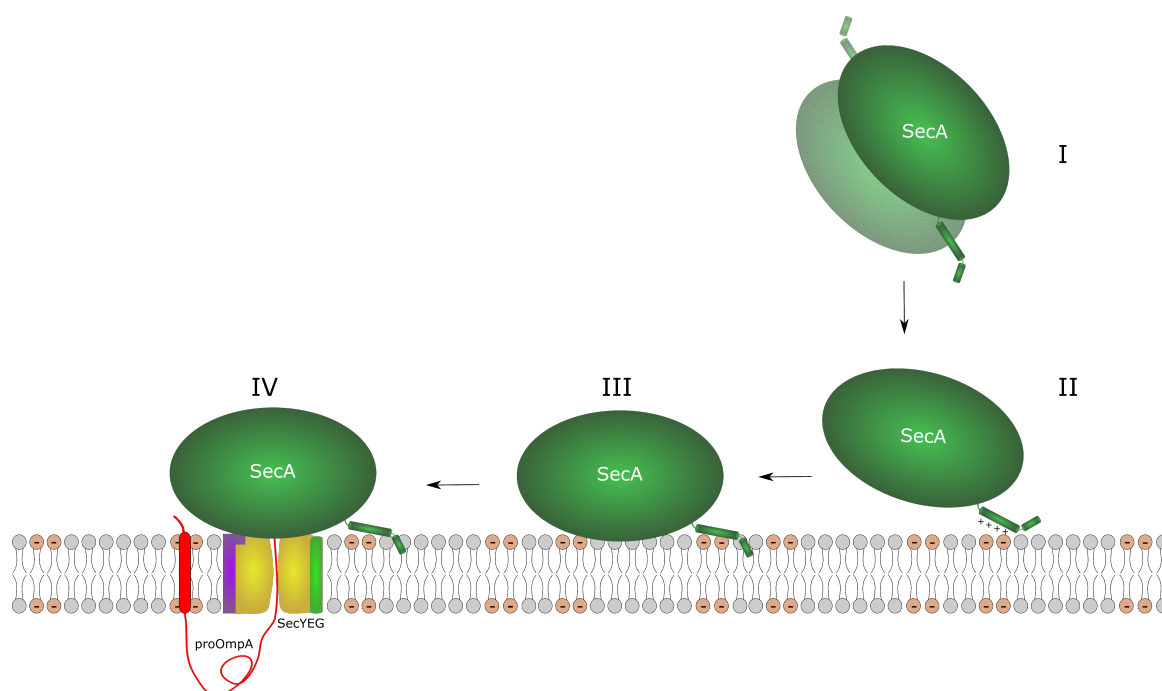
Figure 7.2: A model to describe the interplay between SecA: membrane interaction and protein transport. I) SecA exists as a dimer in the cytoplasm. II) SecA monomerizes once it finds the membrane, and electrostatic interaction between the $\alpha 1$ helix and anionic lipids in the membrane recruits SecA to the membrane. III) The $\alpha 0$ helix inserts into the membrane, and SecA undergoes 2D diffusion to find SecYEG. IV) SecA binds with SecYEG with high affinity and its translocating ATPase activity is stimulated and the protein transport cycle starts.

Therefore, based on these results combined with previous reports, a model was built that explains the interplay between SecA membrane interaction and protein transport. First, SecA exists as a dimer in the cytoplasm, probably the *B. subtilis* dimer (PDB: 1M6N). Once it finds the membrane, the dimer dissociates exposing the $\alpha 1$ helix, which recruits SecA to the membrane via electrostatic interactions. Afterward, the $\alpha 0$ helix inserts into the membrane and SecA undergoes 2D diffusion on the membrane till it finds SecYEG. Once it binds SecYEG, its translocating ATPase activity is stimulated and the protein transport cycle starts (Figure 7.2).

7.1.4   The N-terminal helix regulates SecA: membrane interaction

Different bacterial species have broadly diverse lipid compositions in their membrane. Consequently, it is tempting to predict that the N-terminal helices of SecA homologs have different properties that allow them to interact with the respective membrane. To test this hypothesis, SecA homologs from other gram-negative bacteria (*P. aeruginosa*), gram-positive bacteria (*B. subtilis*), and thermophilic bacteria (*T. maritima*) were purified and tested for membrane binding. Interstingly, all the examined homologs showed a preference for the mono UFAs-rich membrane, which could be explained by the fact that all the helices of the homologs have an amphipathic property (Figure 7.3).

Gram-positive bacteria have a higher content of negatively charged lipids compared to gram-negative bacteria in their cytoplasmic membrane. Investigating the N-terminal helices of different SecA homologs from gram-positive bacteria showed that the helices of these proteins are weakly

positively charged compared to gram-negative bacteria. Therefore, high anionic lipids content in the membrane will still ensure efficient recruitment of SecA to the membrane. This was confirmed by the fact that the *B. subtilis* SecA could only bind efficiently to the membrane when high content of anionic lipids was present. The membrane of the gram-positive bacteria is enriched with branched-chain fatty acids, which have also been shown to induce a disorder in the lipid packing in the membrane, a similar effect to that caused by mono-UFAs in the membrane [41]. Once bound to the membrane via electrostatic interactions, hydrophobic interactions with the exposed hydrophobic groove due to lipid packing disorder in the membrane might stabilize the membrane-bound state of SecA. This could be clearly observed when the binding of the *B. subtilis* SecA was not affected in high salt conditions. Moreover, the N-terminal helix of the *B. subtilis* SecA has two bulky aromatic amino acids in its hydrophobic face (phenylalanine and tyrosine) which might mediate the hydrophobic interactions with the membrane. A similar pattern is also observed from the thermophilic species *Thermus*. The membrane of this species is enriched with branched-chain fatty acids [42], and the N-terminal helix of SecA from this strain is weakly positively charged, while its hydrophobic face is enriched with three aromatic amino acids, two tyrosines, and phenylalanine (Figure 7.3).

The membrane composition of the thermophilic bacteria *Thermotoga maritima* is enriched with membrane-spanning and saturated lipids, therefore, it is predicted here that the electrostatic interactions might play a more important role. This was supported by two pieces of evidence. First, in high salt conditions *T. maritima* SecA substantially loses membrane binding. Second, the crystal structure of the *T. maritima* SecA shows that it lacks the $\alpha 0$ helix, which as mentioned above might mediate hydrophobic interactions with the membrane.

Therefore, this work sheds light on the importance of the N-terminal helix of SecA in regulating the membrane binding of SecA to the different biological membranes. Consequently, this may regulate protein transport through the Sec translocon in the different bacterial species, under different temperatures, growth, and environmental conditions.
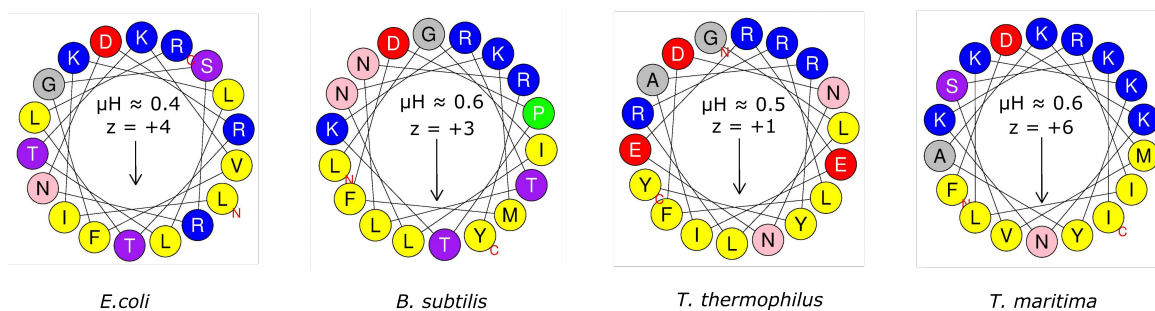
Figure 7.3: Helical wheel projection showing the hydrophilic and hydrophobic faces of the N-terminal helices of SecA from different species. SecA from *E. coli* has a moderately hydrophobic face and a moderately positively charged face. SecA from *B. subtilis* and *T. thermophilus* have a weakly positively charged face and a highly hydrophobic face. While SecA from *T. maritima* has a highly positively charged face and a highly hydrophobic face.

7.2   Probing the dynamics of the Sec translocon

In order to transport protein across or into the membrane, SecYEG interacts either with SecA or ribosome nascent chain complexes (RNCs) respectively. The aim of this part was to investigate the dynamics of the SecYEG channel alone and when bound to both SecA or RNCs in physiologically relevant conditions. To that aim, single-molecule total internal reflection microscopy (TIRFm) was employed to monitor the dynamics of SecYEG that was reconstituted in a supported lipid bilayer. TIRFm is a surface imaging method that has been proven to provide valuable information on the dynamics of membrane protein in the membrane, for instance, diffusion coefficients, oligomeric states, and assembly of protein complexes [43–45].

The exact oligomeric state of SecYEG has been extensively disputed. Detergent solubilized SecYEG can be purified as monomers [36, 46] and dimers [24, 47, 48]. SecYEG dimers have been suggested by crosslinking studies [49–51]. Both front-to-front [48] and back-to-back dimers [24, 47, 49] have been detected with the latter being more logical as it provides a passage for the TMHs and signal peptides to reach the membrane through the lateral gate. Nevertheless, it has been shown that a single copy is sufficient for protein transport and ribosome nascent chain binding [16, 27, 49] and the reported structures show only one copy of SecYEG engaging with either SecA [36, 37, 52, 53] or RNCs [54–56]. Therefore, the physiological relevance of a dimeric SecYEG is not clear. However, it was suggested that even though a single copy is sufficient, a dimeric SecYEG may enhance protein transport and stabilize the interaction with SecA [57, 58].

The dynamics of SecYEG were previously reported, either in supported lipid bilayer using atomic force microscopy [59, 60] or in giant unilamellar vesicles (GUVS) using fluorescence correlation spectroscopy (FCS) [16]. Using brightness analysis of fluorescently-labeled SecYEG, both monomeric and dimeric SecYEG were detected in the membrane with the monomer being approximately three times as abundant as the dimer. This agrees with what was observed in the GUVs-based study, where only monomeric SecYEG was observed [16]. Similarly, AFM imaging showed that both monomeric and dimeric SecYEG exist, but they showed that 40 % of the molecules were in a dimeric state [59]. When SecYEG engaged with SecA, the fraction of the dimeric species increased, consistent with what was previously observed that the dimers stabilize the interaction with SecA [57, 58]. But the fraction of the dimers did not change when SecYEG was engaged with RNCs with a hydrophobic nascent chain.

Single particle tracking was employed to extract trajectories of individual freely diffusing SecYEG molecules. The microscopy glass used was coated with a long amino silane (1.5 nm in length) to prevent the contact of the periplasmic loops of SecYEG with the surface of the glass allowing its free diffusion. Slow and fast diffusion modes were detected for SecYEG molecules and the individual molecule could also switch between the two diffusion modes. The slow diffusion mode might be explained by specific interactions with the lipid molecules. It was recently shown by MD simulations that anionic lipids contact SecYEG in various positions [22, 23]. Therefore, once SecYEG molecules dissociate from these specific lipids contacts, they can switch to the fast diffusing mode.

When SecYEG was bound to SecA, only a slight decrease in the fast diffusion coefficient was observed, in good agreement with what was previously measured in GUVs using FCS. However, RNCs with a hydrophobic nascent chain decreased the fast diffusion coefficient of SecYEG by

30%. This can be explained by the interaction of the ribosomes with both the cytoplasmic loops of SecY and the proximate lipid bilayer. It was previously reported that rRNA helix H59 of the ribosome interacts with the lipid bilayer [61]. Structural rearrangements within SecYEG itself might also contribute to the decrease in the diffusion coefficient.

Single-molecule observations of biological processes can provide valuable information about complex molecular mechanisms. Here, this single-molecule setup provided some insights into the dynamics of SecYEG in native-like membranes. The same setup can then be further utilized to describe the dynamics of the membrane protein insertase, YidC. YidC has been shown to function as a monomer. However, dimers have also been detected [62, 63]. Therefore, single-molecule observation of fluorescently- labeled YidC molecules in the bilayer might provide more information about the oligomeric state of YidC and determine its diffusion coefficient when alone or in complex with ribosomes in a similar manner to what was performed here with SecYEG. Moreover, using single-molecule FRET, the assembly of the rather transient complex between SecYEG and YidC can be monitored once a ribosome translating a nascent chain that requires both of them for membrane insertion is provided.

7.3 Reconstitutuion of the bacterial insertion machinery using CFPS for structural studies

The insertion of membrane proteins into the membrane is mediated in a co-translational mode through the Sec translocon [64] or the insertase, YidC [65, 66], or through both of them [67–69]. Different structures of the membrane insertion machinery with ribosomes nascent chains translating membrane proteins have been reported. Despite the fact that these structures provided many valuable insights into the architecture and the mechanism of membrane protein insertion. Nevertheless, many of these structures show the complex in a detergent micelle, which might influence the native interactions between the individual components of the complex [48, 55, 70–72]. Also, many structures report on a late-stage of membrane insertion where the TMH is already inserted into the membrane without a clear explanation of the pathway of the nascent chain to reach this position [55, 61]. Additionally, many of the reported structures were not assembled in a native state, the ribosome nascent chain complexes (RNCs) and the insertion machinery were individually purified and mixed in a tube to form the complex [56, 61, 73].

Cell-free protein synthesis (CFPS) has developed as an attractive approach for expressing and producing different protein and macromolecular complexes for structural biology [74]. It has also been successfully used to express and produce milligram amounts of membrane proteins from both prokaryotes and eukaryotes [75, 76]. Moreover, it has been used for the co-translational spontaneous insertion of membrane proteins into nanodiscs [77, 78]. Membrane proteins were also directly reconstituted in nanodiscs from CFPS reactions [79]. Interestingly, the CFPS of the Sec translocon itself and its insertion into liposomes was reported. It was then further used for the translocation of the precursor of the outer membrane protein A, and the insertion of the LepB and YidC into the membrane [80]. The membrane insertion and the activity of the multidrug resistance protein, EmrE was improved when liposomes containing the *in vitro* transcription-translation system with reconstituted SecYEG were used [81]. Similarly, the insertion of the LeuT

was also checked using CFPS reactions supplied with SecYEG proteoliposomes [82]. Therefore, CFPS is a very attractive approach to be employed to study mechanisms behind membrane protein biogenesis.

In this work, CFPS was used to co-translationally form a complex between RNCs and the membrane protein insertion machinery reconstituted beforehand in nanodiscs. The CFPS setup allowed for the co-translational assembly of the complex since the ribosomes that are actively translating the nascent chain of interest can directly engage with the supplied SecYEG/YidC-containing nanodiscs that contain the insertion machinery. Different types of nanodiscs were also employed. The typical membrane scaffold protein-based nanodiscs were used as they provided an easy way to check the performance of the system due to their homogeneity and their extensive use in structural studies. Maleic acid copolymers were also utilized which can directly isolate the insertion machinery from the membrane without the need to use any detergents providing a native environment. DIBMA was the chosen copolymer as it can tolerate high concentrations of magnesium ions supplied to the reaction to ensure the integrity of the 70S ribosomes. Moreover, DIBMA does not interfere with the UV absorbance of proteins facilitating the estimation of their concentration [83].

It is a very appealing idea to directly use DIBMA copolymer to isolate the insertion machinery in complex with RNCs that were formed *in vivo*. And, it was previously reported that DIBMA was used to purify membrane-attached RNCs directly from the membrane [84]. However, this is in conflict with our own observation that mixing DIBMA at membrane solubilizing concentrations with purified RNCs caused the aggregation of the 70S ribosomes. Still, it is noteworthy to mention that in this experiment only DIBMA and RNCs were present, but when used in a more complex environment like membranes, the majority of DIBMA molecules might have served to solubilize the membrane decreasing its destructive ability on ribosomes. Therefore, a sufficient amount of RNCs could still be purified providing a reasonable argument to employ this strategy to isolate the complex.

A modified version of the well-known arrest peptide, SecM was introduced in the constructs to stall the ribosomes and trap an insertion intermediate [85, 86]. The arrest peptide prevents the full insertion of the nascent chain into the lipid bilayer of the nanodisc and the disassembly of the RNCs- insertion machinery complex. This allows trapping an intermediate state of membrane protein insertion. Using an in-house established CFPS setup, successful complexes between FtsQ RNCs and SecYEG in either MSP2N2 or DIBMA nanodiscs were co-translationally assembled. Similar results were also obtained for YidC in MSP1D1 nanodiscs with both MscL and F_oc RNCs were obtained.

A first cryo-EM analysis trial was performed and no nanodiscs were observed at the exit tunnel of the ribosome. This could be explained by a loosely bound state of the SecYEG to the ribosomes, either due to the long GSG linker that was present in the construct used or due to the complete insertion of the nascent chain into the membrane. The long GSG linker might have also promoted the release of the nascent chain from the exit causing the disassembly of the whole complex. Therefore, the GSG linker was shortened to decrease the flexibility, and it lead to decreasing the release of the nascent chain from the ribosome exit tunnel. Another possible reason is the disassembly of the complex due to freezing and thawing before preparing the cryo-

EM grids. Thereby, preparing the sample in situ just before preparing the grids should eliminate this problem. Once all these reasons were fixed, our recent cryo-EM analysis showed the presence of the SecYEG MSP2N2 at the ribosome exit tunnel confirming the reliability of the established platform.

This setup can be further employed, for instance when using nascent chains stalled at different lengths to provide different snapshots of the insertion pathway through SecYEG, or YidC. Moreover, the structure of the SecYEG- YidC- RNCs complex could be obtained using a nascent chain that requires both of them for insertion. FtsQ can be a good example since crosslinking studies showed that it contacts both SecYEG and YidC during membrane insertion [87]. NuoK and CyoA are other suitable candidates since they have been reported to require both SecYEG and YidC for membrane insertion [67–69]. Again, constructs that are stalled at different lengths can be generated to provide different snapshots of the insertion pathway. SecYEG- YidC complex has been reported to be a transient complex, consequently it is quite challenging to purify and get the structure of this complex to this date. A construct was generated that contain a fusion protein between YidC and SecE separated by a 3C cleavage site, SecY and SecG in the same construct. This fusion protein was successfully purified and reconstituted in MSP2N2 and DIBMA nanodiscs. The YidC and SecE could then be uncoupled by the 3C protease and the complex can then assemble naturally and be trapped once a ribosome translating a nascent chain that requires both proteins for insertion is supplied.

Therefore, this work provided a reliable platform that can be easily employed for the co-translational assembly and the *in-vitro* reconstitution of the membrane protein insertion pathway (Figure 7.4). Additionally, it provided the initial steps towards obtaining the structure and understanding the mechanism of membrane protein biogenesis using a native-like environment.
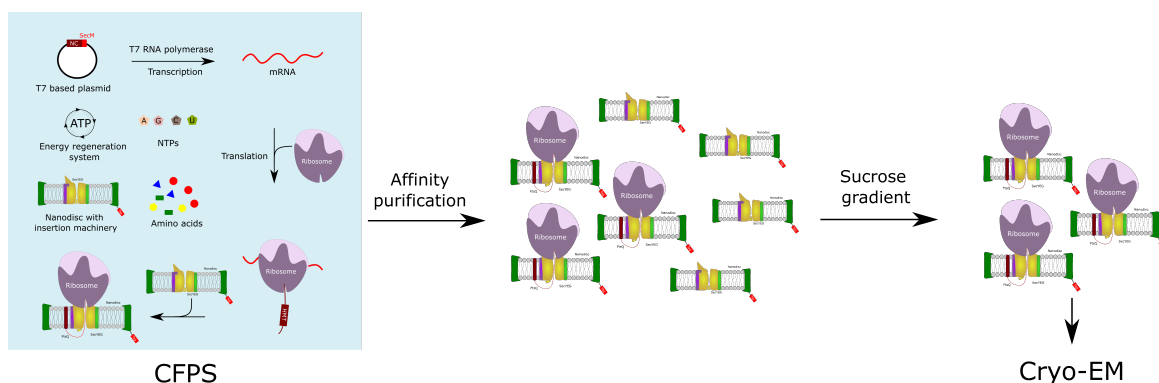
Figure 7.4: The established platform for the in vitro reconstitution and the co-translational assembly of the membrane protein insertion pathway.

References

[1] S. Koch, J. G. de Wit, I. Vos, J. P. Birkner, P. Gordiichuk, A. Herrmann, A. M. van Oijen, and A. J. Driessen, "Lipids activate SecA for high affinity binding to the SecYEG complex," *Journal of Biological Chemistry*, vol. 291, no. 43, pp. 22534–22543, 2016.

[2] R. Cabelli, K. M. Dolan, L. Qian, and D. B. Oliver, "Characterization of membrane-associated and soluble states of SecA protein from wild-type and SecA51 (ts) mutant strains of Escherichia coli.," *Journal of Biological Chemistry*, vol. 266, no. 36, pp. 24420–24427, 1991.

[3] A.-B. Seinen, D. Spakman, A. M. van Oijen, and A. J. Driessen, "Cellular dynamics of the SecA ATPase at the single molecule level," *Scientific reports*, vol. 11, no. 1, pp. 1–16, 2021.

[4] V. Corradi, B. I. Sejdiu, H. Mesa-Galloso, H. Abdizadeh, S. Y. Noskov, S. J. Marrink, and D. P. Tieleman, "Emerging diversity in lipid–protein interactions," *Chemical reviews*, vol. 119, no. 9, pp. 5775–5848, 2019.

[5] T. De Vrije, R. De Swart, W. Dowhan, J. Tommassen, and B. De Kruijff, "Phosphatidylglycerol is involved in protein translocation across Escherichia coli inner membranes," *Nature*, vol. 334, no. 6178, pp. 173–175, 1988.

[6] R. Lill, W. Dowhan, and W. Wickner, "The ATPase activity of SecA is regulated by acidic phospholipids, SecY, and the leader and mature domains of precursor proteins," *Cell*, vol. 60, no. 2, pp. 271–280, 1990.

[7] E. Breukink, R. A. Demel, G. De Korte-Kool, and B. De Kruijff, "SecA insertion into phospholipids is stimulated by negatively charged lipids and inhibited by ATP: a monolayer study," *Biochemistry*, vol. 31, no. 4, pp. 1119–1124, 1992.

[8] J. Hendrick and W. Wickner, "SecA protein needs both acidic phospholipids and SecY/E protein for functional high-affinity binding to the Escherichia coli plasma membrane.," *Journal of Biological Chemistry*, vol. 266, no. 36, pp. 24596–24600, 1991.

[9] J. H. Floyd, Z. You, Y.-H. Hsieh, Y. Ma, H. Yang, and P. C. Tai, "The dispensability and requirement of SecA N-terminal aminoacyl residues for complementation, membrane binding, lipid-specific domains and channel activities," *Biochemical and biophysical research communications*, vol. 453, no. 1, pp. 138–142, 2014.

[10] B. W. Bauer, T. Shemesh, Y. Chen, and T. A. Rapoport, "A "push and slide" mechanism allows sequence-insensitive translocation of secretory proteins by the SecA ATPase," *Cell*, vol. 157, no. 6, pp. 1416–1429, 2014.

[11] A. G. Marr and J. L. Ingraham, "Effect of temperature on the composition of fatty acids in Escherichia coli," *Journal of bacteriology*, vol. 84, no. 6, pp. 1260–1267, 1962.

[12] A. Kropinski, V. Lewis, and D. Berry, "Effect of growth temperature on the lipids, outer membrane proteins, and lipopolysaccharides of Pseudomonas aeruginosa PAO," *Journal of bacteriology*, vol. 169, no. 5, pp. 1960–1966, 1987.

[13] M. F. Siliakus, J. van der Oost, and S. W. Kengen, "Adaptations of archaeal and bacterial membranes to variations in temperature, pH and pressure," *Extremophiles*, vol. 21, pp. 651–670, 2017.

[14] V. A. Gold, A. Robson, H. Bao, T. Romantsov, F. Duong, and I. Collinson, "The action of cardiolipin on the bacterial translocon," *Proceedings of the National Academy of Sciences*, vol. 107, no. 22, pp. 10044–10049, 2010.

[15] B. K. Tan, M. Bogdanov, J. Zhao, W. Dowhan, C. R. Raetz, and Z. Guan, "Discovery of a cardiolipin synthase utilizing phosphatidylethanolamine and phosphatidylglycerol as substrates," *Proceedings of the National Academy of Sciences*, vol. 109, no. 41, pp. 16504–16509, 2012.

[16] A. Kedrov, I. Kusters, V. V. Krasnikov, and A. J. Driessen, "A single copy of SecYEG is sufficient for preprotein translocation," *The EMBO journal*, vol. 30, no. 21, pp. 4387–4397, 2011.

[17] A. Driessen and W. Wickner, "Proton transfer is rate-limiting for translocation of precursor proteins by the Escherichia coli translocase.," *Proceedings of the National Academy of Sciences*, vol. 88, no. 6, pp. 2471–2475, 1991.

[18] F. Duong and W. Wickner, "The SecDFyajC domain of preprotein translocase controls preprotein movement by regulating SecA membrane cycling," *The EMBO journal*, vol. 16, no. 16, pp. 4871–4879, 1997.

[19] T. Tsukazaki, H. Mori, Y. Echizen, R. Ishitani, S. Fukai, T. Tanaka, A. Perederina, D. G. Vassylyev, T. Kohno, A. D. Maturana, *et al.*, "Structure and function of a membrane component SecDF that enhances protein export," *Nature*, vol. 474, no. 7350, pp. 235–238, 2011.

[20] S. Morein, A.-S. Andersson, L. Rilfors, and G. Lindblom, "Wild-type Escherichia coli Cells Regulate the Membrane Lipid Composition in a "Window" between Gel and Non-lamellar Structures ," *Journal of Biological Chemistry*, vol. 271, no. 12, pp. 6801–6809, 1996.

[21] I. Prabudiansyah, I. Kusters, A. Caforio, and A. J. Driessen, "Characterization of the annular lipid shell of the Sec translocon," *Biochimica et Biophysica Acta (BBA)-Biomembranes*, vol. 1848, no. 10, pp. 2050–2056, 2015.

[22] R. A. Corey, E. Pyle, W. J. Allen, D. W. Watkins, M. Casiraghi, B. Miroux, I. Arechaga, A. Politis, and I. Collinson, "Specific cardiolipin–SecY interactions are required for proton-motive force stimulation of protein secretion," *Proceedings of the National Academy of Sciences*, vol. 115, no. 31, pp. 7967–7972, 2018.

[23] S. Koch, M. Exterkate, C. A. López, M. Patro, S. J. Marrink, and A. J. Driessen, "Two distinct anionic phospholipid-dependent events involved in SecA-mediated protein translocation," *Biochimica et Biophysica Acta (BBA)-Biomembranes*, vol. 1861, no. 11, p. 183035, 2019.

[24] D. Hizlan, A. Robson, S. Whitehouse, V. A. Gold, J. Vonck, D. Mills, W. Kühlbrandt, and I. Collinson, "Structure of the SecY complex unlocked by a preprotein mimic," *Cell reports*, vol. 1, no. 1, pp. 21–28, 2012.

[25] R. M. Voorhees and R. S. Hegde, "Structure of the Sec61 channel opened by a signal sequence," *Science*, vol. 351, no. 6268, pp. 88–91, 2016.

[26] W. J. Allen, R. A. Corey, P. Oatley, R. B. Sessions, S. A. Baldwin, S. E. Radford, R. Tuma, and I. Collinson, "Two-way communication between SecY and SecA suggests a brownian ratchet mechanism for protein translocation," *Elife*, vol. 5, 2016.

[27] I. Taufik, A. Kedrov, M. Exterkate, and A. J. Driessen, "Monitoring the activity of single translocons," *Journal of Molecular Biology*, vol. 425, no. 22, pp. 4145–4153, 2013.

[28] M. Giménez-Andrés, A. Čopič, and B. Antonny, "The many faces of amphipathic helices," *Biomolecules*, vol. 8, no. 3, p. 45, 2018.

[29] A. Fagarasanu, M. Fagarasanu, and R. A. Rachubinski, "Maintaining peroxisome populations: a story of division and inheritance," *Annu. Rev. Cell Dev. Biol.*, vol. 23, pp. 321–344, 2007.

[30] Ł. Opaliński, J. A. Kiel, C. Williams, M. Veenhuis, and I. J. Van Der Klei, "Membrane curvature during peroxisome fission requires Pex11," *The EMBO Journal*, vol. 30, no. 1, pp. 5–16, 2011.

[31] H. T. McMahon and I. G. Mills, "COP and clathrin-coated vesicle budding: different pathways, common approaches," *Current opinion in cell biology*, vol. 16, no. 4, pp. 379–391, 2004.

[32] A. K. Gillingham and S. Munro, "Finding the Golgi: Golgin coiled-coil proteins show the way," *Trends in cell biology*, vol. 26, no. 6, pp. 399–408, 2016.

[33] G. Drin, J.-F. Casella, R. Gautier, T. Boehmer, T. U. Schwartz, and B. Antonny, "A general amphipathic α-helical motif for sensing membrane curvature," *Nature structural & molecular biology*, vol. 14, no. 2, pp. 138–146, 2007.

[34] M. Magdeleine, R. Gautier, P. Gounon, H. Barelli, S. Vanni, and B. Antonny, "A filter at the entrance of the Golgi that selects vesicles according to size and bulk lipid composition," *Elife*, vol. 5, p. e16988, 2016.

[35] H. F. Hofbauer, M. Gecht, S. C. Fischer, A. Seybert, A. S. Frangakis, E. H. Stelzer, R. Covino, G. Hummer, and R. Ernst, "The molecular recognition of phosphatidic acid by an amphipathic helix in Opi1," *Journal of Cell Biology*, vol. 217, no. 9, pp. 3109–3126, 2018.

[36] J. Zimmer, Y. Nam, and T. A. Rapoport, "Structure of a complex of the ATPase SecA and the protein-translocation channel," *Nature*, vol. 455, no. 7215, pp. 936–943, 2008.

[37] C. Ma, X. Wu, D. Sun, E. Park, M. A. Catipovic, T. A. Rapoport, N. Gao, and L. Li, "Structure of the substrate-engaged SecA-SecY protein translocation machine," *Nature communications*, vol. 10, no. 1, pp. 1–9, 2019.

[38] J. F. Hunt, S. Weinkauf, L. Henry, J. J. Fak, P. McNicholas, D. B. Oliver, and J. Deisenhofer, "Nucleotide control of interdomain interactions in the conformational reaction cycle of SecA," *Science*, vol. 297, no. 5589, pp. 2018–2026, 2002.

[39] G. Gouridis, S. Karamanou, M. F. Sardis, M. A. Schärer, G. Capitani, and A. Economou, "Quaternary dynamics of the SecA motor drive translocase catalysis," *Molecular cell*, vol. 52, no. 5, pp. 655–666, 2013.

[40] S. Das, E. Stivison, E. Folta-Stogniew, and D. Oliver, "Reexamination of the role of the amino terminus of SecA in promoting its dimerization and functional state," *Journal of bacteriology*, vol. 190, no. 21, pp. 7302–7307, 2008.

[41] D. Poger, B. Caron, and A. E. Mark, "Effect of methyl-branched fatty acids on the structure of lipid bilayers," *The Journal of Physical Chemistry B*, vol. 118, no. 48, pp. 13838–13848, 2014.

[42] Y.-L. Yang, F.-L. Yang, S.-C. Jao, M.-Y. Chen, S.-S. Tsay, W. Zou, and S.-H. Wu, "Structural elucidation of phosphoglycolipids from strains of the bacterial thermophiles Thermus and Meiothermus," *Journal of lipid research*, vol. 47, no. 8, pp. 1823–1832, 2006.

[43] P. A. Nguyen, C. M. Field, A. C. Groen, T. J. Mitchison, and M. Loose, "Using supported bilayers to study the spatiotemporal organization of membrane-bound proteins," in *Methods in cell biology*, vol. 128, pp. 223–241, Elsevier, 2015.

[44] E. M. Kudalkar, T. N. Davis, and C. L. Asbury, "Single-molecule total internal reflection fluorescence microscopy," *Cold Spring Harbor Protocols*, vol. 2016, no. 5, pp. pdb–top077800, 2016.

[45] S. Wilmes, M. Hafer, J. Vuorio, J. A. Tucker, H. Winkelmann, S. Löchte, T. A. Stanly, K. D. Pulgar Prieto, C. Poojari, V. Sharma, *et al.*, "Mechanism of homodimeric cytokine receptor activation and dysregulation by oncogenic mutations," *Science*, vol. 367, no. 6478, pp. 643–652, 2020.

[46] B. V. D. Berg, W. M. Clemons, I. Collinson, Y. Modis, E. Hartmann, S. C. Harrison, and T. A. Rapoport, "X-ray structure of a protein-conducting channel," *nature*, vol. 427, no. 6969, pp. 36–44, 2004.

[47] C. Breyton, W. Haase, T. A. Rapoport, W. Kühlbrandt, and I. Collinson, "Three-dimensional structure of the bacterial protein-translocation complex SecYEG," *Nature*, vol. 418, no. 6898, pp. 662–665, 2002.

[48] K. Mitra, C. Schaffitzel, T. Shaikh, F. Tama, S. Jenni, C. L. Brooks III, N. Ban, and J. Frank, "Structure of the E. coli protein-conducting channel bound to a translating ribosome," *Nature*, vol. 438, no. 7066, pp. 318–324, 2005.

[49] K. Deville, V. A. Gold, A. Robson, S. Whitehouse, R. B. Sessions, S. A. Baldwin, S. E. Radford, and I. Collinson, "The oligomeric state and arrangement of the active bacterial translocon," *Journal of Biological Chemistry*, vol. 286, no. 6, pp. 4659–4669, 2011.

[50] S. Das and D. B. Oliver, "Mapping of the SecA· SecY and SecA· SecG interfaces by site-directed in vivo photocross-linking," *Journal of Biological Chemistry*, vol. 286, no. 14, pp. 12371–12380, 2011.

[51] Z. Zheng, A. Blum, T. Banerjee, Q. Wang, V. Dantis, and D. Oliver, "Determination of the oligomeric state of SecYEG protein secretion channel complex using in vivo photo-and disulfide cross-linking," *Journal of Biological Chemistry*, vol. 291, no. 11, pp. 5997–6010, 2016.

[52] L. Li, E. Park, J. Ling, J. Ingram, H. Ploegh, and T. A. Rapoport, "Crystal structure of a substrate-engaged SecY protein-translocation channel," *Nature*, vol. 531, no. 7594, pp. 395–399, 2016.

[53] L. Dong, S. Yang, J. Chen, X. Wu, D. Sun, C. Song, and L. Li, "Structural basis of SecA-mediated protein translocation," *Proceedings of the National Academy of Sciences*, vol. 120, no. 2, p. e2208070120, 2023.

[54] E. Park, J.-F. Ménétret, J. C. Gumbart, S. J. Ludtke, W. Li, A. Whynot, T. A. Rapoport, and C. W. Akey, "Structure of the SecY channel during initiation of protein translocation," *Nature*, vol. 506, no. 7486, pp. 102–106, 2014.

[55] L. Bischoff, S. Wickles, O. Berninghausen, E. O. Van Der Sluis, and R. Beckmann, "Visualization of a polytopic membrane protein during SecY-mediated membrane insertion," *Nature communications*, vol. 5, no. 1, p. 4103, 2014.

[56] L. Kater, B. Frieg, O. Berninghausen, H. Gohlke, R. Beckmann, and A. Kedrov, "Partially inserted nascent chain unzips the lateral gate of the Sec translocon," *EMBO reports*, vol. 20, no. 10, p. e48191, 2019.

[57] K. Dalal, C. S. Chan, S. G. Sligar, and F. Duong, "Two copies of the SecY channel and acidic lipids are necessary to activate the SecA translocation ATPase," *Proceedings of the National Academy of Sciences*, vol. 109, no. 11, pp. 4104–4109, 2012.

[58] A. R. Osborne and T. A. Rapoport, "Protein translocation is mediated by oligomers of the SecY complex with one SecY copy forming the channel," *Cell*, vol. 129, no. 1, pp. 97–110, 2007.

[59] R. R. S. Gari, N. C. Frey, C. Mao, L. L. Randall, and G. M. King, "Dynamic structure of the translocon SecYEG in membrane: direct single molecule observations," *Journal of Biological Chemistry*, vol. 288, no. 23, pp. 16848–16854, 2013.

[60] R. R. Sanganna Gari, K. Chattrakun, B. P. Marsh, C. Mao, N. Chada, L. L. Randall, and G. M. King, "Direct visualization of the E. coli Sec translocase engaging precursor proteins in lipid bilayers," *Science Advances*, vol. 5, no. 6, p. eaav9404, 2019.

[61] J. Frauenfeld, J. Gumbart, E. O. v. d. Sluis, S. Funes, M. Gartmann, B. Beatrix, T. Mielke, O. Berninghausen, T. Becker, K. Schulten, *et al.*, "Cryo-EM structure of the ribosome–SecYE complex in the membrane environment," *Nature structural & molecular biology*, vol. 18, no. 5, pp. 614–621, 2011.

[62] R. Kohler, D. Boehringer, B. Greber, R. Bingel-Erlenmeyer, I. Collinson, C. Schaffitzel, and N. Ban, "YidC and Oxa1 form dimeric insertion pores on the translating ribosome," *Molecular cell*, vol. 34, no. 3, pp. 344–353, 2009.

[63] D. Spann, E. Pross, Y. Chen, R. E. Dalbey, and A. Kuhn, "Each protomer of a dimeric YidC functions as a single membrane insertase," *Scientific reports*, vol. 8, no. 1, p. 589, 2018.

[64] T. Welte, R. Kudva, P. Kuhn, L. Sturm, D. Braig, M. Müller, B. Warscheid, F. Drepper, and H.-G. Koch, "Promiscuous targeting of polytopic membrane proteins to SecYEG or YidC by the Escherichia coli signal recognition particle," *Molecular biology of the cell*, vol. 23, no. 3, pp. 464–479, 2012.

[65] M. van der Laan, P. Bechtluft, S. Kol, N. Nouwen, and A. J. Driessen, "F_1F_0 ATP synthase subunit c is a substrate of the novel YidC pathway for membrane protein biogenesis," *The Journal of cell biology*, vol. 165, no. 2, pp. 213–222, 2004.

[66] S. A. Neugebauer, A. Baulig, A. Kuhn, and S. J. Facey, "Membrane protein insertion of variant MscL proteins occurs at YidC and SecYEG of Escherichia coli," *Journal of molecular biology*, vol. 417, no. 4, pp. 375–386, 2012.

[67] N. Celebi, L. Yi, S. J. Facey, A. Kuhn, and R. E. Dalbey, "Membrane biogenesis of subunit II of cytochrome bo oxidase: contrasting requirements for insertion of N-terminal and C-terminal domains," *Journal of molecular biology*, vol. 357, no. 5, pp. 1428–1436, 2006.

[68] E. van Bloois, G.-J. Haan, J.-W. de Gier, B. Oudega, and J. Luirink, "Distinct requirements for translocation of the N-tail and C-tail of the Escherichia coli inner membrane protein CyoA," *Journal of Biological Chemistry*, vol. 281, no. 15, pp. 10002–10009, 2006.

[69] C. E. Price and A. J. Driessen, "Conserved negative charges in the transmembrane segments of subunit K of the NADH: Ubiquinone Oxidoreductase determine its dependence on YidC for membrane insertion 2," *Journal of Biological Chemistry*, vol. 285, no. 6, pp. 3575–3581, 2010.

[70] J.-F. Menetret, J. Schaletzky, W. M. Clemons, A. R. Osborne, S. S. Skånland, C. Denison, S. P. Gygi, D. S. Kirkpatrick, E. Park, S. J. Ludtke, *et al.*, "Ribosome binding of a single copy of the SecY complex: implications for protein translocation," *Molecular cell*, vol. 28, no. 6, pp. 1083–1092, 2007.

[71] S. Wickles, A. Singharoy, J. Andreani, S. Seemayer, L. Bischoff, O. Berninghausen, J. Soeding, K. Schulten, E. O. van der Sluis, and R. Beckmann, "A structural model of the active ribosome-bound membrane protein insertase YidC," *Elife*, vol. 3, p. e03035, 2014.

[72] R. M. Voorhees, I. S. Fernández, S. H. Scheres, and R. S. Hegde, "Structure of the mammalian ribosome-Sec61 complex to 3.4 Å resolution," *Cell*, vol. 157, no. 7, pp. 1632–1643, 2014.

[73] A. Kedrov, S. Wickles, A. H. Crevenna, E. O. van der Sluis, R. Buschauer, O. Berninghausen, D. C. Lamb, and R. Beckmann, "Structural dynamics of the YidC: ribosome complex during membrane protein biogenesis," *Cell reports*, vol. 17, no. 11, pp. 2943–2954, 2016.

[74] T. Terada, S. Kusano, T. Matsuda, M. Shirouzu, and S. Yokoyama, "Cell-free protein production for structural biology," *Advanced Methods in Structural Biology*, pp. 83–102, 2016.

[75] D. Schwarz, F. Junge, F. Durst, N. Frölich, B. Schneider, S. Reckel, S. Sobhanifar, V. Dötsch, and F. Bernhard, "Preparative scale expression of membrane proteins in Escherichia coli-based continuous exchange cell-free systems," *Nature protocols*, vol. 2, no. 11, pp. 2945–2957, 2007.

[76] E. Henrich, V. Dotsch, and F. Bernhard, "Screening for lipid requirements of membrane proteins by combining cell-free expression with nanodiscs," in *Methods in enzymology*, vol. 556, pp. 351–369, Elsevier, 2015.

[77] N. J. Harris, E. Reading, K. Ataka, L. Grzegorzewski, K. Charalambous, X. Liu, R. Schlesinger, J. Heberle, and P. J. Booth, "Structure formation during translocon-unassisted co-translational membrane protein folding," *Scientific reports*, vol. 7, no. 1, pp. 1–15, 2017.

[78] O. Peetz, E. Henrich, A. Laguerre, F. Löhr, C. Hein, V. Dötsch, F. Bernhard, and N. Morgner, "Insights into cotranslational membrane protein insertion by combined LILBID-mass spectrometry and NMR spectroscopy," *Analytical chemistry*, vol. 89, no. 22, pp. 12314–12318, 2017.

[79] E. Henrich, O. Peetz, C. Hein, A. Laguerre, B. Hoffmann, J. Hoffmann, V. Dötsch, F. Bernhard, and N. Morgner, "Analyzing native membrane protein assembly in nanodiscs by combined non-covalent mass spectrometry and synthetic biology," *Elife*, vol. 6, p. e20954, 2017.

[80] H. Matsubayashi, Y. Kuruma, and T. Ueda, "In vitro synthesis of the E. coli Sec translocon from DNA," *Angewandte Chemie*, vol. 126, no. 29, pp. 7665–7668, 2014.

[81] N. Ohta, Y. Kato, H. Watanabe, H. Mori, and T. Matsuura, "In vitro membrane protein synthesis inside Sec translocon-reconstituted cell-sized liposomes," *Scientific Reports*, vol. 6, no. 1, pp. 1–9, 2016.

[82] L. R. Blackholly, N. J. Harris, H. E. Findlay, and P. J. Booth, "Cell-free expression to probe co-translational insertion of an alpha helical membrane protein," *Frontiers in Molecular Biosciences*, vol. 9, p. 52, 2022.

[83] A. O. Oluwole, B. Danielczak, A. Meister, J. O. Babalola, C. Vargas, and S. Keller, "Solubilization of membrane proteins into functional lipid-bilayer nanodiscs using a diisobutylene/maleic acid copolymer," *Angewandte Chemie International Edition*, vol. 56, no. 7, pp. 1919–1924, 2017.

[84] G. A. Pellowe, H. E. Findlay, K. Lee, T. M. Gemeinhardt, L. R. Blackholly, E. Reading, and P. J. Booth, "Capturing membrane protein ribosome nascent chain complexes in a native-like environment for co-translational studies," *Biochemistry*, vol. 59, no. 30, pp. 2764–2775, 2020.

[85] F. Cymer, R. Hedman, N. Ismail, and G. von Heijne, "Exploration of the arrest peptide sequence space reveals arrest-enhanced variants," *Journal of Biological Chemistry*, vol. 290, no. 16, pp. 10208–10215, 2015.

[86] N. Kempf, C. Remes, R. Ledesch, T. Züchner, H. Höfig, I. Ritter, A. Katranidis, and J. Fitter, "A novel method to evaluate ribosomal performance in cell-free protein synthesis systems," *Scientific reports*, vol. 7, no. 1, p. 46753, 2017.

[87] M. L. Urbanus, P. A. Scotti, L. Fröderberg, A. Sääf, J.-W. L. de Gier, J. Brunner, J. C. Samuelson, R. E. Dalbey, B. Oudega, and J. Luirink, "Sec-dependent membrane protein insertion: sequential interaction of nascent FtsQ with SecY and YidC," *EMBO reports*, vol. 2, no. 6, pp. 524–529, 2001.

Chapter 8

Conclusion

In order to gain more insights into protein transport to and across the membrane via the bacterial Sec translocon, this work combined advances in membrane mimetics with biochemical and biophysical characterization. The effect of the membrane on the SecYEG: SecA translocon has been characterized. The dynamics of SecYEG in the membrane have been addressed. A reliable platform for the assembly of the bacterial membrane protein insertion pathway has been established.

To sum up, this work has provided the following findings (Figure 8.1):

1. Mono-UFAs stimulate protein transport across the SecYEG: SecA translocon.

2. The motor protein, SecA interacts with the membrane via both electrostatic and hydrophobic interactions.

3. The hydrophobic interactions of SecA with the membrane promote SecA insertion and stimulate its translocating ATPase activity.

4. The N-terminal helix of SecA regulates SecA homologs from different species binding to different membranes.

5. Observing SecYEG at the single-molecule level reveals variations in the lateral diffusion within the membrane and the dynamics of its quaternary state.

6. Established platform for the co-translational assembly of the membrane insertion pathway is to be further utilized for studying membrane protein biogenesis by structural and biophysical methods.
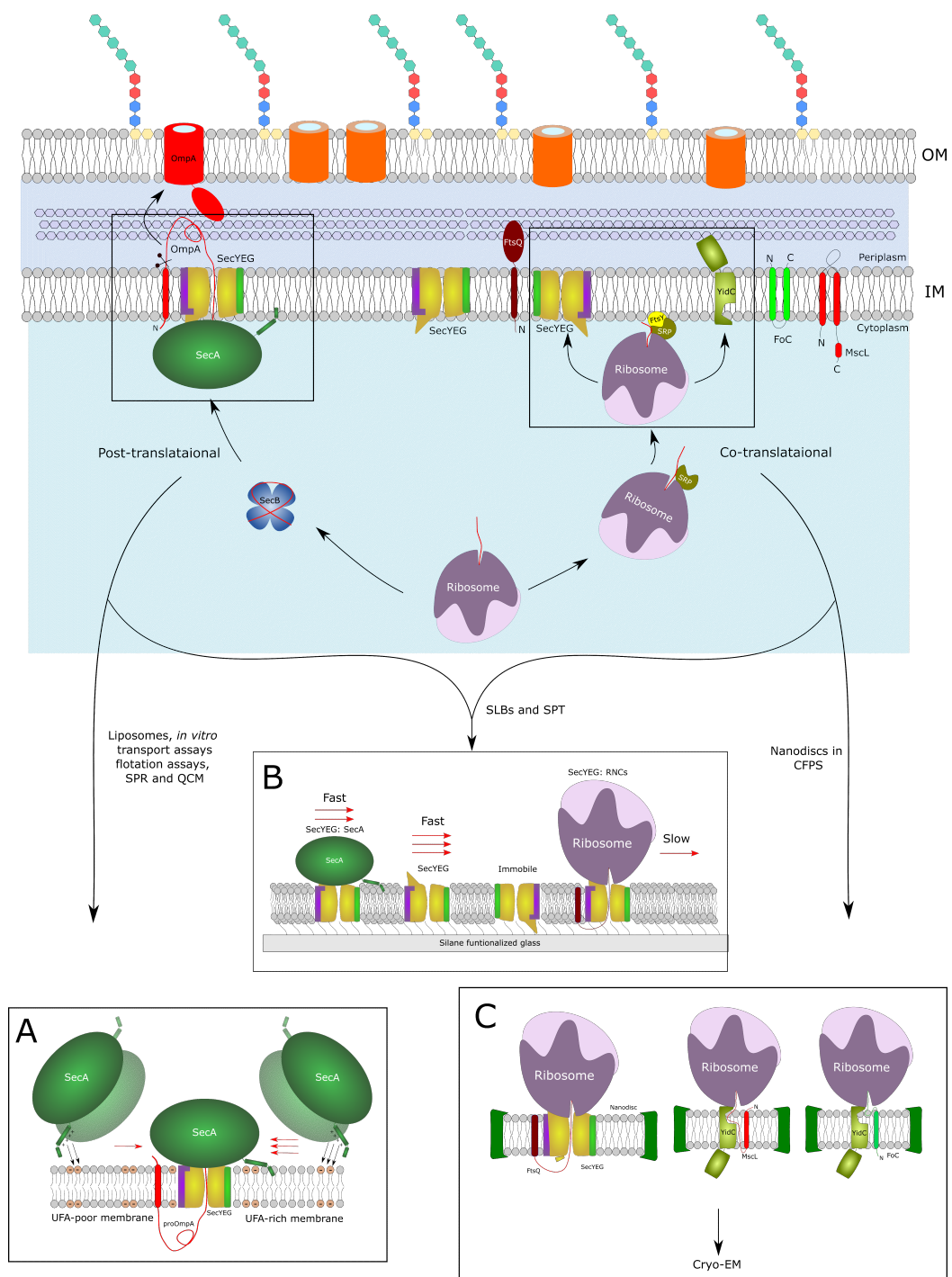
Figure 8.1: Summary of the results obtained in this thesis. A) Mono-UFAs stimulate protein transport via SecYEG: SecA translocon. The N-terminal helix of SecA is splitted into two helices $\alpha 0$ and $\alpha 1$. $\alpha 1$ helix promote electrostatic interaction with the membrane, while $\alpha 0$ promote hydrophobic interaction and SecA insertion into the membrane. Decreasing the positive charge on the $\alpha 1$ helix decrease SecA membrane binding, but has no effect on protein transport. Increasing the polarity of th$\alpha 0$ helix reduce both SecA: membrane binding and transport activity. B) The lateral mobility of SecY in the membrane is not affected by binding SecA. On the other hand, it becomes slower once SecY bind RNCs. C) The co-translational assembly of SecYEG/YidC reconstituted in nanodiscs was established using CFPS. Reconstituted complexes were isolated for structural studies.

Chapter I

Appendix I

Table I.1: Constructs used in Chapter 3

Plasmid name	Description
pEK20 Cless	cysteine less variant of *E. coli* SecY with N terminal histidine tag + SecE + SecG.
pEK20 C148	*E. coli* SecY with L148C mutation with N terminal histidine tag+ SecE + SecG.
pMK2O	*E. coli* SecA wild-type + C terminal histidine tag.
pMK22	SecA Δ N20, *E. coli* SecA with deletion of the first 20 amino acids.

Table I.2: Constructs used in Chapter 4

pEK20 Cless	cysteine less variant of *E. coli* SecY with N-terminal deca-histidine tag + SecE + SecG.
pEK20 C148	*E. coli* SecY with L148C mutation with N-terminal deca-histidine tag+ SecE + SecG.
pMK2O	*E. coli* SecA wild-type + C terminal hexahistidine tag.
pMK21	SecA ΔN10 mutant, *E. coli* SecA with deletion of the first 10 amino acids.
pMK22	SecA ΔN20 mutant, *E. coli* SecA with deletion of the first 20 amino acids.
pMK27	*E. coli* SecA ΔN30 mutant + first 30 amino acids of *B. subtilis* SecA.
pMK28	*E. coli* SecA ΔN30 mutant + first 30 amino acids of *T. maritima* SecA.
pMK29	*E. coli* SecA ΔN30 mutan + first 30 amino acids of *P. aeruginosa* SecA.
pMK40	SecA H1 mutant, *E. coli* SecA I3K, K4I, T8K and K9T.
pMK41	SecA H2 mutant, *E. coli* R19L, L18R, K23V and V24K.
pMK42	SecA H3 mutant, *E. coli* SecA I3K, K4I, T8K, K9T, R19L, L18R, K23V and V24K.
pMK50	*E. coli* SecA Q655A.
pMK51	*E. coli* SecA R656A.
pMK52	*E. coli* SecA Y660A.
pMK53	*E. coli* SecA R663A.
pMK54	*E. coli* SecA F10A.
pMK55	*E. coli* SecA F10W.
pMK56	*E. coli* SecA F10N.
pMK240	*B. subtilis* SecA + C-terminal hexahistidine tag.
pMK240	*T. maritima* SecA + C-terminal hexahistidine tag.
pAT	*P. aeruginosa* SecA + C-terminal hexahistidine tag.

Table I.3: Constructs used in Chapter 6

Plasmid name	Description
pEK20 Cless	cysteine less variant of *E. coli* SecY with N terminal histidine tag + SecE + SecG.
pEK20 C148	*E. coli* SecY with L148C mutation with N terminal histidine tag+ SecE + SecG.
pEM183	*E. coli* YidC with an N-terminal deca-histidine tag.
pEM472	*E. coli* YidC-SecE fusion + SecY with N-terminal deca-histidine tag + SecG.
pKAD186.1	FtsQ FL, *E. coli* FtsQ 1-84 + HA tag + 6 copies of GSG + SecM (FSTPVWIWWWPRIRGPP).
pKAD186.2	FtsQ Δ1, *E. coli* FtsQ 1-73 + HA tag + 6 copies of GSG + SecM (FSTPVWIWWWPRIRGPP).
pKAD186.3	FtsQ Δ2, *E. coli* FtsQ 1-63 + HA tag + 6 copies of GSG + SecM (FSTPVWIWWWPRIRGPP).
pKAD186.4	FtsQ Δ3, *E. coli* FtsQ 1-53 + HA tag + 6 copies of GSG + SecM (FSTPVWIWWWPRIRGPP).
pKAD184	Foc, *E. coli* Foc 1-36 + HA tag + 6 copies of GSG + SecM (FSTPVWIWWWPRIRGPP).
pNCS6	FtsQ FL, *E. coli* FtsQ 1-84 + HA tag + SecM (FSTPVWIWWWPRIRGPP).
pNCS7	FtsQ Δ1, *E. coli* FtsQ 1-73 + HA tag + SecM (FSTPVWIWWWPRIRGPP).
pNCS8	FtsQ Δ2, *E. coli* FtsQ 1-63 + HA tag + SecM (FSTPVWIWWWPRIRGPP).
pNCS9	FtsQ Δ3, *E. coli* FtsQ 1-53 + HA tag + SecM (FSTPVWIWWWPRIRGPP).
pNCS10	FtsQ FL, *E. coli* FtsQ 1-84 + HA tag + 1 copy of GSG + SecM (FSTPVWIWWWPRIRGPP).
pNCS11	FtsQ Δ1, *E. coli* FtsQ 1-73 + HA tag + 1 copy of GSG + SecM (FSTPVWIWWWPRIRGPP).
pNCS12	FtsQ Δ2, *E. coli* FtsQ 1-63 + HA tag + 1 copy of GSG + SecM (FSTPVWIWWWPRIRGPP).
pNCS13	FtsQ Δ3, *E. coli* FtsQ 1-53 + HA tag + 1 copy of GSG + SecM (FSTPVWIWWWPRIRGPP).
pNCS14	Foc, *E. coli* Foc 1-36 + HA tag +1 copy of GSG + SecM (FSTPVWIWWWPRIRGPP).
pNCS23	MscL FL, *E. coli* MscL 1-74 + 1 copy of GSG + SecM (FSTPVWIWWWPRIRGPP).
pNCS24	MscL Δ1, *E. coli* MscL 1-64 + 1 copy of GSG + SecM (FSTPVWIWWWPRIRGPP).
pNCS25	MscL Δ2, *E. coli* MscL 1-54 + 1 copy of GSG + SecM (FSTPVWIWWWPRIRGPP).

Chapter II

Acknowledgments

First, I would like to thank my supervisor and my friend **Junior Professor Alexej Kedrov**. First I would like to thank him for all the support during all the years that I was a member of his lab. This work would have not been possible without you. I have to say that I really had a pleasant time during my Ph.D. time without any stress. I have learned a lot from you during this time not only because you advised me through my project, but because I have watched how you think in different projects and through many conversations that we had through the years, this was very helpful to me to develop myself. Thanks a lot for the trust that I have felt through the last few years and the encouragement to come up with and pursue my own ideas. Thanks a lot for your patience during the mistakes that I have done every now and then. I will miss the bier hour that we used to have every now and then on Friday evenings. I really wish you all the best.

I thank my second supervisor **Professor Lutz Schmitt**. Thanks a lot for the support and for being there through many of my progress reports and for all the critical questions that you have asked that helped me rethink my project, which was very helpful for me to improve my project. Thanks for the tough time you gave me during my last progress report and for all the useful information that you provided me that is definitely very helpful for my defense.

I would like to thank Professor Sander Smits and Dr Jens Reiners from the center of structural studies (CSS) for the support and the SAXS measurements.

I would like to thank all my previous students, Dounia M. Rastani, Ana Mara Popovic, Kai Lange, Anuja Joseph, Nadejda Boicenco, Schinya Ibrahim, and Christian Mammen for all the nice work that they have done and the nice time we spent together in the lab.

Special thanks go to my previous master's student and my friend, Yulia Schaumkessel for the amazing work she has done. She contributed a lot to this work by going through the hard work for optimizing and obtaining a very reliable cell-free protein synthesis reaction setup and testing different stalling sequences for efficient ribosome stalling and initiating the first SecYEG/YidC-RNCs complex assembly experiments.

I would like to thank all the people who have contributed to this work all over the years: Stephan-Schott Verdugo and Professor Holger Gohlke for doing the MD simulations in chapter 3 of the thesis. Jennifer Loschwitz and Professor Birgit Strodel for the nice MD simulations that they have done which supported the work done in chapter 4 of the thesis. Dr. Wieland Steinchen and Professor Gerd Bange for performing the HDX-MS experiments. Thanks to Daniel Kuckla and Professor Cornelia Monzel for helping me with all the microscopy experiments and for analyzing

the data for the part that we contributed to in chapter 5 of the thesis. I would like also to thank Cristian Rosales Hernandez, Hannah Kratzat and Professor Roland Beckmann for performing the cryo-EM measurements and single particle analysis in chapter 6 of the thesis.

I thank Athanasios Papadopoulos, my friend and colleague for the nice time, all the fun we had in the lab, and the late nights that we stayed together in the lab fighting for our projects. All the jokes and the laughs we had together and the nice shisha time discussing and talking about our projects.

I thank Maryna Löwe, my friend and colleague for the nice time and the fun we had in the lab. All the nice conversations we had about food and nutrition, soaps, and bacterial culture drinks. Well, you have taught me a lot I have to say.

I thank my close friend, Max Busch, I have known him since he was a bachelor's student in the lab. It was really nice having you around, and all the funny discussions, the laughs, and the great time we had together in and outside the lab. Thanks for the suffering and the patience you had to go through my horrible German skills and my flachwitze.

Thanks to my close friend, Dr. Marten Exterkate for all the fun times we had together and the Holy Craft time, and the intense discussion we had together on all different topics. And of course for all the scientific discussions we had that I have found useful for my project.

I would like to thank all my colleagues and friends from the Institute of Biochemistry for all the useful discussions that we had over the years that helped me with my project and for all the fun times and discussions that we had during the coffee breaks and the fun outings that we had together outside the lab.

Thanks to Florestan Bilsing and Junior Professor Miriam Kutsch for proofreading certain chapters of my thesis.

I would like to thank Martina Wesemann and Silke Mavaro for always being so helpful and being there whenever I needed anything.

I like to thank Professor Sandro Keller from the University of Graz for the support provided in establishing maleic acid copolymer nanodiscs for our proteins.

Special thanks go to my family, my father **Nady Boshra**, and my sister Sandy Nady. Without my father, I wouldn't have been here today. He is the reason I am in Germany doing and now finishing my Ph.D. studies.

Thanks to all my Egyptian best friends, Mina Moheb, Fady Youssef, and Mina Atef for believing in me all these years.

Chapter III

Publications

1. **Michael Kamel***, Jennifer Loschwitz*, Martin Wolff, Wieland Steinchen, Gerd Bange, Salvatore Chiantia, Birgit Strodel , Alexej Kedrov. (2023). Characterization of SecA: membrane interaction and its role in protein transport. In preparation.

2. C. Vivian Knospe, **Michael Kamel**, Olivia Spitz, Astrid Hoeppner, Stefanie Galle, Jens Reiners, Alexej Kedrov, Sander H.J Smits, Lutz Schmitt. (2023). The structure of MadC from Clostridium maddingley reveals new insights into class I lanthipeptide cyclases. Frontiers in Microbiology, 13, 1057217.

3. Andrea J. Weiler, Olivia Spitz, Mirja Gudzuhn, **Michael Kamel**, Björn Thiele, Wolfgang R. Streit, Alexej Kedrov, Lutz Schmitt, Holger Gohlke, Filip Kovacic. (2022). A phospholipase B from Pseudomonas aeruginosa with activity towards endogenous phospholipids affects biofilm assembly. Biochimica et Biophysica Acta (BBA)-Molecular and Cell Biology of Lipids, 1867(4), 159101.

4. **Michael Kamel**, Maryna Löwe, Stephan N. Schott-Verdugo, Holger Gohlke, Alexej Kedrov. (2022). Unsaturated fatty acids augment protein transport via the SecA: SecYEG translocon. The FEBS journal, 289(1), 140-162

5. Sabrina Koch, Anne-Bart Seinen, **Michael Kamel**, Daniel Kuckla, Cornelia Monzel, Alexej Kedrov, Arnold J.M. Driessen. (2021). Single-molecule analysis of dynamics and interactions of the SecYEG translocon. The FEBS Journal, 288(7), 2203-2221.

6. Maryna Löwe, Athanasios Papadopoulos, **Michael Kamel**, Alexej Kedrov. (2019). Membranproteinfaltung—Kernwissen aus (nicht zu) vereinfachten Systemen. BIOspektrum, 25(4), 385-387.

Chapter IV

Curriculum Vitae

Michael Kamel

━━━━━ Personal Details

Date of Birth	1 October 1991.
Nationality	Egyptian.

━━━━━ Education

2018- present	**Ph.D. in Natural Sciences/ Biochemistry**, *Heinrich Heine Universität Düsseldorf*, still to be completed.
2015–2017	**Master of Science in Molecular Bioengineering**, *Technische Universität Dresden*, Dresden, Germany, Graduation grade: *1.7/1.0*
2008–2013	**Bachelor of Science in Pharmaceutical Sciences**, *Ain Shams University*, Cairo, Egypt, Graduation grade: *87.47%/100%*
2005–2008	**General Secondary certificate**, *Saint Fatima Language School*, Cairo, Egypt, Graduation grade: *96.8%/100%*

━━━━━ Experience

2018 till now	**Ph.D. Candidate**, *Synthetic Membrane Systems, Institute of Biochemistry Heinrich Heine Universität Düsseldorf*, Düsseldorf, Germany,

Ph.D. Topic: SecYEG/YidC mediated protein biogenesis.

Project 1: Unraveling the mechanism of Sec mediated protein transport. Within the scope of the project, I studied the effect of the membrane composition on SecYEG: SecA translocon, where I demonstrated the stimulatory role of unsaturated fatty acids on the Sec machinery.

Project 2: Analysis of the structure and dynamics of co-translational membrane protein insertion and folding. I reconstituted the bacterial membrane protein insertion machinery in nanodiscs and DIBMA particles. By using a cell-free protein synthesis platform, the co-translational assembly of the ribosome nascent chain complex with the reconstituted insertion machinery was established for structural studies using cryo-EM.

Project 3: Single-molecule analysis of the dynamics and interactions of the SecYEG translocon. I contributed to a study to analyze the dynamics of SecYEG in a planar lipid bilayer on a single molecule level.

2017	**Research Assistant**, *Leibniz Insitut Für Polymerforschung*, Dresden, Germany

Optimization of a microfluidic method for the preparation of pH-switchable giant vesicles using the block copolymer (PEG-PDEAMA-s-PDMIBM).

2017	**Master's student**, *Leibniz Insitut Für Polymerforschung*, Dresden, Germany,

Topic: pH-switchable giant vesicles using microfluidics.

Description: Preparation of pH-switchable giant vesicles via microfluidics from the pH-switchable diblock copolymer (PEG-PDEAMA-s-PDMIBM) using the double emulsion method. .

2013–2015 **Research and Development Specialist**, *Eva Pharma*, Giza, Egypt
Research and development department in the analytical section.
Responsibilities:
○ Development of analytical methods of analysis for pharmaceutical drugs using high-performance liquid chromatography, gas chromatography, UV spectroscopy.
○ Validation of analytical methods of analysis for pharmaceutical drugs to satisfy five parameters repeatability, accuracy, specificity, precision, and robustness.
○ Establishment of in vitro experiments to test the dissolution for pharmaceutical drugs.
○ Stability follow-up (Long term and accelerated) studies for pharmaceutical products.
○ Raw material analysis.

Chapter V

Declaration

I declare under oath that I have produced my thesis independently and without any undue assistance by third parties under consideration of the 'Principles for the Safeguarding of Good Scientific Practice at Heinrich Heine University Düsseldorf

Düsseldorf, den _____ Signature: _____